PB-231 067

FOUNDATION FOR MODELING NOx AND SMOKE FORMATION IN DIESEL FLAMES

R. P. Wilson, Jr., et al

Coordinating Research Council, Incorporated

Prepared for:

Environmental Protection Agency

January 1974

DISTRIBUTED BY:

NTIS
National Technical Information Service
U. S. DEPARTMENT OF COMMERCE
5285 Port Royal Road, Springfield Va. 22151

BIBLIOGRAPHIC DATA SHEET

1. Report No. CRC-APRAC-CAPE-20-71-1

2.

PB 231 067

4. Title and Subtitle
Foundation for Modeling NO_x and Smoke Formation in Diesel Flames

5. Report Date
January 1974

6.

7. Author(s)
R.P. Wilson, Jr.; C.H. Waldman; and L.J. Muzio

8. Performing Organization Rept. No.

9. Performing Organization Name and Address
Ultrasystems, Inc.
2400 Michelson Drive
Irvine, California 92664

10. Project/Task/Work Unit No.

11. Contract/Grant No.

12. Sponsoring Organization Name and Address
Coordinating Research Council, Inc., 30 Rockefeller Plaza, New York, N.Y. 10020 and Environmental Protection Agency, 2565 Plymouth Road, Ann Arbor, Michigan 48105

13. Type of Report & Period Covered
Final -- 7-1-71-6-30-73

14.

15. Supplementary Notes

16. Abstracts

A mechanistic model has been established by four activities: (1) Emissions data were correlated with engine parameters; (2) Existing models were assessed; (3) a model of heat release was outlined; (4) diesel flame measurements were conceived. Exhaust measurements of NO, soot, and hydrocarbons were made on a 2340-cm^3 displacement, single-cylinder diesel engine. In addition to confirmation of the well known effects of A/F and timing the following parameters were found to change NO_x emissions by 40% or more (with corresponding soot changes):

Engine Geometry	State of the Intake	Mixing Parameters
Divided chamber	EGR	Fuel orifice size
Prechamber volume ratio	Water injection	Air swirl
Compression ratio		

17. Key Words and Document Analysis. 17a. Descriptors

Air Pollution
NO
Soot
Diesel Engine
Emissions
Oxides of Nitrogen
Exhaust
Hydrocarbons

17b. Identifiers/Open-Ended Terms

17c. COSATI Field/Group 13B; 7B; 21B; 20M; 7C.

18. Availability Statement
Releasable to the General Public

19. Security Class (This Report)
UNCLASSIFIED

20. Security Class (This Page
UNCLASSIFIED

21. No. of Pages
181

22. Price
5.50/1.45

i.

FORM NTIS-35 (REV. 3-72)

THIS FORM MAY BE REPRODUCED

USCOMM-DC 14952-P72

EPA-460/3-74-002a

FOUNDATION FOR MODELING NO_x AND SMOKE FORMATION IN DIESEL FLAMES

By

R. P. Wilson, Jr., C. H. Waldman, and L. J. Muzio
Ultrasystems, Inc., Irvine, California

Final Report for Phase I

Studies Performed From
1 July 1972 - 30 June 1973

Prepared for:

U. S. Environmental Protection Agency
2565 Plymouth Road
Ann Arbor, Michigan 48105

Contract No. 68-02-0222

Coordinating Research Council
30 Rockefeller Plaza
New York, New York 10020

APRAC Project CAPE 20-17

ii.

January 1974

ACKNOWLEDGEMENTS

The eventual usefulness of an applied research study hinges on whether efforts are focussed on questions of real importance to industry and society. The EPA and the CAPE 20-71 Steering Committee of the Coordinating Research Council, having conceived the original project outline, have aligned this study to be "on target" through numerous critical reviews and suggestions. The following individuals have been of service in this regard:

J. L. Bascunana	Environmental Protection Agency
T. C. Belian	Coordinating Research Council
J. E. Bennethum	General Motors Research Laboratory
W. L. Brown	Caterpillar Tractor
F. J. Hills	Mobil R&D (Committee Chairman)
J. C. Hoelzer	International Harvester
G. D. Kittredge	Environmental Protection Agency
D. F. Merrion	General Motors
P. C. Meurer	International Harvester
J. M. Perez	Caterpillar Tractor
S. M. Shahed	Cummins Engine
A. V. Wilson	Cummins Engine
A. E. Zengel	Coordinating Research Council

In addition, the following fluid physics specialists and advisors from the academic community have shared their experience and technical expertise during Phase I of the study

G. L. Borman	University of Wisconsin
P. S. Myers	University of Wisconsin
J. Shipinski	John Deere Tractor
F. A. Williams	University of California, San Diego

Finally, the support and competent engineering of the Advanced Products Division of White Motors Corporation, especially the following persons, is warmly acknowledged

W. F. Dittman	President
E. B. Muir	Product Development
F. A. Pellicciotti	Engineer
J. Salyer	Technician
H. LaHomme	Design

Description of Project Team

The study is being conducted by the Applied Combustion Research Group of Ultrasystems, Inc. During Phase I, staff members participating were as follows:

R. P. Wilson, Jr.	Program Management, Single Cylinder Emissions, Photography, Spectroscopy, Model Evaluation, New Mechanistic Model
C. H. Waldman	Model Evaluation, Diffusion Flame Studies, New Mechanistic Model
L. J. Muzio	Spectroscopy, New Mechanistic Model

In addition, T. J. Tyson provided substantial technical guidance in modeling cylinder fluid dynamics and, as Division Vice President, garnered vital resources (e.g. instrumentation) for the program. Technical support was provided by E. Madsen, C. McComis, and C. Bradley. Typing and artwork were by G. Cresswell and J. Stewart, respectively.

TABLE OF CONTENTS

Section | Page

I. SYNOPSIS AND RECOMMENDATIONS 1

II. ORIENTATION 3

A. Practical Reasons for an Attempt to Characterize NO and Smoke Formation in Diesel Flames 3
B. Characterizing NO and Soot Formation will Demand a Clear Picture of the Diesel Flame 4
C. Program Strategy to Identify NO_x and Smoke Mechanisms 5

III. EVIDENCE FROM DIESEL EMISSIONS BEHAVIOR 7

A. Single-Cylinder Experimental Technique 8
B. Observed Emissions 11
C. Summary of Emissions Evidence 45

IV. AN INTERPRETATION OF DIESEL COMBUSTION AND POLLUTANT FORMATION 48

A. Mixing and Combustion Mechanisms 50
B. Outline of an Emissions Model 53
C. Flame Studies Needed 64
D. Droplet Diffusion Flame as a NO_x-Source 67

V. ASSESSMENT OF EXISTING MODELS 74

A. The NREC Model 77
B. The CAV Model 84
C. The Cummins Model 89

VI. DIESEL FLAME STUDIES 93

A. Spectroscopic Observations 93
B. Diesel Flame Photography 102

NOMENCLATURE 104

REFERENCES 107

APPENDICES

A. Essentials of NO_x and Smoke Formation 111
B. Single-Cylinder Experimental Technique 121
C. Complete Data from Single Cylinder Emission Tests 133
D. Compilation of Published Diesel Emissions Data 143
E. Equilibrium Analysis of Diffusion Flame Structure 149
F. Unsteady Diffusion as a Factor in Droplet Combustion 155
G. Experience in the Use of Windowed Combustion Chambers 169

II. ORIENTATION

A. PRACTICAL REASONS FOR AN ATTEMPT TO CHARACTERIZE NO AND SMOKE FORMATION IN DIESEL FLAMES

The modern diesel engine enjoys widespread use in heavy duty transport, due in large part to its simplicity and relatively low fuel consumption. The high flame temperatures and mixture heterogeneity which produce the advantages of the compression ignition engine also give rise to the side effects which concern us in this study--NO and smoke formation. An investigation was undertaken to attempt to better understand the diesel flame, so that the formation of these pollutants can be controlled--without compromising the basic advantages of the diesel engine by complex add-on gadgetry or higher fuel consumption.

Through a number of past studies, the industry has determined certain simple measures which will reduce nitric oxide and smoke emissions from specific engines, foremost among them retarded timing and aftercooled turbocharging. Other measures such as EGR, water injection, fuel injection variations, and prechamber designs have also shown emissions control potential but require further research and development. If engines are to be optimized, it will be helpful to know why these methods work. In the long term, the industry may be considering advanced designs for the diesel engine; designs which may be so different from current engines that existing emissions data cannot be extrapolated with reasonable confidence. At this point, a predictive framework of understanding of diesel-generated NO and soot will be valuable. In the meantime, model predictions could be used to improve and guide the "cut-and-try" emissions testing which is currently being carried out on major production engines. When smoke and fuel consumption limits are reached on a given engine, the test engineer could use a table of predicted influence coefficients to assist the intuition in selecting promising test set-ups. It is the intent of this study to forge such a tool by setting down in a mathematical model all we know or can learn about the complex, coupled flame phenomena in which NO and smoke are produced: spray combustion, radiation, and pollutant kinetics.

B. CHARACTERIZING NO AND SOOT FORMATION WILL DEMAND A CLEAR PICTURE OF THE DIESEL FLAME

NO and soot formation are activated by combinations of temperature and species composition which fortunately are not widespread in a diesel flame (for a complete discussion, see Appendix A). Therefore, in a given diesel combustion chamber, there are only certain zones which are actively producing NO or soot during certain crank-angle intervals. An accurate description of NO and soot formation requires detailed temperature and species profiles in these local regions. Details such as temperature and O-atom gradients, supercritical envelope or wake flames, turbulent eddy size, and spray droplet size distribution may be required.

None of these actual happenings have been measured or described for the flame of any production diesel engine. To date, it has simply not been worth the trouble. In order to simulate or predict performance, it sufficed to describe the heat release either with empirical formulas [after Lyn (1957) or Shipinski (1968)], or to assume burning of homogeneous regions of prescribed fuel/air ratio. Such "global" models paid a penalty for whitewashing the physical mechanisms with prescribed empiricism: A new set of empirical constants for each new engine or fuel system had to be developed to make the computer simulation work. Only Shipinski et al. (1968) and Khan and Wang (1971) have attempted more universally applicable treatments of diesel combustion based on the diffusion flame. These models are evaluated in Section V. The basic limitation to formulating a more applicable model is lack of measurements on the diesel flame. The available evidence essentially consists of high-speed movies, chamber pressure (heat release) recordings, and heat transfer measurements.

Substantial experimental and theoretical effort is required to go deeper into the details of diesel spray combustion. If the empiricism is to be replaced, ultimately this effort must be made. The current program is oriented toward this goal.

C. PROGRAM STRATEGY TO IDENTIFY NO_x AND SMOKE MECHANISMS

The program is structured to focus on the missing diesel flame information needed to predict NO and soot formation. Tasks are grouped into five main activities as summarized below in Table 1, along with the approximate percent completion as of this writing. Note that the diesel flame studies and analytical modeling are at a very preliminary stage. The Phase I report should be read as an interim report; except for the emissions data (Chapter III), a reasonable number of the interpretive notions about diesel combustion in this report are likely to be revised or even abandoned as new data becomes available.

Table 1

FIVE MAJOR PROGRAM ELEMENTS

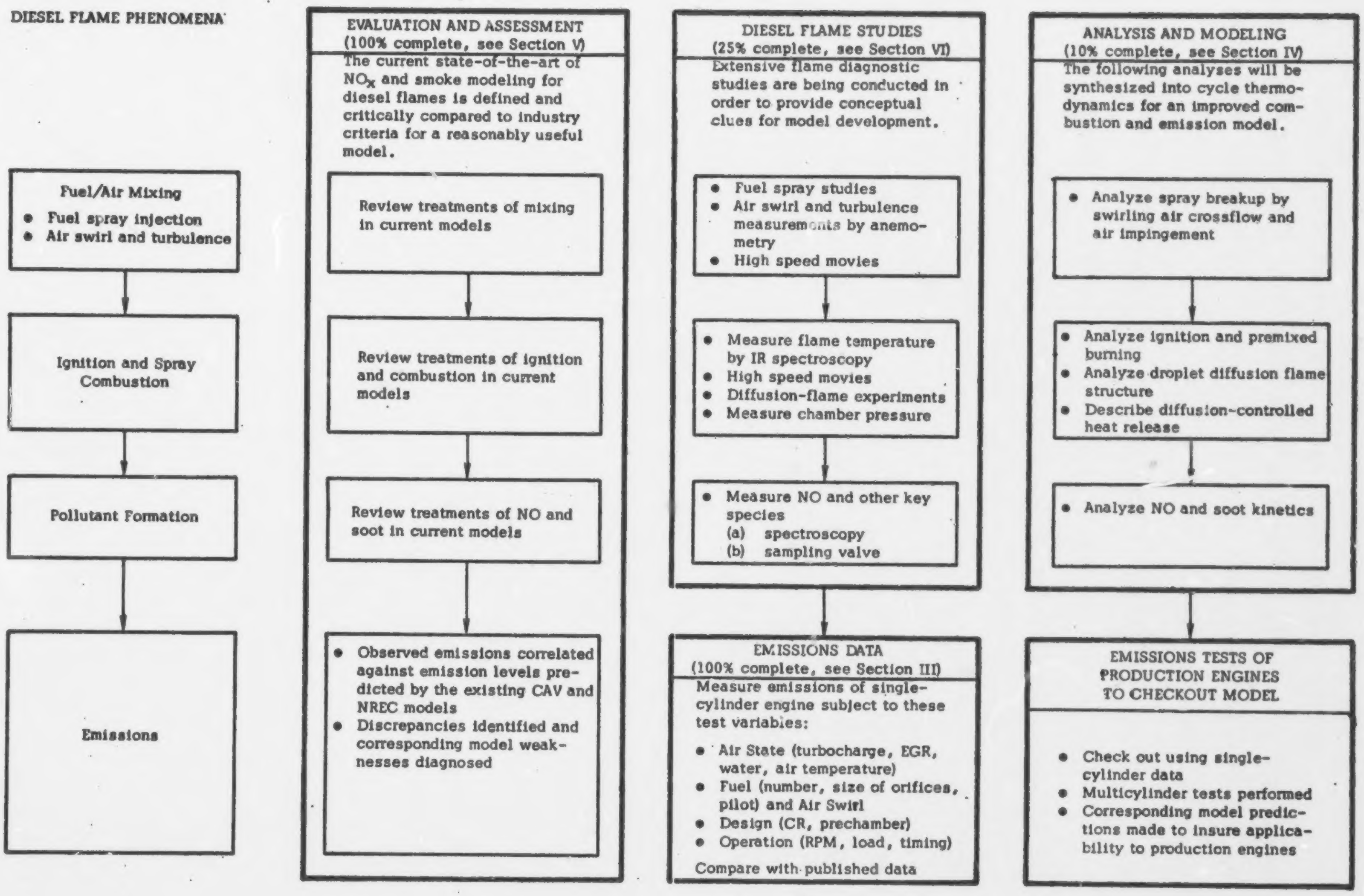

DIESEL FLAME PHENOMENA

Fuel/Air Mixing
- Fuel spray injection
- Air swirl and turbulence

Ignition and Spray Combustion

Pollutant Formation

Emissions

EVALUATION AND ASSESSMENT
(100% complete, see Section V)

The current state-of-the-art of NO_x and smoke modeling for diesel flames is defined and critically compared to industry criteria for a reasonably useful model.

Review treatments of mixing in current models

Review treatments of ignition and combustion in current models

Review treatments of NO and soot in current models

- Observed emissions correlated against emission levels predicted by the existing CAV and NREC models
- Discrepancies identified and corresponding model weaknesses diagnosed

DIESEL FLAME STUDIES
(25% complete, see Section VI)

Extensive flame diagnostic studies are being conducted in order to provide conceptual clues for model development.

- Fuel spray studies
- Air swirl and turbulence measurements by anemometry
- High speed movies

- Measure flame temperature by IR spectroscopy
- High speed movies
- Diffusion-flame experiments
- Measure chamber pressure

- Measure NO and other key species
  - (a) spectroscopy
  - (b) sampling valve

EMISSIONS DATA
(100% complete, see Section III)

Measure emissions of single-cylinder engine subject to these test variables:

- Air State (turbocharge, EGR, water, air temperature)
- Fuel (number, size of orifices, pilot) and Air Swirl
- Design (CR, prechamber)
- Operation (RPM, load, timing)

Compare with published data

ANALYSIS AND MODELING
(10% complete, see Section IV)

The following analyses will be synthesized into cycle thermodynamics for an improved combustion and emission model.

- Analyze spray breakup by swirling air crossflow and air impingement

- Analyze ignition and premixed burning
- Analyze droplet diffusion flame structure
- Describe diffusion-controlled heat release

- Analyze NO and soot kinetics

EMISSIONS TESTS OF PRODUCTION ENGINES TO CHECKOUT MODEL

- Check out using single-cylinder data
- Multicylinder tests performed
- Corresponding model predictions made to insure applicability to production engines

III. EVIDENCE FROM DIESEL EMISSIONS BEHAVIOR

A. SINGLE-CYLINDER EXPERIMENTAL TECHNIQUE

A 2340-cm^3 (143 in^2) displacement research engine was constructed for the experimental program. The engine and test procedures are described in detail in Appendix B. The selected chamber geometry is a 5-1/2" bore, 6" stroke, with 12" connecting rod to minimize piston slap at TDC. Two cylinder head configurations were fabricated--a direct injection head and a prechamber version, hereafter referred to as the DI engine and PC engine (Figure 1). Piston and bowl geometry are given in Figure 1 for both types of heads. Changes in piston geometry gave compression ratios of 20:1, 17:1, and 14:1 for the DI configuration; changes in piston caps and prechamber gave four combinations of PC ratio and compression ratio, as listed in Figure 1.

The M.A.N. and Lanova combustion chambers were also tested in order to examine emissions sensitivity to substantial changes in provisions for fuel/air mixing. These systems were tested as standard multicylinder engines of comparable displacement. Sketches of the head design appear in Figure 1.

The nozzle for the DI head was a Roosa pencil injector, popularly used in farm tractors, nominally with six .010" orifices at 160 deg. cone angle. For the PC head a single pintle orifice at .37 mm^2 size with 12 deg. cone angle was standard.

By means of changes in the fuel line length, injectors, cam profiles, fuel valve opening pressure, and plunger diameter, it was possible to study the following variations:

No. of orifices: 4, 6, 8
Orifice size: .008, .010, .012, .014 inches
Rate of fuel injection: 3 to 8 mm^2/$^\circ$CA
Pilot injection: 10 to 20% of fuel injected at -40°CA
Cone angle: 120 deg. vs. 160 deg. for DI
8 to 12 deg. for PC

Air was taken from the laboratory compressed air supply and heated (or cooled) after the filter and flowmeter. A throttle valve in the exhaust line was used in some tests to build up exhaust pressure to simulate turbocharging.

Figure 1

CYLINDER HEADS

PRECHAMBER

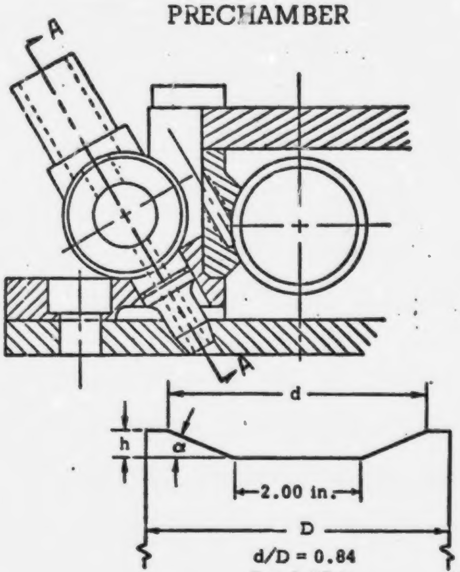
A
A
d
h
α
2.00 in.
D

d/D = 0.84
D = 5.50 in.

CR	V/V_{tot}	h(in.)	α	Plug (Projection) x
17:1	25%	0.395	16°45'	0.690
19.4:1	15%	0.395	16°45'	1.113
17:1	35%	0.345	14°44'	0.398
19.4:1	25%	0.345	14°94'	0.826

DIRECT INJECTION

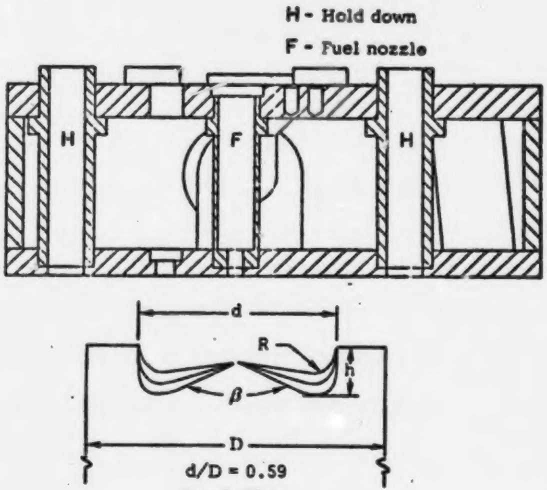
H - Hold down
F - Fuel nozzle
H
F
H
d
R
h
β
D

d/D = 0.59
D = 5.50 in.

CR	β	h(in.)	R(in)	Serial No.
17:1	119°	0.877	.500	TE 02650
14:1	100°	1.125	.500	TE 02697
20:1	140°	0.715	.500	TE 02696

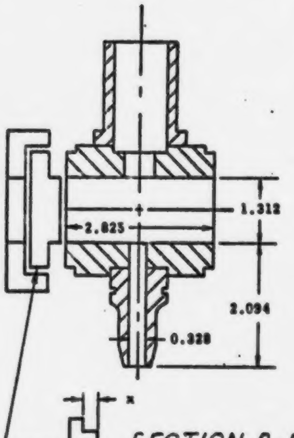
1.312
2.825
2.094
0.328
x

SECTION A-A

M.A.N.

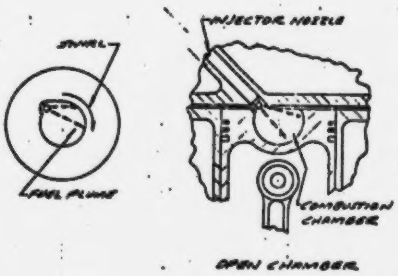
SWIRL
FUEL PLUME
INJECTOR NOZZLE
COMBUSTION CHAMBER

OPEN CHAMBER

LANOVA

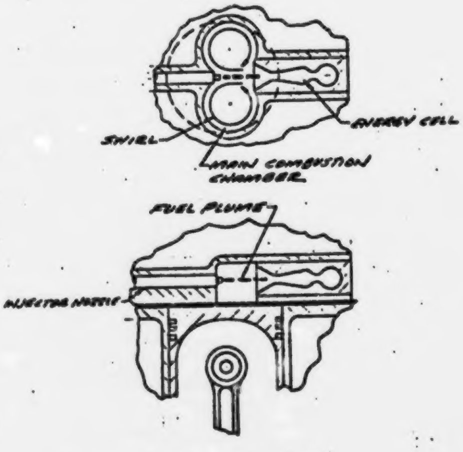
SWIRL
ENERGY CELL
MAIN COMBUSTION CHAMBER
FUEL PLUME
INJECTOR NOZZLE

DIVIDED CHAMBER

Preceding page blank

Water mist was available at the intake, and an EGR system was available to supply measured amounts of exhaust gas to the intake. In this manner, the state of the intake air could be controlled and varied as follows:

Water injection: $\dot{m}_{H_2O}/\dot{m}_f$ = 0 to 1.0
EGR: $\dot{m}_{egr}/\dot{m}_{tot}$ = 0 to 30%
Air pressure: 30 to 60" Hg
Air temperature: 100 to 200°F

A masked valve was used to generate swirl (see Figure 2); rotation of the valve controlled both the sense and degree of swirl. In addition, for each "top-end", baseline tests were run over a 20-point matrix of speed, load, and timing.

Variables were changed one at a time in order to clarify the NO and smoke behavior. Runs with two effects which compensate or amplify one another would be appropriate for a low-emissions development program, but not for this study of mechanisms. In each case, extreme levels of the variables (for example, 30% EGR; a range of X5 in swirl, etc.) were selected in order to bring to the surface whatever NO and smoke changes were occurring.

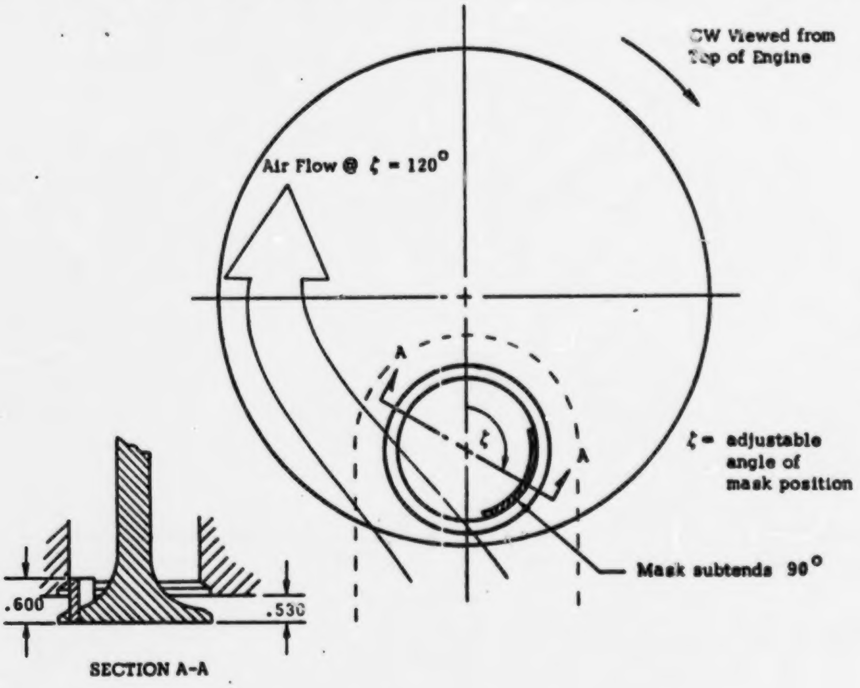
CW Viewed from Top of Engine
Air Flow @ ζ = 120°
A
ζ
A
ζ = adjustable angle of mask position
Mask subtends 90°
.600
.530
SECTION A-A

Figure 2
PROVISION FOR AIR SWIRL

B. OBSERVED EMISSIONS

In this section we report how diesel emissions responded as operating parameters were changed. A substantial bank of data has been acquired in a closely controlled, highly instrumented manner. Complete data records are supplied as Appendix C to this report. This data bank serves the three functions of (1) providing diverse emissions data against which model predictions can be compared, (2) stimulating mechanistic thinking about NO_x behavior which the model must simulate, and (3) suggesting the most interesting emissions behavior for planned diesel flame studies.

The form of the graphical data presentation is designed to facilitate comparison with model predictions. All values are normalized by baseline emissions and performance data; what appears on the graph is the fractional change in NO_x (lb/1000 lb fuel), soot (% opacity) or indicated specific fuel consumption (lb/IHP-hr) due to the test variable. This reflects our predisposition that it is more realistic to expect relative trends or influence coefficients from a model than absolute predictions. In addition, values of brake specific NO_x (g/BHP-hr)* are given to permit direct comparison with multicylinder engines.

Results from earlier studies generally corroborate our findings. A compilation of published emission data may be found in Appendix D. This data listing includes the studies of Abthoff and Luther (1969), Landen (1963), Khan and Wang (1971), Schmidt et al. (1966), Marshall and Fleming (1971), Bascom et al. (1971), Hames et al. (1971), Pischinger and Cartellieri (1972), Parker and Walker (1972), Shahed, Chiu and Yumlu(1973), Walder (1973), and McConnell (1963).

Even though the combustion chamber was treated as a "black box", these measurements of external behavior can provide valuable clues about the flame processes which produce NO_x and smoke. Possible interpretations are hypothesized in preparation for synthesizing these interpretations into a model of diesel-generated pollutants.

---

*A slight FMEP correction was applied to the BMEP in order to simulate the lower specific mechanical friction experienced in a multicylinder engine. This correction is minor (2 to 7 FMEP, depending on engine configuration).

1. Effect of Different Combustion Chambers

The behavior at baseline RPM and air/fuel ratio of the single cylinder engine is shown in Table 6. Results for the MAN and Lanova multicylinder engines are listed for comparison. It cannot be overstressed that none of the engines, except the MAN and Lanova engines, were tuned or adjusted into optimum performance; they represent single cylinder designs which were simply set up and run. In comparing PC engines to DI engines, it should be noted that the fuel system differed.

Table 6

COMPARATIVE BEHAVIOR OF ENGINES TESTED
(Baseline: 1500 RPM; A/F = 32, N.A.)

Type	Compression	Volume Ratio	Fuel Nozzle	Timing (°BTDC)	NO_x (lb/1000 lb fuel)	Soot (% Opac)	BSFC
DI	17:1	--	6-hole	-20	92.1	5.3	.397
DI	14:1	--	6-hole	-20	46.7	5.3	.412
PC	17:1	25%	Pintle	- 6	26.4	1.8	.397
PC	17:1	35%	Pintle	- 6	37.0	1.0	.409
PC	19.4:1	25%	Pintle	- 6	17.2	4.0	.428
PC	19.4:1	15%	Pintle	- 6	11.7	24.0	.490
MAN	17:1	--	Not avail.	-21	51.2	1.2	.408
Lanova	17:1	--	Not avail.	-20	51.8	2.0	.358

A significant variation in NO_x can be seen between engine configurations. The main trends are as follows:

- The prechamber generally gives lower NO_x with higher fuel consumption.
- Increased volume ratio produces increased NO_x but reduced soot.
- As compression ratio is increased, nitric oxide emissions increase.

a. Effect of Prechamber

Prechamber engines exhibit markedly lower NO_x than DI engines. A popular hypothesis is that premixed burning occurs at a lower temperature because the overall mixture is richer in the prechamber. The merit of this hypothesis is questionable since there are some indications that the combustion is diffusion limited. In a diffusion flame, the overall A/F ratio does not affect the local flame temperature but only affects the final mean temperature of the product mixture. An alternative hypothesis is the staged-combustion argument: following partial combustion in the prechamber, the hot gases lose heat as they are pumped out into the main chamber (for this reason, PC engines have relatively large radiators). Thus the heat release is staged, and the intervening heat transfer presumably reduces peak temperatures and NO_x.

b. Effect of Volume Ratio

The effects of prechamber volume ratio are presented in detail in Figures 3 and 4. It is plausible that the larger prechamber volumes contain enough air to burn more of the fuel before expulsion occurs, thus reaching higher flame temperatures and generating more NO_x. To corroborate this hypothesis, we have extended the plot to include the DI engine which is, in effect, 100% prechamber. The NO_x emissions for DI and PC engines are related systematically as shown in Figure 4.

c. Effect of Compression Ratio

As to the effect of compression ratio shown in Figures 5 and 6, clearly more than one mechanism is at work since Figure 5 shows the opposite trend of Figure 6. The higher compression temperatures associated with an increase in the compression ratio might stimulate thermal NO formation. Even though NO_x production is presumably confined to flame fronts and other local zones, the local peak temperatures associated with these "active" zones will be boosted along with any increase in the average gas temperature, increasing NO formation. Increased heat transfer and dissociation will of course attenuate such an effect. Compression ratio also affects the rate of fuel/air mixing by governing the swirl at TDC when fuel is injected. If fuel mixes and burns earlier in the cycle, before volume expansion drops the temperature, NO emissions may increase. Furthermore, compression ratio may affect ignition delay.

2. Effect of Operational Parameters (Load, Speed, and Timing)

a. Effect of Load

The effect of equivalence ratio (ϕ)* upon NO formation supports the notion that overall mixture ratio is not as relevant a parameter as it would be in a premixed flame. Comparison of DI and PC engines in Figures 7 and 8 show that NO peaks at $\phi \simeq 0.3$ in both cases, whereas for a premixed system NO would peak at $\phi \approx .95$. Nitric oxide emissions per unit fuel actually decrease as ϕ approaches stoichiometric for $\phi > 0.3$, as shown in Figures 7 and 8. There are at least two possible factors which could cause NO to drop with equivalence ratio:

(i) The start of injection and rate of injection are fixed. As the period of injection increases with ϕ, more burning occurs later in the expansion cycle, where the gas temperature has dropped due to expansion and heat losses, so that NO may be produced at a reduced rate.

(ii) Each successive fuel element introduced is likely to see an oxidizer which is progressively more diluted with products. At high loads, the available oxygen concentration for late-burning fuel is lower and local flame temperature and NO formation rates may be lowered accordingly.

b. Effect of Timing

Looking at further evidence, we document in Figure 9 the well-known effect of retarded timing on emissions from DI engines. For each 10°CA that the start of fuel feed is delayed, i.e., "retarded" from normal, the exhaust NO_x level drops about 50%. The effect is most pronounced at high loads, that is, when the duration of fuel injection is largest. Several flame alterations may occur when timing is retarded; their relative importance on NO_x is not yet known:

(i) Aerodynamic Effect: Late fuel is injected into a different air-flow environment, probably lower angular momentum but higher turbulence intensity. Also the piston ledge becomes accessible at late crank angles so that one might expect more stratification of the heavier unused air which is thrown outward away from the fuel.

---

*Equivalence ratio is taken as $(F/A)/(F/A)_{stoic}$. Equivalence ratio was selected over BMEP or IMEP as the "load" variable because the latter are inherently dependent variables.

(ii) Thermal Effect: Fuel burning well into the expansion stroke presumably enjoys an environment of lower temperature and pressure (corresponding to lower performance and lower NO production).

(iii) Residence Time Effect: With late injection, the time for NO-formation in the hot products throughout the cylinder may be cut short.

(iv) Ignition Delay Effect: Evidence shows that the preparation-to-burn time shortens with injection retard.

The effect of timing for the prechamber engines is shown in Figure 10. Note the marked minimum in the NO_x curve at start of injection (about 4°BTDC), which seems to be uniformly characteristic of all four PC engines. Before commenting on this minimum at -4° BTDC, let us review the prechamber combustion phenomena. The fuel is injected into the prechamber, which nominally contains 25% of the air by volume. As heat is released, the prechamber pressure rises, expelling the products and remaining fuel through an orifice into the main chamber. At low loads ($\phi < .25$), none of the main chamber air is needed to complete combustion--the NO_x becomes insensitive to timing as shown by Landen (1963).

For normal operation ($.5 < \phi < .7$), the sensitivity of NO to timing is greatest for small prechambers (see Figure 10). In fact, Walder (1973) reports no timing effect for large prechambers with $V_{PC}/V = 50\%$; again we suspect enough air in the prechamber to complete combustion. This suggests that NO formation in the main chamber is causing the NO changes with timing. Perhaps prechamber activity is complete by the time volume changes occur at high crank angle ($\Theta > +20^{\circ}$).

The minimum in NO vs. timing seems peculiar to PC engines tested in the present program [previous studies by Landen (1963), McConnell (1963), and Eyzat (1967) showed no minimum with retarded timing]. The sharp edged, rather long ($L/D \approx 3$) passageway connecting prechamber to main chamber may be responsible: If large ΔP's exist between the two chambers without combustion (due to the flow restriction), then the timing of fuel injection and prechamber ignition would couple with the timing of this natural pumping. The NO could increase at retarded timings because of a phase lag (between pumping and ignition) more favorable to expulsion and rapid heat release in the main chamber. Indeed the NO minimum is seen to be more severe at 19:1 compression ratio than at 17:1, and pumping lag might be more marked at 19:1.

c. Effect of Speed

From Figure 11, the effect on DI engines of increasing engine speed is to reduce NO emissions. The increase from peak-torque speed to maximum speed results in about a 15% penalty in BSFC. One interpretation of this NO_x trend is based on fixed burning time: recall that residence time between TDC and 60^o ATDC is inversely related to engine speed, ranging from 15 to 5 millisec as speed ranges from 800 to 2400 RPM. So if heat release requires a fixed 5 millisec, more burning will occur on the expansion stroke at high speeds (lower temperature and lower NO). Actually, burning time is reported to decrease somewhat for higher engine speeds [Shipinski (1968)*], but not enough to make burning duration a constant crank angle interval.

Other effects of speed must be considered. Higher piston velocities at high speeds will cause greater air turbulence (earlier burning and higher NO). Engine breathing is reduced at high RPM, while residual gas is increased by the higher valve overlap. Both of these effects might reduce NO emissions. Fuel injection pressure rises with speed and thus might produce smaller drops. Finally, the compressed air temperature is higher at high speeds due to lower heat losses and more pumping work. The prechamber NO_x emissions behave oppositely (increase) as engine speed is increased (Figure 12). The dip in the curve for the baseline case does not appear for cases 2 to 6, however, intermediate data at 1800 RPM was not taken for cases 2 to 6.

---

*This observation is incompatible with droplet-burning models for quiescent oxidizers of invariant composition, but may be consistent with diffusion flames with an "RPM-sensitive" air environment and drop size distribution.

3. Effect of Alterations to the Intake Charge

a. Effect of EGR

Figures 13 and 14 display the effect of EGR on NO_x, smoke, and engine performance. One of the strongest implications that diffusion flames may dominate diesel combustion and NO formation arises from a close examination of the EGR emissions behavior. The effect of exhaust gas recirculation is to replace a portion of the incoming air with exhaust gases. This has three results:

(i) The new mixture is warmer than the air alone (by virtue of introduction of heated combustion products).

(ii) The new mixture has a higher mean specific heat (since the combustion products H_2O and CO_2 have more degrees of freedom than air, which is diatomic).

(iii) The mixture has a reduced oxygen concentration.

All three of these alterations in the intake charge have an effect on the flame structure (temperature and species profiles) following ignition. It is the purpose of this brief analysis to show that the measured nitric oxide reductions with EGR can be "explained" on the basis of the predicted decrease of peak flame temperature in a diffusion flame. The factor dominating this suppression is neither item (i) nor item (ii), (in fact, these effects are small and tend to cancel each other), but rather item (iii), the reduced oxygen mass fraction. The conditions surrounding the diffusion flame were taken arbitrarily to be the intake charge compressed adiabatically to TDC; thus the calculation is representative of burning early in the cycle.

The Zeldovich mechanism for NO formation [Zeldovich and Raizer (1966)] tells us that the rate of formation rises exponentially with temperature:

$$\frac{d(NO)}{dt} \sim \exp(-E/RT), \quad E/R = 123{,}000^{\circ}R \qquad (1)$$

where the activation energy is derived from the activation energy of the controlling reaction, $O + N_2 \rightarrow NO + N$, and the O_2 dissociation energy.

We examine the rate of NO formation at the place most likely to produce significant amounts of nitric oxide, i.e., at the flame front of a diffusion flame. Here the temperature can be written [Williams (1965)]:

$$T_{fl} = T_f + \frac{1}{C_p}\left\{\frac{(Q-L)\dfrac{Y_{ox}^{\infty}}{i} + C_p(T_{\infty} - T_f)}{\left(1 + \dfrac{Y_{ox}^{\infty}}{i}\right)}\right\} .$$

where

T_{fl} = flame temperature

T_f = fuel-droplet surface temperature

C_p = specific heat (at constant pressure) of the gas

Q = heat of combustion per unit mass of fuel

L = latent heat of vaporization of the fuel

Y_{ox}^{∞} = ambient oxygen mass fraction

i = stoichiometric oxygen to fuel ratio (by mass)

T_{∞} = gas temperature far from droplet

Although this expression is accurate enough to suit our purposes, it was derived subject to simplifying assumptions, the most serious of which are

(i) Infinitely fast irreversible hydrocarbon oxidation (completely diffusion-controlled)

(ii) Dissociation not considered

(iii) Single C_p common to both sides of the flame

For diesel fuel we take $T_f = 973^{\circ}R$ (boiling point), $Q = 19{,}000$ Btu/lb, $L = 144$ Btu/lb, and $i = 3.36$. For T_{∞}, we take the compression temperature of a 19:1 engine (approx. 1200°F), and assume that the EGR is 100°R hotter than the air in the intake manifold. These relative magnitudes permit the following approximation:

$$T_{fl} \cong \left(1 - \frac{Y_{ox}^{\infty}}{i}\right)\left[\left(\frac{Q-L}{i\,C_p}\right)Y_{ox}^{\infty} + T_{\infty}\right] . \qquad (2)$$

The remaining quantities, C_p, Y_{ox}^{∞}, and T_∞ depend on the % EGR according to the following recipes (derived for a 17:1 compression ratio at 24:1 overall air/fuel ratio):

$$T_\infty = 1677 + 300 \times (\%\ \mathrm{EGR}),\ {}^{\circ}\mathrm{R} \qquad (3)$$

$$C_p = .30 + .02 \times (\%\ \mathrm{EGR}),\ \mathrm{Btu/lb\text{-}}{}^{\circ}\mathrm{F} \qquad (4)$$

$$Y_{ox}^{\infty} = .232 - .143 \times (\%\ \mathrm{EGR}) \qquad (5)$$

Based on expressions (1) through (5) we can calculate the relative NO-formation rate at the diffusion flame surface with different amounts of recirculation:

% EGR	Y_{ox}^{∞}	C_p Btu/lb-°F	T_∞, °R	T_{fl}, °R	Calculated dNO/dt (relative)
0	.232	.300	1677	5610	1.00
10	.218	.302	1707	5360	.41
20	.203	.304	1737	5157	.17
30	.189	.306	1767	4947	.07

It is important to note that the Y_{ox}^{∞} effect dominates; for example, at 30% EGR, C_p and T_∞ give rise to offsetting 2% changes in T_{fl} whereas Y_{ox}^{∞} causes an 11% suppression.

Figure 15 compares the observed NO reductions with the calculated reductions in the rate of NO formation. The shapes of the curves agree rather well for values of EGR above 10%; the leveling off of measured values at 0% EGR is not simulated by the present calculations.

b. Effect of Water Injection

The introduction of one part water for every two parts fuel into the intake air causes NO to drop about 50%, as shown in Figures 16 and 17. Abthoff and Luther (1969) have shown that the effect occurs in the combustion chamber and is not due to NO_2 absorption by recondensed water in the exhaust.

The interpretation for this effect presumably lies in thermal quenching of NO-producing reactions. The effect of adding 0.5 gm water/gm fuel on the temperature of the combustion products at $\phi = 1$ is about $-150^{\circ}K$*. It can be readily shown that, for the Zeldovich mechanism at $\phi \approx 1.0$, a $100^{\circ}K$ drop would cause a factor of three reduction in NO-production rate. The measurements bear these facts out: When water is injected into the air intake and hence throughout the cylinder, some water is wasted; by contrast, the potential for NO_x reductions for fuel/water emulsions appear to be greater (see Appendix D). It might be noted that water injection seems to have a greater potential for reduction at high speeds and low-to-medium loads.

c. Effect of Intake Air Temperature

Since the effects of water injection on NO emissions are so substantial, it is somewhat surprising to find the small effect of air temperature shown in Figure 18. The compression temperature should be boosted about $300^{\circ}R$ by a $100^{\circ}R$ rise in intake temperature, according to the adiabatic approximation:

$$\frac{T_2}{T_1} = \left(\frac{V_1}{V_2}\right)^{\gamma-1} \approx 3 \quad \text{for } V_1/V_2 = 17,\ \gamma = 1.4 \quad .$$

Offsetting this $300^{\circ}R$ rise is a slight increase in heat loss during compression. Nevertheless the flame temperature for the first fuel elements which burn is bound to be boosted at least $100^{\circ}R$, even considering dissociation. Whereas a flame temperature change of this order should increase NO production rate by 50 to 100%, only 10 to 15% increase in NO emission is observed (Figure 18). One is led to the hypothesis that the early burning matters relatively little and NO-formation is more sensitive to the conditions at later stages of combustion. Due to heat transfer, the memory of the initial compression temperature is washed out. Another conceivable effect of greater air temperature is greater fuel evaporation prior to ignition, so that heat release is weighted more toward the premixed "spike" than the ensuing diffusion flame burning. Also, ignition delay is smaller with air preheat.

---

*The temperature decrease would be much less if the entire contents of the cylinder were homogeneous and at a uniform temperature ($\Delta \overline{T} \approx -75^{\circ}K$).

d. Effect of Intake Air Pressure (Turbocharging)

As shown in Figures 19 and 20, the effect of simulated turbocharge with aftercool on NO is not substantial, provided A/F rather than BMEP is held constant as in the current tests. As the air density goes up, the fuel burning rate increases; counteracting this is the fact that the average point of fuel injection is delayed because the duration of fuel injection is increased to keep A/F constant. Increased air density also shortens ignition delay and alters spray penetration. The diffusion flame temperature should not change significantly, because for a given engine the compression temperature depends only on the intake temperature and not on the intake density. Because of these compensating effects, NO_x remains at about the same level as might be expected. However, the BSFC drops about 20% with turbocharging due to the improved ratio of BMEP/FMEP (the incremental heat release is not taxed by friction). It is primarily this BSFC factor which reduces the gm NO_2/BHP-hr and has made turbocharging popular as an emission control technique.

4. Effect of Air/Fuel Mixing Parameters

a. Effect of Fuel Orifice Diameter

Variations in those parameters which affect dispersion of fuel and rate of mixing provide significant clues about the diesel flame. Fuel orifice size was varied in an attempt to find the effect of fuel dispersion (e.g., initial mean droplet diameter). In these tests the total orifice area (and hence the rate of injection) was maintained near constant by making compensating changes in the number of orifices. The results are shown in Figure 21. The system with fewer, larger orifices displayed substantially lower NO_x emissions. This result is in accord with the data of Hames et al. (1971) as shown in Appendix D.

At least three mechanisms may be at work here:

(i) The system with fewer fuel jets will have a smaller surface-to-volume ratio of the fuel spray, creating delayed mixing and heat release, and hence lower NO_x.

(ii) The larger diameter jets will penetrate further, perhaps splashing off the chamber walls.

(iii) The larger orifices should produce larger droplets (in the mean). On the one hand, large droplets will take longer to burn (reducing NO_x), however for constant ambient conditions, Seery and Bowman have suggested $NO_x \sim d^2$.

b. Effect of Injection Rate

The rate of injection was varied by changing orifice size for a given number of orifices. Although orifice area was doubled in these tests, the rate of injection increased only a factor of 1.3 (because the fuel line pressure relaxed for larger orifices). The results are given in Figures 22 and 23 and show opposite trends for 14 and 17 compression ratio. Hames et al.(1971) and Landen (1963) found lower NO emissions for larger rates of injection through large orifices. Several factors come into play:

(i) Larger orifices produce larger droplets. The larger droplets could increase NO_x (the diffusion-flame structure argument) or decrease NO_x (the retarded burning argument).

(ii) Faster injection permits faster burning (which would increase NO_x.

c. Effect of Air Swirl

Increasing air swirl apparently promotes NO formation, as documented in Figure 24. The effect is stronger in our engine than previous studies have observed (Appendix D) and may be due to faster mixing in the high swirl case, which would lead to earlier heat release. Thus NO might be increased because the active subzones would be hotter due to (a) faster heat release for a given heat loss, and (b) burning before expansion cools the bulk gases. Another effect which probably occurs with high swirl is an increased tendency for both fuel and cool air to be thrown outward to the chamber walls.

Figure 3
EFFECT OF VOLUME RATIO
(Prechamber Engines)

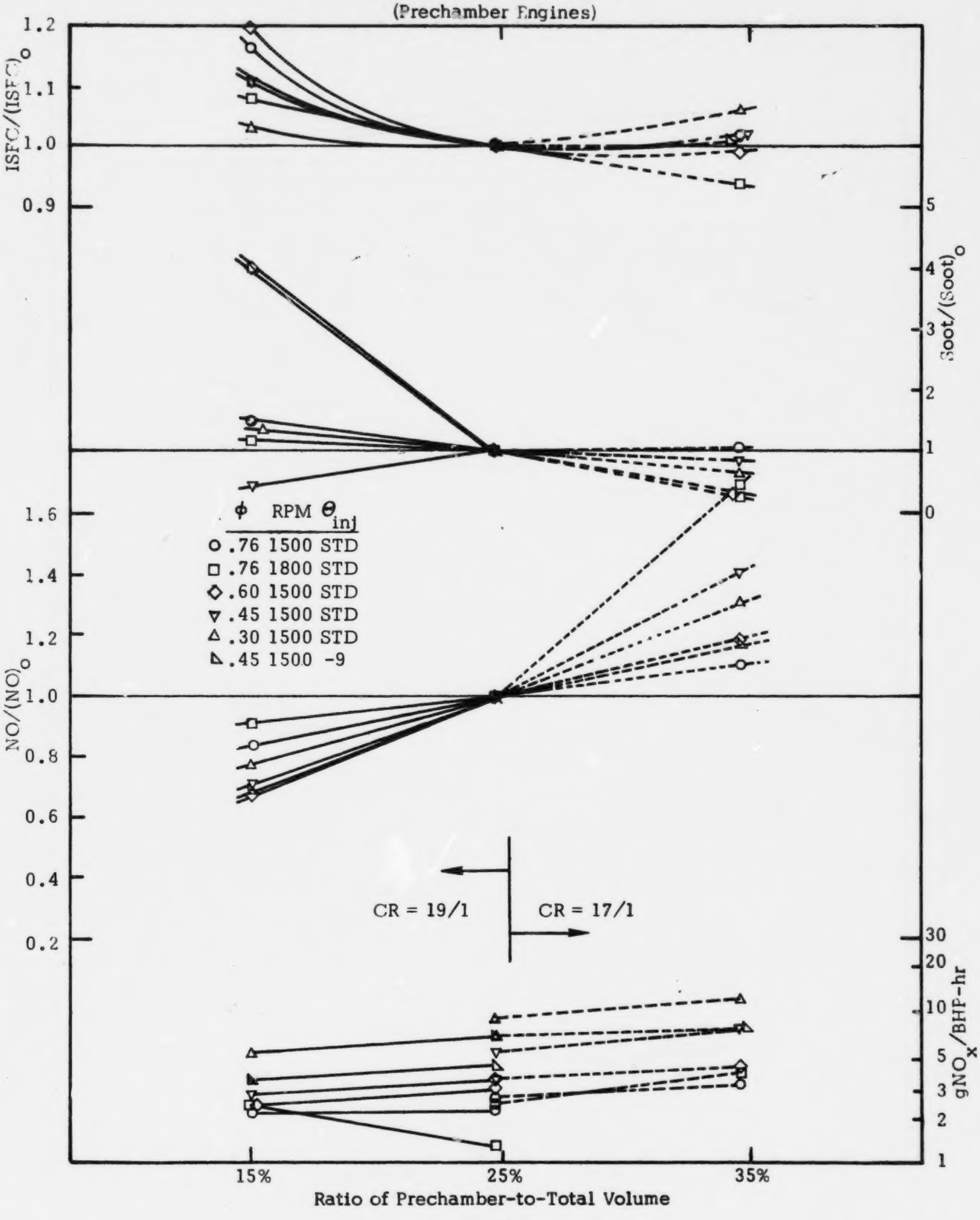

Figure 4
EFFECT OF VOLUME RATIO
(All Engines of CR = 17)

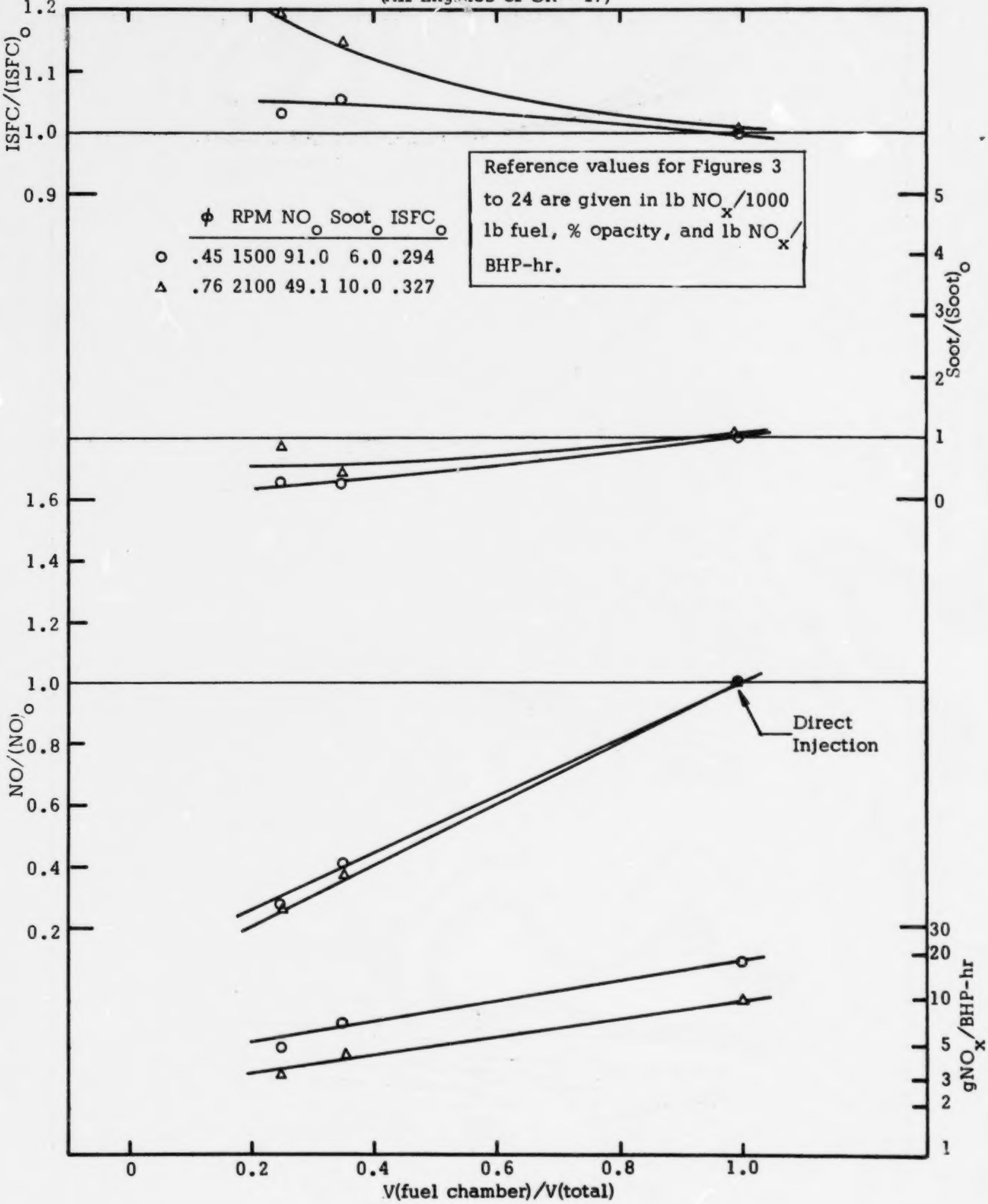

Reference values for Figures 3 to 24 are given in lb NO$_x$/1000 lb fuel, % opacity, and lb NO$_x$/BHP-hr.

Figure 5
EFFECT OF COMPRESSION RATIO
(Direct Injection Engines)

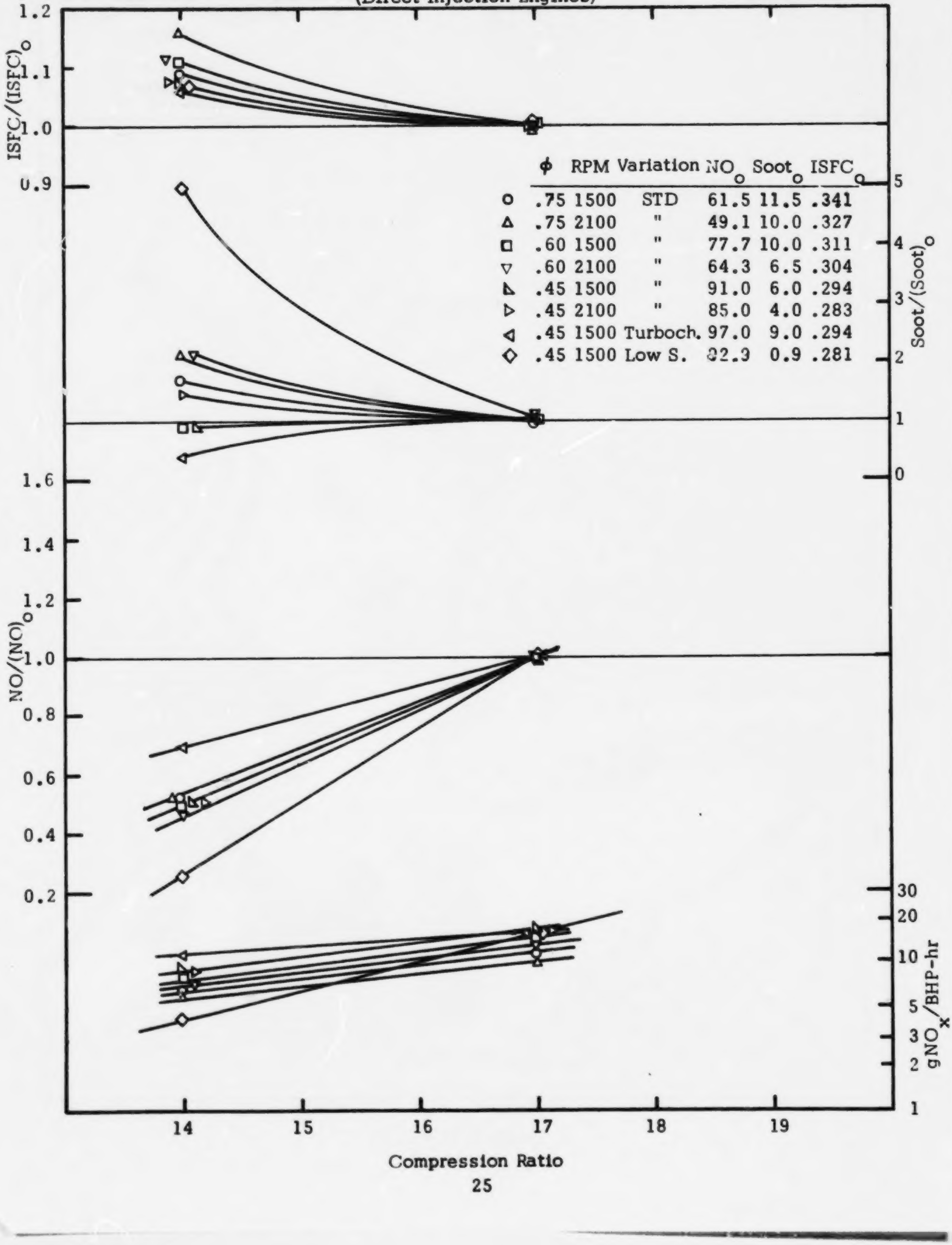

	ϕ	RPM	Variation	NO_o	$Soot_o$	$ISFC_o$
○	.75	1500	STD	61.5	11.5	.341
△	.75	2100	"	49.1	10.0	.327
□	.60	1500	"	77.7	10.0	.311
▽	.60	2100	"	64.3	6.5	.304
◺	.45	1500	"	91.0	6.0	.294
▷	.45	2100	"	85.0	4.0	.283
◁	.45	1500	Turboch.	97.0	9.0	.294
◇	.45	1500	Low S.	82.3	0.9	.281

Figure 6
EFFECT OF COMPRESSION RATIO
(Prechamber Engines, Volume Ratio = 25%)

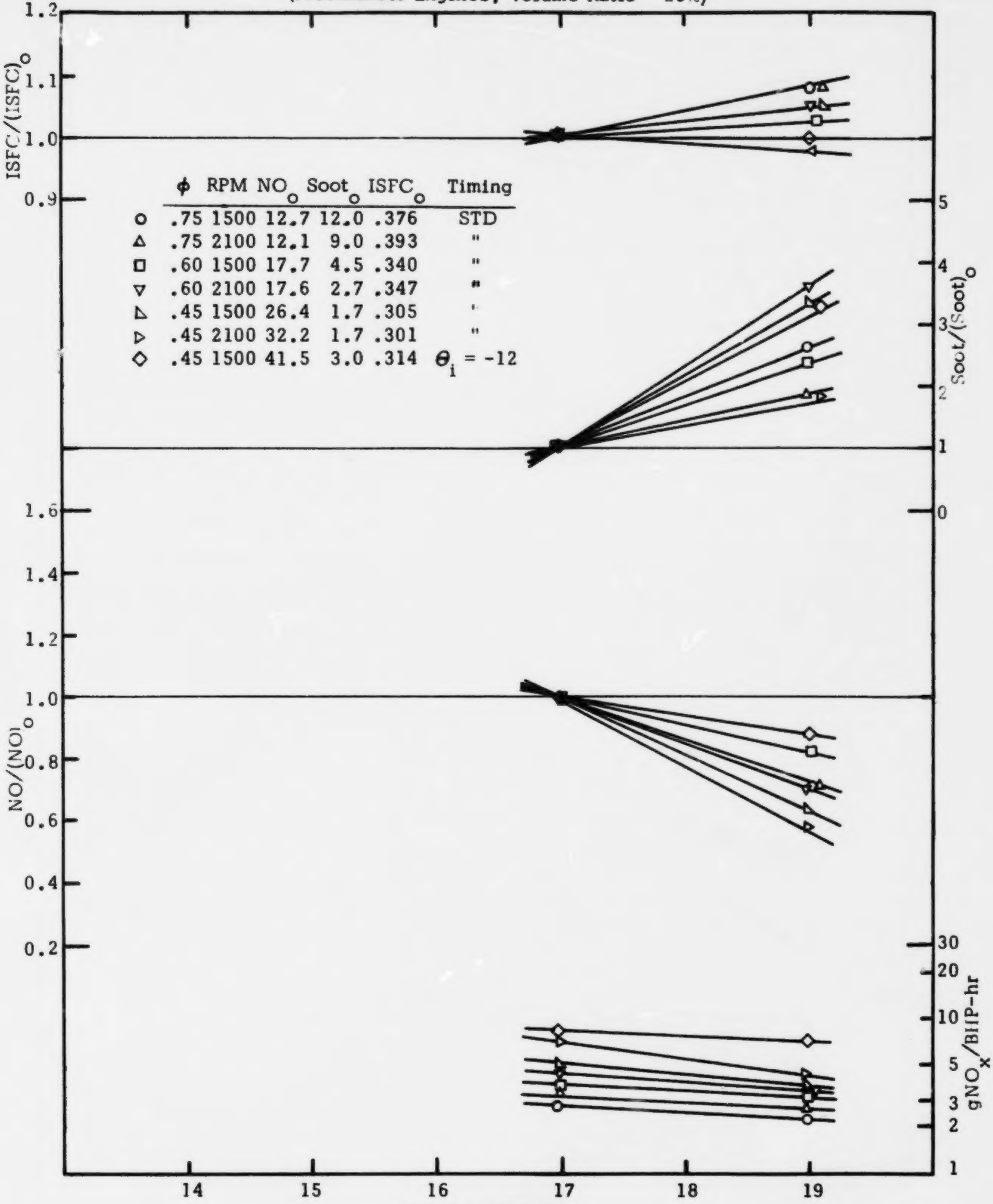

	ϕ	RPM	NO_o	$Soot_o$	$ISFC_o$	Timing
○	.75	1500	12.7	12.0	.376	STD
△	.75	2100	12.1	9.0	.393	"
□	.60	1500	17.7	4.5	.340	"
▽	.60	2100	17.6	2.7	.347	"
◺	.45	1500	26.4	1.7	.305	"
▷	.45	2100	32.2	1.7	.301	"
◇	.45	1500	41.5	3.0	.314	$\theta_i = -12$

Figure 7
EFFECT OF LOAD
(Direct Injection Engines)

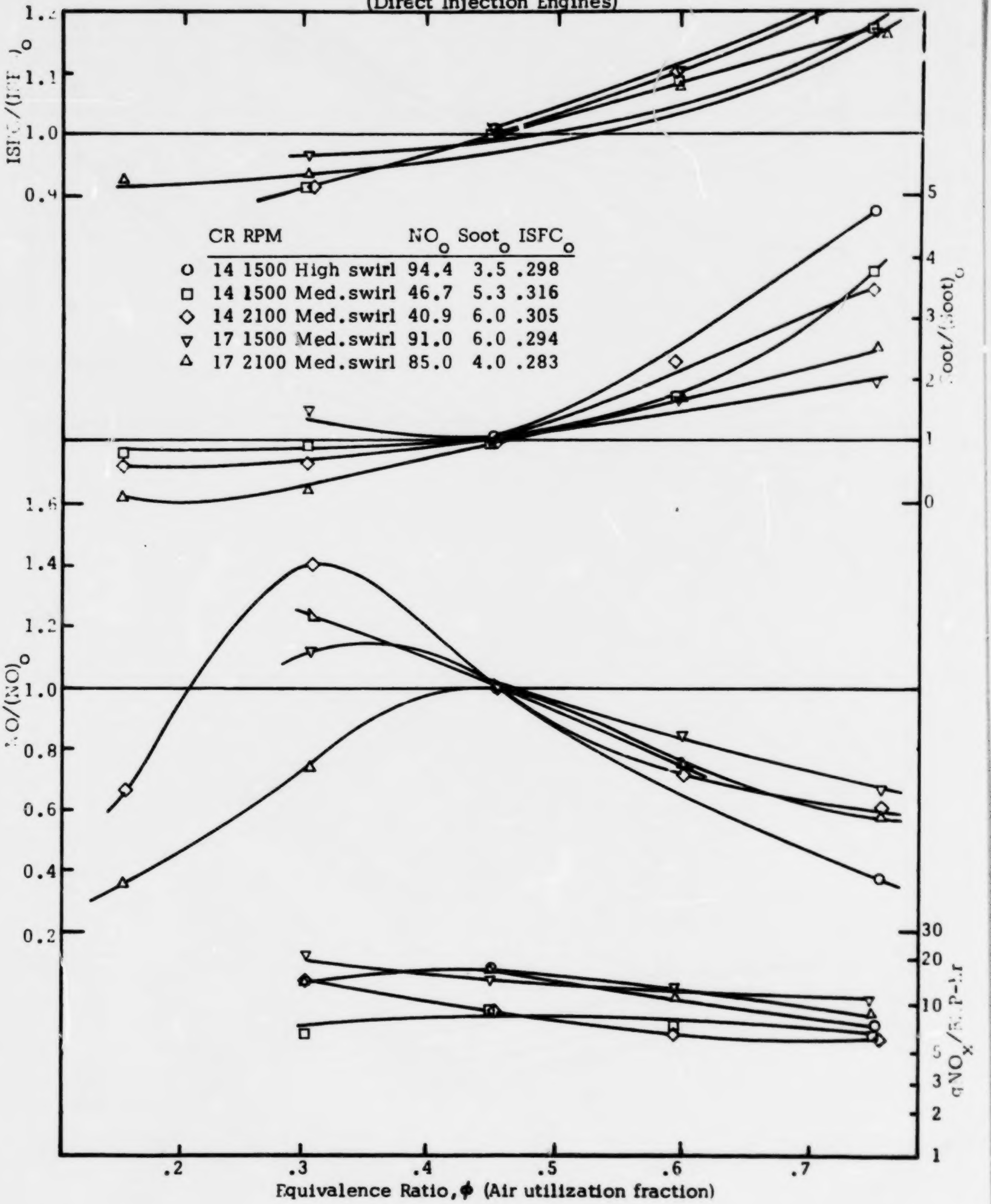

Figure 8
EFFECT OF LOAD
(Prechamber Engines)

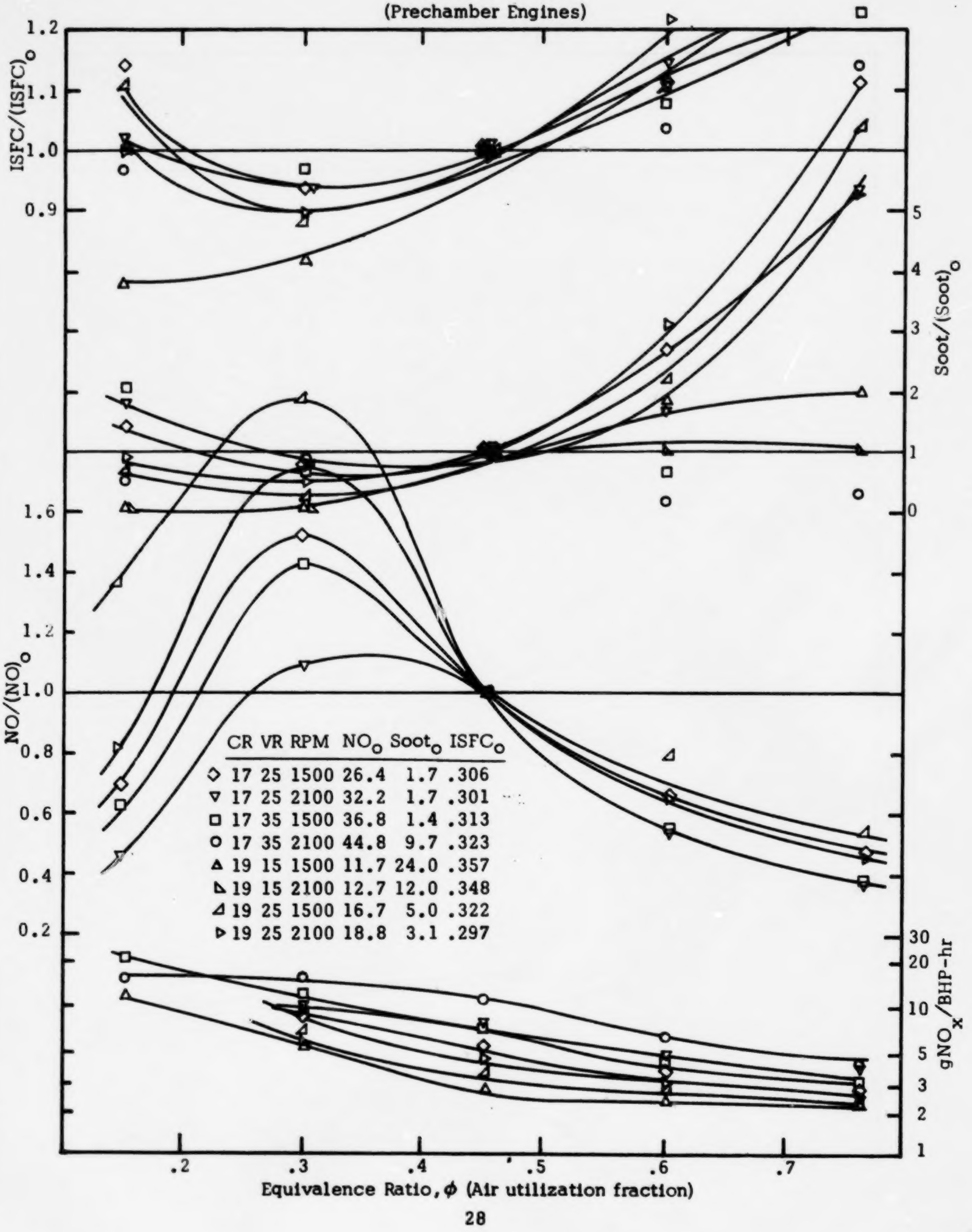

Figure 9
EFFECT OF TIMING
(Direct Injection Engines)

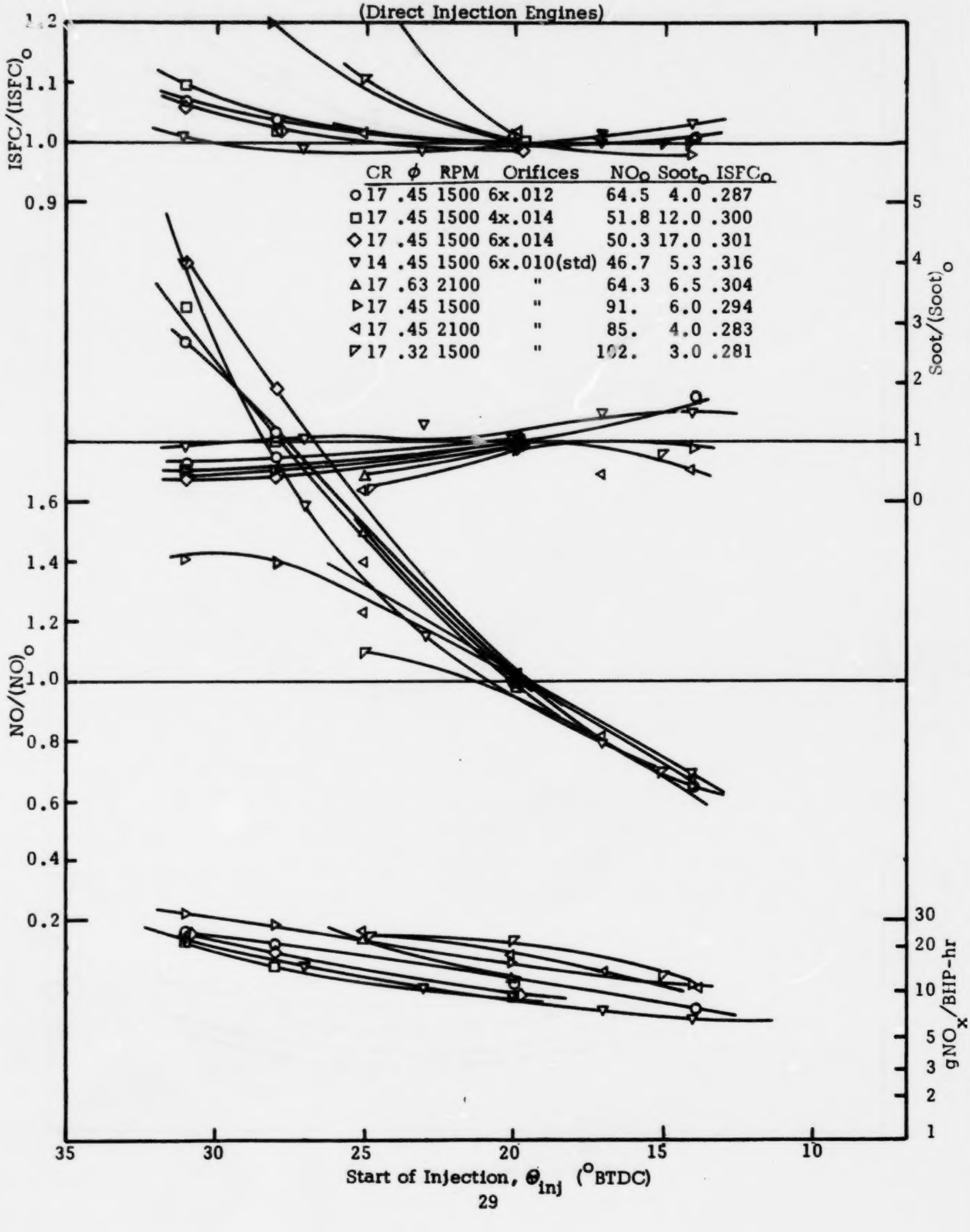

Figure 10
EFFECT OF TIMING
(Prechamber Engines)

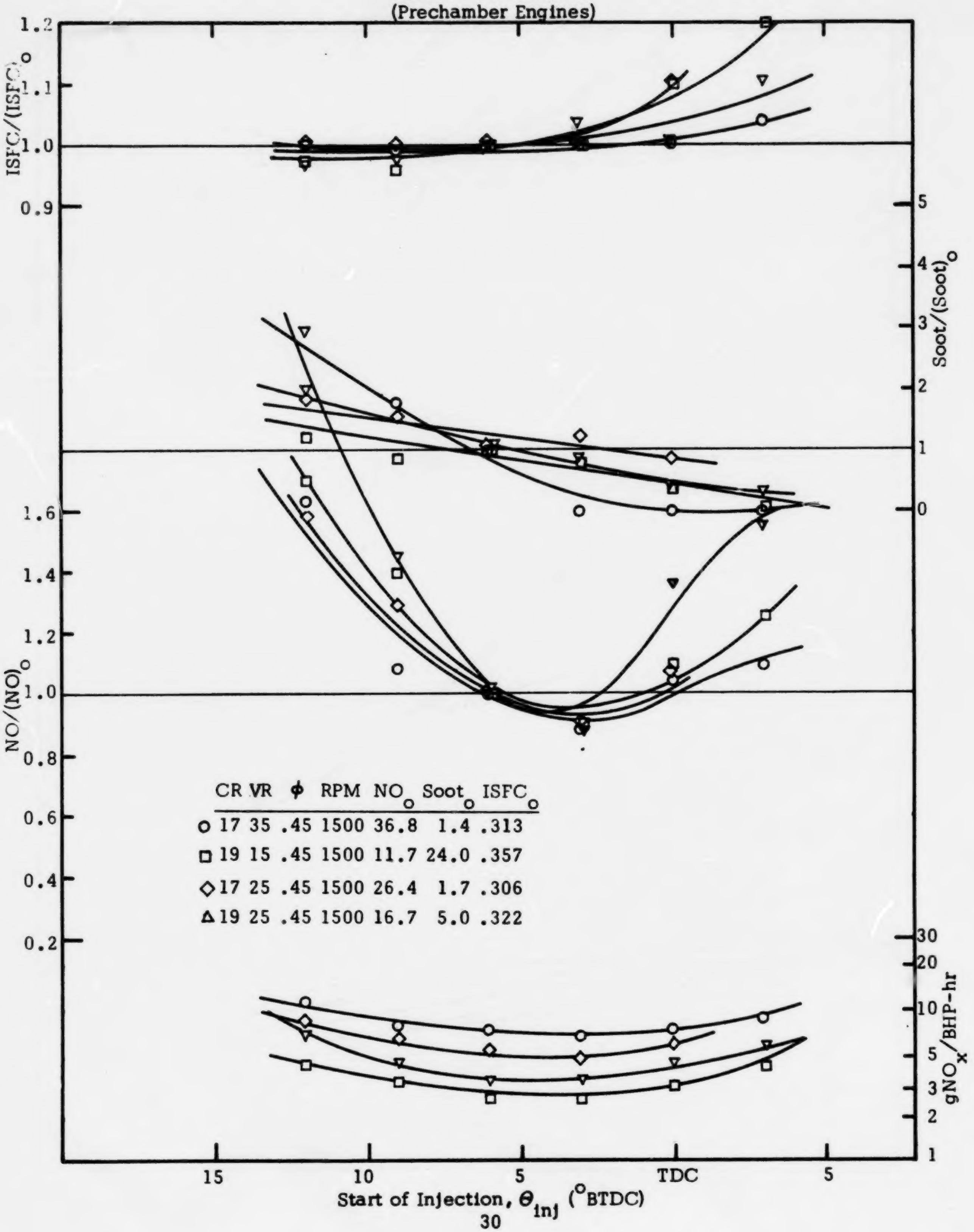

Figure 11
EFFECT OF ENGINE SPEED
(Direct Injection Engines)

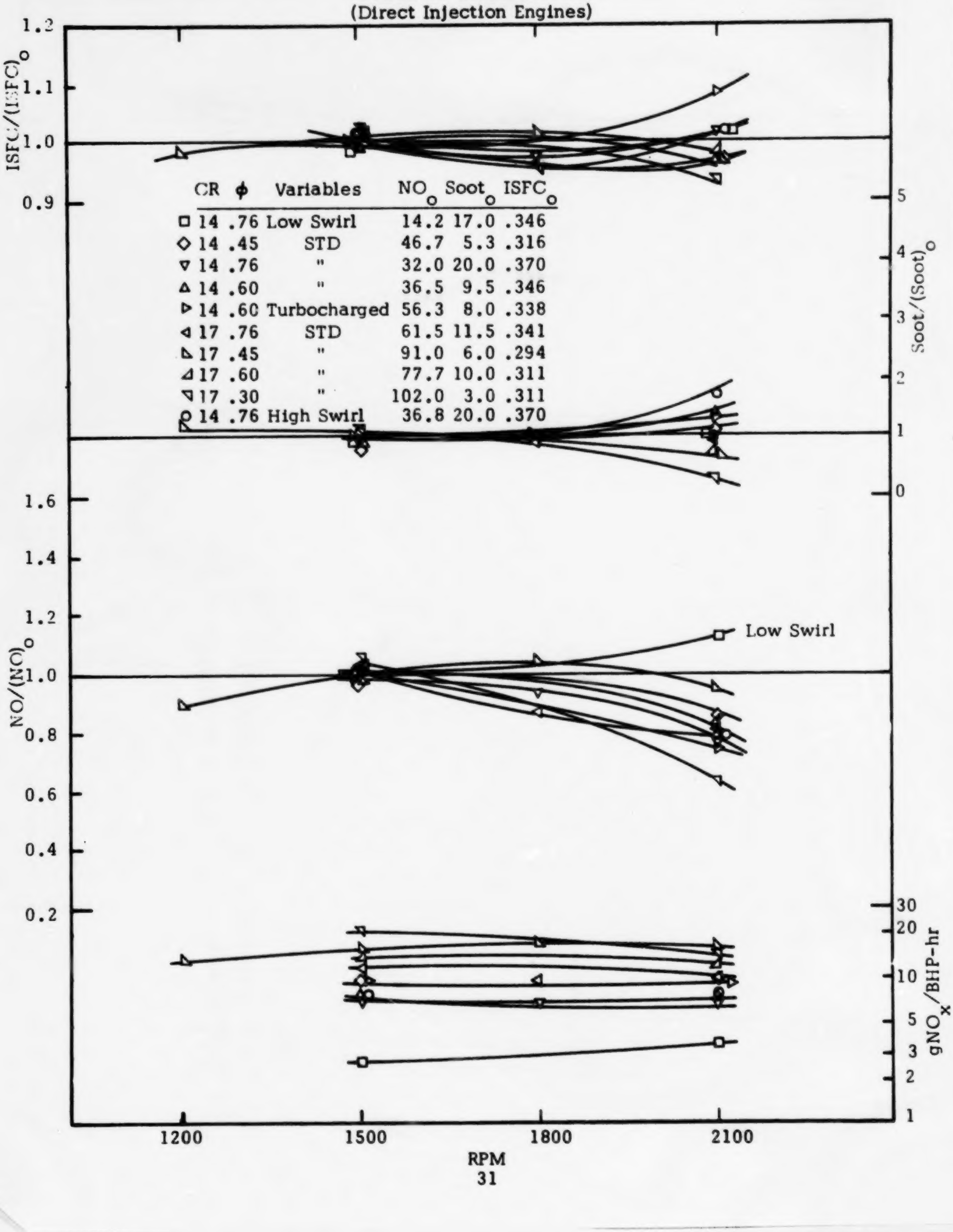

	CR	ϕ	Variables	NO$_o$	Soot$_o$	ISFC$_o$
□	14	.76	Low Swirl	14.2	17.0	.346
◇	14	.45	STD	46.7	5.3	.316
▽	14	.76	"	32.0	20.0	.370
△	14	.60	"	36.5	9.5	.346
▷	14	.60	Turbocharged	56.3	8.0	.338
◁	17	.76	STD	61.5	11.5	.341
◺	17	.45	"	91.0	6.0	.294
◿	17	.60	"	77.7	10.0	.311
◸	17	.30	"	102.0	3.0	.311
○	14	.76	High Swirl	36.8	20.0	.370

Figure 12
EFFECT OF ENGINE SPEED
(Prechamber Engines)

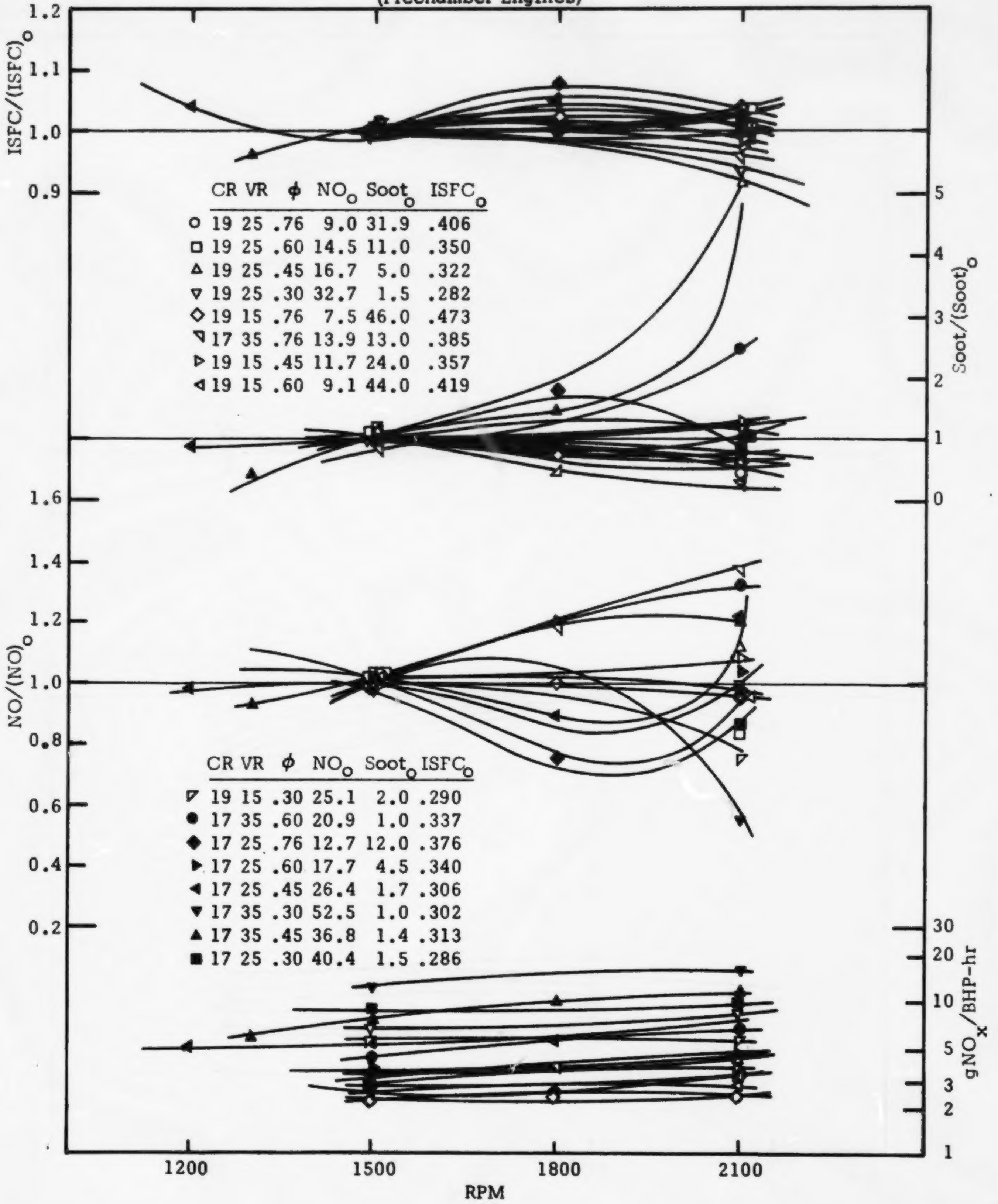

Figure 13
EFFECT OF EGR
(Direct Injection Engines)

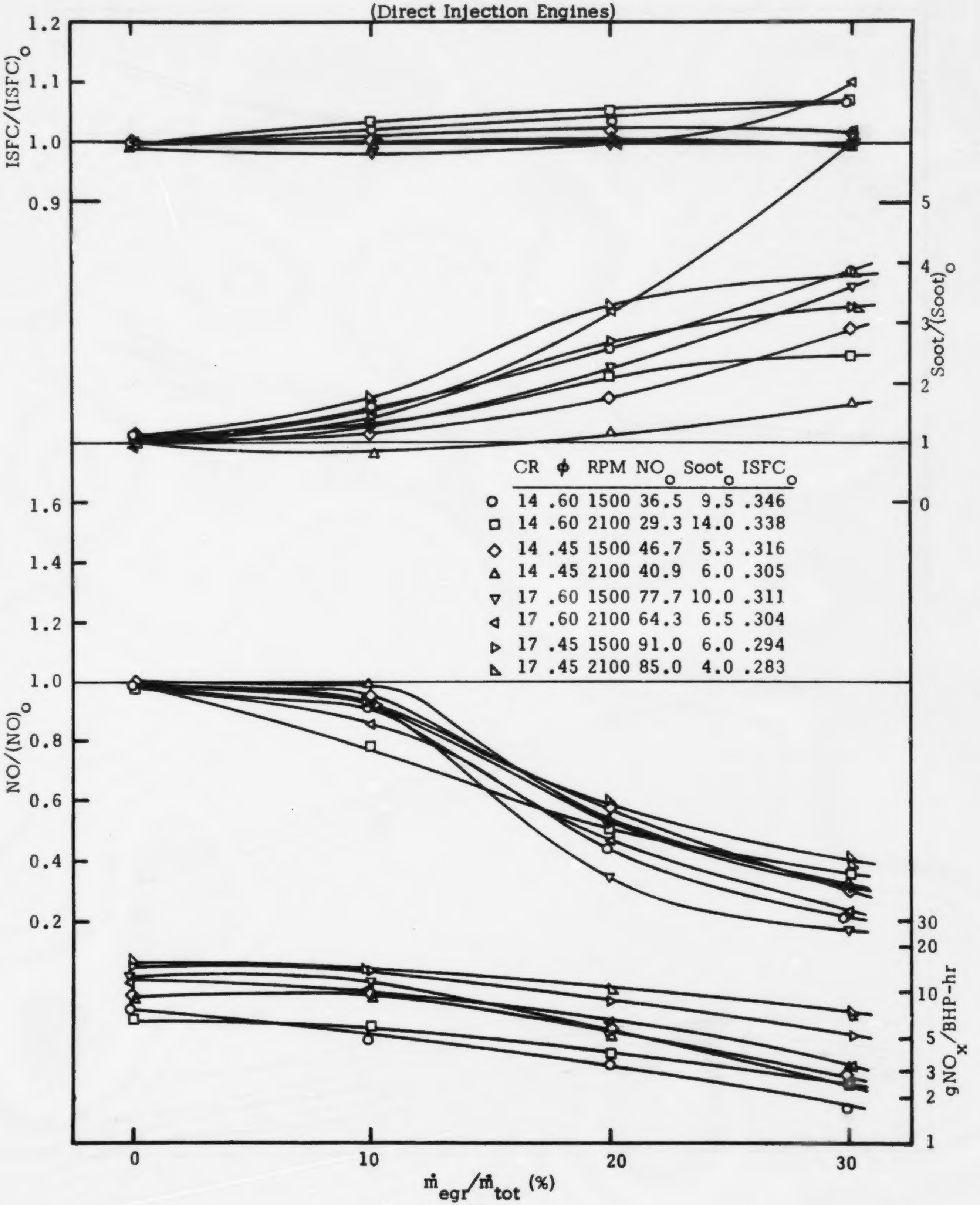

	CR	ϕ	RPM	NO_o	$Soot_o$	$ISFC_o$
○	14	.60	1500	36.5	9.5	.346
□	14	.60	2100	29.3	14.0	.338
◇	14	.45	1500	46.7	5.3	.316
△	14	.45	2100	40.9	6.0	.305
▽	17	.60	1500	77.7	10.0	.311
◁	17	.60	2100	64.3	6.5	.304
▷	17	.45	1500	91.0	6.0	.294
◺	17	.45	2100	85.0	4.0	.283

Figure 14
EFFECT OF EGR
(Prechamber Engines)

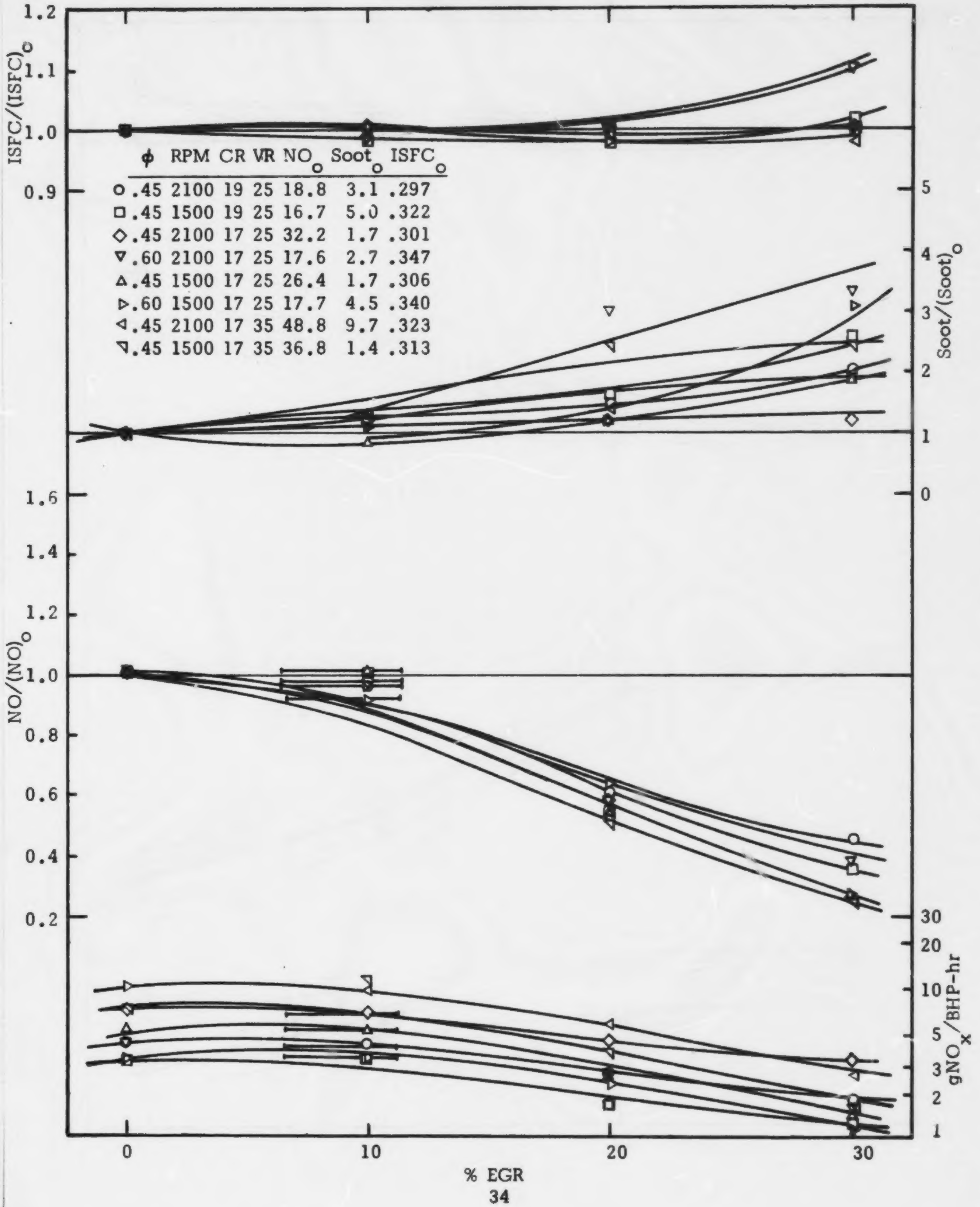

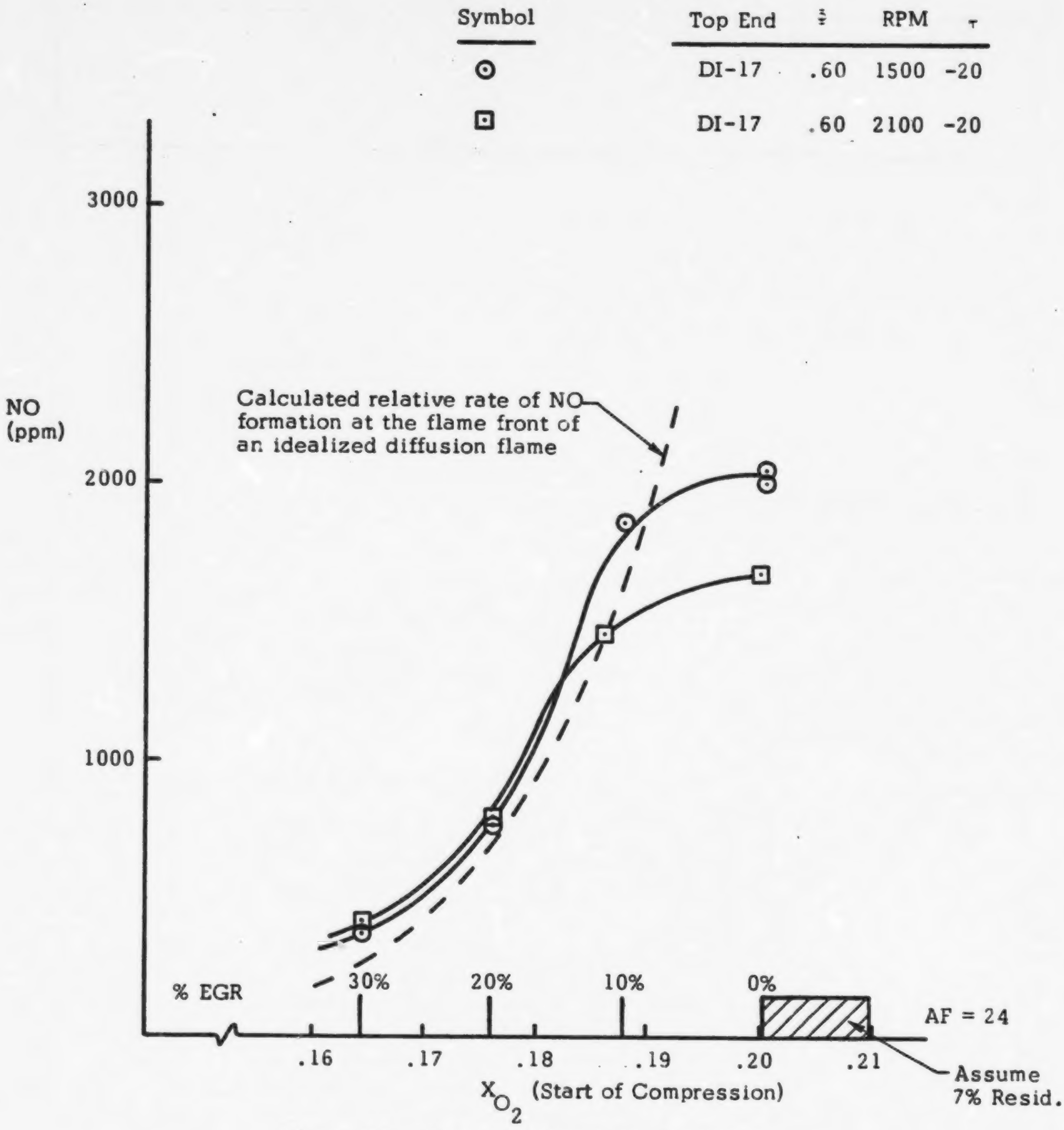

Figure 15. Effect of Exhaust Recirculation

Figure 16
EFFECT OF WATER INJECTION
(Direct Injection Engines)

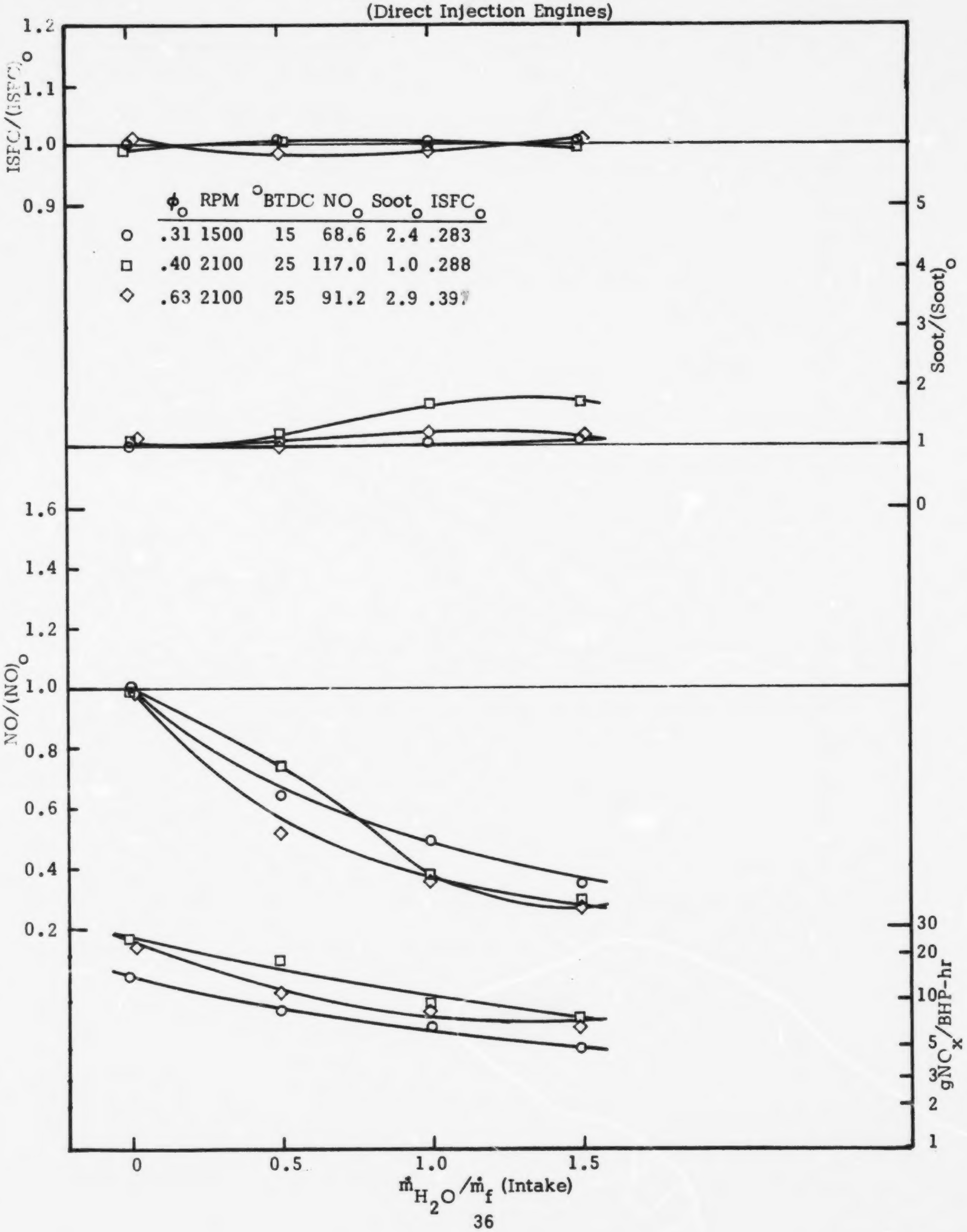

Figure 17
EFFECT OF WATER INJECTION
(Prechamber Engines)

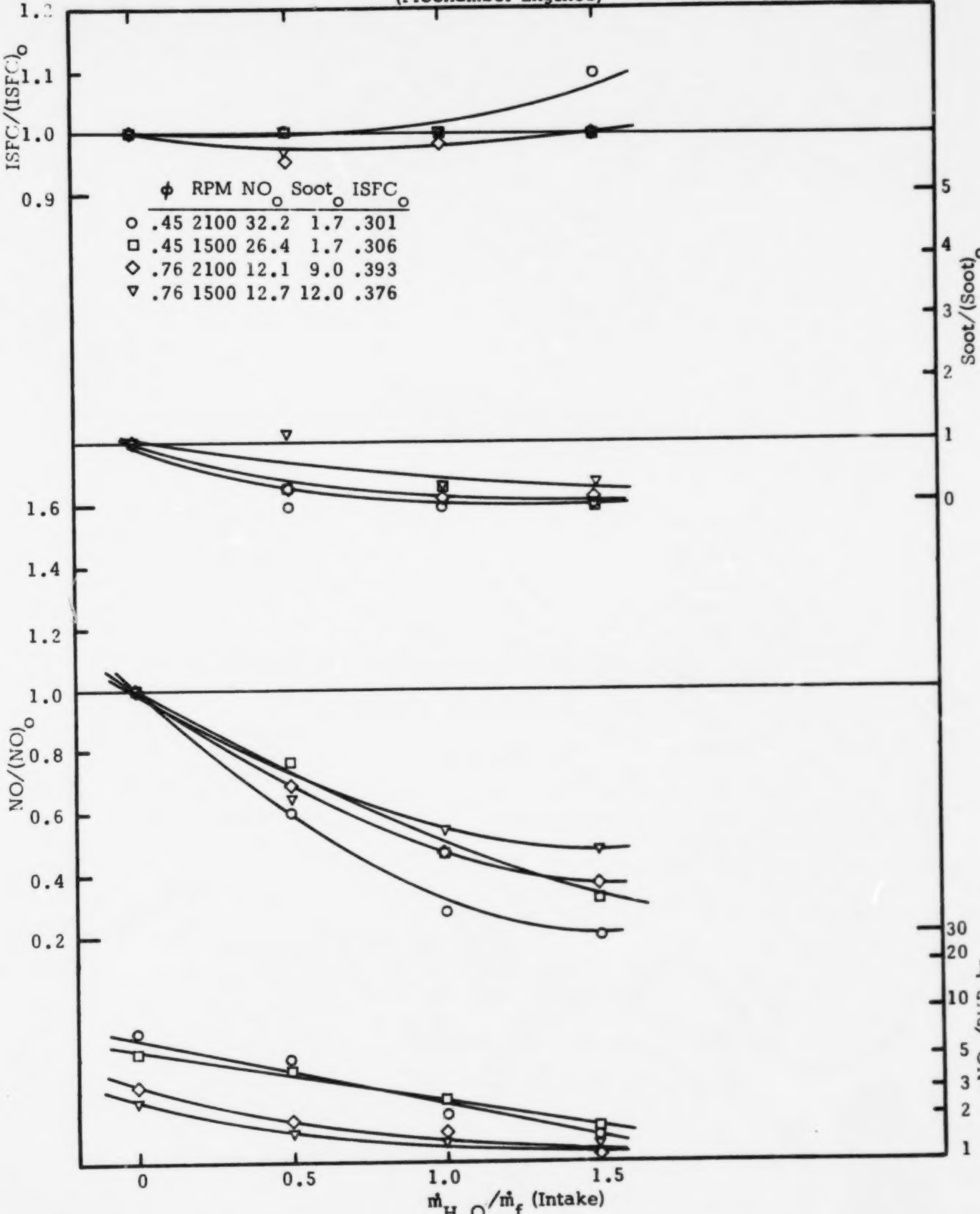

Figure 18
EFFECT OF INTAKE AIR TEMPERATURE

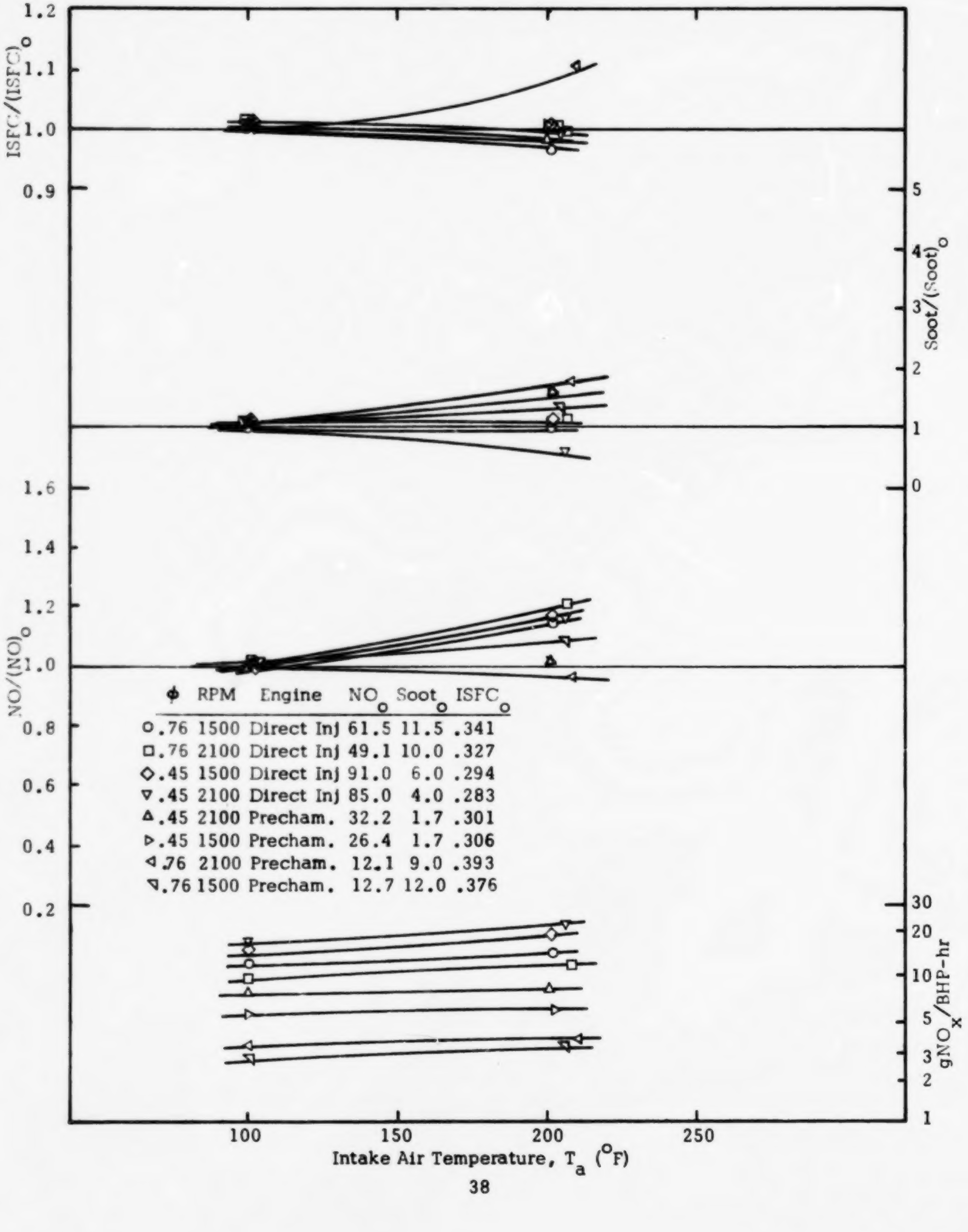

Figure 19
EFFECT OF AIR PRESSURE (TURBOCHARGING)
(Direct Injection Engines)

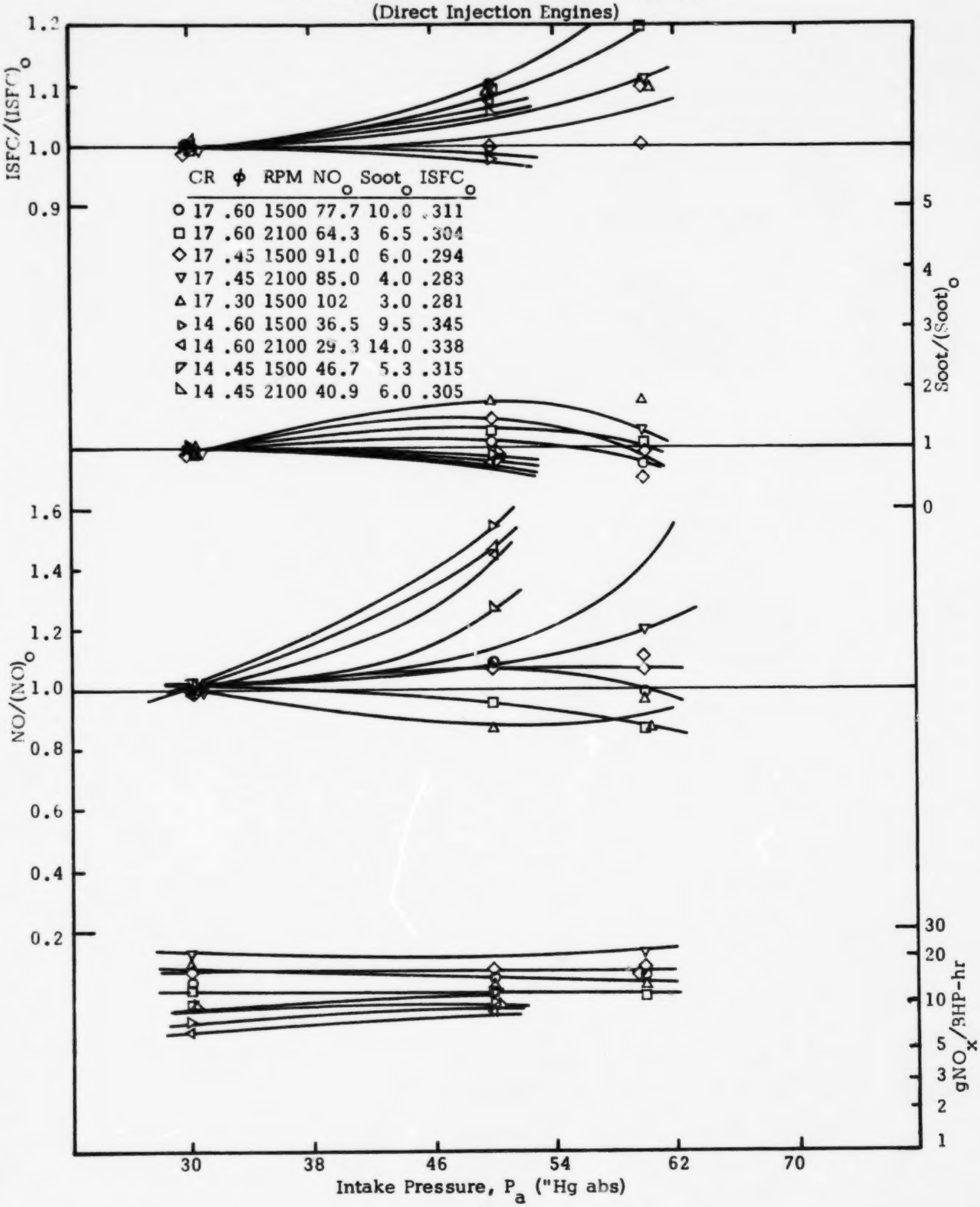

Figure 20
EFFECT OF AIR PRESSURE (TURBOCHARGING)
(Prechamber Engines)

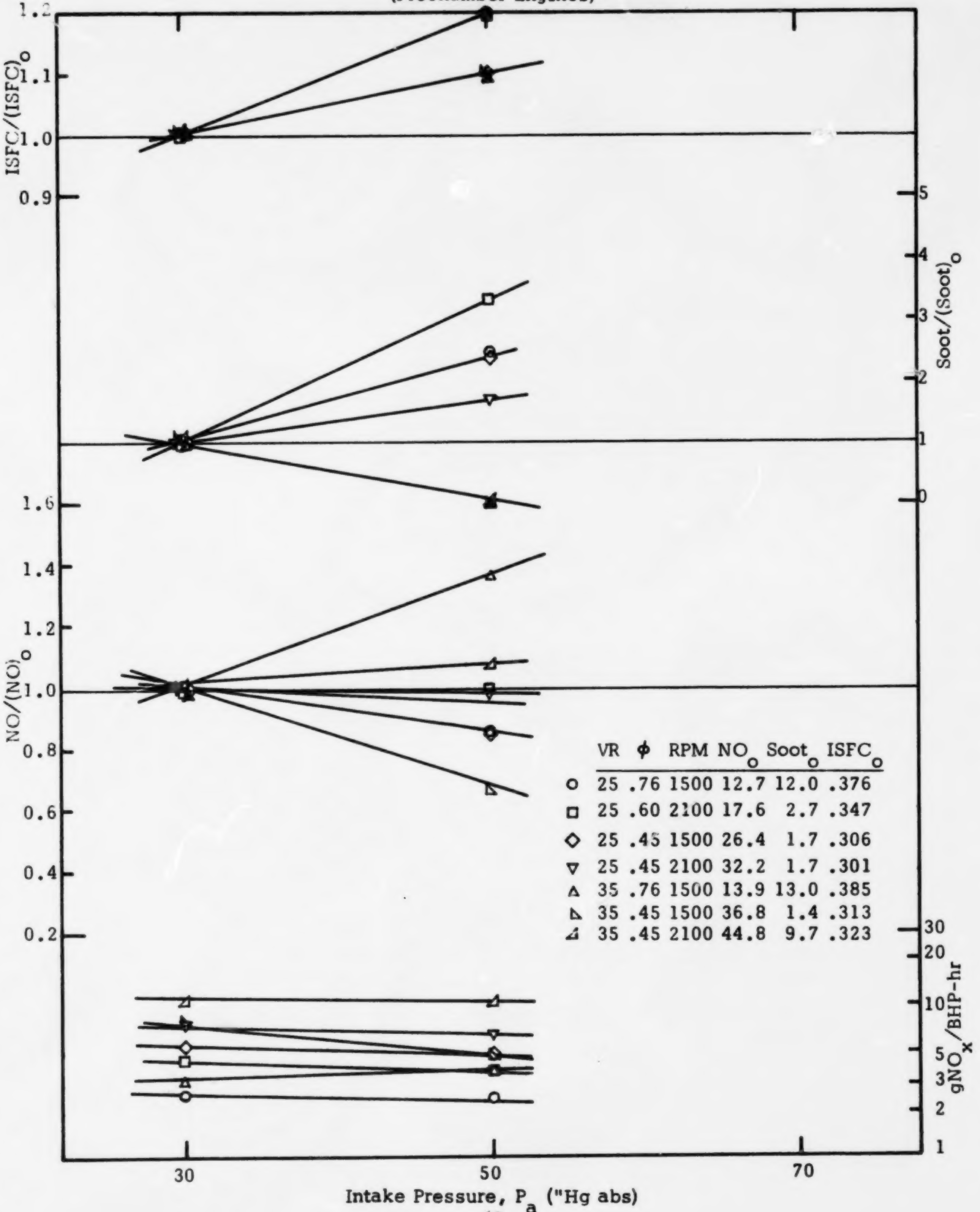

	VR	ϕ	RPM	NO$_o$	Soot$_o$	ISFC$_o$
○	25	.76	1500	12.7	12.0	.376
□	25	.60	2100	17.6	2.7	.347
◇	25	.45	1500	26.4	1.7	.306
▽	25	.45	2100	32.2	1.7	.301
△	35	.76	1500	13.9	13.0	.385
◺	35	.45	1500	36.8	1.4	.313
◿	35	.45	2100	44.8	9.7	.323

Figure 21

EFFECT OF ORIFICE DIAMETER

(Direct Injection Engines)

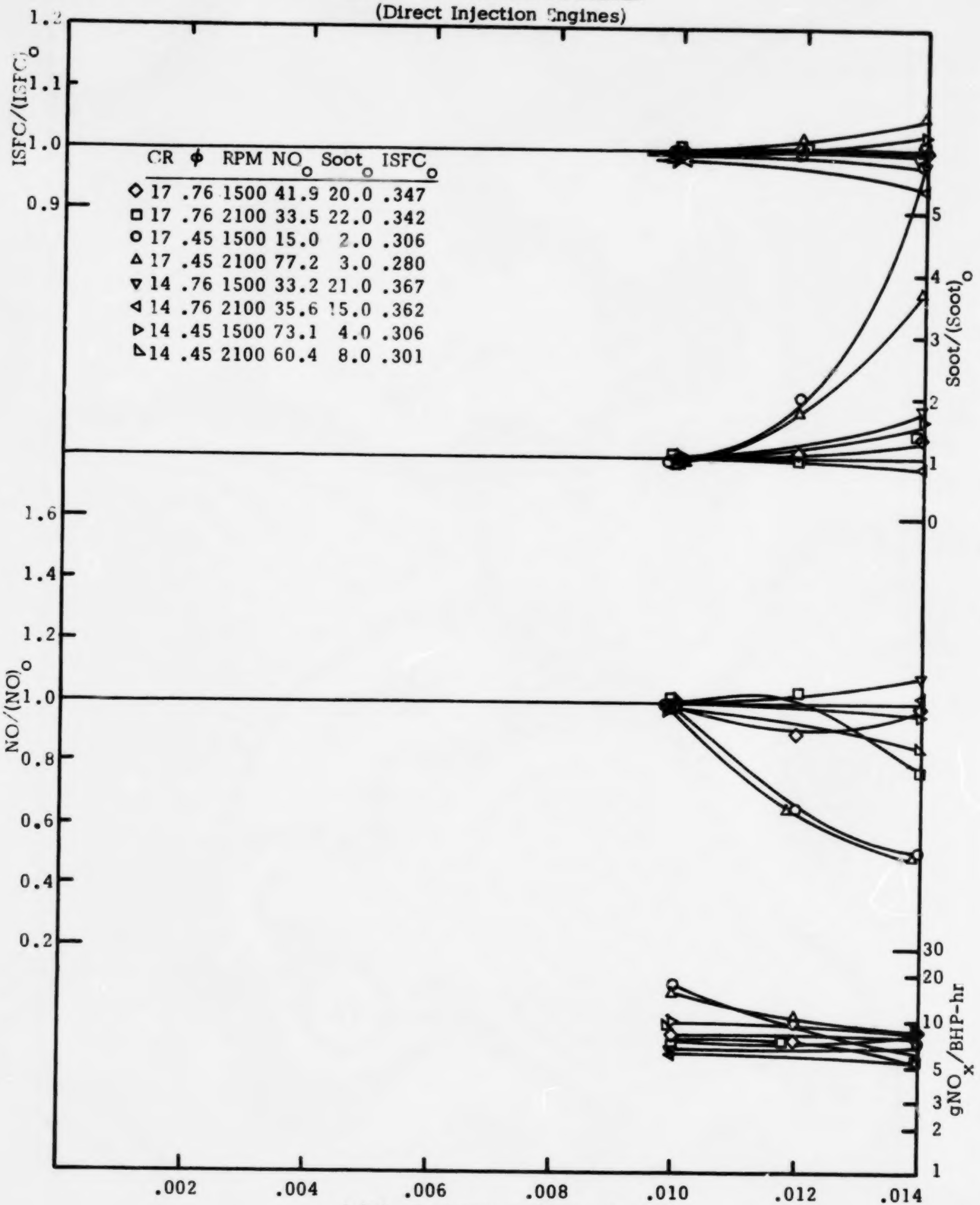

Figure 22
EFFECT OF FUEL RATE
(Direct Injection Engines)

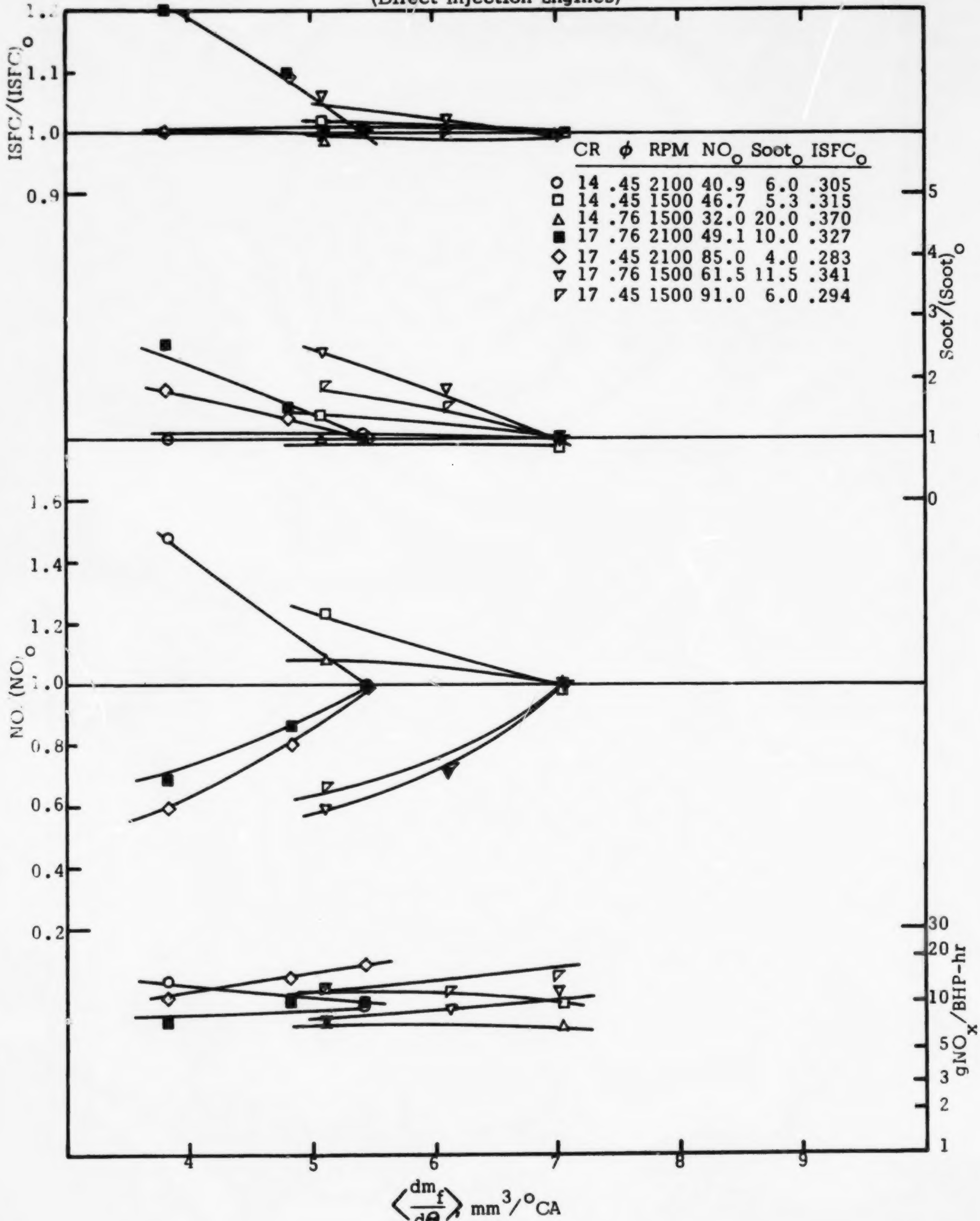

	CR	ϕ	RPM	NO_o	$Soot_o$	$ISFC_o$
○	14	.45	2100	40.9	6.0	.305
□	14	.45	1500	46.7	5.3	.315
△	14	.76	1500	32.0	20.0	.370
■	17	.76	2100	49.1	10.0	.327
◇	17	.45	2100	85.0	4.0	.283
▽	17	.76	1500	61.5	11.5	.341
◸	17	.45	1500	91.0	6.0	.294

Figure 23
EFFECT OF FUEL RATE
(Prechamber Engines)

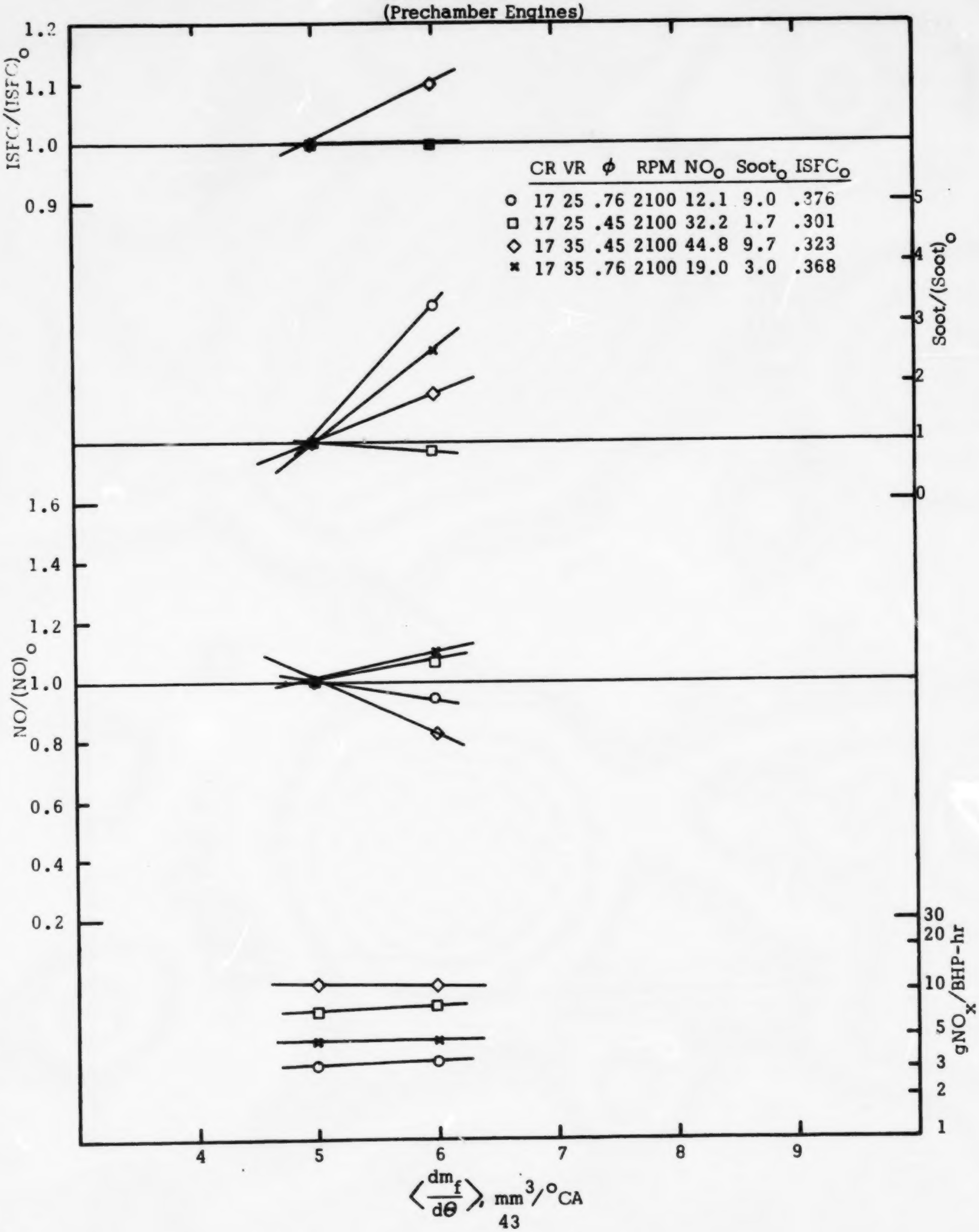

Figure 24
EFFECT OF SWIRL
(Direct Injection Engines)

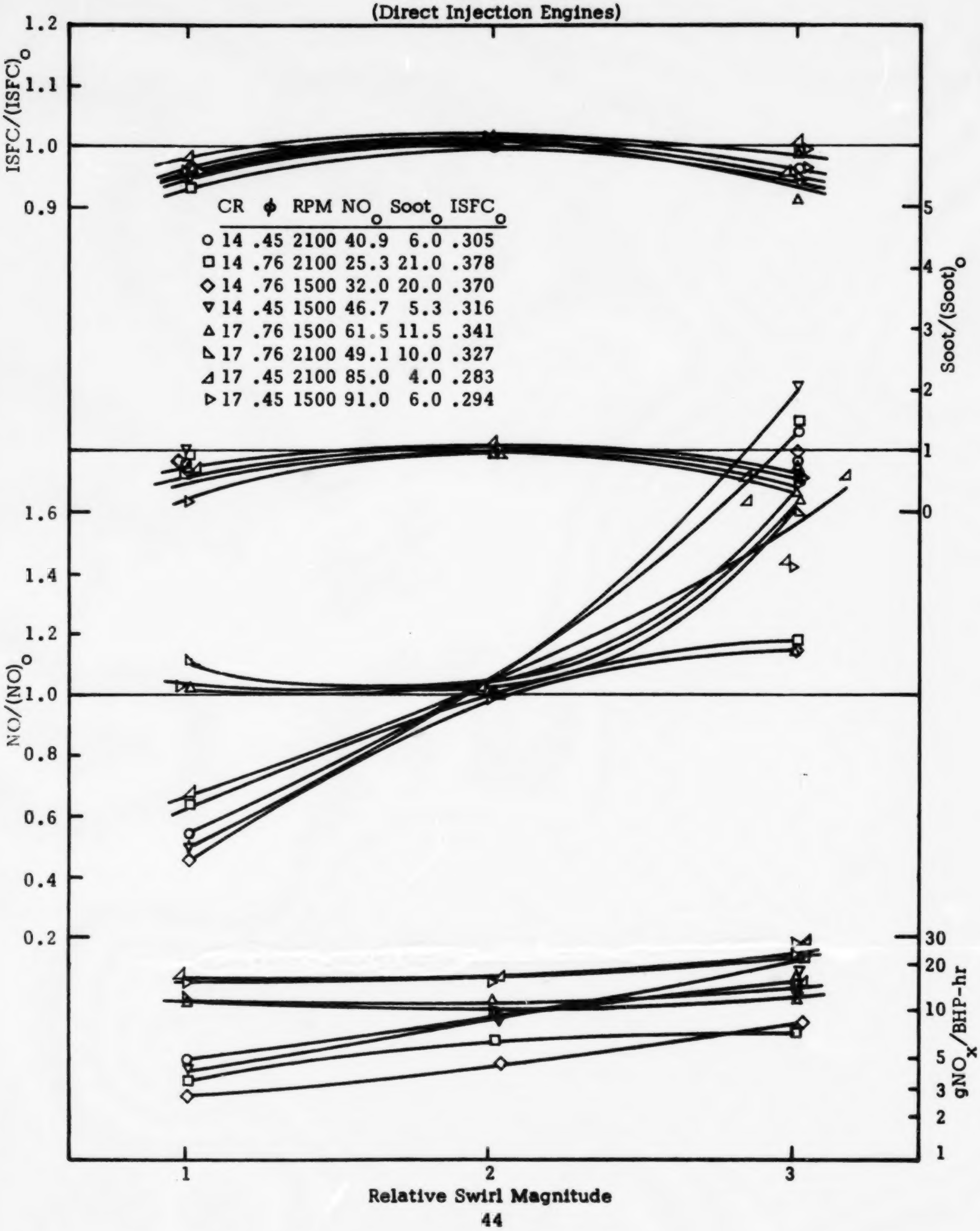

C. SUMMARY OF EMISSIONS EVIDENCE

Seven parameters were found to change NO_x emissions by at least 40%, as summarized in Table 7 and Figure 25. Corresponding changes in soot were observed; typically the soot increased when NO_x was reduced, although some exceptions such as use of divided chamber and water injection were found. Other measures have increased soot with very little NO_x change--these might be avoided if other tests corroborate these trends.

Table 7
LINEAR INFLUENCE COEFFICIENTS
DERIVED FROM SINGLE CYLINDER TESTS

CAUTION

- **Test engine not optimized, results not strictly representative of production engines.**
- **% changes are relative to arbitrarily selected baseline--this allows numerical values of $\Delta Y/Y$ to exceed 100%.**
- **Emissions variations were non-linear in most cases; a linear fit was imposed.**
- **Most coefficients averaged over several cases involving distinct combinations of speed, load, etc.**

Engine	Variable X	Range of Variable ΔX	Figure	Observed % Change in Emissions and Output		
				ΔNO/NO	ΔSoot/Soot	ΔISFC/ISFC
Direct Injection	Compression Ratio	3 units	5	+ 90%	- 30%	- 9%
	Timing	$\Delta\theta_i = 17^\circ$CA retard	9	-160%	+120%	- 14%
	Load (Equivalence Ratio)	$\Delta\phi = .30$	7	+ 5%	+210%	+ 17%
	Speed	ΔRPM = 600	11	- 20%	- 10%	- 2%
	EGR	$\Delta\dot{m}_{egr}/\dot{m}_{tot} = 30\%$ $\Delta X_{O_2} = -.037$	13	- 70%	+220%	+ 6%
	Water Injection	$\Delta(\dot{m}_{H_2O}/\dot{m}_f) = 1.5$	16	- 70%	+ 40%	+ 1%
	Turbocharging	$\Delta P_a = 20"$ Hg	19	+ 12%	+ 50%	+ 7%
	Air Temperature	$\Delta T_a = 100^\circ F$	18	+ 20%	- 10%	- 1%
	Air Swirl	"med" to "high"	24	+ 60%	- 50%	- 5%
	Fuel Orifice Size	$\Delta d_f = .004"$	21	- 30%	- 10%	*
	Fuel Rate	$\Delta\langle d_{m_f}/d\theta\rangle = 1.5$ mm$^3/^\circ$CA	22	*	- 40%	- 10%
	Fuel Temperature	$100^\circ F$	--	- 12%	- 30%	- 3%
	Pilot Injection	ON/OFF (15% fuel at -40°CA)	--	+ 40%	+ 30%	- 2%
Prechamber	Compression Ratio	2 units	6	- 30%	+170%	+ 4%
	Divided Chamber	DI vs. PC	Table 6	- 60%	- 50%	+ 1%
	Prechamber Volume	$\Delta(V/V_{tot}) = 20\%$	3	+ 75%	- 80%	- 12%
	Timing	$\Delta\theta_i = 15^\circ$CA	10	*	-150%	+ 13%
	Load (Equivalence Ratio)	$\Delta\phi = .30$	8	- 30%	+500%	+ 28%
	Speed	ΔRPM = 600	12	*	*	*
	EGR	$\Delta\dot{m}_{egr}/\dot{m}_{tot} = 30\%$ $\Delta X_{O_2} = -.037$	14	- 64%	+150%	+ 3%
	Water Injection	$\Delta(\dot{m}_{H_2O}/\dot{m}_f) = 1.5$	17	- 66%	- 80%	+ 2%
	Turbocharging	$\Delta P_a = 20"$ Hg	20	- 8%	+140%	+ 15%
	Air Temperature	$\Delta T_a = 100^\circ F$	18	+ 2%	+ 70%	+ 1%
	Fuel Rate	$\Delta\langle d_{m_f}/d\theta\rangle_3 = 1$ mm$^3/^\circ$CA	23	*	+120%	*

*Excessive variation among cases or excessive non-linearity

Figure 25

EMISSIONS SUMMARY ILLUSTRATING THE SOOT-NO TRADEOFF

CAUTION

- **Test engine not optimized, results not strictly representative of production engines.**
- **% changes are relative to arbitrarily selected baseline--this allows numerical values of $\Delta Y/Y$ to exceed 100%.**
- **Emissions variations were non-linear in most cases; a linear fit was imposed.**
- **Most coefficients averaged over several cases involving distinct combinations of speed, load, etc.**

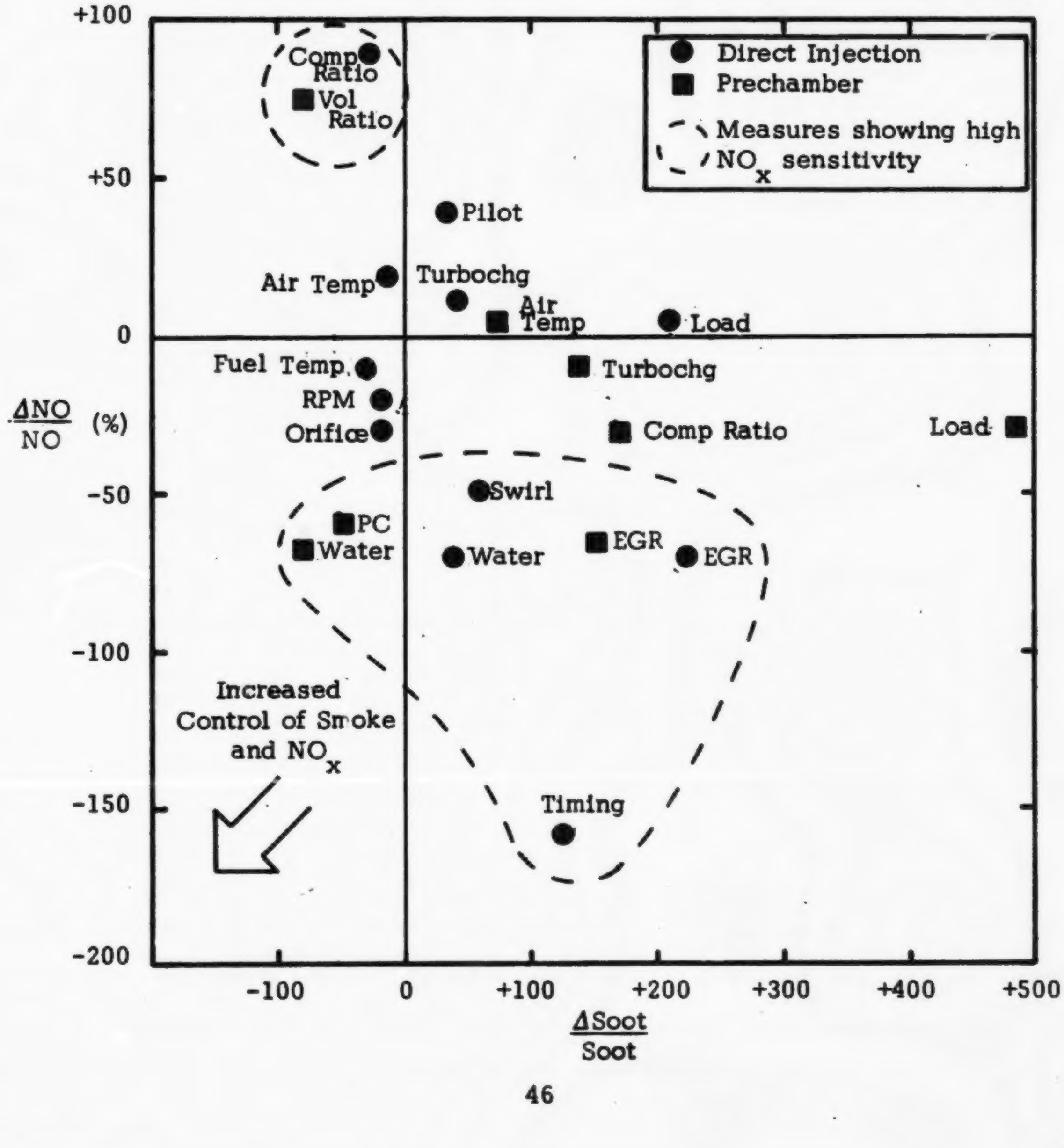

In Table 8 we have noted some of the NO_x mechanisms which were hypothesized to explain the data. A qualitative picture of what may be affecting pollutant formation in the diesel flame emerges from the common network of arguments in Table 8.

Reproduced from best available copy.

Table 8

HYPOTHETICAL MECHANISMS CITED TO RATIONALIZE NO_x EMISSIONS BEHAVIOR

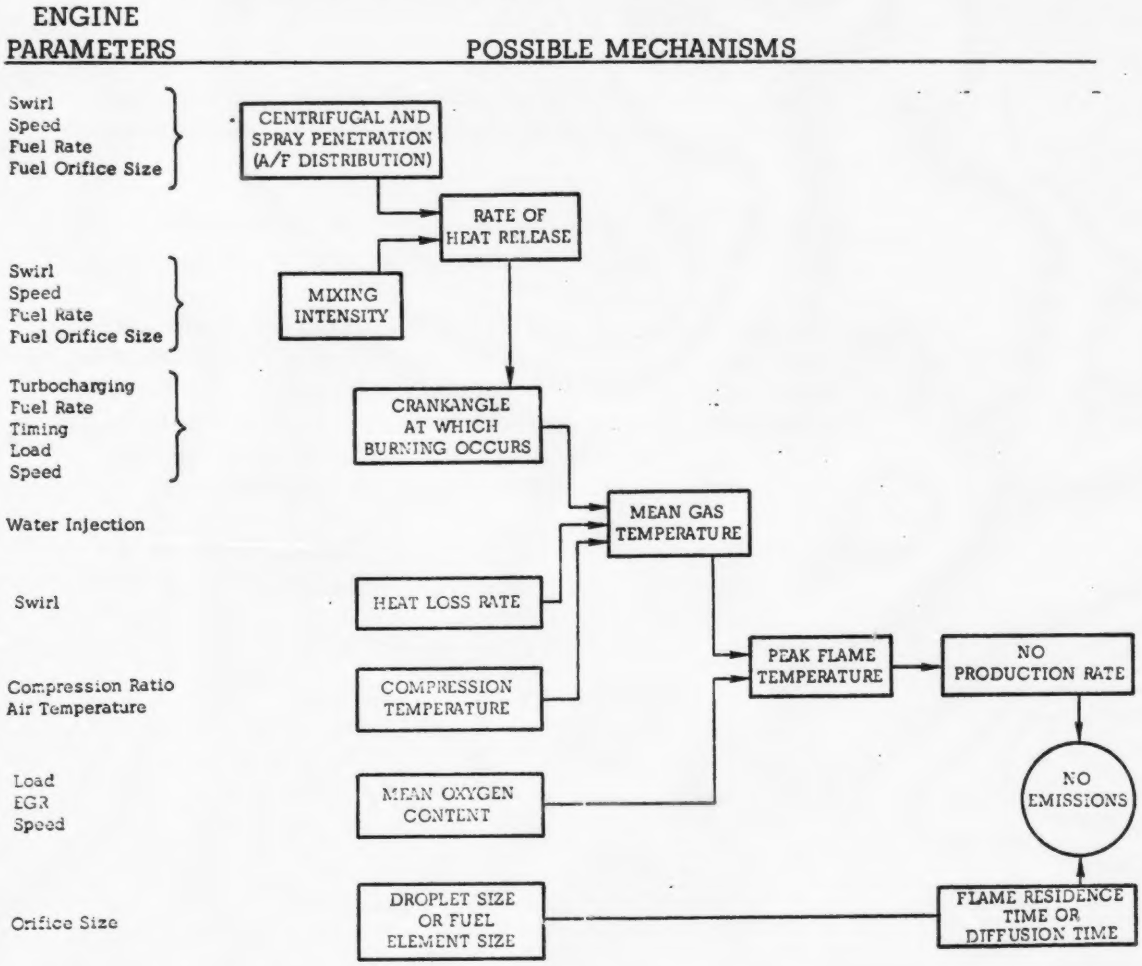
ENGINE PARAMETERS
POSSIBLE MECHANISMS
Swirl
Speed
Fuel Rate
Fuel Orifice Size
CENTRIFUGAL AND SPRAY PENETRATION (A/F DISTRIBUTION)
RATE OF HEAT RELEASE
Swirl
Speed
Fuel Rate
Fuel Orifice Size
MIXING INTENSITY
Turbocharging
Fuel Rate
Timing
Load
Speed
CRANKANGLE AT WHICH BURNING OCCURS
Water Injection
MEAN GAS TEMPERATURE
Swirl
HEAT LOSS RATE
PEAK FLAME TEMPERATURE
NO PRODUCTION RATE
Compression Ratio
Air Temperature
COMPRESSION TEMPERATURE
Load
EGR
Speed
MEAN OXYGEN CONTENT
NO EMISSIONS
Orifice Size
DROPLET SIZE OR FUEL ELEMENT SIZE
FLAME RESIDENCE TIME OR DIFFUSION TIME

According to these results, the following phenomena should be subjected to rigorous theoretical analysis and experimental studies in order to reach a better understanding of diesel-flame generated NO and smoke:

Local Diffusion Flames: The temperature and burning rate of such flames is independent of the overall fuel/air ratio. Many forms are conceivable: wake burning as studied by Natarajan and Brzustowski (1970), envelope flames classically studied by Godsave (1950), and spray combustion as investigated by McCreath and Chigier (1972).

Swirl Effects: Angular motion and entrainment of fuel, radial stratification due to centrifugal effects, and turbulence levels.

Fuel Spray Details: Penetration, drop size distribution, possible wall impingement, and entrainment by air.

Time-Dependent Phenomena: Must be precisely characterized and overlayed with an exactly (± .5° CA) specified piston motion and fuel delivery schedule. The phasing of key phenomena such as ignition, mixing rates, burning rates, evaporation rates, and heat transfer rates must be characterized as precisely as possible.

Prechamber Phenomena: Such as fluid transfer between the two chambers, including phase lags and heat transfer.

IV. AN INTERPRETATION OF DIESEL COMBUSTION AND POLLUTANT FORMATION

A. MIXING AND COMBUSTION MECHANISMS

The emissions data present definite arguments about the nature of the diesel flame. Emissions and performance are quite sensitive to chamber shape, swirl, and fuel dispersion. The fuel specific NO_x emissions appear insensitive to A/F ratio. The EGR data is well correlated by a simplified droplet diffusion flame theory. These behavioral patterns suggest that the combustion is mixing-controlled; by this we mean that the time for chemical reaction, once fuel and air are brought into molecular contact, is quite short compared to the mixing time. In the combustion literature [e.g. Fendell (1967)], the mixing-controlled flame is recognized as the limit of large Damkohler number:

$$N_D = \frac{\dot{\omega} L^2}{\rho D} \sim \frac{\text{(Characteristic Mixing Time)}}{\text{(Characteristic Reaction Time)}} \rightarrow \infty$$

Such flames have the singular property of locating themselves at the interface region between the unreacted fuel and the unburned air. Product/reactant mixing occurs on each side of the flame but fuel/air mixing per se does not occur (the flame intervenes)*.

Mixing occurs in two distinct stages, and it will be useful to define two scales of mixing:

(1) The scale on the order of the fuel spray or piston bowl (the term "macromixing" has been suggested by Khan). The zones and rate of fuel accessibility are defined by mixing on this scale.

(2) The scale on the order of the fuel elements (droplets or fuel vapor eddies). The "micromixing" on a molecular scale, and hence the detailed flame structure itself, is defined on this scale.

---

*Fuel/air mixing occurs to the extent that $N_D < \infty$ and the heat releasing reaction is reversible.

The suggestion of a mixing-limited heat release rate is corroborated if we look beyond the emissions behavior to chamber-pressure measurements and high speed movies. Appealing to energy conservation, the rate of heat release can be deduced from the pressure trace and known volume changes:

$$\dot{q} = f[P(\Theta), V(\Theta), \dot{q}_{loss}] \quad .$$

Figure 26 shows the pressure and derived heat release traces for a typical DI engine, as recorded by Lyn (1963). The first feature one might notice is that characteristically the duration of heat release exceeds the period of fuel injection. This means fuel is not consumed immediately upon entering the chamber, and a rate-limiting process is at work. Knowing that hydrocarbon burning times are short (10^{-4} sec) at these temperatures, the flame is suspected to be mixing-limited.

A curious feature noted by Lyn (1963) is the brief period of intense heat-release at the start of combustion (often termed the "spike"). Typically only 10 to 15% of the energy release occurs during the spike, which implies that after ignition the combustion slows down for some reason. This would not occur in a premixed flame; thus we infer that sufficient fuel is not available and the burning is modulated by the mixing processes.

High-speed movies provide additional clues as a qualitative explanation of the spike followed by the plateau. Lyn (1963) observed that the spike emission was blue (indicative of a combustion wave passing through premixed fuel vapor and air), whereas the plateau appeared yellow-orange (suggesting the carbon-laden diffusion flames--the most familiar of which is the ordinary candle). Movies taken by Scott (1969) show the same yellow-white emission, and reveal that the fuel distribution is non-uniform. Burning starts locally on the outer edges of the fuel spray and quickly envelops the spray. Apparently, adjacent burning sprays do not interact, at least early in

Preceding page blank

Figure 26
Overlay of Combustion and Mixing Processes

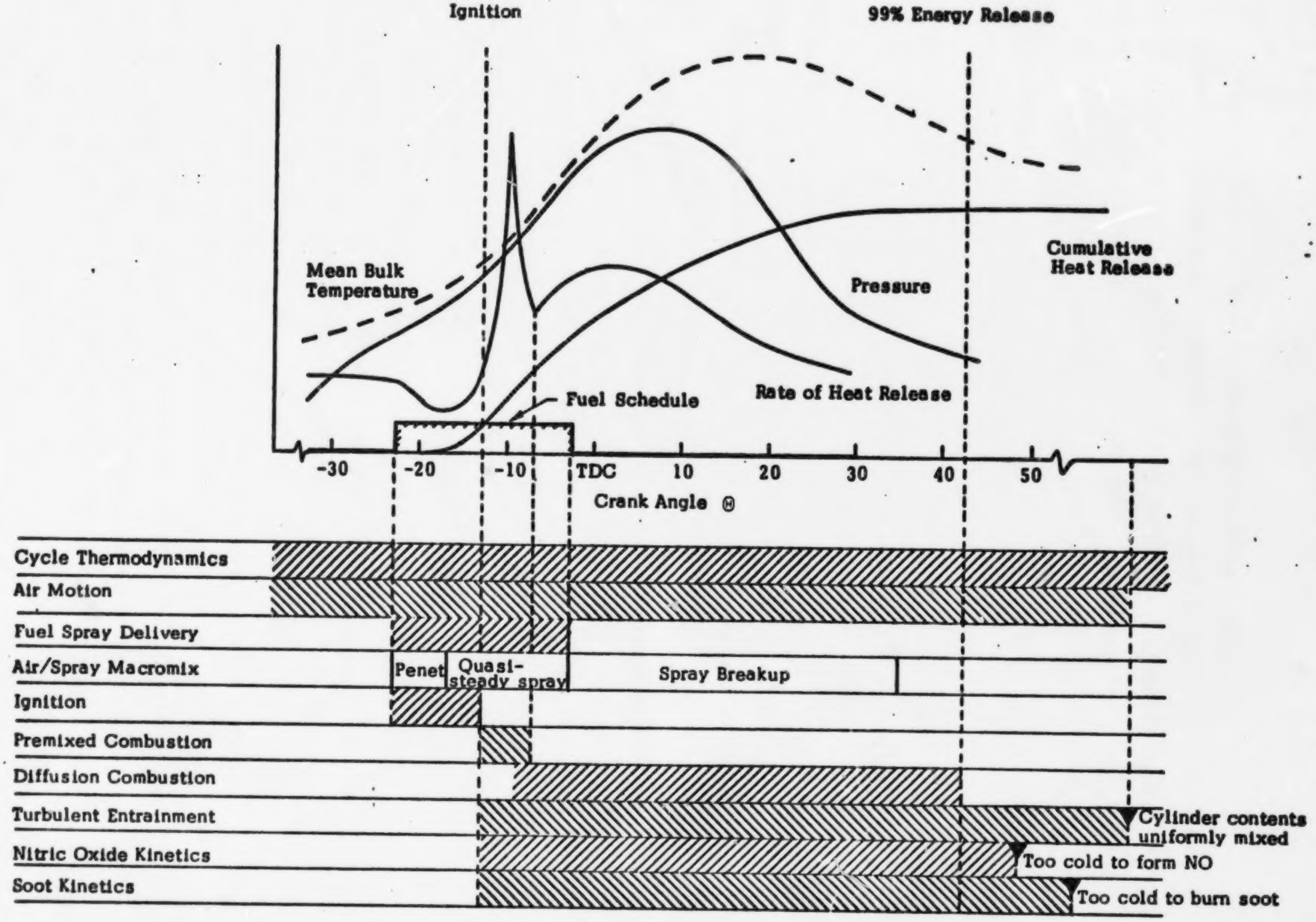

the heat release period. The air swirl in Scott's engine was sufficient that wall-impingement of fuel occurred; wall markings of the single-cylinder test engine indicated little or no wall impingement.

To recapitulate, the clues examined above indicate the following mechanisms may account for mixing and combustion:

(i) Non-uniform distribution of liquid fuel spray.

(ii) Ignition after a 5 to 15°CA delay.

(iii) Rapid premixed combustion of evaporated "fines", yielding the blue emission and the "spike" accounting for 10 to 15% of the heat release.

(iv) Mixing-controlled burning, accounting for most of the heat release and the continuous emission from soot. Mixing occurs simultaneously on two scales:

  a. Macromixing, whereby fuel elements (e.g. droplets) are delivered to an oxidizing zone.
  b. Molecular diffusion, whereby fuel and air molecules approach the interfacial flame zone, actually collide, and burn.

B. OUTLINE OF AN EMISSIONS MODEL

1. Model Components Identified

The complexity of the diesel flame is widely appreciated; our approach is to break such a problem into simpler subproblems which are more amenable to analysis. It is conceptually helpful to disassemble the diesel model into the following ten recognizable phenomena (rather than by crank angle regimes or gas vs. liquid phase, say):

1. Cycle Thermodynamics (Volume Change and Heat Transfer)
2. Air Motion
3. Fuel Spray Delivery
4. Air/Spray Entrainment (Macromixing)
5. Delay to Spontaneous Ignition
6. Heat-Release "Spike"
7. Combustion (Diffusion-Controlled Combustion; Micromixing)

8. Air/Product Entrainment
9. Nitric Oxide Kinetics
10. Soot Kinetics

A reasonable procedure in developing the computer code will be to write distinct subroutines for each component; then improvements to any one component can be introduced with a minimum of alterations to the basic program.

It is recognized that the model components interact for two reasons: (1) certain phenomena may be physically coupled if they happen simultaneously as represented in Figure 26, and (2) late phenomena will be influenced by the cumulative effect of previous processes. The overall model must account for physical coupling and "memory" interactions with iteration loops as shown in Figure 27.

2. Specifications for the Computer Code

The computer routine has other guidelines and specifications as well. Once developed, the model should help the engineer to focus valuable experimental test resources on those engine configurations indicated by computer runs to be most promising. The extent to which this can be done cost-effectively depends upon how well the following criteria are met:

(i) The model must be human engineered, with input/output in diesel engine jargon, and not requiring extra subprograms for the compression stroke, etc. In short, ideally the model will be accessible to the engineer.

(ii) The model must be versatile enough to describe a reasonable variety of engine changes.

(iii) The numerical computation scheme must be efficient; typical run times on modern computers should be in the 10^2 to 10^3 second range for a 360^o revolution of the crank. (Computer time/engine time $\approx 10^4$.)

(iv) The relative accuracy should be about $\pm$ 10% so that predictions of substantial (20 to 80%) NO changes are reliable.

(v) As far as possible, the model should be free of non-universal empiricism.

Figure 27
Interaction of Model Components

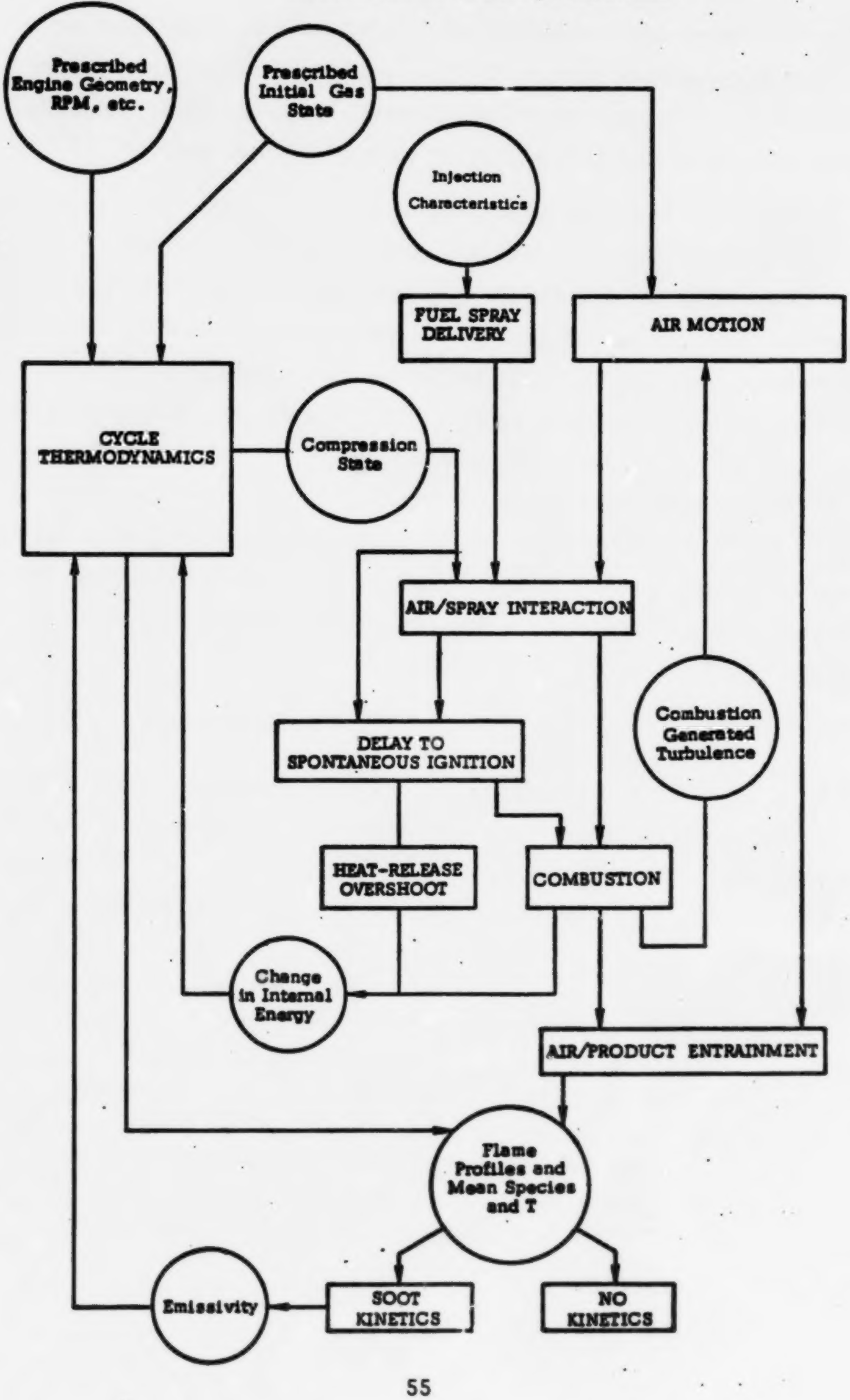

Prescribed Engine Geometry, RPM, etc.
Prescribed Initial Gas State
Injection Characteristics
FUEL SPRAY DELIVERY
AIR MOTION
CYCLE THERMODYNAMICS
Compression State
AIR/SPRAY INTERACTION
Combustion Generated Turbulence
DELAY TO SPONTANEOUS IGNITION
HEAT-RELEASE OVERSHOOT
COMBUSTION
Change in Internal Energy
AIR/PRODUCT ENTRAINMENT
Flame Profiles and Mean Species and T
Emissivity
SOOT KINETICS
NO KINETICS

Item (v) is particularly important and bears further comment. If several flame-related constants must be adjusted for each diesel engine design or operational change, then the model will not markedly reduce the test matrix. Thus as a modeling objective, we seek a model which has been formulated from first principles as much as possible.

Here the choice of simplifying assumptions is critical. Attempts to use empirical "fits" to describe complicated flame processes which are little understood will open the door for several adjustable constants. These constants make the model produce answers, however they are merely a substitute for our ignorance of complex flame couplings. In this sense the model is not useful except as a simulation; it performs the task,"given-A, calculate-A". In short, we recommend that the model incorporate processes which are well understood and can be described by physical laws. Some phenomena known to occur in the diesel flame may have to be idealized (or even ignored) to achieve a physical treatment. Other phenomena about which little is known (turbulence and diffusion flame geometry) will have to be hypothesized.

3. Alternative Treatments of Increasing Completeness and Physical Basis

The ten model components have been examined using a ladder of alternative assumptions which moves toward the ideal of representing precisely what is happening in the flame. The modeling program can move up this hierarchy to more and more accurate plateaus until one of four limits is reached:

(i) Lack of knowledge of what is happening in the flame (e.g. nature of diffusion flame).

(ii) Lack of ability to write and solve the governing equations for a known phenomenon (e.g. turbulent mixing).

(iii) Lack of program resources to complete a solvable component analysis (e.g. 3 dimensions, spectral radiation).

(iv) Lack of usefulness of increased component accuracy relative to predicting NO from all ten components.

As shown in Table 9, the most coarse assumption which can be taken to handle a phenomena is to assume a limiting case which circumvents any detailed description. Frequent choices are that the process is assumed to occur instantaneously or that it does not occur at all. For example, non-premixed flames are frequently assumed to have instantaneous chemical reaction rates, so that burning is diffusion-limited. Simplified models of combustion such as the NREC model may not be able to use fuel spray or air swirl information; in these cases A-1 and F-1 would be selected.

Moving down to the next row, phenomenological models are postulated wherein the process is assumed to exist (e.g., have a finite rate), but the mathematical expression describing the process can be arbitrary. This mathematical form may or may not have a basis in physics; coefficients are introduced and adjusted to give agreement with the behavior of as large a class of engine data as possible. Typical of this level of approach are the arbitrary ignition relay, the relaxation law for transport (flux equals coefficient times perturbation), and the Arrhenius rate expression for soot formation with adjustable coefficients. Current state-of-the-art in modeling diesel-generated NO_x appears to adopt this "phenomenological" approach in six of the ten model components.

The proposed model for Phase II attempts to reach the next level of sophistication, which replaces the phenomenological laws with expressions based on fluid-physics mechanisms. These expressions contain transport and rate coefficients just like the coarser models, but now the values must be measured or derived rather than being freely adjustable. For example, T-5 derives a value for emissivity from non-negotiable quantities such as the overall fuel/air ratio. In model NO-4, the highly respected Leeds data on the Zeldovich mechanism of NO formation is taken in place of arbitrary coefficients as appearing in NO-3. Once the coefficients are fixed by the physics, the burden of achieving agreement with engine data is shifted to other model components. Inadequacies in, say, the entrainment will be forced to the surface which otherwise might be hidden in the NO component.

Table 9

ALTERNATE APPROACHES FOR MODEL COMPONENTS

	Cycle Thermodynamics	Air Motion	Fuel Spray Delivery	Air/Spray Entrainment	Delay to Spontaneous Ignition	Heat-Release Overshoot	Combustion	Air/Product Entrainment	Nitric Oxide Kinetics	Soot Kinetics
Role of This Component	Given the initial state, chamber geometry, composition, heat release rate and mass injection, describe the state of the gas (P,T) as a function of crank angle.	Given the inlet angular momentum and RPM, describe whatever swirl, squish, and turbulence characteristics are needed for mixing and combustion models.	Given the fuel schedule, number and diameter of orifices, describe the droplet dispersion spreading angle, and injection velocity.	Given the air motion and fuel spray, describe the macromixing of spray before burning can be considered.	Given the state and motion of the air at start of injection, describe the delay before first noticable net heat release.	Account for the "spike" in the heat release profiles.	Given the fuel and air distribution, describe the heat release rate and flame T and species profiles.	Given the air motion and combustion products, describe how turbulent transport will disperse and cool the products.	Given the species and temperature fields, compute the net accumulation of nitric oxide.	Given the species and temperature fields, compute the net accumulation of soot.
Bypass Component by Taking Limiting Case	T-1 Adiabatic compression and expansion (no heat loss).	A-1 Swirl not considered.	F-1 Fuel dispersion not considered (spray structure not considered).	A/S-1 Instantaneous entrainment of spray upon injection: no velocity lag.	D-1 Instantaneous ignition at start of injection (no delay).	O-1 Instantaneous heat release from all prepared fuel.	C-1 Instantaneous burning upon fuel availability. Burning specified to occur at stoichiometric A/F ratio. C-2 Same as C-1 but A/F ratio is distributed.	A/P-1 No mixing. A/P-2 Instantaneous mixing of products (uniform gas composition).	NO-1 Full equilibrium.	S-1 Soot formation ignored.
Phenomenological Models with Adjustable Components	T-2 Adjustable heat loss, cycle averaged. T-3 Adjustable heat loss, released during combustion only.	A-2 Adjustable swirl coefficient.	F-2 Adjustable fuel dispersion coefficient (no structure). F-3 Homogeneous jet (droplets not recognized); adjustable spreading coefficient.	A/S-2 Arbitrary mixing law (e.g., Lyn's triangular profiles); adjustable coefficient.	D-2 Arbitrary ignition delay, adjustable coefficient. D-3 Ignition delay derived from both chemical rate and mixing rate (adjustable coefficient).	O-2 Arbitrary heat release law for accumulated fuel (e.g., Lyn's triangular profiles).	C-3 Well-stirred reactor giving finite burning rate. Adjustable coefficients include size, residence time. C-4 Macro size diffusion flame based on droplet clusters. Shape arbitrary.	A/P-3 Proportional to unmixed air, adjustable mixing coefficient.	NO-2 Empirical correlation of exhaust NO with key combustion parameters (e.g., peak temperature). NO-3 Arrhenius rate law with adjustable coefficients.	S-2 Empirical correlation of exhaust soot with key combustion parameters (e.g., overall A/F). S-3 Rate law involving cylinder-averaged T, A/F, P.; adjustable coefficients.
Mechanistic Models with Derived Coefficients	T-4 Convective and radiative heat loss from T and T_w coefficients assigned. T-5 Same as T-4 but transfer coefficients derived or measured.	A-3 Mean swirl from conservation of angular momentum.	F-4 Homogeneous jet, width derived from momentum and entrainment.	A/S-3 Entrainment based on cylinder of fuel in crossflow (without drop size). A/S-4 Entrainment as A/S-3 but gives drop size and velocity lag.	D-4 Time delay based on physical transport (heat-up, evaporation, mixing). Stoichiometry criteria for ignition. D-5 Rate of buildup of radicals to critical level. D-6 Rate of buildup of temperature to critical level. D-7 Same as D-3 but coefficients derived from physics.	O-3 Sequence of spontaneous ignition for premixed pockets progressively resistant A/F. O-4 Flame speed model for premixed mixture consumption. O-5 Finite rate of energy release due to premixed combustion kinetics.	C-5 Spherical droplet diffusion flame, quasi-steady "flame sheet". C-6 Droplet diffusion flame; instead of flame sheet, use chemical equilibrium diffusion profile. C-7 Macro-size diffusion flame with equilibrium profiles as in C-6.	A/P-4 Proportional to ΔT, ΔV, or ΔO_2, turbulent diffusivity derived or measured.	NO-4 Zeldovich rate mechanism, O/O_2 equilibrated. NO-5 Same as NO-3 but extended to include OH effect and NO decomposition.	S-4 Basis for formation: Mechanism for fuel pyrolysis and carbon agglomeration.
Models with Spatial Resolution	T-6 Same as T-5 but allow local hot zones to radiate independently.	A-4 $\omega(r)$ solid body or free vortex. A-5 $\omega(r)$ solid body inner, free vortex outer 2 parameters.	(Not applicable: spray trajectory determined from A/S models.	A/S-5 Radial jet in crossflow analyzed to give peel off of droplets.	D-8 Describe ignition of liquid fuel droplets, including trajectories and droplet boundary layer.			A/P-5 Local turbulent diffusivity based on local gradients.		S-5 Local soot formation rate (e.g., higher in fuel-rich regions).
Models with Other Refinements		A-6 Consider squish. A-7 Consider wall boundary layer.	F-5 Monodisperse spray. F-6 Drop-size distribution: (a) upper limit log normal (b) Rosin-Rammler (c) Nukigama (d) Bi-disperse	A/S-6 High swirl model with body forces analyzed to give ballistic droplet trajectories. A/S-7 Wall impingement analysis.			C-8 Velocity lag effects in droplet diffusion flame; possible wake flame. (Amend C-6 model). C-9 Account for rising T and falling O_2 due to neighboring droplets. (Amend C-6). Droplet spacing must be assumed.	A/P-6 Diffusivity derived from conservation equation for turbulence A/P-7 Turbulent cross correlations allowed.	NO-6 O-atom concentration in partial equilibrium with CO but not with O_2. NO-7 Non-equilibrium O-atom concentration (complete C-H-O-N scheme required).	S-6 Include soot combustion rate.

The description of spatial variations in temperature, species, and velocity represents a substantial leap in complexity and accuracy. Although spatial considerations such as the shape of spray flames (C-3) are likely to be necessary to predict NO to high accuracy, we do not project that a complete spatial model can be achieved under the current program scope. However, spatial distributions and gradients can be partially included in a few model elements without requiring all ten elements to be 3-dimensional. For example, a fraction of the chamber volume can be described as radiating at a higher temperature than the remainder. Or the fuel spray trajectory as influenced by the swirling air can be analyzed to give better estimates of the velocity lags and characteristic dimensions of droplets or macro sized flame zones.

Finally, at the bottom of Table 9 are listed a number of further refinements pertaining to the individual model components.

4. Tentative Model

With reference to Table 9, the tentative model can be described as follows:

Cycle Thermodynamics (T-6)

Convective heat loss from an Annand type expression, with coefficients measured or derived, not freely adjustable. Radiation will be considered allowing local hot zones to radiate independent of the bulk mean temperature to accurately describe NO formation. Internal energy changes will be converted to species distributions and temperature by means of the equilibrium program "ODE" developed under NASA auspices. This program allows for dissociation effects. Residual gas effects will be included, but subroutines for valve flow are not to be re-invented.

Air Motion (S-5)

Rigorous swirl radial profiles will be derived for the bowl based on chamber geometry and angular momentum after compression. Both an inner solid body rotation and an outer free vortex flow will be assumed. Squish will not be considered, nor will the wall boundary layer. Turbulence levels will be derived from Reynolds number considerations and scale lengths.

Fuel Spray (F-6)

The injection velocity will be computed from known injection schedule and orifice dimensions. Spreading angle will be measured or derived from jet theory. A drop size distribution is needed because its decay (shift of mass mean size upward) will affect NO production, heat release, and entrainment differently. A single drop size would force inaccuracies in the relative rates of these three processes.

Air/Spray Entrainment (A/S-4)

Entrainment will be based on the well-studied behavior of a cylindrical spray in a crossflow of air. Since swirl and spray structure are known as a function of chamber radius, this entrainment analysis will be conducted at a number of discrete radial positions. The analysis will yield the rate of entrainment of a distribution of drop sizes, each having certain velocity lag (if required).

Ignition Delay (D-7)

Ignition delay will be derived from both a chemical delay τ_c, taken from D-5 or D-6, coupled with a physical transport delay τ_p, taken from D-4, into an expression of the form

$$\tau^{-1} = (\tau_c^{-1} + C\,\tau_p^{-1})/(1 + C) \qquad .$$

Clearly, when C is large, transport controls; whereas when $C \rightarrow 0$, chemistry controls. The expression for τ_p will be derived from heat-up, evaporation and mixing, with a limiting stoichiometry criterion. The expression for τ_c will be derived from an Arrhenius expression for local temperature buildup or from a chain-branching expression for radical buildup.

Heat-Release Overshoot (O-3)

The ignition model D-7 will be generalized to permit a succession of ignitions. If τ_p controls, then premixed pockets of progressively "resistant" A/F ratio will be allowed to ignite. If τ_c controls, the critical kinetic condition will be progressively reached. In this way a sudden but controlled burst of heat-release will occur. The constant controlling the rate of successive ignitions will be adjustable if necessary to match observed ignition delay; essentially this will be an empirical flame speed.

Combustion (C-6)

Diesel combustion and emissions behavior strongly suggest that heat release is not homogeneous and is controlled by the rate of diffusive transport. Current models represent these main features by assuming instantaneous combustion at a prescribed stoichiometry, occurring with a rate limited by a prescribed mixing coefficient. We propose to treat a distribution of droplet sizes burning with quasi-steady spherical diffusion flames. Broadening of the heat release zone due to dissociation/recombination will be treated by using the local equilibrium diffusion model[*] for the flame. The temperature and composition of the oxidizer in which the droplets burn would be derived from macromixing (the air/spray entrainment hypothesis--see A/S-4). The rate of heat release will be derived from (1) the burning rate (molecular transport rate) of individual droplets, and (2) the rate of entrainment of droplets of different sizes into the flame regions.

It should be noted that the value of the droplet diffusion flame is not in an improved heat-release prediction, nor do we claim it describes the actual burning process. Rather, it is a useful artifice to describe in detail the high temperature diffusion flames which give rise to nitric oxide and soot. The nature of the diffusion flame (wake-type, ensemble-type, or single-droplet-type) is not known. But regardless of type, the flame itself is expected to take on a profile universal to any type.

The use of droplet burning laws to describe measured diesel heat release rates was first attempted by Lyn (1960), who was not able to obtain good agreement. However, in Lyn's model, size distribution was not considered, nor was the change in droplet burning conditions (key offsetting effects of oxygen depletion and average temperature increase). Shipinski et al. (1968) made an effort to extend Lyn's model to account for size distribution and time-dependent boundary conditions. Tanasawa (1960) had started with a size distribution f(d), and applied the burning law $d^2 = d^2(t=0) - \beta t$, which resulted in a fuel mass history of the form

---

[*] Obviously, nitric oxide will be exempted from the equilibrium calculations and treated separately by kinetic overlay.

$$\frac{m_f(t)}{m_f(t=0)} = \exp\left[\left(-3\,\frac{\beta t}{4\langle d\rangle^2}\right)^{3/4}\left(1-\frac{\beta t}{4\langle d\rangle^2}\right)^{-1/4}\right] .$$

When Shipinski used this expression directly for diesel flames, he allowed a distribution f(d) but attempted to empirically modify β to account for air dilution with hot products. This procedure has two shortcomings as follows:

(i) The physically-derived expression for the effect of ambient conditions (P_∞, $Y_{0\infty}$, T_∞), as given by Williams (1965) for a thin flame, is not used.

(ii) The expression for $m_f(t)/m_f(t=0)$ derived by Tanasawa is not valid for gradual oxygen dilution and must be re-derived (numerically) for time-dependent boundary conditions.

The above assumptions about diesel combustion may be said to set the pace or calibre of the entire model. The level of sophistication with which any remaining single component is approached must not be out of balance with the combustion component, or else data will be required/generated which has not been generated/required. For example, the fuel spray model need not compute a distribution of droplet velocity lags if a quiescent diffusion flame is assumed. Assumptions about the nature of the main diffusion burning will largely determine not only the requirements of the air, spray, and entrainment components, but also determine the information available for NO formation, soot formation, and local heat transfer.

Air/Product Entrainment (A/P-4)

Entrainment of hot combustion products in cooler air is crucial to limiting the NO formation process. We will assume turbulent transport proportional to macroscopic (~1 cm) gradients in temperature, oxygen, or velocity set up between the flame zone and the environment. The turbulent diffusivity will be derived from transport theory. Preliminary calculations indicate that the turbulent microscale may be on the order of the droplet size (10 to 30 μ). If this is true, the progressive turbulent convolutions may bring fresh cool air into contact with the hot products produced by single droplets within the time scale of burning (~1 msec). Otherwise turbulent should only be considered for the subsequent breakup of hot gaseous regions on the macroscale size (1mm to 1cm).

Nitric Oxide Formation (NO-5)

The extended Zeldovich mechanism will be employed, with oxygen atoms in equilibrium with O_2:

$$\begin{aligned} O/O_2 &= K_{eq}(T,P) \\ O + N_2 &\rightleftarrows NO + N \\ N + O_2 &\rightleftarrows NO + O \\ N + OH &\rightleftarrows NO + H \end{aligned}$$

Soot Kinetics (S-6)

Both soot combustion and soot formation will be included, with local kinetics described to allow intense soot activity in the fuel-rich zones. The mechanism for soot combustion appears to be well enough established to use measured coefficients, whereas the soot formation rate will involve an adjustable coefficient.

It should be emphasized that this set of assumptions is a current tentative guess for an improved model which is still realizable in 12 months, and does not preclude a number of alternative combustion models which are being considered. For example, it may be important to describe (1) a macro-size diffusion flame fed by a cluster of droplets, (2) non-equilibrium hydrocarbon burning at the flame front to permit O-atom overshoots, and (3) supercritical effects. The achievement of this model should achieve a substantial broadening of the engine data which can be described without adjusting coefficients. The model outlined above would have 27 coefficients, most physico-chemical properties, distributed as follows:

	Adjustable Coefficients	Universal or Derived Coefficients
Cycle Thermodynamics	---	a(conv) ϵ(rad) K(equilibrium consts) h(T) for species i
Air Motion	C_1(fraction of air in solid body rotation)	N_{Re}
Fuel Spray Delivery	C_2(drop size distribution parameter)	c_D(discharge coeff)
Air/Spray Interaction	---	D (spray/air diffusivity)
Ignition Delay	C_3(relative importance of chem. and physical delay)	A, E for chem β for evaporation D for vapor diffusivity
Heat-Release "Spike"	C_4(flame speed)	---
Combustion	---	$Q, \nu, \bar{c}_p$(gas) L, κ(gas)
Air/Product Entrainment	---	D (turbulent diffusivity)
Nitric Oxide Kinetics	---	$K_{eq}(O/O_2)$ $A\ (O + N)$ rate constants $E\ (O + N_2)$
Soot Kinetics	C_{s+}, N_{s+} (formation rate coeff)	A_{s-}, E_{s-} (combustion rate coeff)
Total number	6	21

C. FLAME STUDIES NEEDED

In Sections A and B above, we have offered the skeleton of an improved diesel flame model (spray/air mixing with local diffusion flames). Within this framework, certain pivotal questions arise. The remaining unresolved issues in our understanding of diesel flames can be set forth as in Table 10, with possible approaches toward resolving these issues.

Table 10

UNRESOLVED QUESTIONS ABOUT THE DIESEL FLAME

Issue	Method of Resolution
Is the air swirl best described by solid body rotation, potential vortex flow, or a combination?	Measure air speeds as a function of radius and crank angle using anemometry.
Can the spray be described by the same drop-size distribution law for all crank angles? Do differences in droplet velocity transform the effective size distribution?	High magnification photography or holography of sprays.
Is the spray/air interaction dominated by either the spray or the air swirl for the research engine under consideration? Is wall impingement significant? Do rotational body forces need to be considered in the air/fuel mixing process?	High speed photography will provide qualitative information. Analysis of the processes will be revealing.
Is ignition controlled by fuel availability (mixing and evaporation), by chemical induction times, or by both?	High speed movies can provide qualitative clues. Heat release traces give indirect evidence.
Is there any particular crank angle interval (e.g., the "spike") which produces most of the NO?	Time resolved (± 5°CA) measurement of nitric oxide and other key species.
Is NO production widespread or primarily confined to localized regions of heat release?	Spatially resolved (± 0.5cm) measurements of nitric oxide and other key species. On a microscale, probably cannot be resolved; only indirect evidence.
Heat release is postulated to occur in diffusion flames. Are these flames droplet envelope flames, wake burning flames, or zones on the scale of a cluster of droplets?	High speed photography may identify large flame zones, but limited information is expected.
Are combustion products rapidly diluted with air or does the mixture remain stratified during the heat release period?	Measure temperature and species with spatial resolution. Measure turbulence levels by anemometry.
What are the details of NO and smoke production in a diffusion flame?	Out-of-cylinder steady-state diffusion flame experiments.

Engine improvements due to timing shifts or EGR are relatively easy to understand (in terms of thermodynamics) and optimize. By contrast, the effects of air swirl, fuel orifice size, and chamber geometry are poorly comprehended and engine improvements are only made by trial and error. It is worthwhile to note that the unresolved questions about diesel combustion (fluid physics of fuel spray interacting with swirling air, and diffusion flame structure) correspond one-to-one to these gaps in our ability to optimize diesel efficiency and emissions. There is little sense in embarking on a major costly model development without more insight as to flame behavior than we have at present. Anticipating this need, the single-cylinder engine was designed to accommodate a variety of diagnostic probes, windows, and inserts. The flame techniques listed in Table 11 and described in Section VI are selected to begin to remedy this situation.

Table 11

SUMMARY OF RECOMMENDED TECHNIQUES

Flame Characteristic	Measurement Technique
Local NO level	UV absorption at 2260Å/direct sampling
Local Temperature	Two wavelength infrared measurements/ cooled film anemometry
Droplet-generated NO	Porous sphere simulation of droplet burning; UV detection of NO radial distribution
Air Flow Patterns	Hot-wire anemometry of motored engine Cooled film anemometry High speed photograph with tracers Radial pressure variation indicates swirl
Pressure	Piezoelectric transducers
Flame Appearance	High speed photography
Fuel Spray Characteristics	Various methods under study

D. DROPLET DIFFUSION FLAME AS A NO_x-SOURCE

1. Considerations in Calculating NO_x from Diffusion Flames

The extent to which significant NO_x is generated in diffusion flames is an extremely crucial point. The flame envelope which surrounds an element of fuel vapor (such as the mantle of a liquid fuel droplet), has somewhat mixed qualifications for generating nitric oxide. In Figure 28 we display the relevant theoretical species and temperature profiles*.

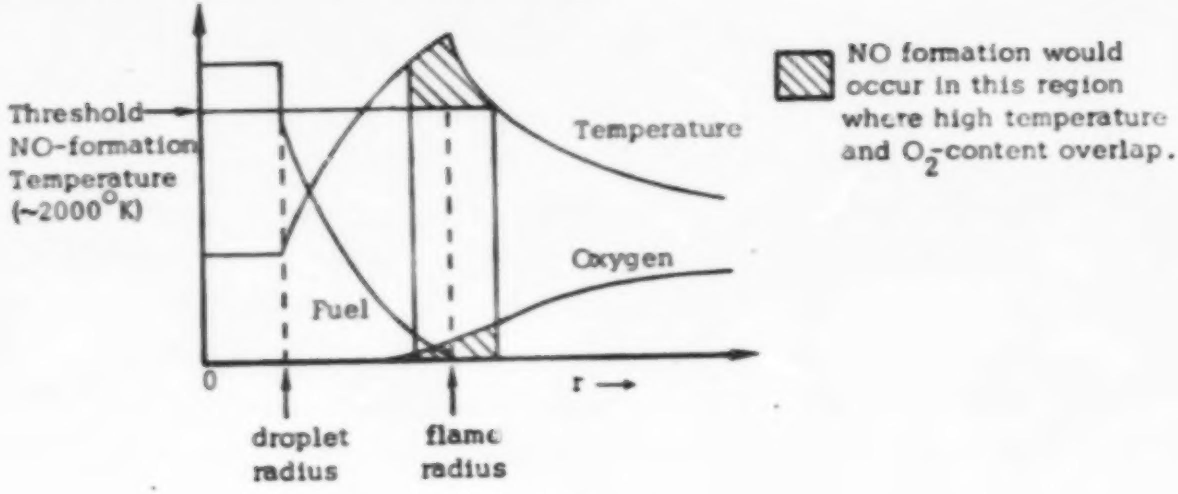
Threshold NO-formation Temperature (~2000°K)
Temperature
Oxygen
Fuel
0
r →
droplet radius
flame radius
▨ NO formation would occur in this region where high temperature and O_2-content overlap.

Figure 28

Temperature and Mass Fraction Profiles for a Burning Fuel Droplet in the Flame Surface Approximation [Williams (1965)]

On one hand, the peak temperature is near adiabatic with considerable dissociation; on the other hand, the oxygen concentration tapers off to extremely low values at the flame, so that dissociation of the product species might have to serve as the principle source of O-laden radicals. There are a number of complications which must be closely examined to evaluate the diffusion flame as a source of nitric oxide:

(i) Dropping the flame surface approximation in favor of a realistic treatment of dissociation behavior.

---

*For diesel engines, the droplets burn at elevated pressure; upon transition to the supercritical regime, the mathematical description replaces the boundary condition of equal partial pressure and vapor pressure with a condition of equal fugacity [see Rosner (1967), Spalding (1958), Natarajan and Brzustowski (1970), and Tarifa et al.(1971)].

(ii) Integration of dNO/dt over radius and droplet lifetime.

(iii) Drop size effects.

(iv) Dropping the quasi-steady approximation in favor of a rigorous treatment of the flame envelope movement during combustion.

(v) Supercritical boundary conditions applied at the droplet surface.

Let us review each of these items in turn. Detailed analysis of points (i) and (iv) has been initiated and preliminary results are found in Appendices E and F.

2. Detailed Flame Profile Calculations Necessary

It is necessary to execute a careful theoretical analysis superimposing N-O kinetics on computed species and temperature profiles, and to check the results with simple measurements of NO-profiles in the immediate neighborhood of isolated burning oil droplets (or in some other idealized diffusion flame geometry). Theoretical predictions of nitric oxide production in diffusion flames have been carried out by Bracco (1973), and Bowman and Kesten (1971). Since the results on NO_x are extremely sensitive to the choice of diffusion flame model, it is imperative that a sufficiently accurate model be used. For example, "flame-surface" models derived from the original work of Burke-Schumann (1928) are popular because one can obtain a closed-form solution. However, the flame-surface models are inadequate for NO_x prediction because they overestimate the peak flame temperature and correspondingly manhandle the species profiles*. For a more sophisticated approach, one must turn to formulation requiring numerical integration, such as the Coffin model (1957), which is based on H-C-O chemical equilibrium throughout the field, or to recent studies which incorporate certain aspects of non-equilibrium chemical kinetics into the diffusion flame model [Kassoy and Williams (1968), and Fendell (1967)].

---

*The merit of the Burke-Schumann approach lies in accurate description of the burning rate, which proves to be more less insensitive to species and temperature profiles in the near field of the droplet [Wilson (1970)].

As a first simplifying step, we neglect bulk convection and nonsteady effects and consider only the balance between the molecular-diffusion transport term and chemical source terms. We postulate that this flame balance is independent of the geometric configuration. That is to say, it is a universally valid approximation and will apply equally as well to burning droplets, sprays, jets, or gaseous counter-flow. It is assumed here that all of the reactions are in equilibrium with the exception of the NO_x-formation reactions.

If we further assume (1) diffusion pairs with equal diffusion coefficients and obey Fick's Law, and (2) unit Lewis number, and (3) spherical symmetry, then the governing equations take the form

$$\rho \frac{\mathcal{D}\tilde{Y}_j}{\mathcal{D}t} = \nabla \cdot (\rho D \nabla \tilde{Y}_j)$$

$$\rho \frac{\mathcal{D}h}{\mathcal{D}t} = \nabla \cdot (\rho D \nabla h) \quad ,$$

where

$$\tilde{Y}_j = \Sigma \mu_{ij} \frac{M_j}{M_i} Y_i$$

$\tilde{Y}_j$ = element mass fraction

Y_i = species mass fraction

μ_{ij} = number of atoms of element j in molecule of specie i

M = atomic or molecular weight

Once the element mass functions $\tilde{Y}_j$ and enthalpy h have been solved as a function of radius (see Appendix E), the actual species distribution can be found from an equilibrium analysis. Equilibrium composition through the diffusion flame is accomplished with the aid of the NASA One-Dimensional Equilibrium (ODE) Program. Results are shown in Figure 29 for $N_{Pe'}=.51$, where the thin flame solution is given for comparison. Note the effect of dissociation. Clearly the NO production rate would differ markedly for the two models.

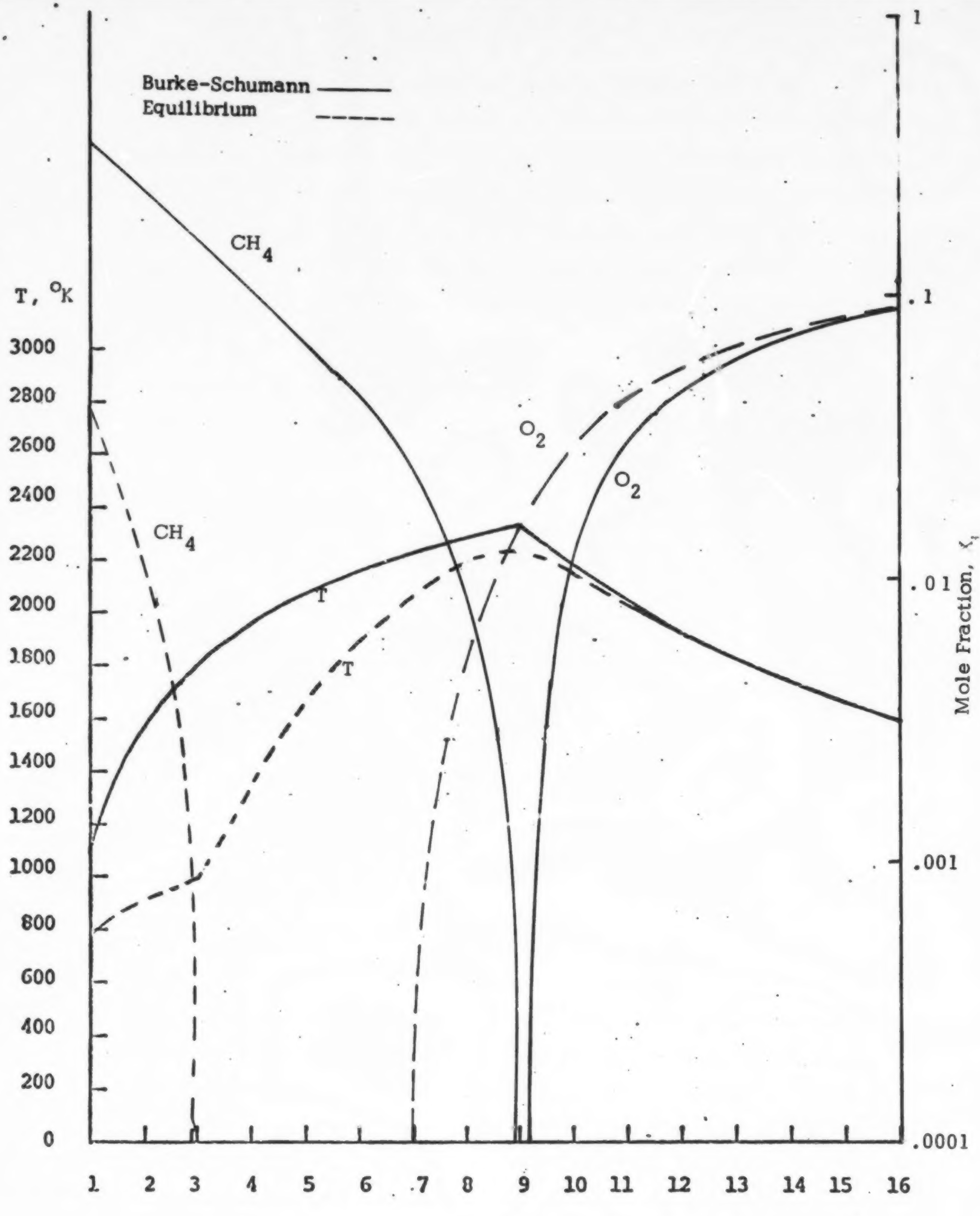
Burke-Schumann
Equilibrium
T, °K
3000
2800
2600
2400
2200
2000
1800
1600
1400
1200
1000
800
600
400
200
0
CH$_4$
CH$_4$
T
T
O$_2$
O$_2$
1
.1
.01
.001
.0001
Mole Fraction, X$_i$
1
2
3
4
5
6
7
8
9
10
11
12
13
14
15
16
Dimensionless Distance $\eta = r/r_f$

Figure 29

3. Integration over Radial Coordinate and Burning Time

Another point concerns the estimation of the contribution of burning droplets to NO_x production. Because the lifetime in the flame zone is quite brief, it is not enough merely to establish the production rate (in ppm/sec) as a function of radial coordinate for given droplet diameter and ambient composition and temperature. One must estimate the cumulative flux of NO outward from the droplet at some radial point far from the flame (say, 10 flame radii out), and combine this with the fuel burning rate (e.g. kg/sec) to obtain the grams NO/kg fuel produced. This emission level will be valid only within the framework of the quasi-steady model--i.e., it will only apply instantaneously for a given droplet size. In reality the droplet size changes, and one must average the NO_x-production rate over the lifetime of the droplet. Then it will be possible to evaluate NO_x production by burning diesel fuel droplets, and to optimize the size distribution of fuel spray nozzles to minimize NO formation.

4. Importance of Droplet Size Distribution

The preliminary calculations of Bowman and Kesten (1971) show that the droplet emission index (gNO/g fuel) goes up with the square of droplet diameter. The greater NO_x emission was due to the broader diffusion flames associated with larger drops, such that NO-breeding gaseous products take longer to move out from the hot flame. In any case, droplet sizes must be established if possible.

5. Asymptotic Analysis of Non-Steady Effects

The quasi-steady approximation is often made to simplify the analysis of diffusion flames. Under this hypothesis, the burning time is assumed much longer than other potentially complex relaxation times such as (1) the time for thermal equilibration of the droplet interior, and (2) the time required to set up a diffusive mixing field centered about the flame envelope. The validity of this approximation has been analyzed by introducing non-steady effect (2) into the equations and observing the predicted flame behavior. An analysis by matched asymptotic expansions was conducted to distinguish the droplet vicinity (quasi-steady) and the unsteady effects which predominate further out in the field, and which may affect the flame position. Typical values for the evaporation constant and the diffusion coefficient ($\beta \approx 10^{-3}$ cm^2/sec, $D_\infty \approx 10^{-1}$ cm^2/sec) suggest taking the expansion parameter

$$\delta = \sqrt{\frac{\beta}{D_\infty}} \quad .$$

Details of the analysis are presented in Appendix F; here we outline the major conclusions.

After the analysis given in Appendix F , one obtains the following results: The flame radius (r_{fl}) is given implicitly by the equation

$$\bar{Y}_{ox_\infty} = \frac{(\bar{Y}^\infty_{ox} + \bar{Y}_{f-})}{4\pi\rho D[r_{fl}(t) - r_f(t)]} \Big\{ \dot{m}_f(t) - \dot{m}_f(o) \operatorname{erfc} \frac{r_{fl}(t) - r_f(t)}{2\sqrt{Dt}}$$

$$- \int_0^t \frac{d\dot{m}}{dt} f(t'-t) \operatorname{erfc} \frac{r_{fl}(t') - r_f(t')}{2\sqrt{Dt'}}\, dt' - 4\pi\rho D[r_{fl}(t) - r_f(t)] \Big[\exp\Big(\frac{-\dot{m}_f(t)}{4\pi\rho D r_{fl}(t)}\Big) - 1 \Big]\Big] \Big\}$$

where $r_f(t)$ and $\dot{m}_f(t)$ are given by the quasi-steady solution in the inner region and hence are known. Here $\bar{Y}$ is defined by $\bar{Y} = Y \sum \nu'' M/(\nu'' - \nu')M$, where ν are stoichiometric coefficients. This implicit equation for flame radius was numerically solved, and the results are given in Figure 30.

Likewise, the flame temperature can be determined as shown in Appendix F and is given by the expression

$$\bar{T}_{fl} = \frac{\bar{T}_\infty \bar{Y}_{f-} + \bar{Y}^\infty_{ox} \bar{Y}_{f-} + \bar{T}_{f-} \bar{Y}^\infty_{ox}}{\bar{Y}^\infty_{ox} + \bar{Y}_{f-}}$$

where $\bar{T} = C_p T/Q$.

This equation shows that flame temperature is constant in spite of the motion of the flame. This results runs counter to the exact numerical solutions of Kotake and Okazaki (1969) which exhibit temporally varying flame temperature. This discrepancy conceivably is attributable to the neglect of liquid-phase heat conduction in the present case.

Figure 30 shows that over this envelope of validity the flame to droplet radius does not change very much and may perhaps be treated as constant (this is not examined here). This is not to be interpreted, however, as an acceptance of the quasi-steady theory which predicts such a constant ratio somewhat in excess of the mean value obtained by the unsteady theory.

Figure 30

FLAME ENVELOPE EXPANDS RELATIVE TO DROPLET SURFACE
(BOTH DECREASE DURING BURNING)

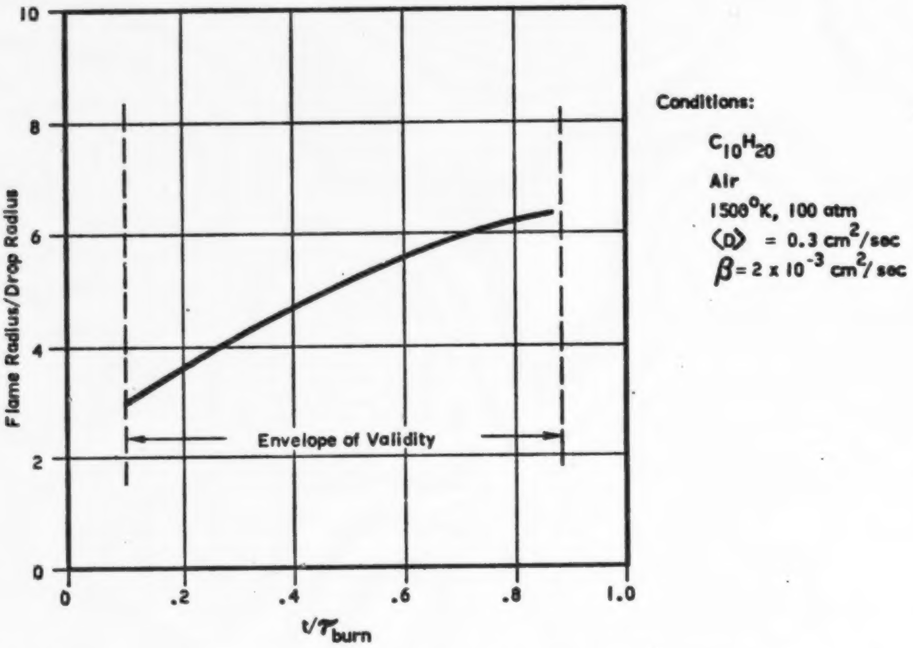

It is also interesting to note that the parameter δ, which may be rewritten as

$$\delta = \sqrt{2N_{Pe'}\frac{\rho}{\rho_\ell}} = \sqrt{\frac{2N_{Pe'}}{RT}\frac{P}{\rho_\ell}}$$

is seen to be proportional to the gas-to-liquid phase density ratio. Owing to the high pressure environment found in diesel combustion chambers it may yet turn out that unsteady effects are minimized in diesel engines. From the form of the solution, it appears that flame temperature variations are due to the transient heat up of the liquid surface whereas the flame position may change due to transient gas phase processes. These points require further examination before any definite conclusions can be reached.

Table 14

ALTERNATE APPROACHES FOR MODEL COMPONENTS

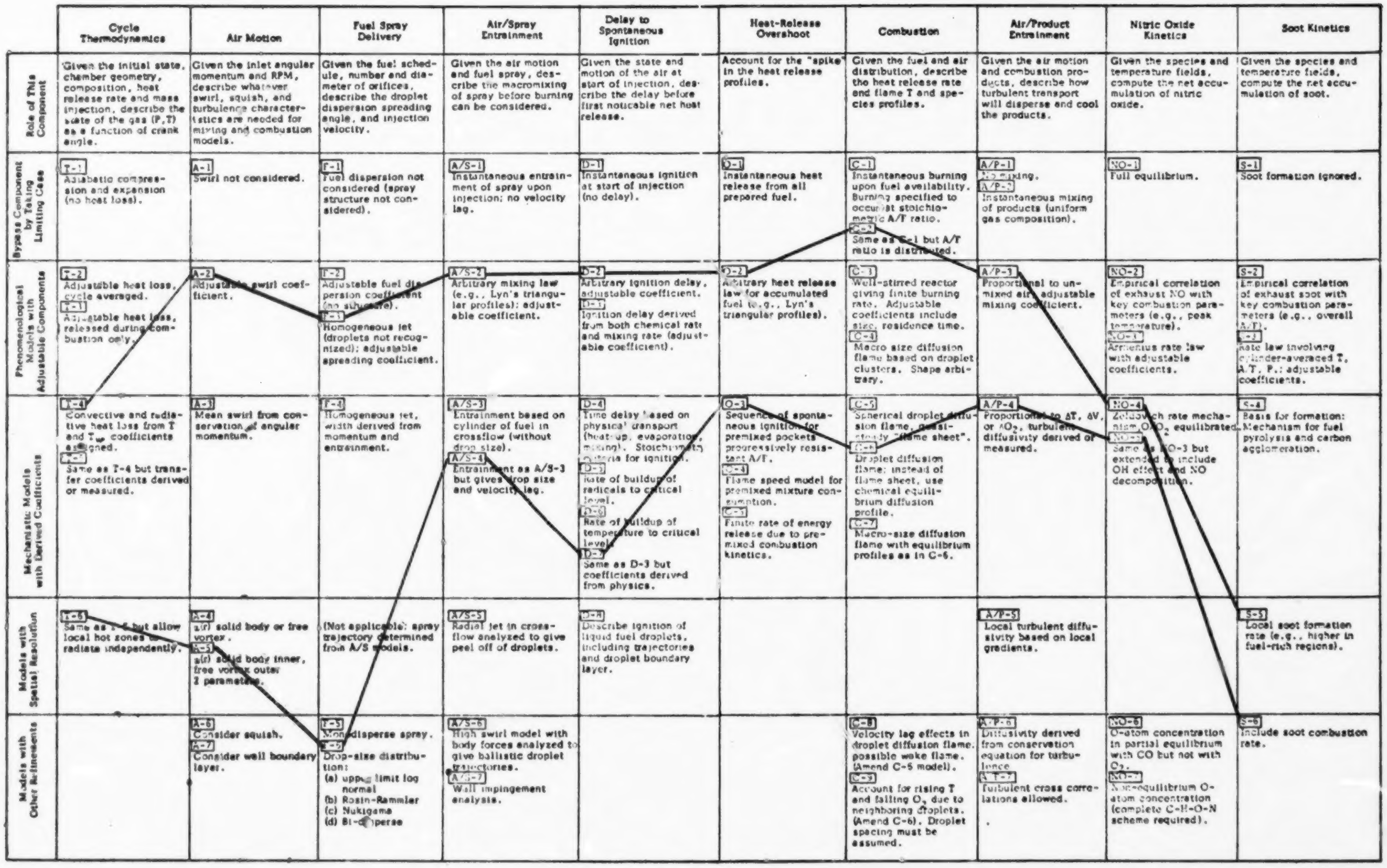

	Cycle Thermodynamics	Air Motion	Fuel Spray Delivery	Air/Spray Entrainment	Delay to Spontaneous Ignition	Heat-Release Overshoot	Combustion	Air/Product Entrainment	Nitric Oxide Kinetics	Soot Kinetics
Role of This Component	Given the initial state, chamber geometry, composition, heat release rate and mass injection, describe the state of the gas (P,T) as a function of crank angle.	Given the inlet angular momentum and RPM, describe whatever swirl, squish, and turbulence characteristics are needed for mixing and combustion models.	Given the fuel schedule, number and diameter of orifices, describe the droplet dispersion spreading angle, and injection velocity.	Given the air motion and fuel spray, describe the macromixing of spray before burning can be considered.	Given the state and motion of the air at start of injection, describe the delay before first noticable net heat release.	Account for the "spike" in the heat release profiles.	Given the fuel and air distribution, describe the heat release rate and flame T and species profiles.	Given the air motion and combustion products, describe how turbulent transport will disperse and cool the products.	Given the species and temperature fields, compute the net accumulation of nitric oxide.	Given the species and temperature fields, compute the net accumulation of soot.
Bypass Component by Taking Limiting Case	T-1 Adiabatic compression and expansion (no heat loss).	A-1 Swirl not considered.	F-1 Fuel dispersion not considered (spray structure not considered).	A/S-1 Instantaneous entrainment of spray upon injection; no velocity lag.	D-1 Instantaneous ignition at start of injection (no delay).	O-1 Instantaneous heat release from all prepared fuel.	C-1 Instantaneous burning upon fuel availability. Burning specified to occur at stoichiometric A/F ratio. C-2 Same as C-1 but A/F ratio is distributed.	A/P-1 No mixing. A/P-2 Instantaneous mixing of products (uniform gas composition).	NO-1 Full equilibrium.	S-1 Soot formation ignored.
Phenomenological Models with Adjustable Components	T-2 Adjustable heat loss, cycle averaged. T-3 Adjustable heat loss, released during combustion only.	A-2 Adjustable swirl coefficient.	F-2 Adjustable fuel dispersion coefficient (no structure). F-3 Homogeneous jet (droplets not recognized); adjustable spreading coefficient.	A/S-2 Arbitrary mixing law (e.g., Lyn's triangular profiles); adjustable coefficient.	D-2 Arbitrary ignition delay, adjustable coefficient. D-3 Ignition delay derived from both chemical rate and mixing rate (adjustable coefficient).	O-2 Arbitrary heat release law for accumulated fuel (e.g., Lyn's triangular profiles).	C-3 Well-stirred reactor giving finite burning rate. Adjustable coefficients include size, residence time. C-4 Macro size diffusion flame based on droplet clusters. Shape arbitrary.	A/P-3 Proportional to unmixed air; adjustable mixing coefficient.	NO-2 Empirical correlation of exhaust NO with key combustion parameters (e.g., peak temperature). NO-3 Arrhenius rate law with adjustable coefficients.	S-2 Empirical correlation of exhaust soot with key combustion parameters (e.g., overall A/F). S-3 Rate law involving cylinder-averaced T, A/F, P.; adjustable coefficients.
Mechanistic Models with Derived Coefficients	T-4 Convective and radiative heat loss from T and T_w coefficients assigned. T-5 Same as T-4 but transfer coefficients derived or measured.	A-3 Mean swirl from conservation of angular momentum.	F-4 Homogeneous jet, width derived from momentum and entrainment.	A/S-3 Entrainment based on cylinder of fuel in crossflow (without drop size). A/S-4 Entrainment as A/S-3 but gives drop size and velocity lag.	D-4 Time delay based on physical transport (heat-up, evaporation, mixing). Stoichiometry criteria for ignition. D-5 Rate of buildup of radicals to critical level. D-6 Rate of buildup of temperature to critical level. D-7 Same as D-3 but coefficients derived from physics.	O-3 Sequence of spontaneous ignition for premixed pockets progressively resistant A/F. O-4 Flame speed model for premixed mixture consumption. O-5 Finite rate of energy release due to premixed combustion kinetics.	C-5 Spherical droplet diffusion flame, quasi-steady "flame sheet". C-6 Droplet diffusion flame; instead of flame sheet, use chemical equilibrium diffusion profile. C-7 Macro-size diffusion flame with equilibrium profiles as in C-6.	A/P-4 Proportional to ΔT, ΔV, or ΔO_2, turbulent diffusivity derived or measured.	NO-4 Zeldovich rate mechanism, O/O_2 equilibrated. NO-5 Same as NO-3 but extended to include OH effect and NO decomposition.	S-4 Basis for formation: Mechanism for fuel pyrolysis and carbon agglomeration.
Models with Spatial Resolution	T-6 Same as T-5 but allow local hot zones to radiate independently.	A-4 $\omega(r)$ solid body or free vortex. A-5 $\omega(r)$ solid body inner, free vortex outer 2 parameters.	(Not applicable): spray trajectory determined from A/S models.	A/S-5 Radial jet in crossflow analyzed to give peel off of droplets.	D-8 Describe ignition of liquid fuel droplets, including trajectories and droplet boundary layer.			A/P-5 Local turbulent diffusivity based on local gradients.		S-5 Local soot formation rate (e.g., higher in fuel-rich regions).
Models with Other Refinements		A-6 Consider squish. A-7 Consider wall boundary layer.	F-5 Monodisperse spray. F-6 Drop-size distribution: (a) upper limit log normal (b) Rosin-Rammler (c) Nukigama (d) Bi-disperse	A/S-6 High swirl model with body forces analyzed to give ballistic droplet trajectories. A/S-7 Wall impingement analysis.			C-8 Velocity lag effects in droplet diffusion flame; possible wake flame. (Amend C-5 model). C-9 Account for rising T and falling O_2 due to neighboring droplets. (Amend C-6). Droplet spacing must be assumed.	A/P-6 Diffusivity derived from conservation equation for turbulence A/P-7 Turbulent cross correlations allowed.	NO-6 O-atom concentration in partial equilibrium with CO but not with O_2. NO-7 Non-equilibrium O-atom concentration (complete C-H-O-N scheme required).	S-6 Include soot combustion rate.

Upper curve: Current models
Lower curve: Tentative model for Phase II

Reproduced from best available copy.

A. THE NREC MODEL

1. Approach to Modeling the Mixing, Heat Release and Pollutant Formation

The mixing and heat release process is entirely artificial and prescribed by four parameters, C_1, C_2, $\overline{F}$, and ΔF. Two stages of heat release are represented, following Lyn (1963):

(a) An initial triangular "spike" of heat release having width specified by C_2.

(b) Heat release according to a Gaussian profile with half width C_1:

$$\frac{dm_f}{d\theta} \sim \frac{(\theta - \theta_{inj})}{C_1^{\,2}} \exp\left[-\frac{\theta - \theta_{inj}}{C_1}\right] .$$

In both cases, the chemical reactions are instantaneous (equilibrium prevails). C_1 and C_2 are mixing coefficients prescribing fuel availability. During the second heat release plateau, heat release occurs at a specified mixture ratio $\overline{F}$, often taken at stoichiometric to simulate a diffusion flame zone. Excursions from the nominal value $\overline{F}$ are permitted during the spike; these excursions are characterized by the parameter ΔF.

Subsequent dilution of combustion products by air is specified by a parameter C_3. Successive pockets of combustion products are distributed randomly in the chamber and no attempt is made to describe temperature or concentration gradients. Heat transfer is prescribed in proportion to the temperature of each pocket by an exchange of coefficient C_4 (10^{-3} ft-lb $^{o}R^{-1}$ - CA^{-1}-ft^{-2}). The kinetics of NO formation are represented adequately by the Zeldovich mechanism, although in practice the program is difficult to use because NO production is a tabular entry based on given C/H ratio, pressure, F/A ratio, and temperature. Soot is not considered.

Preceding page blank

There are a number of interacting systems and processes which seem important to incorporate in an improved model for diesel combustion and emissions. These are outlined in Figure 31(a). The approach of the NREC model is outlined for comparison in Figure 31(b), with bracketed criticisms, omissions, and characterizations.

The main objection to this approach is obvious. The incorporation of six parameters which are to be specified arbitrarily (C_1, C_2, C_3, C_4, $\overline{F}$, ΔF) reduces the method to little more than a data correlation technique. The physics of fuel spray macromixing, ignition, and diffusion-controlled burning has been bypassed with these six parameters. It is not clear how to relate these six parameters to measurable or calculable fluid physics properties. Such a method will allow the correlation of data from a tightly defined family of engines and will allow a certain amount of extrapolation to the boundaries of this family. However, it will tell very little if anything about how engine design parameters are related to fundamental combustion and pollution-formation phenomena. The method cannot be used for new optimum engine design.

To be more specific in our criticism, the program in effect specifies a priori the local stoichiometry to which the products of combustion will immediately mix and the quench rate to which these products are then subjected. It further specifies a priori the "delay" (preparation time) which injected fuel experiences before it burns. Furthermore the program assumes that fuel vapor combines only with fresh air and that no combustion product dilution of the air prior to combustion is present. All of these points are factors which must be dictated by the physics of fuel spray-air interaction and diffusion flame mechanics.

Such a model cannot be used as a basis for soot formation prediction. Soot formation kinetics depends on the lifetime at high temperature of rich zones. Clearly these features are built into the program a priori rather than derived.

Figure 31(a)

BLOCK DIAGRAM OF SYSTEM INTERACTIONS FOR DIESEL COMBUSTION

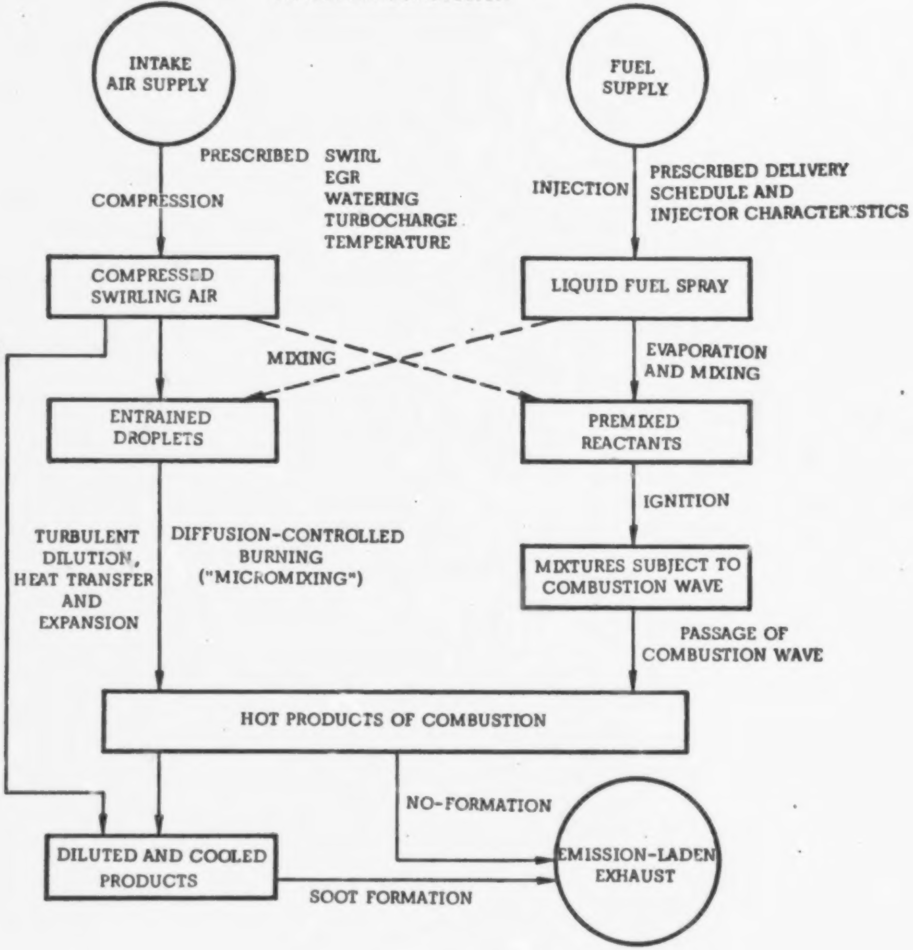
INTAKE AIR SUPPLY
FUEL SUPPLY
PRESCRIBED
COMPRESSION
SWIRL
EGR
WATERING
TURBOCHARGE
TEMPERATURE
INJECTION
PRESCRIBED DELIVERY SCHEDULE AND INJECTOR CHARACTERISTICS
COMPRESSED SWIRLING AIR
LIQUID FUEL SPRAY
MIXING
EVAPORATION AND MIXING
ENTRAINED DROPLETS
PREMIXED REACTANTS
IGNITION
TURBULENT DILUTION, HEAT TRANSFER AND EXPANSION
DIFFUSION-CONTROLLED BURNING ("MICROMIXING")
MIXTURES SUBJECT TO COMBUSTION WAVE
PASSAGE OF COMBUSTION WAVE
HOT PRODUCTS OF COMBUSTION
NO-FORMATION
DILUTED AND COOLED PRODUCTS
SOOT FORMATION
EMISSION-LADEN EXHAUST

Figure 31(b)

BLOCK DIAGRAM OF NREC MODEL

[ ] = CHARACTERIZATION OR CRITICISM

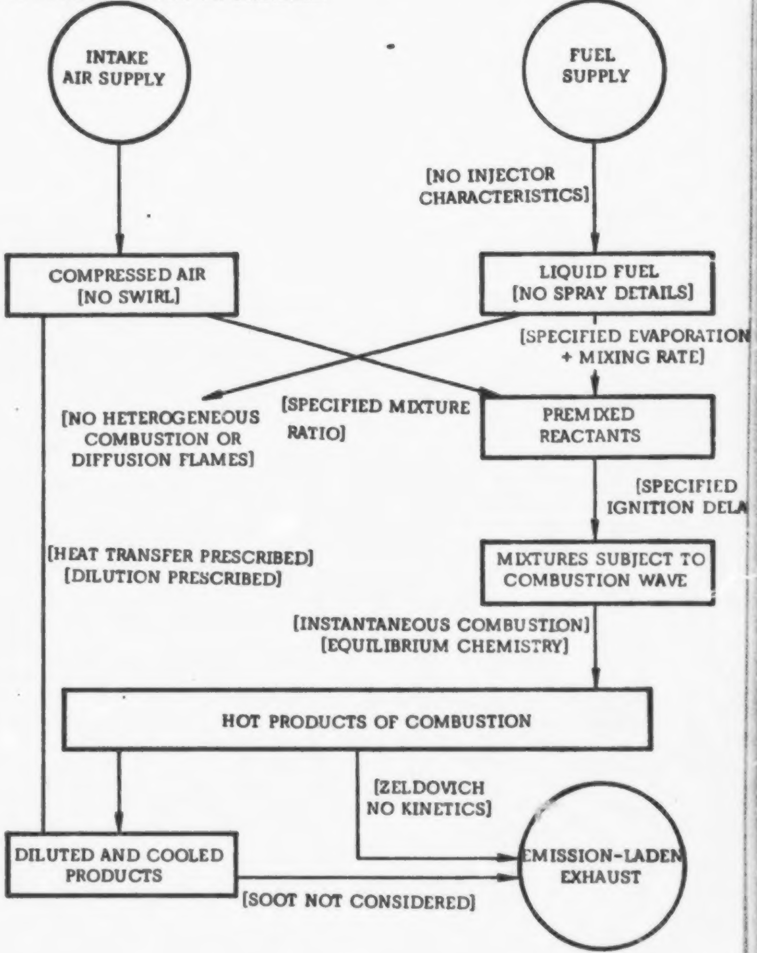
INTAKE AIR SUPPLY
FUEL SUPPLY
[NO INJECTOR CHARACTERISTICS]
COMPRESSED AIR [NO SWIRL]
LIQUID FUEL [NO SPRAY DETAILS]
[SPECIFIED EVAPORATION + MIXING RATE]
[NO HETEROGENEOUS COMBUSTION OR DIFFUSION FLAMES]
[SPECIFIED MIXTURE RATIO]
PREMIXED REACTANTS
[SPECIFIED IGNITION DELA
[HEAT TRANSFER PRESCRIBED]
[DILUTION PRESCRIBED]
MIXTURES SUBJECT TO COMBUSTION WAVE
[INSTANTANEOUS COMBUSTION]
[EQUILIBRIUM CHEMISTRY]
HOT PRODUCTS OF COMBUSTION
[ZELDOVICH NO KINETICS]
DILUTED AND COOLED PRODUCTS
[SOOT NOT CONSIDERED]
EMISSION-LADEN EXHAUST

2. Predictive Capability of the NREC Model

The NREC model has been run under the following conditions which match the baseline test matrix of the experimental single cylinder tests:

Engine:

Bore	5.50"
Connecting Rod Length	12.00"
Crank Radius	3.00"
Clearance Volume	0.00485 ft^3 (CR = 17:1)

Fuel System:

Fuel injection schedule shown in Figure 32

θ_{inj} = 15, 20, 25° CA BTDC

θ_2 = adjusted to give desired A/F (maximum 126 mm^3/stroke)

Operating Parameters:

Air Temperature	100°F
Initial Air Pressure	1 atm
Fuel Temperature	100°F
Engine Speed	1500, 1800, 2100 RPM

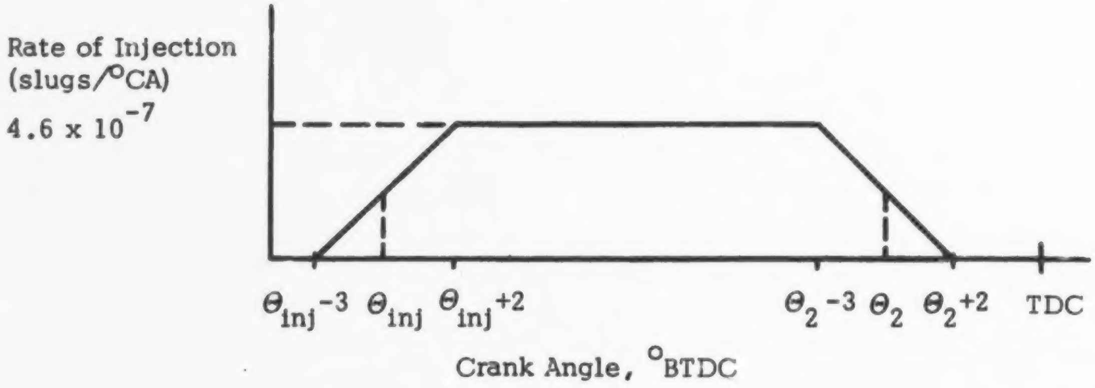
Rate of Injection (slugs/°CA)
4.6×10^{-7}
$\theta_{inj}-3$
θ_{inj}
$\theta_{inj}+2$
θ_2-3
θ_2
θ_2+2
TDC
Crank Angle, °BTDC

Figure 32
Fuel Injection Schedule

In addition, a number of model parameters were first arbitrarily set as follows:

Fuel Vaporization Rate	(C_1)	10°CA
Fuel Burning Rate	(C_2)	10°CA
Dilution Rate	(C_3)	$.05^{\circ}\mathrm{CA}^{-1}$
Heat Transfer	(C_4)	10^{-3} lbf-ft/ft^{2}-$^{\circ}$R-$^{\circ}$CA
Fuel Mass Fraction Increment	ΔF	.01

The results are compared with observed emissions in Table 15.

Table 15

ϕ	RPM	Timing	Run #	Observed NO (ppm)	Calc. NO (ppm)
.15	1500	-20°	33-8	620	611
.33	1500	-20°	33-11	2000	1091
.63	1500	-20°	34-2	2900	726
.62	2100	-25°	35-11	2420	783
.60	2100	-15°	39-4	1200	554

Generally, while these original NREC predictions agreed at low load, the predicted NO levels were a factor of three too low at high load. The relative trend with increasing load was opposite to that observed, and the relative trend with timing was correct, but quantitatively less (3% reduction rather than 5% reduction per $^{\circ}$CA retard).

Certain adjustments to the NREC model parameters were made and the results were much more reasonable. The original and revised sets are given below.

	Original	First Revision	Second Revision
Fuel Vaporization Rate (C_1)	10°CA	17°CA	17°CA
Fuel Gas Burning Rate (C_2)	10°CA	5°CA	10°CA
Dilution Rate (C_3)	$.05^{\circ}$CA	$.01^{\circ}\mathrm{CA}^{-1}$	$.01^{\circ}\mathrm{CA}^{-1}$
Heat Transfer (C_4)	10^{-3}	2×10^{-3}	10^{-3}
Fuel Mass Fraction Increment (ΔF)	.01	.001	.003

In order to explain the model's behavior, it is useful to recall that the original set of parameters gave NO_x decreasing with load (see Table 15). Apparently no air was left for combustion when the last several "packages" of fuel were ready. Our first remedy was to decrease the air dilution rate (C_3), hoping to save air for later in the cycle. The result was unsatisfactory. Closer analysis showed all of the air consumed during the ignition "spike", which in a real engine amounts to only 5 to 10% of the heat release. The root cause of the spike's appetite for air was the distribution of fuel/air ratios specified during the ignition spike. With $\Delta F = .01$, the distribution was so wide that extremely lean "packages" were created--so lean that all of the air was promptly assigned. The remedy for this was to reduce the width of the spike (C_2) and to reduce the F/A dispersion (ΔF). These changes gave rough agreement with the data; fine tuning was then done by adjusting C_1 to favor delayed burning. The "tuned" results are shown in Table 16. The model could have been further tuned by assigning an individual set (C_1, C_2) for each fuel package.

The agreement on load effects (Columns 2, 8, 9 and 10) was better than 15%. The 50% reduction in NO with 10° CA retard was also well simulated (Columns 11 and 12). The reduction of NO with increased speed was overpredicted by the model (Column 7). Turbocharging effects were well represented while increased air effects were overpredicted. Neither compression ratio changes nor rate of injection effects were very well described.

In short, the model performed reasonably well only on emissions behavior with changes in load, timing, and turbocharging. The predictive capability of the NREC model for variations in air temperature, compression ratio, RPM, or rate of injection appeared inadequate for practical use by engineers.

3. Versatility and Adjustment of Parameters

The NREC model is not set up to investigate the effect of EGR, water injection, air swirl, fuel dispersion, or chamber shape. In fact the residual exhaust is ignored in the cycle thermodynamics; pure air is taken as the intake charge. Thus the model is quite limited in its ability to predict a wide variety of emissions control variations.

Three iterations were necessary to find a set of six parameters which gave reasonable baseline agreement. However, when extended beyond the baseline the predictive capability was quite limited, so three iterations is not unexpectedly few. A more rigorous procedure would be to attempt to fit the heat release profile by adjustment of the six parameters.

Table 16

COMPARISON OF NREC PREDICTIONS TO SINGLE CYLINDER EMISSIONS

Description			Original	#1	#2	#3	#4	#5	#6a	#6b	#7	#8	#9	#10	#11	#12
Arbitrary Parameters	C_1	Fuel Vaporization Rate (^oCA)	10	17	17	17	17	17	17	17	23.8	17	17	17	17	17
	C_2	Fuel Gas Burning Rate (^oCA)	5	10	10	10	10	10	10	10	14.0	10	10	10	10	10
	C_3	Dilution Rate ($^oCA^{-1}$)	.05	.01	.01	.01	.01	.01	.01	.00715	.01	.01	.01	.01	.01	.01
	C_4	Heat Transfer (ft-lbs/ft^2-^oR-^oCA)	.001	.002	.001	.001	.001	.001	.001	.001	.000715	.001	.001	.001	.001	.001
	ΔF	Fuel Mass Fraction Increment	.01	.001	.003	.003	.003	.003	.003	.003	.003	.003	.003	.003	.003	.003
	F	Mean Fuel/Air Ratio	.01	.066	.066	.066	.066	.066	.066	.066	.066	.066	.066	.066	.066	.066
Engine Conditions		P_a (lb_f/ft^2)		1900	3800	1900	1900	1900	1900	1900	1900	1900	1900	1900	1900	1900
		T_a (^oR)		560	560	560	660	560	560	560	560	560	560	560	560	560
		VC Clearance Volume (ft^3)		.00485	.00485	.00485	.00589	.00485	.00485	.00485	.00485	.00485	.00485	.00485	.00485	.00485
		Fuel Schedule (as represented by $\dot{m}_{f\,max} \times 10^7$)		4.6	4.6	9.2	3.9	4.6	6.8	9.2	4.6	4.6	4.6	4.6	4.6	4.6
		Timing		-20°	-20°	-20°	-20°	-20°	-20°	-20°	-20°	-20°	-20°	-20°	-25°	-15°
		ϕ		.45	.45	.45	.45	.45	.45	.45	.45	.15	.33	.60	.60	.60
		RPM		1500	1500	1500	1500	1500	1500	1500	2100	1500	1500	1500	2100	2100
Results		NO_x Predicted		2300	1875	1936	2300	1700	1925	1916	700	1500	1500	1500	2100	2265
		NO_x Experimental		1800	1800	1910	2060	920	825	990	1670	620	2000	2900	2420	1200

Legend:

#2:	New Baseline	#6a:	High Rate of Fuel Injection	#11:	Increase RPM
#3:	Turbocharge (Double Air Pressure)	#6b:	Very High Rate of Fuel Injection	#12:	Retard
#4:	Increase Air Temperature by 100°F	#7:	Increased RPM		
#5:	Decrease Compression Ratio to 14:1	#8-10:	A/F Variation		

B. THE CAV MODEL

1. Approach to Modeling the Mixing, Heat Release, and Pollutant Formation

In contrast to the NREC approach, the CAV model considers the mixing of a fuel spray with high density swirling air. Khan, Greeves and Probert (1971) derived their mixing model from Grigg and Syed (1970) . Starting (as all models must) with a prescribed fuel schedule, a conical plume of half angle θ_f is described, as shown in Figure 33.

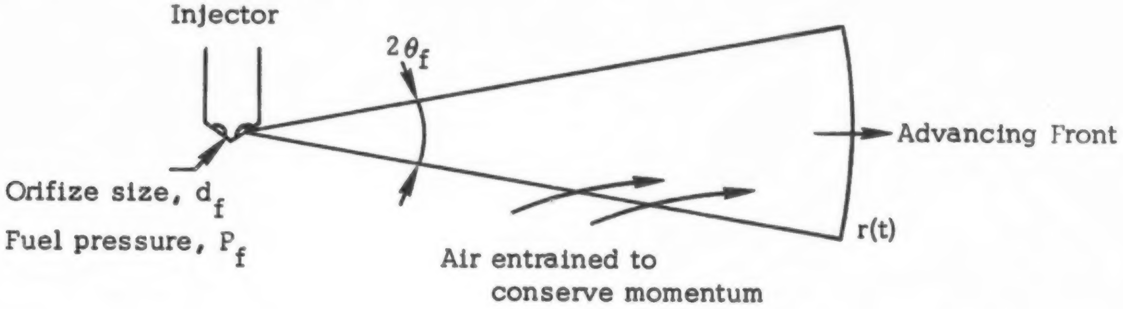

Figure 33

Conical Plume Schematic

The front advances according to the Schweitzer (1938) expression

$$r^2 \sim \frac{d_f P_f^{1/2}}{t\,[\rho(\text{intake})/\rho(\text{stp})]}$$

where the notation is given in Figure 32. The rate of air entrainment is such that the plume density is constant. Thus air fills in the widening plume at a rate which can be derived from geometrical considerations:

$$\frac{d(m_a)_{jet}}{dt} = \frac{E_r\, \rho_a \pi \tan^2\theta_f\, r^3}{t[\rho(\text{intake})/\rho(\text{stp})]}$$

where E_r is an "entrainment" coefficient, empirically fitted as a function of speed and swirl to data on soot emission. A similar "macromix" model has been worked out for wall impingement.

Heat release is described as follows: An ignition delay is specified from measured chamber pressure data, followed by a triangular heat release "spike" with a base arbitrarily set at 6°CA. The major heat release occurs by a diffusion-controlled process within the entrainment cone defined above. The rate of diffusion (and instantaneous heat release) is given by a quasi-Fick's law proportional to not only the concentration difference but also to the velocity of the advancing conical plume:

$$\frac{d(m_a)_{burn}}{dt} = D' \frac{dr}{dt} \left[(m_a)_{jet} - (m_a)_{burn}\right] \quad ,$$

where $D'(cm^{-1})$ is a "diffusion coefficient" selected as an empirical function of swirl and speed to give good agreement with heat release data. A peak temperature T_p for NO formation, unique to this zone of hot products, is derived from equilibrium considerations. However, heat loss occurs at the same rate as for the cylinder-averaged temperature.

Let us turn to the assumed pollutant production mechanisms. Within this heat release zone, a fuel-rich zone (denoted ▒ in Figure 34) is defined

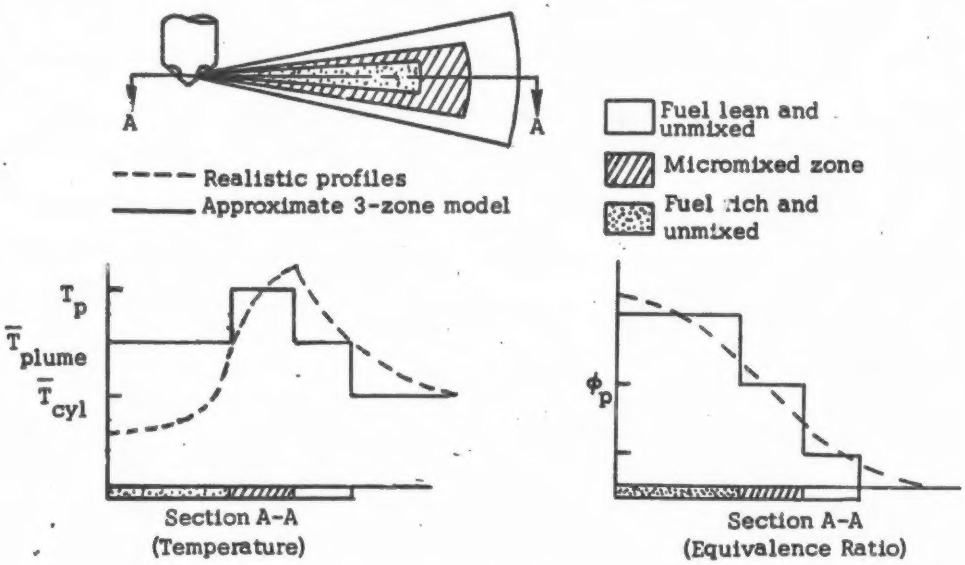
A
A
Fuel lean and unmixed
Micromixed zone
Fuel rich and unmixed
Realistic profiles
Approximate 3-zone model
T_p
$\bar{T}_{plume}$
$\bar{T}_{cyl}$
Section A-A (Temperature)
ϕ_p
Section A-A (Equivalence Ratio)

Figure 34

THREE-ZONE MODEL FOR MICROMIXING AND POLLUTANT FORMATION where smoke is formed at a rate given by

$$\frac{dm_s}{dt} = C_s \frac{V_s}{V(\theta=-180)} \phi_s^{\,n} P \cdot \exp(-E_s/RT_s) \quad ,$$

where the subscript s denotes the fuel rich soot zone, and the remaining parameters are set by an array of recipes as follows:

C_s	=	9.3×10^5	(Best fit to soot data)
E_s	=	40 kcal/mole	(Best fit to soot data)
n	=	3	(Best fit to soot data)
ϕ_s	=	$\frac{m_f}{(m_f)_{burn}} \langle\phi\rangle_{unmixed}$	(Equivalence ratio for unmixed reactants in entire plume, weighted to fuel rich in early stages of burning)
T_s	=	$\overline{T}_{plume}$	(Ranges from compression temperature of unburned air up to final temperature of conical plume after combustion is complete)
V_s	=	Volume of fuel rich zone, given by thermodynamics, and the definitions of ϕ_s and T_s.	

Soot oxidation is acknowledged to occur but is not included because it did not seem to heavily influence the emission data, relative to soot formation.

Nitric oxide is formed by the modified Zeldovich mechanism* within the zone of hot products, where the temperature T_p and equivalence ratio ϕ_p are given by the micromixed fuel and air taken to equilibrium. The pre-exponential factor was boosted a factor of 5 over the literature values; otherwise NO emissions were predicted too low. Peak temperatures and oxygen profiles are ignored with the details of the diffusion flame, so this correction is not unexpected.

Figure 35(b) gives the block diagram of the CAV approach.

---

*Adopted by Khan and Greeves (1973) as a significant improvement over the earlier model [Khan et al (1971)].

Figure 35(a)

BLOCK DIAGRAM OF SYSTEM INTERACTIONS FOR DIESEL COMBUSTION

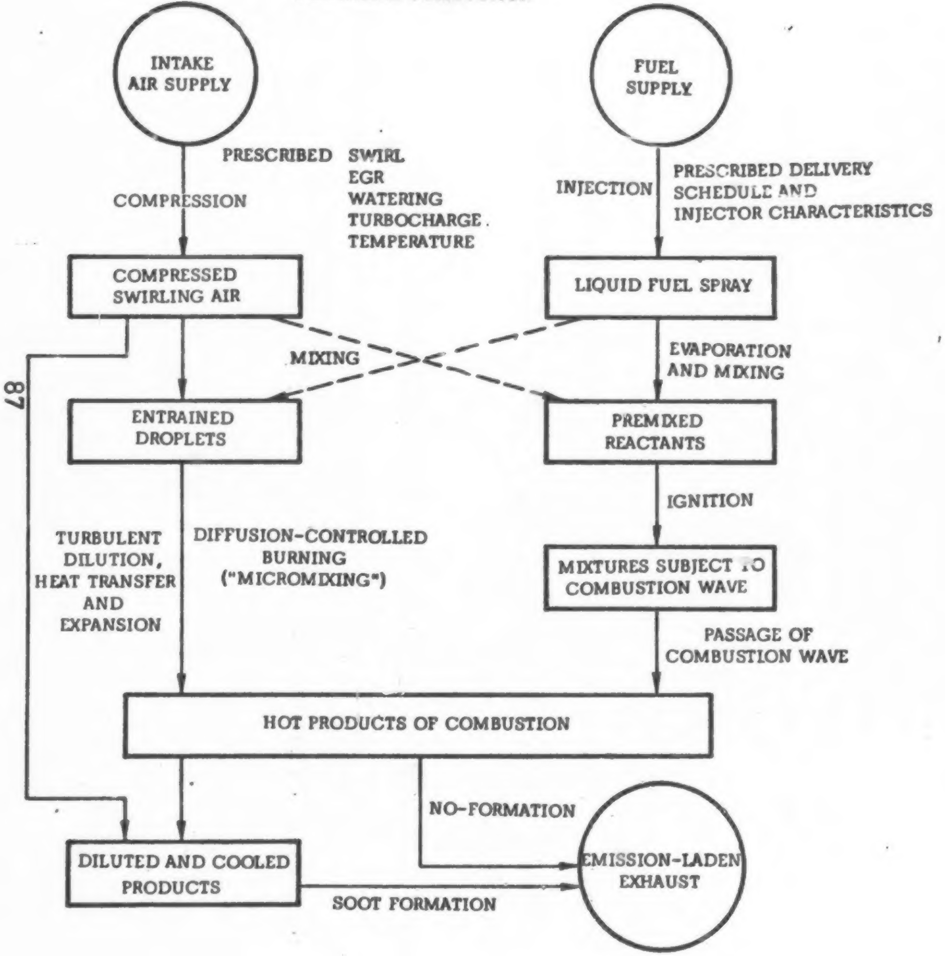
INTAKE AIR SUPPLY
FUEL SUPPLY
COMPRESSION
PRESCRIBED SWIRL
EGR
WATERING
TURBOCHARGE
TEMPERATURE
INJECTION
PRESCRIBED DELIVERY SCHEDULE AND INJECTOR CHARACTERISTICS
COMPRESSED SWIRLING AIR
LIQUID FUEL SPRAY
MIXING
EVAPORATION AND MIXING
ENTRAINED DROPLETS
PREMIXED REACTANTS
IGNITION
TURBULENT DILUTION, HEAT TRANSFER AND EXPANSION
DIFFUSION-CONTROLLED BURNING ("MICROMIXING")
MIXTURES SUBJECT TO COMBUSTION WAVE
PASSAGE OF COMBUSTION WAVE
HOT PRODUCTS OF COMBUSTION
NO-FORMATION
DILUTED AND COOLED PRODUCTS
SOOT FORMATION
EMISSION-LADEN EXHAUST

Figure 35(b)

BLOCK DIAGRAM OF CAV MODEL

[ ] = Characterization or Criticism

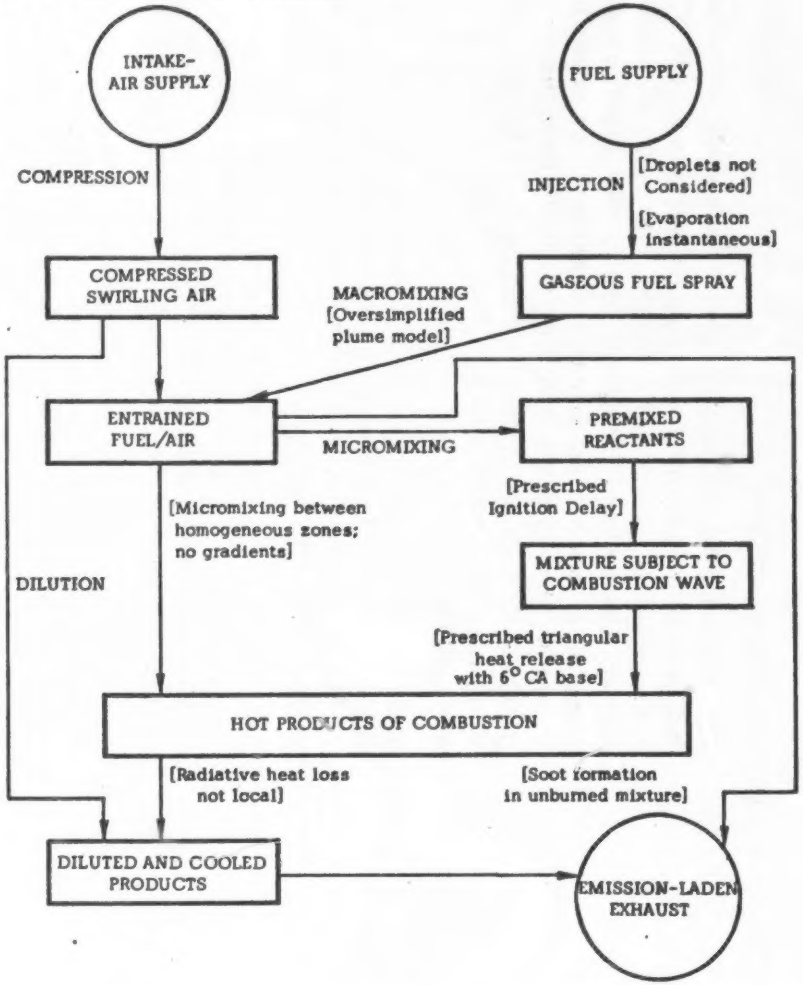
INTAKE-AIR SUPPLY
FUEL SUPPLY
COMPRESSION
INJECTION
[Droplets not Considered]
[Evaporation instantaneous]
COMPRESSED SWIRLING AIR
GASEOUS FUEL SPRAY
MACROMIXING [Oversimplified plume model]
ENTRAINED FUEL/AIR
MICROMIXING
PREMIXED REACTANTS
[Micromixing between homogeneous zones; no gradients]
[Prescribed Ignition Delay]
DILUTION
MIXTURE SUBJECT TO COMBUSTION WAVE
[Prescribed triangular heat release with 6° CA base]
HOT PRODUCTS OF COMBUSTION
[Radiative heat loss not local]
[Soot formation in unburned mixture]
DILUTED AND COOLED PRODUCTS
EMISSION-LADEN EXHAUST

Our main criticisms are as follows:

(i) The macromixing model may work as a mental construct, but is far from reality as high speed movies reveal (CAV acknowledges this). For example, the spray cone penetration time is small compared to the heat release time; some other mechanism of entrainment such as crossflow stripping of droplets appears more likely from the photographs. The effect of swirl would be more fundamental in a crossflow model and E_r = f(swirl) would be more mechanistic.

(ii) Droplet details such as the dropsize distribution, evaporation, or local diffusion flames are not treated. This would be a more fundamental approach to the effect of orifice size, for example.

(iii) The smoothing out of gradients (temperature and concentration) in the heat-release zone will underpredict nitric oxide. The established Zeldovich mechanism should not have to be "doctored" as in the 1971 CAV model.

(iv) The NO emissions are quite sensitive to heat losses from the heat-release zone, yet the CAV approach was to assign the same radiation as for the entire chamber. Doubtless this decision was tied to the underprediction of NO (the need for higher temperature). This again reflects the need for detailed flame profiles where heat losses would be allowed along with actual "unclipped" peak temperatures.

(v) The rate of micromixing or molecular diffusion is assumed proportional to the plume velocity $\dot{r}$. It would be more fundamental to derive a turbulent diffusivity from Prandtl mixing length considerations using the air swirl and/or piston speed.

In many respects, the CAV model is the most advanced model currently in existence, particularly in regard to the fuel/air mixing and soot formation processes.

2. Predictive Capability of the CAV Model

The CAV model was exercised and predictions compared against our single cylinder data. Results were not available at this writing.

3. Versatility and Adjustment of Parameters

The CAV model is expressly structured to handle a wide variety of parameter variations including variations in air swirl, engine speed, load, rate of injection, timing, and compression ratio. According to communications from the CAV, the program is not general enough to accommodate EGR, water injection, turbocharging, fuel orifice size, or pilot injection as parameter variations. The computer code was not available for direct evaluation.

The diffusivity coefficient, D', must be adjusted using cumulative heat release diagrams from precise cylinder pressure measurements. Apparently, a unique set of coefficients must be derived for each engine speed and swirl level.

C. THE CUMMINS MODEL

The approach of the Cummins model to the following physical aspects which should be included in a model of NO_x formation in a diesel cylinder will be commented on:

1. Aerodynamics of the macromixing of air/fuel and air/combustion products
2. Local mechanism of combustion, including diffusion if necessary
3. Thermodynamic cycle processes
4. Detailed description of the chemical kinetic mechanism of NO_x formation

The model presented by the authors correctly represents cycle thermodynamics but incorporates empirical treatments of NO_x kinetics and rate of heat release. With this simple approach, and with suitable adjustment of parameters, the model is able to simulate the NO_x effects of compression ratio, inlet pressure, temperature, composition (EGR), injection timing and schedule, and engine speed. However, mixing is not treated. Consequently, the NO_x-influences of swirl, spray parameters, and bowl geometry cannot be explained.

The model adopts the assumption of stoichiometric burning, which is quite remarkable despite its common acceptance. The authors note that "stoichiometric combustion represents approximately the mid range of combustible mixtures". An alternate justification, which seems more reasonable to us, is that nonpremixed combustion manifests itself in the form of a diffusion-controlled flame, which will self-regulate itself to be "fed" stoichiometrically.

The next aspect of the model which deserves comment is the rate expression used to describe NO formation. Based on the Zeldovich mechanism for NO formation, the authors' rate equation contains two parameters, A and E, which the authors have arbitrarily adjusted to give agreement with NO emission data for a number of diesel engines. The difference between the adjusted (A, E) and the values calculated from basic kinetic data ($A = 1.3 \times 10^9$ mole $^\circ K/atm^{1/2}$ Btu $^\circ CA$, and E = 137 kcal/mole) might be attributed to other effects, such as mixing, which have been inadequately treated in the model.

Also regarding the empirical parameters, the parameter A includes the square root of the oxygen concentration. It is consistent with the authors' assumptions of equilibrium combustion, $\phi = 1$, and no mixing to assign a constant value of O_2 concentration (say 1%). In reality during NO formation the oxygen concentration may change by a factor of 3 due to dilution or oxygen consumption. The omission of a rigorous description of O-atom profiles and temperature in the flame is also serious (although common to all existing models).

We are also concerned with the lack of mixing between a stoichiometric package of combustion products and excess air in the model. This can have two ramifications on predicted nitric oxide formation. First, the cooling effect of air dilution is neglected and thus NO_x production may be overestimated. However, without air dilution, the amount of oxygen available for NO formation is also artificially curtailed, reducing the amount of NO predicted. By holding the oxygen concentration constant throughout the process, the authors have partially compensated for the latter effect.

Finally, concerning the heat release calculation, the model has been exercised with two options: (1) empirical burning law following Lyn, and (2) a spray mixing model which is mentioned but not elaborated. It would be of interest to have details of the spray mixing model and to learn whether the two calculations of heat release give comparable results.

In commenting on the preliminary Cummins model, it is useful to reflect on two key characteristics which a model should incorporate in order to be useful to an engineer in explaining observed system performance or predicting performance of untested systems. First, as the authors have pointed out, assigned constants should be universal to the entire class of direct injection engines. Second, the model should be able to accurately predict the performance and emissions behavior over a broad range of combustion system parameters. In order to accomplish these goals, the model must curtail empiricism in favor of principles describing underlying mechanisms. Unfortunately, many of these mechanisms are not understood and like all other current models, the preliminary Cummins model must rely on empirically adjusted constants. A block diagram is given as Figure 36(b).

Figure 36(a)

BLOCK DIAGRAM OF SYSTEM INTERACTIONS FOR DIESEL COMBUSTION

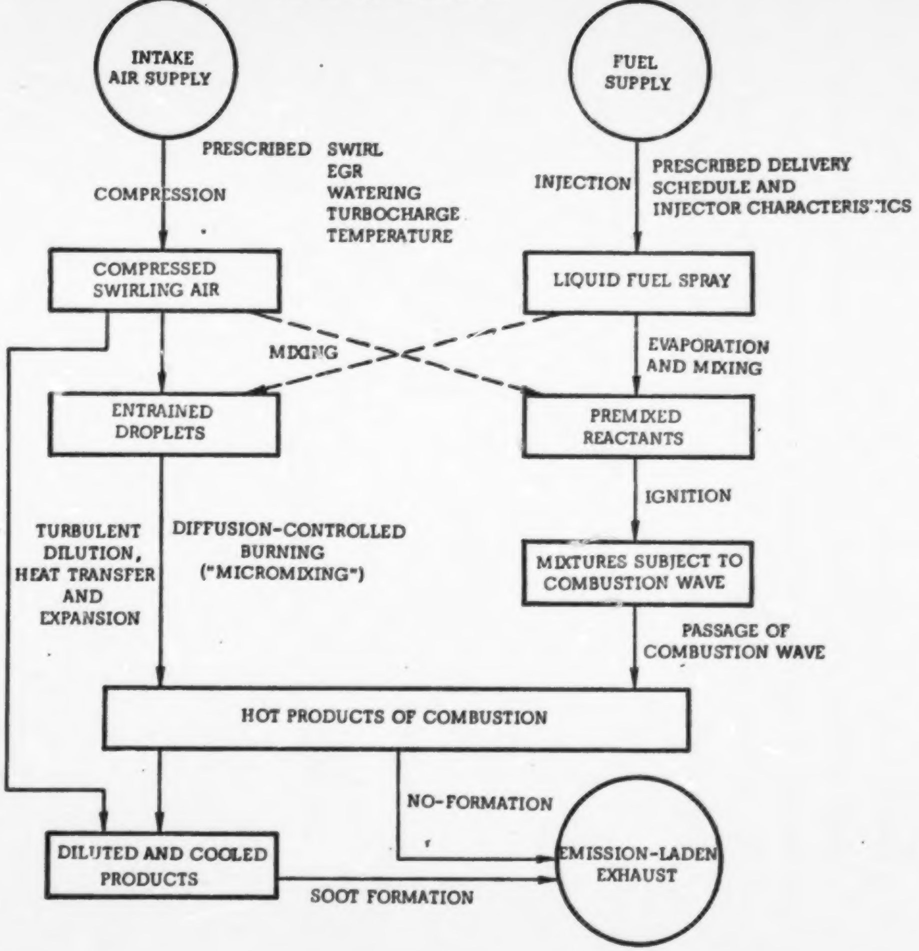
INTAKE AIR SUPPLY
FUEL SUPPLY
PRESCRIBED SWIRL
EGR
WATERING
TURBOCHARGE
TEMPERATURE
COMPRESSION
INJECTION
PRESCRIBED DELIVERY SCHEDULE AND INJECTOR CHARACTERISTICS
COMPRESSED SWIRLING AIR
LIQUID FUEL SPRAY
MIXING
EVAPORATION AND MIXING
ENTRAINED DROPLETS
PREMIXED REACTANTS
IGNITION
TURBULENT DILUTION, HEAT TRANSFER AND EXPANSION
DIFFUSION-CONTROLLED BURNING ("MICROMIXING")
MIXTURES SUBJECT TO COMBUSTION WAVE
PASSAGE OF COMBUSTION WAVE
HOT PRODUCTS OF COMBUSTION
NO-FORMATION
DILUTED AND COOLED PRODUCTS
EMISSION-LADEN EXHAUST
SOOT FORMATION

Figure 36(b)

BLOCK DIAGRAM OF CUMMINS MODEL

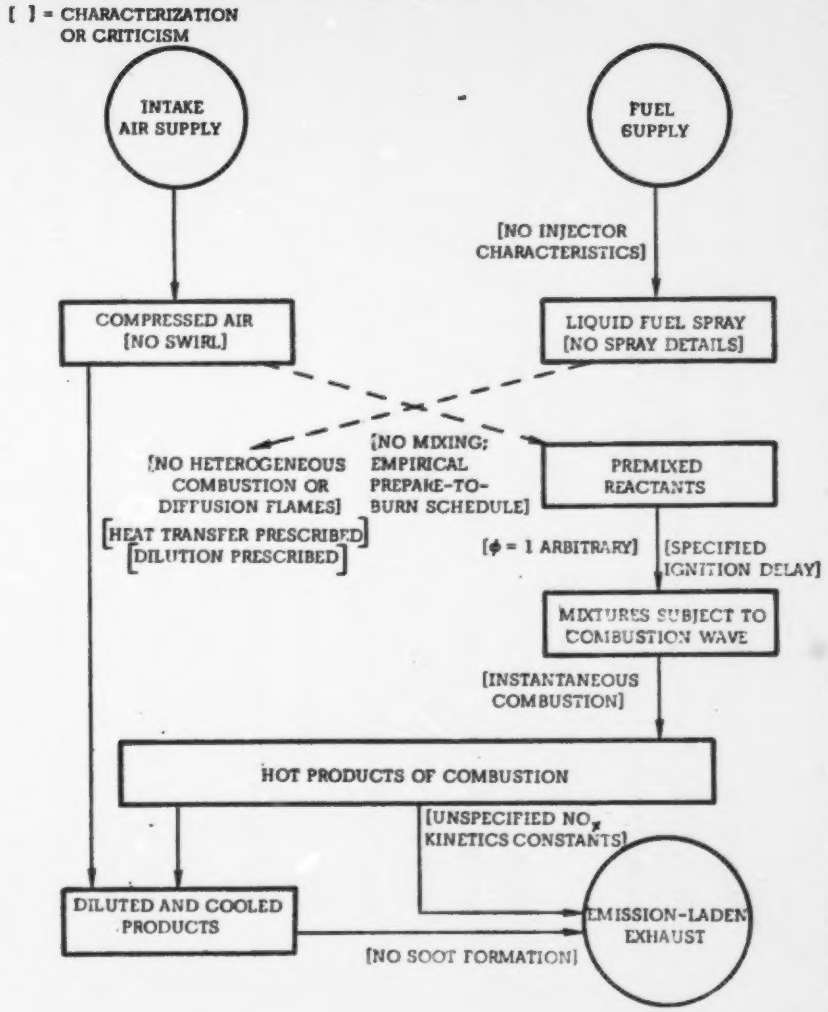
[ ] = CHARACTERIZATION OR CRITICISM
INTAKE AIR SUPPLY
FUEL SUPPLY
[NO INJECTOR CHARACTERISTICS]
COMPRESSED AIR [NO SWIRL]
LIQUID FUEL SPRAY [NO SPRAY DETAILS]
[NO HETEROGENEOUS COMBUSTION OR DIFFUSION FLAMES]
[NO MIXING; EMPIRICAL PREPARE-TO-BURN SCHEDULE]
PREMIXED REACTANTS
[HEAT TRANSFER PRESCRIBED]
[DILUTION PRESCRIBED]
[ϕ = 1 ARBITRARY]
[SPECIFIED IGNITION DELAY]
MIXTURES SUBJECT TO COMBUSTION WAVE
[INSTANTANEOUS COMBUSTION]
HOT PRODUCTS OF COMBUSTION
[UNSPECIFIED NO_x KINETICS CONSTANTS]
DILUTED AND COOLED PRODUCTS
EMISSION-LADEN EXHAUST
[NO SOOT FORMATION]

VI. DIESEL FLAME STUDIES

A. SPECTROSCOPIC OBSERVATIONS

1. Past Studies and Description of Method

The light radiated from air-fed flames creates three distinct signatures of nitric oxide:

Spectral Region	Wavelength	Type of Transition	Structure	Source
UV	.2260μ	Electronic	Line	$\gamma(0,0)$ transition to lowest vibrational level of upper state $(X^2\Pi \rightarrow A^2\Sigma^+)$
VIS	.5 - .7μ	Chemiluminescent	Continuum	NO + O reaction
IR	5.29μ	Vibrational	Band	Fundamental

Spectroscopic species determinations are notably rare in diesel flame studies. In the IR region there appears to be good reason: Lyn (1963) and others have observed large quantities of smoke in the flame with corresponding continuum emission overshadowing even the strong CO_2 and H_2O bands in the IR. This behavior is illustrated below in an IR scan taken by Lyn (1957). The IR emission from a diesel flame resembles a grey body with very little structure to analyze for species contribution (Figure 37). This strong continuum peaks in the near IR (for a black body, $\lambda_{max} T = 2884^{\circ}K$) and presumably gives rise to the high peak levels of radiant heat transfer (up to 500 watts/cm^2) measured by Henein (1971). The 30% uncertainty encountered by Newhall (1967) for emission determination of NO in spark-ignited engines would definitely be a lower limit for diesel flames with these lower S/N ratios. A further difficulty with emission spectroscopy is the dependence of emission strength on temperature, which in turn depends on crank angle. Thus a decrease in signal could be attributed to either lower temperature or NO decomposition at constant temperature.

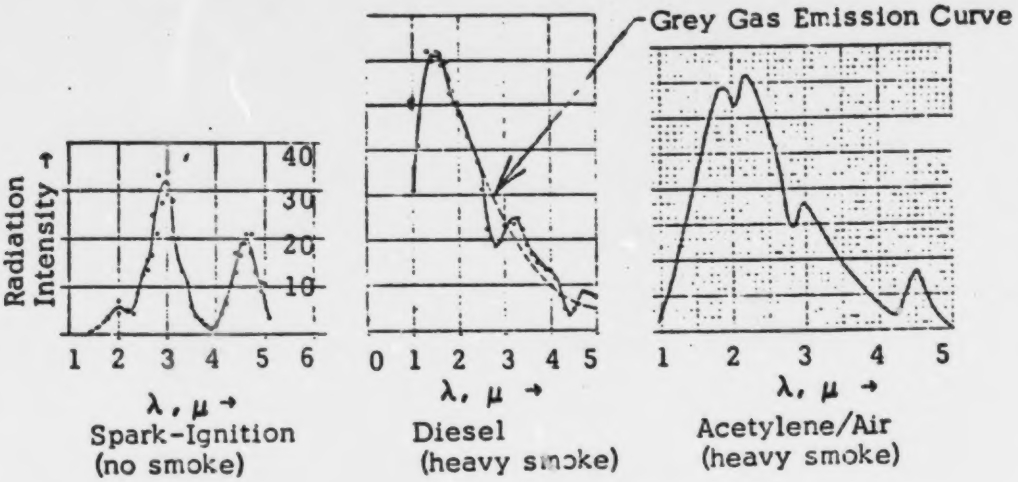

Figure 37

IR SPECTRA SHOWING BLACK BODY EMISSION
FROM DIESEL ENGINE [Lyn (1957)]

The near UV was selected for the NO diagnostic technique primarily because the carbon-smoke continuum at 2500°K was expected to fall off sharply below .4μ, according to blackbody curve shapes. The work of Shahed and Newhall (1971) had shown that the $\gamma(0,0)$ NO band at 2260 Å could be seen above the shoulder of the O_2 Schumann-Runge continuum even at 350 psi (Figure 38), although this result was for smokeless fuel (propane).

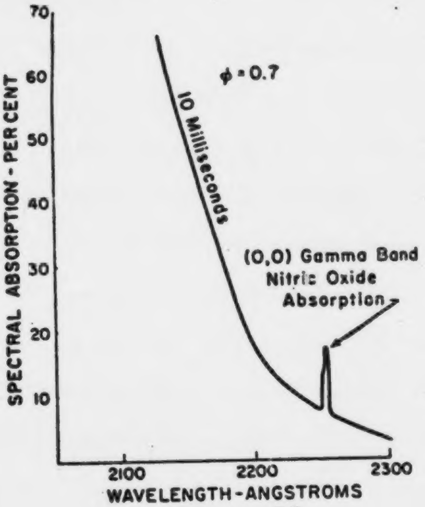

Figure 38

(0,0) gamma band nitric oxide absorption
superimposed on Schumann-Runge background
[Shahed and Newhall (1971)]

Quader (1973) at General Motors Research Laboratories has also attempted to utilize the NO gamma bands to measure the nitric oxide histories in a single cylinder spark ignition engine. The 2358 Å (0,1) band of NO has also proved useful, according to Seery and Bowman (1970) and McGregor (1973). The β band at 2200 Å apparently was obscured by the O_2 absorption. Furthermore we attempted to measure the onset of combustion by monitoring the growth of the key OH radical through the 3064 Å absorption band.

It was hoped that the time-resolved traces of the 2260 Å band of NO and the nearly O_2-smoke continuum (say 2240 Å) would appear as in Figure 39.

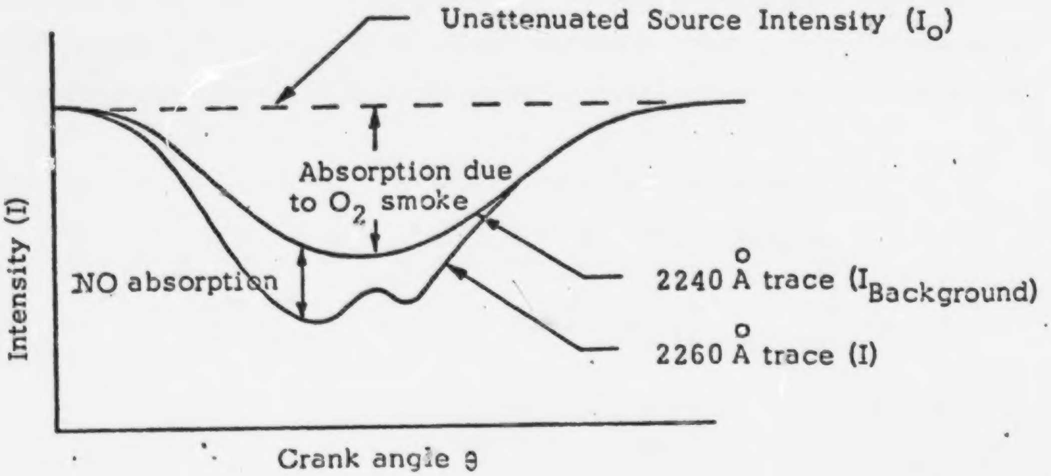

Figure 39

EXPECTED ABSORPTION TRACES

The expression for transmitted intensity in the absence of self absorption will obey Beer's Law:

$$\left.\begin{aligned} \frac{I}{I_{Back.}} &= 1 - \alpha_{NO} = \exp\left[k(X_{NO}, P)\, X_{NO}\, \ell\right] \\ \frac{I_{Back.}}{I_o} &= 1 - \alpha_{Back.} \end{aligned}\right\} \text{where } I,\ I_{Back.},\ \text{and } I_o \text{ are defined in Figure 39}$$

Combining these, we define α_{Total}:

$$\frac{I}{I_o} = \exp(-kX_{NO}\ell)(1-\alpha_{\mathrm{Back.}}) = 1 - \alpha_{\mathrm{Total}}$$

$$\frac{1 - \alpha_{\mathrm{Total}}}{1 - \alpha_{\mathrm{Back.}}} = \exp(-kX_{NO}\ell)$$

One only need calibrate or predict k (cm^{-1}) to solve for X_{NO}.

2. Experimental Technique

Large uncooled windows were developed and used with both open and divided chambers (the experience with windows is documented in Appendix G). After establishing optical access to the flame of an operating prechamber engine, the modulated UV spectroscopic system shown in Figure 40 was set up.

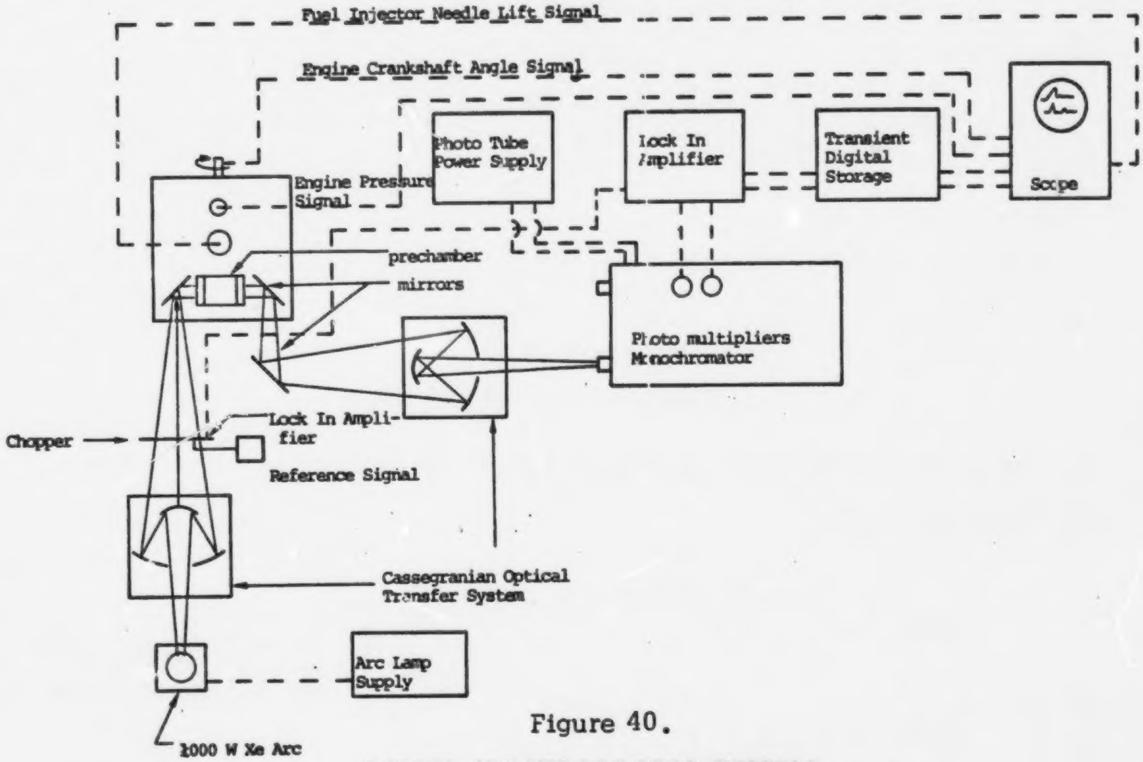
Fuel Injector Needle Lift Signal
Engine Crankshaft Angle Signal
Photo Tube Power Supply
Lock In Amplifier
Transient Digital Storage
Scope
Engine Pressure Signal
prechamber
mirrors
Photo multipliers Monochromator
Chopper
Lock In Amplifier
Reference Signal
Cassegranian Optical Transfer System
Arc Lamp Supply
1000 W Xe Arc

Figure 40.

DIESEL SPECTROSCOPIC SYSTEM

3. UV-Absorption Results

Twenty-second intervals of fuel injection were run with motoring in between these intervals to clean up the windows. Signal strength at the beginning of each interval was 5 volts over a 5Å spectral window. Measurements taken at 2220 Å (background) and 2265 Å (NO band) are reproduced in Figure 41.

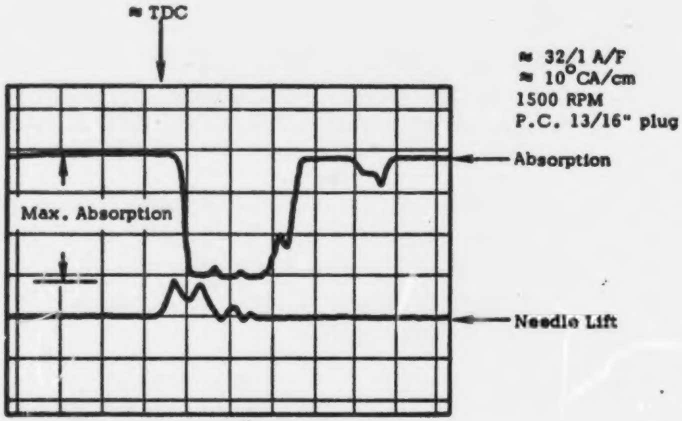

Case (a) λ = 2265Å (NO band max.)

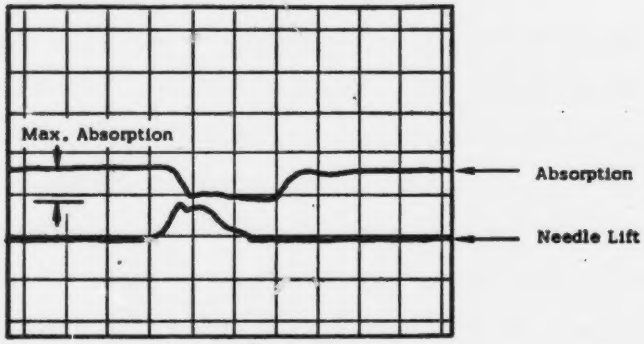

Case (b) λ = 2220Å (Background)

Figure 41.

Salient features of the traces are as follows:

(i) Absorption begins upon needle lift (± 1°CA) and diminishes about 35°ATDC. Absorption signal width is only 30°CA (indicating absorption is combustion related).

(ii) Absorption is optically thick, giving only about 5% transmissivity over the 10 to 20°CA wide peak. This prohibits detecting the NO bands by the method shown in Figure 39.

(iii) Shape of absorption trace includes a "notch". This "notch" is due to emission, as discussed below. The Xenon arc lamp was turned off and emission observed.

(iv) The absorption is diffuse, i.e. has no band structure over the 2200 - 2400 Å region. This was demonstrated by spectroscopic plates taken through a chopper phased to allow only the TDC-30°CA ATDC interval to reach the spectrometer.

(v) When the intake air was doctored with pure NO so that the mixture contained 3000 ppm NO, the peak transmissivity remained at about 5%; however, the absorption began earlier (rise time 5°CA instead of 2°CA to peak value).

(vi) Absorption histories differ for different alignments of the Xenon arc beam through the prechamber. For certain alignments, a secondary absorption 180° ATDC can be observed.

Based on the 95% absorption described in items (ii), (iv), and (v), it can be inferred that nitric oxide cannot be observed by UV absorption in the present prechamber engine. Because the optical depth is so great (item ii), the rise and fall of species concentration X cannot be detected. Since absorption goes as $A \sim 1 - \exp(-kX\ell)$, when the product $k\ell$ is sufficiently large, $A \approx 1$ practically independent of X. There are no changes in A from which to deduce changes in X. There are at least three possible absorption sources which could be responsible for the interference:

(a) Photo dissociation of CO_2, as suggested by McAlevy and Cole (1973).

(b) Interference from Schumann-Runge transitions in O_2 molecules.

(c) Absorption or scattering interference by soot.

Further experimentation is necessary.

NO itself has a large optical depth $k\ell$ at these pressures. Table 17 gives the absorption coefficient k (cm^{-1}) at 1 atm for five γ bands of NO, along with the ratio of NO absorption to Schumann-Runge O_2 absorption.

Table 17

ABSORPTION COEFFICIENTS FOR THE γ-BANDS OF NO*

Fractional Absorption for ℓ=4cm, P=5atm	γ Bands of NO	k cm^{-1}	$[\alpha_{NO}/\alpha_{O_2}]$
97%	(2,0) 2047 Å	17	2
98%	(1,0) 2153	20	4
86%	(0,0) 2262	12	3
50%	(0,1) 2365	3.5	3
15%	(0,2) 2465	0.6	2

---

*Absorption strengths k taken from Golden (1967).

Perhaps more serious is the lack of band structure (item iv), without which it will be impossible to subtract the banded NO absorption from the background absorption. Diedrichsen and Wolfhard (1956) observed the γ bands of NO at high pressure to become quite diffuse even at 20 atm; the pressures encountered here are two or three times higher. These two difficulties would plague an investigator who had comparable absorption from NO and other species, which we call the "background". However, from item (v) it would appear that NO absorption is quite insignificant compared to the background.

4. UV Emission Results

The remaining items (i), (iii), and (vi) led us to use emission spectroscopy. We observed a banded emission, with the wavelength structure recorded in Figure 42, which begins about 2 to 3°CA prior to the "spike" seen in the pressure trace, and falls off with pressure (see Figure 43). Some of the possible emitters are as follows:

Figure 42

OBSERVED EMISSION FROM PC-DIESEL ENGINE

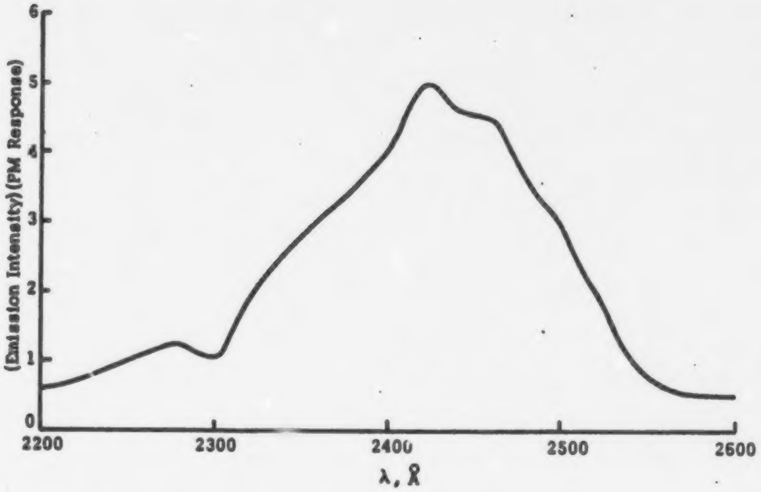

Figure 43

CORRELATION OF DIESEL EMISSION
WITH PRESSURE

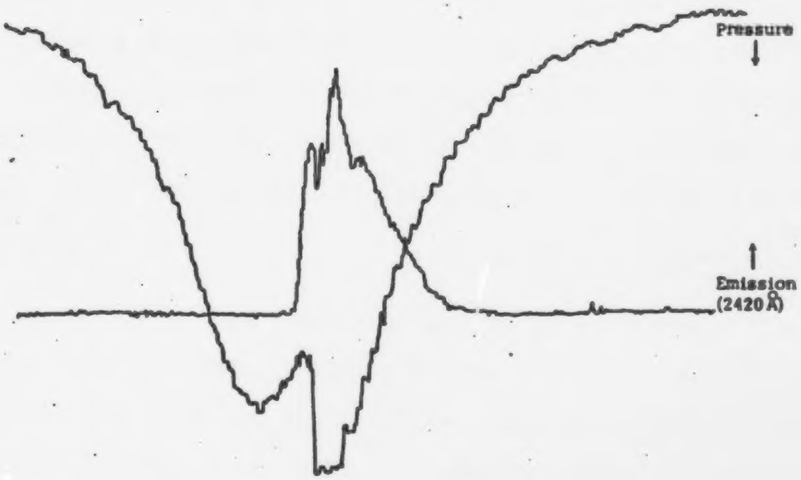

Conditions:

Engine PC - 17:1
1500 RPM
A/F = 32
Volume Ratio 25%

C_2H_2 A - X band system (2400-2500 Å at high temperature)*
OH (3,0) transition of the $A^2\Sigma^+ - X^2\Pi$ band
NO (3,2) transition of the γ band (see Figure 43)
CO Cameron bands $(a^3\Pi - x'\Sigma)$

$h + H_2O \leftarrow H(^2S) + OH\ (X^2\Pi)$
$h + CO_2 \leftarrow CO + O$
} chemiluminescence, as reported by McNesby and Okabe (1964)

Again, NO may be questioned because there seemed to be no effect of adding NO to the intake air; however, the emission spectrum of NO is strongest at 2480 Å in rough agreement with Figure 44. The difficulty in using emission is that the observations are heavily weighted by what happens in the path segment nearest the observer.

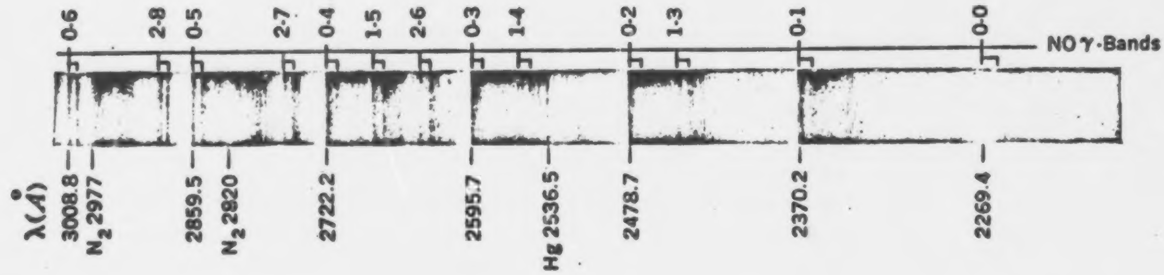

Figure 44

BAND SPECTRUM OF AN AIR-FILLED GEISSLER TUBE

Further spectroscopic tests were run on the precup engine including (1) runs at a low-NO engine setting to see if the emission or absorption traces are altered (no effect), and (2) runs with H_2O injection and observation of spectroscopic changes (no effect in UV).

---

[*] Lyn (1957) observed similarity of diesel and acetylene flame spectra, and Quader (1969) observed a similar phenomenon in the 2500-2600 Å region for preflame reactions. The C_2H_2 bands have been reported by Kistiakowsky (1931) and Woo et al.(1938).

B. DIESEL FLAME PHOTOGRAPHY

A rotating prism camera has been used to observe fuel spray, ignition, and combustion in the prechamber. Both panchromatic and color movies were taken at 5000 fps (approximately 2°CA between frames at 1500 RPM engine speed), under both Xenon backlighting and self-illumination. Magnification was approximately 1/10; an f/11 setting was adequate for ASA 800 processing of Kodak RAR 2479 film.

The qualitative information about diesel spray combustion has been correlated with measurements of chamber pressure, fuel injection, and ultraviolet emission/absorption as shown schematically in Figure 45.

The following observations may be worth noting:

Injection: The first evidence of fuel injection is a small cloud of vapor in the vicinity of the orifice. Three frames (6°CA) are required for the jet to reach the opposite wall. Absorption at 2264 Å begins during this fuel penetration stage and may be simply physical obscuration. Needle lift synchronizes well with the first appearance of fuel. As the spray crosses the chamber, the front is blunted and flattened with waves or ripples on the edges. Conceivably, fuel vapor and small droplets are shredded from these non-uniformities along the edge of the spray. As the spray is established and fuel line pressure builds up, the jet thickness decreases.

Ignition: Ignition begins immediately, but is quite localized (so that the net heat release is negative due to fuel evaporation). Visible emission is observed to emanate from the edges of the spray at the base. This implies that the chemical delay time is negligible and the time required to obtain burning is simply the mixing time for molecular contact of fuel and air. The flame propagates from the base of the spray along the edges parallel to the jet axis. Just as the spray is completely enveloped, a separate ignition zone is often noticed at the impact region where the jet has struck the opposing wall. Emission (2300 - 2500 Å) is first noticed at this time.

Combustion: The entire chamber is engulfed with a bright orange flame one frame (2°CA) after the jet is completely enveloped. This point corresponds precisely to the sudden rise in chamber pressure, often referred to as the ignition "spike". (Perhaps hot main-chamber gases are propelled into the prechamber.) Combustion is optically opaque; even the jet spray is a vague shadow on those runs where it can be seen at all. Turbulent structure is clear with eddy sizes as small as 500μ seen (1/50 chamber diameter). Wall regions are darker, possibly indicating smoke formation. A cone of ordered-motion forms about the throat entry to the main chamber; this cone has an included angle of about 120 deg. As the gases empty out and orange radiation decreases, the UV emission decreases and the pressure trace falls off.

Prechamber and direct injected movie strips are available upon request to the authors.

Figure 45

REPRESENTATION OF HIGH-SPEED PHOTOGRAPHS
OF PRECHAMBER COMBUSTION

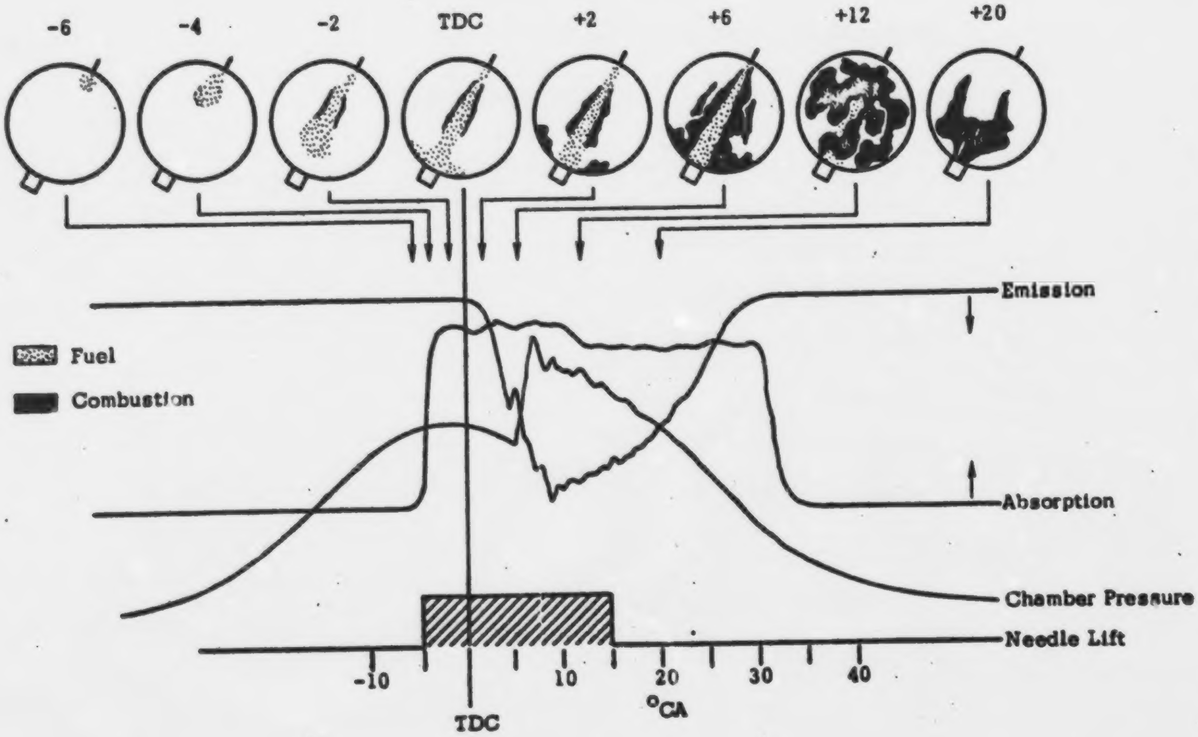

NOMENCLATURE

a,b	Coefficients
A	Pre-exponential factor in Arrhenius rate expression
A/F	Air/fuel ratio (dimensionless) by mass
C	Constant
C_p	Specific heat at constant pressure
d	Droplet size or piston bowl diameter
d_f	Fuel orifice diameter
D	Diffusion coefficient (cm^2/sec) or cylinder bore (cm)
D'	Diffusion coefficient used by CAV (cm^{-1})
DI	Direct-injected combustion chamber
E	Activation energy in Arrhenius rate expression
E_r	Entrainment coefficient of CAV model
f	Function, as for size distribution
F	Mixture ratio of NREC model
h	Specific enthalpy or piston bowl height
i	Stoichiometric oxygen to fuel ratio (by mass)
k	Rate coefficient or absorption coefficient (cm^{-1})
K	Equilibrium constant
L	Latent heat of vaporization
L/D	Length to diameter ratio
m	Mass
$\dot{m}$	Mass flow (g/sec)
M	Molecular mass
n	Coefficient
N_D	Damköhler number (see page 50)
$N_{P\acute{e}}$	Péclet number

$\dot{q}$	Rate of heat release
$\dot{q}_{loss}$	Rate of heat loss to the walls
P	Pressure
PC	Prechamber combustion geometry
Q	Heat of combustion per unit mass of fuel
r	Radius
R	Gas constant, 1.98 cal/°K mole, or piston bown radius of curvature
S	Schvab-Zeldovich variable $\overline{T} + \overline{Y}_{ox}$ or $\overline{T} + \overline{Y}_f$
t	Time
T	Temperature
v	Velocity
$V(\Theta)$	Volume of cylinder
X	Mole fraction
Y	Mass fraction
$\tilde{Y}_j$	Element mass fraction ($\tilde{Y}_j = \sum_i^{\text{All Reactions}} \mu_{ij} \frac{M_j}{M_i} Y_i$) for element j
α	Absorptivity or piston bowl angle
β	Burning rate coefficient (cm^2/sec) or piston bowl angle
γ	Gas property, C_p/C_v
δ	Expansion parameter
ϵ	Emissivity
ζ	Adjustable angle of mask position
η	r/r_f non-dimensional radius
θ	Coordinate in (r, θ, z) system
κ	Thermal conductivity
Θ	Crank angle
μ_{ij}	Number of atoms of element j in molecule of specie i
ν	Stoichiometric coefficients
ρ	Density

τ	Critical time (e.g. for ignition)
τ_c	Chemical reaction time (sec)
τ_p	Physical transport time (sec)
ϕ	Equivalence ratio (fuel/air)/(fuel/air)$_{stoich}$
$\dot{\omega}$	Reaction rate (g/sec-cc)

Subscripts and Superscripts

a	Air
co	Coolant
e	Exhaust
egr	Exhaust gas recycled
f	Fuel
fl	Flame
H_2O	Water
i	Species index
inj	Injection
ℓ	Liquid
ox	Oxygen
P	Products
PC	Prechamber
r	Reference
s	Soot
tot	Total intake flow of air plus EGR, or total chamber volume
1	start
2	end
$(\bar{\ })$	Non-dimensional, transformed, or averaged variable
∞	Far from the droplet surface, surrounding conditions
$\langle\ \rangle$	Averaged quantity

REFERENCES

Abthoff, J. and Luther, H., "The Measurement of Oxide of Nitrogen Emission from Diesel Engines and its Control by Modes of Engine Operation," Auto. Zeits. 71 (4), 1969.

Bascom, R. C., Broering, L. C. and Wulfhorst, D. E., "Design Factors That Affect Diesel Emissions," SAE Paper 710484, 1971.

Bastress, E. K., Chng, K. M., and Dix, D. M., "Models of Combustion and Nitrogen Oxide Formation in Direct and Indirect Injection Compression-Ignition Engines," SAE Paper 719053, 1971.

Bosecker, R. E. and Webster, D. F., "Precombustion Chamber Diesel Engine Emissions--A Progress Report," SAE Paper 710672, 1971.

Bowman, C. T. and Kesten, A. S., "Kinetic Modeling of Nitric Oxide Formation in Combustion Processes," presented at the Western States Section/ Combustion Institute, Fall Meeting, 1971.

Bracco, F. V., "Nitric Oxide Formation in Droplet Diffusion Flames," 14th Symposium (International) on Combustion, p. 831, The Combustion Institute, Pittsburgh, 1973.

Burke, S. P. and Schumann, T. E. W., "Diffusion Flames," Industrial Eng. Chem. 20:998, 1928.

Coffin, K. P. and Brokaw, R. S., "A General System for Calculating Burning Rates of Particles and Drops and Comparison of Calculated Rates for Carbon, Boron, Magnesium, and Isooctane," NACA TN 3929, 1957.

Diederichsen, J. and Wolfhard, H. G., "Spectrographic Examination of Gaseous Flames at High Pressure," Proc. Royal Soc. London, 1956.

Eyzat, P., "Etude Experimental et Theorique de la Formation des oxydes d'Azote Dans les motuers," Rev. de L'Inst. Franc de Petrol 22, 1967.

Fendell, F. E., "Combustion in Initially Unmixed Reactants for One-Step Reversible Chemical Kinetics," Astronautica Acta 13:183, 1967.

Godsave, G.A.E., "The Burning of Single Drops of Fuel. Part I: The Temperature Distribution and Heat Transfer in the Preflame Region," Report R-66, Natl. Gas Turbine Estab. of the Minister of Supply, London, 1950.

Golden, S. A., "Approximate Spectral Absorption Coefficients of Electronic Transitions in Diatomic Molecules," J.Q.S.R.T. 7:225, 1967.

Grigg, H. C. and Syed, M. H., "The Problem of Predicting Rate of Heat Release in Diesel Engines," SAE Paper 700503, 1970.

Hames, R. J., Merrion, D. F., and Ford, H. S., "Some Effects of Fuel Injection System Parameters on Diesel Exhaust Emissions," SAE Paper 710671, 1971.

Henein, N. A., "Combustion and Emission Formation in Fuel Sprays Injected in Swirling Air," SAE Paper 710220, 1971.

Kassoy, D. R. and Williams, F. A., "Effects of Chemical Kinetics on Near Equilibrium Combustion in Nonpremixed Systems," Physics of Fluids 11:1343, 1968.

Khan, I. M., Greeves, G. and Probert, D. M., "Prediction of Soot and Nitric Oxide Concentrations in Diesel Engine Exhaust," Inst. Mech. Engr. Paper C142/71, 1971.

Khan, I. M. and Greeves, G., "A Method of Calculating Emissions of Soot and Nitric Oxide from Diesel Engines," SAE Paper 730169, 1973.

Khan, I. M. and Wang, C.H.T., "Factors Affecting Emissions of Smoke and Gaseous Pollutants from Direct Injection Diesel Engines," Inst. Mech. Engr. Paper C151/71, 1971.

Kistiakowsky, G. B., Phys. Rev. 37, 1931.

Kotake, S. and Okazaki, T., "Evaporation and Combustion of a Fuel Droplet," Int. J. Heat Mass Transfer 12:595, 1969.

Krause, S. R., Merrion, D. F., and Green, G. L., "Effect of Inlet Air Humidity and Temperature on Diesel Exhaust Emissions," SAE Paper 730213, 1973.

Landen, E. W., "Nitrogen Oxides and Variables in Precombustion Chamber Type Diesel Engines," SAE Paper 714B, 1963.

Lyn, W. T., J. Inst. Petr. 43, 1957.

Lyn, W. T., "Calculations of the Effect of Rate of Heat Release on the Shape of Cylinder-Pressure Diagrams and Cycle Efficiency," Proc. Auto. Div. Inst. Mech. Engr. No. 1, p. 34, 1960.

Lyn, W. T., "Study of Burning Rate and Nature of Combustion in Diesel Engines," 9th SIOC, 1963.

Marshall, W. F. and Fleming, R. D., "Diesel Emissions as Related to Engine Variables and Fuel Characteristics," SAE Paper 710836, 1971.

McAlevy, R. F. III, and Cole, R. B., "Nitric Oxide Measurement in a Spark-Ignition Engine," Stevens Inst. Tech. TR #ME-RT 73001, 1973.

McConnell, G., "Oxides of Nitrogen in Diesel Engine Exhaust Gas: Their Formation and Control," Proc. Inst. Mech. Engrs. 178, 1963.

McCreath, C. G. and Chigier, N. A., "Liquid Spray Burning in the Wake of a Stabilizer Disc," 14th SIOC, 1972.

McGregor, W. K., Sieber, G. L. and Few, J. D., "Concentration of OH and NO in YJ93-GE-3 Engine Exhausts Measured in situ by Narrow-Line UV Absorption," AIAA Paper 73-506, 1973.

McNesby, J. R. and Okabe, H., "Vacuum Ultraviolet Photochemistry," Adv. in Photochem. 3, 1964.

Natarajan, R. and Brzustowski, T. A., "Some New Observations on the Combustion of Hydrocarbon Droplets at Elevated Pressures," Comb. Sci. & Tech. 2, 1970.

Newhall, H. K. and Starkman, E. S., Direct Spectroscopic Determination of Nitric Oxide in Reciprocating Engine Cylinders," SAE Paper 670122, 1967.

Parker, R. F. and Walker, J. W., "Exhaust Emission Control in Medium Swirl Rate Direct Injection Diesel Engines," Combined FCIM and Powerplant Meeting, SAE Paper 720755, 1972.

Pischinger, R. and Cartellieri, W., "Combustion System Parameters and Their Effect Upon Diesel Engine Exhaust Emissions," SAE Paper 720756, 1972.

Quader, A. A., Myers, P. S., and Uyehara, O. A., "UV Absorbance Histories and Knock in a Spark Ignited Engine," SAE Paper 690519, 1969.

Quader, A. A., Studies of Diesel-NO by UV Absorption, private communication, 1973.

Rosner, D. E., "On Liquid Droplet Combustion at High Pressures," AIAA J. 5:163, 1967.

Schmidt, R. C., Carey, A. W., and Kamo, R., "Exhaust Characteristics of the Automotive Diesel," SAE Paper 660550, 1966.

Scott, W. M., "Looking in on Diesel Combustion," SAE Paper 690002, 1969.

Seery, D. J. and Bowman, C. T., "An Experimental and Analytical Study of Methane Oxidation Behind Shock Waves," Comb. & Flame 14, 1970.

Shahed, S. M. and Newhall, H. K., "Kinetics of Nitric Oxide Formation in Propane-Air and Hydrogen-Air Diluent Flames," Comb. & Flame 17, 1971.

Shahed, S. M., Chiu, W. S. and Yumlu, V. S., "A Preliminary Model for the Formation of Nitric Oxide in Direct Injection Diesel Engines and its Application in Parametric Studies," SAE Paper 730083, 1973.

Shipinski, J., Uyehara, O. A., and Myers, P. S., "Experimental Correlation Between Rate-of-Injection and Rate-of-Heat-Release in a Diesel Engine," ASME Paper 68-DGP-11, 1968.

Spalding, D. B., ARS Journal 29:828, 1958.

Tanasawa, Y., "On the Combustion Rate of a Group of Fuel Particles," Tech. Rep. Tohoku Univ. 18:61, 1953.

Tarifa, C. S., Crespo, A., Fraga, E., and Munoz, A., "Supercritical Combustion of Fuels and Propellants in Droplets," AD 725 749, 1971.

Valdmanis, E. and Wulfhorst, D. E., "The Effects of Emulsified Fuels and Water Induction on Diesel Combustion," SAE Paper 700736, 1970.

Walder, C. J., "Reduction of Emissions from Diesel Engines," SAE Paper 730214, 1973.

Williams, F. A., Combustion Theory, Addison-Wesley, Reading, 1965.

Williams, G. C. and Sarofim, A. F., "Models for NO Formation in Combustion Processes," Task Order #3 under HEW Contract CPA 22-69-44, Final Report, 1970.

Wilson, R. P. Jr., "Combustion of Aluminum Particles in O_2/Air," Ph.D. Thesis, U.C. San Diego, 1970.

Wise, H., Lorell, J., and Wood, B. J., "The Effects of Chemical and Physical Parameters on the Burning Rate of a Liquid Droplet," 5th SIOC, 1955.

Woo, S. C., Badger, R. J., Chu, T. C., and Chih, W., J.C.P. 6, 1938.

Zeldovich, Ya. B. and Raizer, Yu. P., Physics of Shock Waves and High-Temperature Hydrodynamic Phenomena, Volume 1, Academic Press, 1966.

APPENDIX A

ESSENTIALS OF NO_x AND SMOKE FORMATION IN FLAMES

The processes of heat release and fuel spray/air mixing are not altered by slight traces of NO_x and smoke, therefore these major flame processes can be described as uncoupled to NO_x and smoke mechanisms*. The reverse is definitely not true; nitric oxide and smoke formation are quite sensitive to how mixing and heat release occur in certain parts of the flame. In mathematical terms, smoke and nitric oxide concentration are dependent variables.

In the following section we wish to review which flame conditions dominate the manufacture of NO_x and smoke. The essential mechanisms of NO_x and smoke formation are discussed insofar as current state-of-the-art permits, so that pollutant-active flame conditions can be recognized.

A. NITROGEN OXIDES

Nitric oxide is composed of two atoms, each of which is normally tightly bound in molecules such as N_2 and O_2 or in organic-nitrogen compounds in the fuel. Unless the oxygen and nitrogen bonds are broken, NO cannot form. Once free nitrogen or oxygen are formed, reactions of the following type occur:

$$O + N_2 \longrightarrow NO + \text{fragment} \quad (1)$$

$$\text{N-radical} + O_2 \longrightarrow NO + \text{fragment} \quad (2)$$

$$N + O_2 \longrightarrow NO + \text{fragment} \quad (3)$$

$$N + OH \longrightarrow NO + \text{fragment} \quad (4)$$

Pyrolysis products bearing nitrogen such as CHN and CN are critical since these fuel fragments are readily broken up to yield "loose" N atoms. However, diesel fuels contain only enough chemically-bound nitrogen to produce 30 to 50 ppm at 100% conversion.

---

*An exception is heavy smoke formation which establishes a coupling with the flame processes through increased emissivity and radiative heat loss.

The O_2 bond rather suddenly becomes breakable as the temperature rises above about 2000°K. Oxygen atoms are generated and reaction (1) occurs, followed immediately by reaction (3) or (4). This is known as the extended Zeldovich (1946) mechanism and is widely assumed to be the only NO_x mechanism of importance in the diesel flame. Once formed, nitric oxide does not readily decompose; the NO molecule is surprisingly stable as the flame gases cool. Thus we need only be concerned with NO formation mechanism.

The conditions for generating oxygen radicals are high temperature and high oxygen concentration. At low NO concentrations, the rate of NO formation can be expressed in terms of T and X_{O_2} as follows:

$$\frac{d(NO)}{dt} = 1.1 \times 10^3 (O_2)^{\frac{1}{2}} \exp(-135{,}000/RT) \quad ,$$

where (O_2) is molecular density in cm^{-3} and is related to mole fraction X_{O_2} by the expression $(O_2) = \rho X_{O_2} N_A \overline{M}^{-1}$, where N_A is Avogadro's number. Hot oxygen rich regions can be found in several distinct subzones in a diesel engine:

1. Laminar flame front around burning drop
2. Turbulent diffusion flame front
3. Hot burnt gases

These are discussed briefly below.

1. Droplet Diffusion Flame as an NO_x Source

The extent to which significant NO_x is generated in diffusion flames relative to the other candidate zones is an extremely crucial point. The flame envelope which surrounds a burning liquid fuel droplet moving with low velocity relative to the surrounding air has both the high temperature and high oxygen content needed for generating nitric oxide, as shown in Figure A-1.

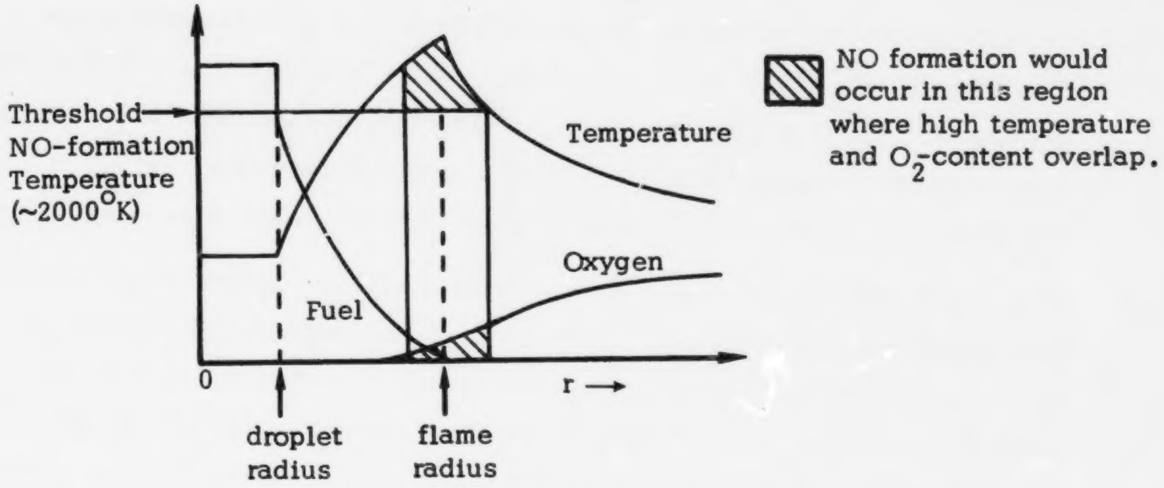

Figure A-1

Temperature and Mass Fraction Profiles
for a Burning Fuel Droplet in the
Flame Surface Approximation [Williams (1965)]

There is some question whether the oxygen content is high where the temperature is large. The peak flame temperature is near adiabatic with considerable dissociation; on the other hand, the oxygen concentration tapers off to extremely low values at the flame, so that dissociation of the product species might have to serve as the principal source of O-atoms. Further discussion of the laminar diffusion flame appears in Appendix E.

2. Turbulent Diffusion Flame Front as an NO_x-Source

In a turbulent unmixed flame, fuel vapor and air mix with hot, previously burnt gases and burn in near-stoichiometric zones. At the flame front itself the temperature approaches the adiabatic maximum; a non-equilibrium distribution of species with a temporary "oversupply" of O-atoms may occur. Thus, conditions may be quite conducive to NO formation.

Here in the flamelets we would require a local fine-scale description of the turbulent diffusion flame. At present this understanding is only available for laminar diffusion flames such as the fuel spray flames with low relative velocity (no "wake burning"). There are a number of speculative theories [Spalding (1971), Libby (1972), Bush and Fendell (1973)] and clever measurements [Batt et al. (1970)] of reaction in a turbulent eddy, but the state of knowledge does not permit a detailed model. Perhaps the most perplexing aspect is the interaction of turbulent fluctuations and chemical conversion rates.

The description of NO_x is tied closely with the description of turbulent mixing with simultaneous kinetics. This will undoubtedly receive intensive long-term research but has yet to be modeled in any satisfactory way. The prospects for including a rigorous treatment of NO_x for turbulent diffusion flames in the proposed program are admittedly quite dim.

3. Hot Combustion Products as an NO_x-Source

The zones of intense diffusion-limited burning produce a steady source of hot gases (mainly CO_2, H_2O, and N_2). This gas may be as hot as 2300 to 2600°K initially (depending on the fuel characteristics, air/fuel ratio, preheat, chamber geometry and emissivity), and this is well above the 2000°K threshold for generating O-radicals which lead to nitric oxide. However, the hot flame products are quenched by mixing with cooler gases, by radiative heat losses to the wall, and by piston expansion, so that gases leave the cylinder at about 850 to 950°K.

The NO-prediction technique in this situation consists of trying to describe the quenching process, i.e., the mean thermal histories of discrete volumes of hot gas originating from given locations in the diffusion flame zone. To this end, it is useful to know mixing patterns and heat transfer coefficients. Heat transfer coefficients can be estimated, but for confined turbulent flames, the product/air mixing should be measured, even if only in cold flow.

B. SOOT FORMATION AND OXIDATION

The presence of carbon particulates in the exhaust gas can be attributed to either excessive formation or inadequate oxidation, or usually both of these.

1. Soot Formation

Soot formation is believed to occur in fuel rich zones fed by massive evaporation such as the apex of the fuel spray, where burning is temporarily incomplete because of (1) lack of air, or (2) quenching by wall contact or cold gases. When partially decomposed fuel vapor mixes with hot combustion products, carbon-forming reactions (e.g., $C_2H_2 + O$, $H_2O + C_2$) are stimulated. This process may also occur on a smaller scale on the fuel side of a diffusion flame mantle. The mechanism of soot formation is illustrated in Figure A-2 [from Meier zu Kocker (1972)]:

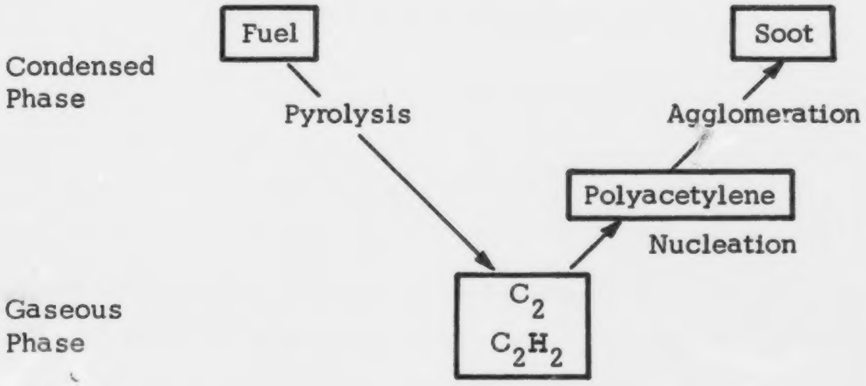

Figure A-2
Mechanism of Soot Formation

Soot formation is a compound process involving both decomposition to acetylene (believed to occur by gas-phase cracking) and subsequent formation of carbon agglomerates. The cracking step is probably rate controlling. As evidence of this, the tendency for soot formation is sensitive to the C/H ratio and boiling temperature of the fuel, as shown by Meier zu Köcker (1968) in Figure A-3.

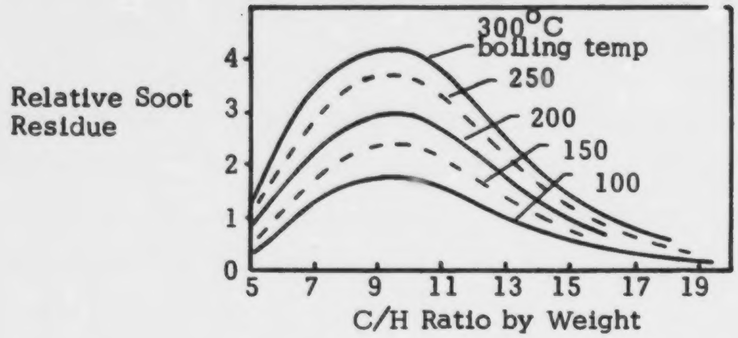

Figure A-3

Soot Formation of Some Hydrocarbons
in One-Dimensional High Pressure Combustion

The soot formation rate is often expressed in the form

$$\frac{1}{m_s}\frac{dm_s}{dt} \sim A_s \phi^{n_s} P^{m_s} \exp(-E_s/RT),$$

where m_s is the mass of soot. Typical values quoted for propane and methane are $n_s = 1$ and $E_s = 32$ to 58 kcal/mole. For diesel engines, Khan and Greeves (1973) found best agreement with emission data by using $n_s = 3$, $m_s = 1$, $E_s = 40.0$ kcal/mole , although the ϕ and T profiles in their calculations were necessarily hypothesized.

The prevention of carbon formation seems to rest on mixing considerations--on air penetration into the fuel spray pattern. In gas turbines and burners this may be accomplished by direct air jets [Bahr et al. (1969), and Faitani (1968)] or by increasing the atomizing air [Durrant (1969)] (if the burner is so equipped. In both diesels and gas turbines, better mixing can be achieved by increasing the spray cone angle [Faitani (1968), Toone (1968), Durrant (1969), and Lefebvre and

Durrant (1960)] or by increasing swirl [Bahr et al. (1969)]. It goes without saying that many of these techniques contradict the principles of delayed mixing to reduce NO_x.

2. Soot Oxidation

Some carbon soot presumably forms in the spray cone no matter what measures are taken. This is evidence by the yellow/white black-body emissions from an ordinary candle. Thus soot oxidation is also a primary goal of combustion system design. Methods to promote oxidation include increasing the temperature [Faitani (1968), Toone (1968), and Gross-Gronowski (1967)], and maintaining uniform air/fuel ratio [$\phi \epsilon (.8, 1.2)$] in the chamber.

The rate of soot combustion can be taken proportional to the exposed area of the particles, the oxygen concentration, and an Arrhenius rate term. Lee, Thring and Beer (1962) found for a laminar diffusion flame an activation energy A_c = 39.3 kcal/mole in an expression of the form:

$$\frac{dm_s}{dA\,dt} = A_c P^{m_c} \phi^{n_c} \exp(-E_c/RT)\, T^{q_c} \quad .$$

Lee also found $n_c = -1$, $m_c = 1$, $q_c = 1/2$. Tesner and Tsibulevsky (1967) also found $n_c = -1$, $m_c = 1$, $q_c = 1/2$, and $E_c = 40$ kcal/mole.

The surface regression rate (micron/sec) can be calculated from $dm_s/dA\,dt$ by using $dr/dt = -10^4(dm_s/dA\,dt)/\rho_s$. Radcliffe and Appleton (1971) have performed such calculations for soot placed in equilibrium products of combustion (C_nH_{2n}/air at 15 atm, preheat $700^\circ K$) and obtain the result shown in Figure A-4. Park and Appleton (1973) determined $dm_s/dA\,dt$ at $2500^\circ K$ as shown in Figure A-5. Measurements of soot particle sizes show the mass mean size in the .05 to .5μ range [DeCorso (1967) and Faitani (1968)], and the residence time for diesel engines is about 3 msec. For $\phi \approx 0.7$ a .1μ particle will require a burnup time of about 6 msec according to Figure A-4, and about 2 msec according to Figure A-5. These values are marginal since the duration of diesel heat release is about 4 msec. Fenimore and Jones (1967) indicate much shorter burning times. However, the conditions giving high soot burnup rates also result in maximum NO_x formation.

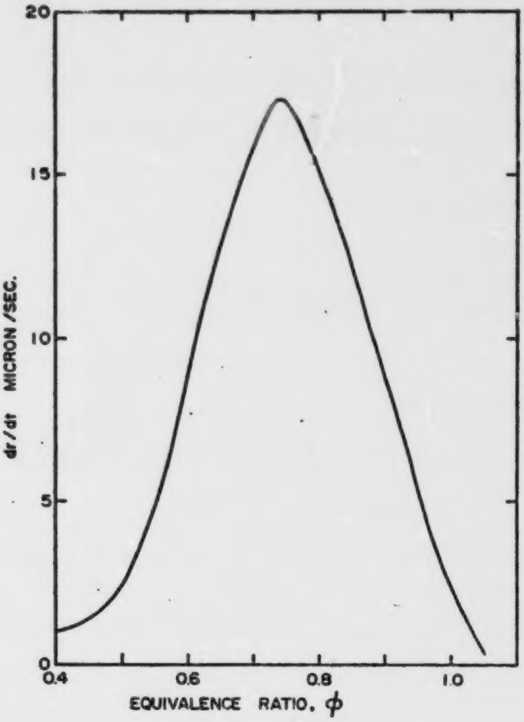

Figure A-4
Estimated Rate of Surface Recession of a Soot Particle
[Radcliffe and Appleton (1971)]

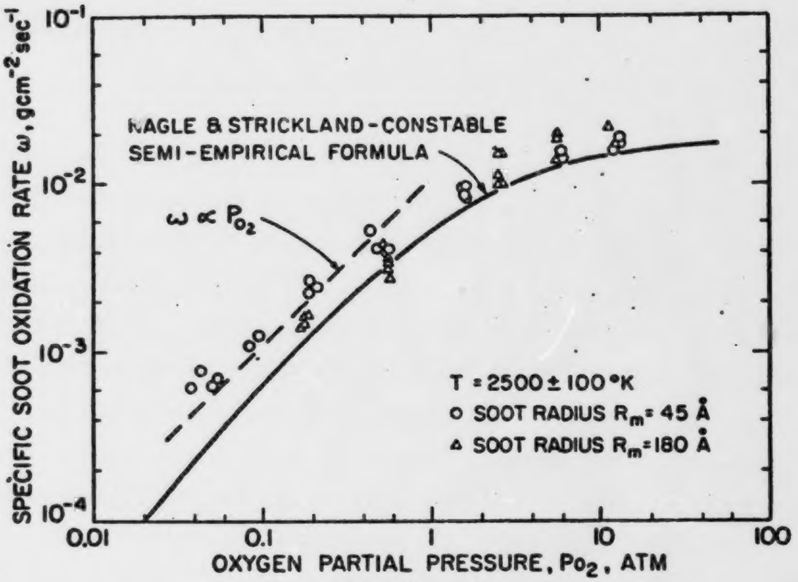

Figure A-5
Specific Soot Oxidation Rate at 2500 ± 100°K vs. Oxygen Partial Pressure
[Park and Appleton (1973)]

REFERENCES FOR APPENDIX A

Bahr, D. W., Smith, J. R. and Kenworthy, M. J., "Development of Low Smoke Emission Characteristics for Large Aircraft Turbine Engines," AIAA Paper 69-493, 1969.

Batt, R. G., Kubota, T. and Laufer, J., "Experimental Investigation of the Effect of Shear-Flow Turbulence on a Chemical Reaction," AIAA Paper No. 70-721, 1970.

Bush, W. B. and Fendell, F. E., "On Diffusion Flames in Turbulent Shear Flows," Project SQUID Technical Report TRW-7-PU, July 1973.

DeCorso, S. M., Hussey, C. E. and Ambrose, M. J., "Smokeless Combustion in Oil Burning Gas Turbines," ASME Paper 67-PWR-5, 1967.

Durrant, T., "The Reduction of Smoke from Gas Turbine Engines," presented to 9th International Aeronautical Congress, A.F.I.T.A.E., Paris, 1969.

Faitani, J. J., "Smoke Reduction in Jet Engines through Burner Design," SAE Paper 680348, 1968.

Fenimore, C. P. and Jones, G. W., "Oxidation of Soot by Hydroxyl Radicals," J. Phys. Chem. 71, 593-597, 1967.

Gross-Gronowski, L., "Smoke in Gas-Turbine Exhaust," ASME Paper 67-WA/GT-5, 1967.

Khan, I. M. and Greeves, G., "Factors Affecting Diesel Smoke and Emissions and a Method of Calculation," SAE Paper 730169, 1973.

Lee, K., Thring, M. and Beer, J., "On the Rate of Combustion of Soot in a Laminar Soot Flame," Combustion and Flame 6, 137-145, 1962.

Lefebve, A. H. and Durrant, T., "Design Characteristics Affecting Gas Turbine Combustion Performance," presented to National Aeronautical Meeting, SAE, Los Angeles, 1960.

Libby, P. A., "On Turbulent Flows with Fast Chemical Reactions. Part I: The Closure Problem," Combustion Science and Technology 6, 22-28, 1972.

Meier zu Kocker, H., Brennstoff-Chemie 49, S 193/198, 1968.

Meier zu Kocker, H., "Kinetics of Soot Formation Investigations into the Mechanism of Soot Formation in Hydrocarbon Diffusion Flames," Combustion Science and Technology 5, 219-224, 1972.

Park, C. and Appleton, J. P., "Shock-Tube Measurements of Soot Oxidation Rates," Combustion and Flame 20, 369-379, 1973.

Radcliffe, S. W. and Appleton, J. P., "Soot Oxidation Rates in Gas Turbine Engines," Combustion Science and Technology 4, 171-175, 1971.

Spalding, D. B., "Mixing and Chemical Reaction in Steady Confined Turbulent Flames," Thirteenth Symposium (International) on Combustion, 649-657, The Combustion Institute, 1971.

Tesner, P. A. and Tsibulevsky, A. M., "Gasification of Dispersed Carbon in Hydrocarbon Diffusion Flames, III. Flames of Acetylene-Hydrogen and Acetylene-Water Vapor Mixtures," Combustion, Explosion and Shock Waves 3, 1963-1967 (Translation from Fizika Gorenya i Vzryva 3, 261-267), 1967.

Toone, B., "A Review of Aero Engine Smoke Emission," Cranfield International Symposium Series 10, Combustion in Advanced Gas Turbine Systems (I. E. Smith ed.), Pergamon Press, 1968.

Zeldovich, Y. B., "The Oxidation of Nitrogen in Combustion and Explosions," Acta Physicochim. USSR 21, 577, 1946.

APPENDIX B

SINGLE CYLINDER EXPERIMENTAL TECHNIQUE

A. Design Specifications

A research engine was built specifically to provide the following features for the experimental program:

(i) Representative of medium output engines (150 to 350 HP)

(ii) Modular interchangeability to permit rapid design changes (head, prechamber volume, piston, fuel system)

(iii) Flexibility to permit operational changes while engine is firing (speed, load, timing, EGR, water injection, air temperature, air density, air swirl)

(iv) Special head design to accommodate flame diagnostics. Cylinder hold down bolts, intake and exhaust porting, valve actuating mechanisms, pencil fuel nozzle, and other hardware necessary to make an engine function are fitted subordinate to the primary objective of making combustion measurements through windows and probe access ports.

Table B-1 indicates the diesel engine types currently in use. The focus of the study is on the open chamber, direct-injection engine because of its geometric simplicity. Larger marine and locomotive engines rely on intense fuel dispersion, whereas the smaller generator and automotive engines operate at high swirl, high speed to promote mixing.

Table B-1
DOMINANT DIESEL CHAMBER TYPES

General Class	Size (HP)	Main Provision for Mixing	Air Swirl	Operating Speed	Bowl/Piston Ratio	Fuel Dispersion	Injector Pressure	No. of Holes	Representative Manufacturers	Application
Direct Injection	1000-20000	High fuel dispersion	Low	To 600 RPM	0.8	High	20,000	8-12	GM Electromotive Nordberg Cooper Bessemer Fairbanks Morse	Marine Locomotive Oil drilling
	150-350	Med. swirl; Med. fuel dispersion	Med	To 2400 RPM	0.6	Med	7,000	3-8	Cummins Detroit Diesel Mack Allis Chalmers John Deere Int. Harvester Caterpillar	Trucks Buses Tractors Construction
	5-100	High swirl; Wall impingement	High	To 4000 RPM	---	Med-Low	---	1-4	M.A.N. Deutz Hercules Perkins	Automotive, Portable generators, Mining, Material handling
Indirect Injection	10-400	Combustion-generated turbulence	Prechamber						Caterpillar Mercedes European and Japenese	Automotive Trucks Buses Tractors Construction
			Lanova/energy cell						Obsolete	
			"Poker" prechamber						McCullogh	

Single cylinder crankcases are made by Waukesha (largely for fuel test work), Labeco (for lubricant test work), AVL and BICERA (for combustion development); but none of these were felt to offer both the size (bore and stroke) and interchangeability of parts that was required to accomplish the objectives of this program.

B. Facility

The selected chamber geometry is a 5-1/2" bore, 6" stroke, with 12" connecting rod to minimize piston slap at TDC. Two cylinder head configurations were fabricated--a direct injection head and a prechamber version, hereafter referred to as the DI engine and PC engine (see Fig. 1, page 9). Only two valves are used in order to leave space in the top deck for probe access and windows. The prechamber design evolved with suggestions by J. Perez and his colleagues at Caterpillar. Piston and bowl geometry are given in Figure 1 for both types of heads. Changes in piston geometry gave compression ratios of 20:1, 17:1, and 14:1 for the DI configuration; changes in piston caps and prechamber gave four combinations of PC ratio and compression ratio, as listed in Figure 1.

Twenty drums of certified fuel were set aside under a nitrogen blanket; the laboratory report on the fuel is given in Table B-2. Fuel was transferred to the nozzle by one cylinder of an American Bosch model APE-6BB pump. Key fuel system parameters are given in Table B-3.

Table B-2
FUEL PROPERTIES

H/C (by mole, approx.)	1.7
Gravity, °API	34.5
Total sulfur, wt %	0.3
Flash point, °F	170
Pour point, °F	20
Cloud point, °F	24
Cetane number	46.7
Viscosity, CS @ 100°F	2.5
Aromatics, %	37.6
Distillation:	
Initial boiling (°F)	386
50% point (°F)	514
End point (°F)	658
Residue	1%
Total nitrogen, wt %	<0.05

Table B-3
NOMINAL FUEL SYSTEM PARAMETERS

Line pressure	10,000 psi
Valve opening pressure	3,500 psi
Duration at full load	20°
Fuel volume at full load	125 mm^3/stroke
A/F at full load	22:1 ($\phi \approx .7$)
Plunger diameter	12 mm
Cam lift	10 mm
Cam profile	#1 (tangential)
Line length	14"
Line ID	.072"

Typical histories of fuel pressure, needle lift, and chamber pressure are given in Figure B-1.Nozzle for the DI head was a Roosa pencil injector, popularly used in farm tractors, nominally with six .010" orifices at 160° cone angle. For the PC head a single pintle orifice at .37 mm^2 size with 12° cone angle was standard.

Figure B- 1
TYPICAL HISTORY OF FUEL PRESSURE,
NEEDLE LIFT AND CHAMBER PRESSURE
(DI engine, 17:1 CR, 6 x .010" fuel orifices)

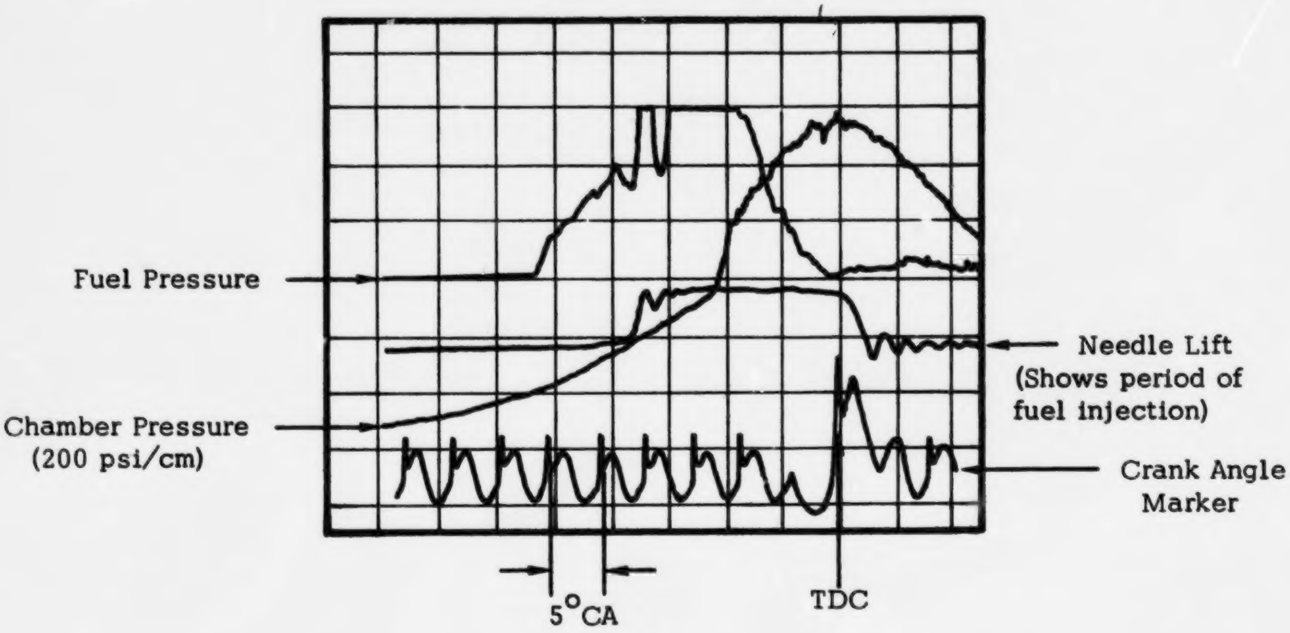

By means of changes in the fuel line length, injectors, cam profiles, fuel valve opening pressure, and plunger diameter, it was possible to study the following variations:

No. of orifices:	4, 6, 8
Orifice size (10^{-3} in.):	.008, .010, .012, .014
Rate of fuel injection:	3 to 8 $mm^3/°CA$
Pilot injection	10 to 20% of fuel injected at -40°CA
Cone angle	120° vs. 160° for DI, 8 to 12° for PC

Air was taken from the laboratory compressed air supply and heated (or cooled) after the filter and flowmeter. A throttle valve in the exhaust line was used in some tests to build up exhaust pressure to simulate turbocharging. Water mist was available at the intake, and the EGR system shown in Figure B-2 was available to supply measured amounts of exhaust gas to the intake.

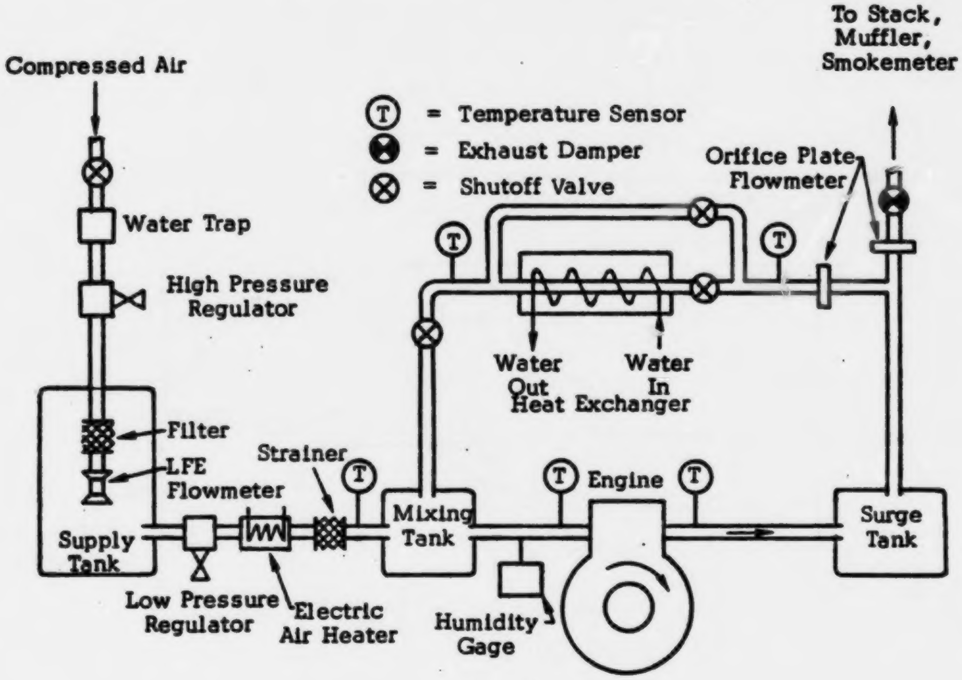
Compressed Air
To Stack, Muffler, Smokemeter
T = Temperature Sensor
● = Exhaust Damper
⊗ = Shutoff Valve
Orifice Plate Flowmeter
Water Trap
High Pressure Regulator
T
T
Water Out
Water In
Heat Exchanger
Filter
LFE Flowmeter
Strainer
T
T
Engine
T
Mixing Tank
Surge Tank
Supply Tank
Low Pressure Regulator
Electric Air Heater
Humidity Gage

Figure B-2
AIR SYSTEM PROVIDING FOR EGR

When introducing EGR, fuel flow was not adjusted to compensate for the displaced intake airflow. Although this procedure caused the A/F parameter (equivalence ratio)* to vary with % EGR, this method permitted comparison with past EGR studies, was simple, and also gave a wider variation in oxygen mole fraction that if air were boosted or fuel reduced. It was necessary to run the intake at a slight vacuum (0.5" Hg) to insure positive flow of EGR into the intake. The state of the intake air from the compressor was not subject to significant changes in humidity during the course of the testing:

---

*Equivalence ratio is taken as $(F/A)/(F/A)_{stoic}$

humidity ranged from 17 to 33 grains/lb air (this corresponds to a ± 1.5% variation in NO emissions, according to Krause, Merrion, and Green (1973). In this manner, the state of the intake air could be controlled and varied as follows:

Water injection: $\dot{m}_{H_2O}/\dot{m}_f = 0$ to 1.0
EGR: $\dot{m}_{egr}/\dot{m}_{tot} = 0$ to 30%
Air pressure: 30 to 60" Hg
Air temperature: 100 to 200°F

Engine breathing efficiency ranged from 80% to a maximum of 87% as RPM dropped from 2100 to 1500. The slightly undersized intake valve was offset by having a larger than normal valve lift (.530").

A masked valve was used to generate swirl; rotation of the valve controlled both the sense and degree of swirl as shown in Figure B-3. The nominal swirl is measured on a standard "paddle wheel" test stand with the valve fixed in open position (.530" lift). Paddle wheel RPM is measured by a proximity transducer. The reason that the values of RPM are a factor of 5 or 10 below those often reported in the literature is that a subnormal air flow was supplied to the intake ($\Delta P = 10$" w.c.). The relative values of swirl are expected to be still valid since typically paddle wheel RPM rises nearly linearly with air flow.

A summary of the instrumentation is given in Table B-4. The sampling train is shown in Figure B-4. Stainless and teflon line was used throughout the total response time of the system was controlled by that of the oxygen analyzer (20 sec).

An automatically controlled cooling tower keeps engine and dynamometer water and oil temperatures within desired limits through a system of heat exchangers and process piping.

Figure B-3
PROVISION FOR AIR SWIRL

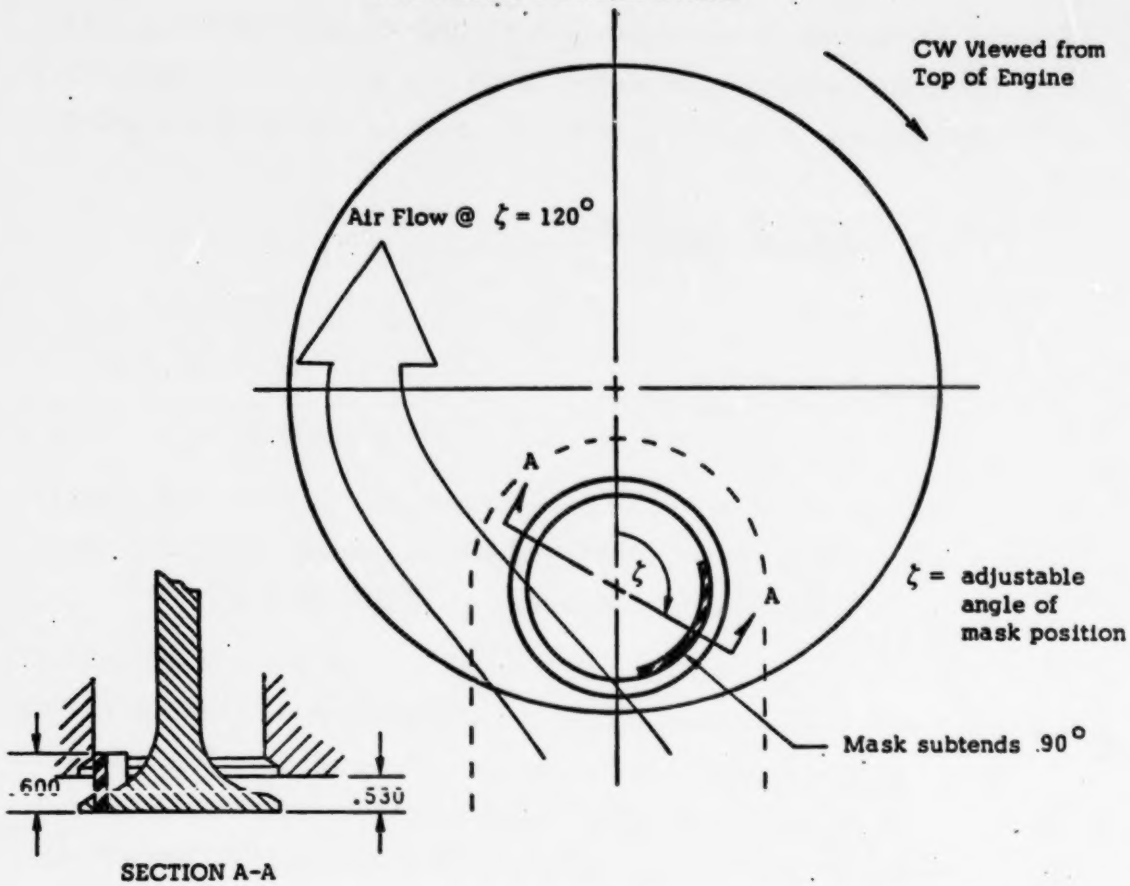

CW Viewed from Top of Engine
Air Flow @ $\zeta = 120^\circ$
A
ζ
A
ζ = adjustable angle of mask position
Mask subtends .90°
.600
.530
SECTION A-A

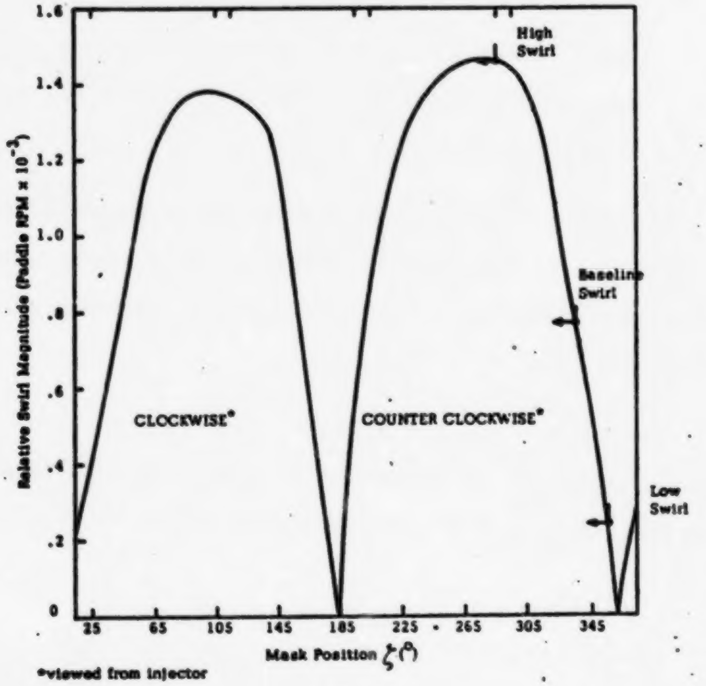

*viewed from injector

Table B-4

	Input Variable	Range Provided	Precision	Instrumentation
$\dot{m}_f$	Fuel flow	0-25 $\frac{lb}{hr}$	1% 1/4%	Rotameter Fuel scale
$\dot{m}_a$	Air flow	0-150 CFM	1 CFM	LFE
T_a	Air temp.	100-200°F	2°F	RTD
T_f	Fuel temp.	100-150°F	1°F	RTD
RPM	Speed	0-2800RPM	2 RPM	Pickup
θ	Timing	-30°to-10° BTDC	1/2° CA	Bentley-Nevada Proximity sensor
P_a	Air pressure	15-30 psia	.1%	Manometer
X_{H_2O}	Air humidity	10-100°F	2°F	Dew point sensor
$\dot{m}_{H_2O}/\dot{m}_f$	Water injection	0-1.00	.05	Rotameter
$\frac{\dot{m}_{egr}}{\dot{m}_a + \dot{m}_{egr}}$	Exhaust Recirculation	0-30%	2%	Orifices
T_{egr}	Temp. of recirc.	200-500°F	5°F	RTD
T_{cool}	Temp.of coolant (in)	0-200°F	1°F	RTD
T_{oil}	Temp. of oil (in)	0-500°F	2°F	RTD

	Output Variable	Range Observed	Precision	Instrumentation
X_{NO}	Nitric Oxide	0-3500 ppm	2%	NDIR
X_{O_2}	Oxygen	0-20%	~5%	Polarographic
X_{HC}	Hydrocarbon	0-1000ppm	1%	FID
	Smoke	0-50% Opacity	1%	PHS smoke-meter
		0-10 Bosch	.2	Bosch spot
X_{CO}	Carbon Monoxide		2%	NDIR
	BMEP	0-150ft-lb	.25%	Load cell
T_e	Exhaust temp.	0-1500°F	5°F	RTD
T_{cool}	Temp. of coolant (out)	0-200	1°F	RTD
T_{oil}	Temp. of oil (out)	0-500	2°F	RTD
P_e	Exhaust pressure	15-30 psia	± 1%	Manometer
P	Cylinder press.	0-7000 psia	10 psia	Cooled AVL transducer

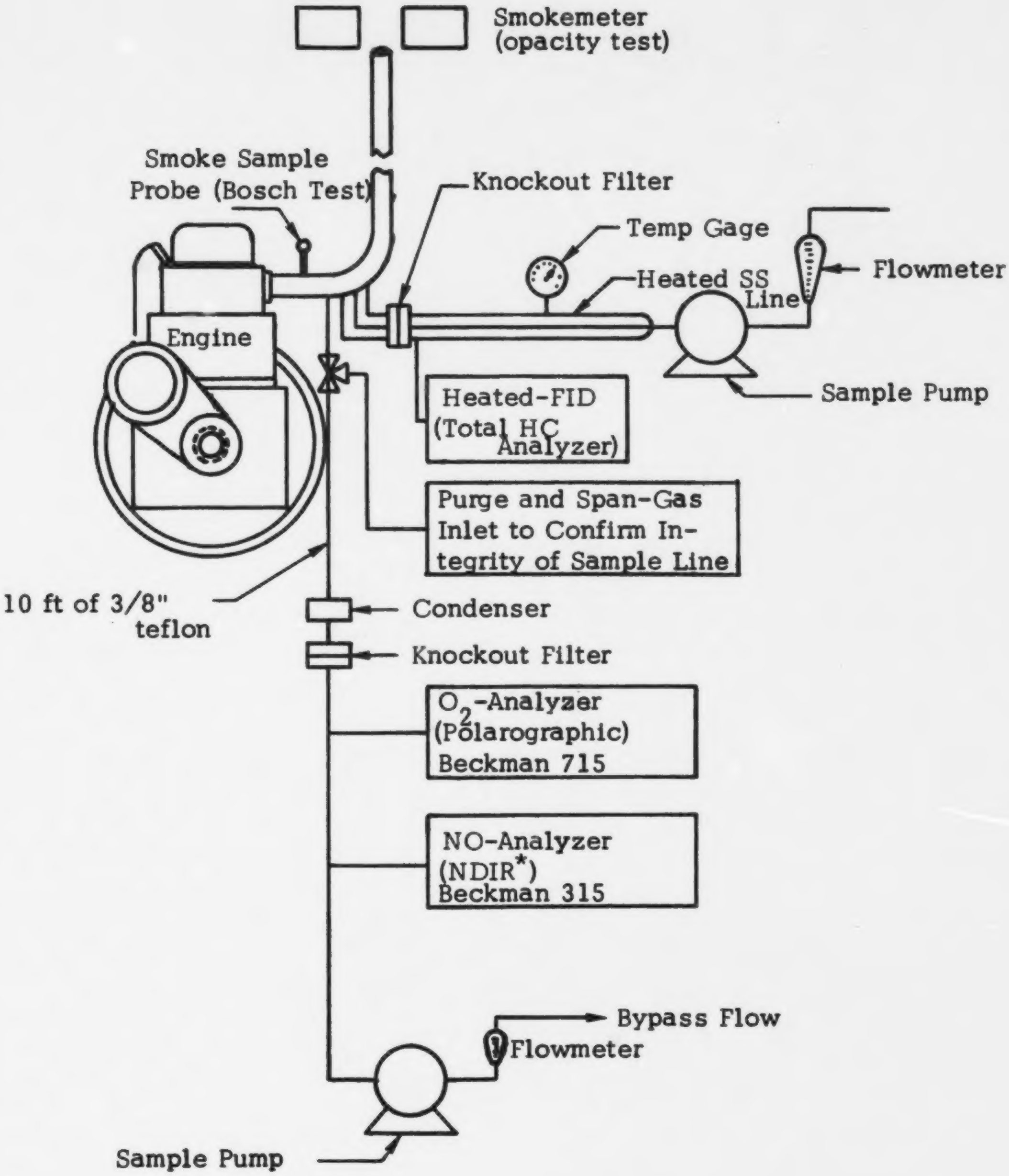
Smokemeter
(opacity test)
Smoke Sample
Probe (Bosch Test)
Knockout Filter
Temp Gage
Heated SS
Line
Flowmeter
Engine
Sample Pump
Heated-FID
(Total HC
Analyzer)
Purge and Span-Gas
Inlet to Confirm Integrity of Sample Line
10 ft of 3/8"
teflon
Condenser
Knockout Filter
O_2-Analyzer
(Polarographic)
Beckman 715
NO-Analyzer
(NDIR*)
Beckman 315
Bypass Flow
Flowmeter
Sample Pump

*Chemiluminescent analyzer available to check NO_x: normally $NO \approx NO_x$

Figure B-4
SAMPLING TRAIN

C. Procedures and Test Matrix

Reproducibility of emissions and performance behavior has been methodically tested. As one returns to a given set fuel-air ratio, timing, and engine speed, the BMEP is reproduced to ± 1%, nitric oxide emission to ± 2%, smoke level to ±.3 Bosch number. Oscilloscope traces of needle lift, combustion chamber pressure, and fuel line pressure manifest no discernable differences.

Response time or equilibration time after adjustments in speed, load or timing is 2 minutes to 90% of final reading, 5 minutes to 99% of final reading. Slowest to respond are the O_2-meter and exhaust temperatures. The rate of data acquisition was paced at about 10-15 minutes per point to allow change in operating parameter, 5 minute equilibration, and data recording. Naturally some changes in engine variables require longer times to set up (e.g., fuel injector changes).

Friction tests were performed for all engine configurations. The DI head fitted with 17:1 compression piston manifested friction losses under motoring conditions rising linearly with engine speed from 22 MEP at 700 RPM to 35 MEP at 2100 RPM.

Each engine configuration was run 20 hours break-in before testing as a standard shakedown procedure. During this time, minor oil leaks were sealed and counterbalance weights were adjusted to reduce engine vibration amplitude to below 0.5 mm. Upon first start up, the prechamber engine showed credible BMEP and specific fuel consumption, low smoke, and baseline NO_x levels (ppm) about a factor of three less than DI emission levels. This performance was unexpected for an untried chamber geometry; fortunately the customary development work was bypassed.

Emissions instrumentation was calibrated before and after testing. Spot checks of the NDIR nitric oxide analyzer against a chemiluminescent analyzer gave agreement to ± 3%, and the difference between NO and NO_x was found to be less than 5% of the NO reading.

Following the shakedown runs for each "top-end", baseline tests were run over a 20-point matrix of speed, load, and timing as shown in Figure B-5. All other runs were conducted over a simpler 4-point matrix. Both test matrices were set up to emphasize peak torque and rated speed conditions, and closely reflect the 13-Mode Cycle.

Figure B-5
TEST MATRIX

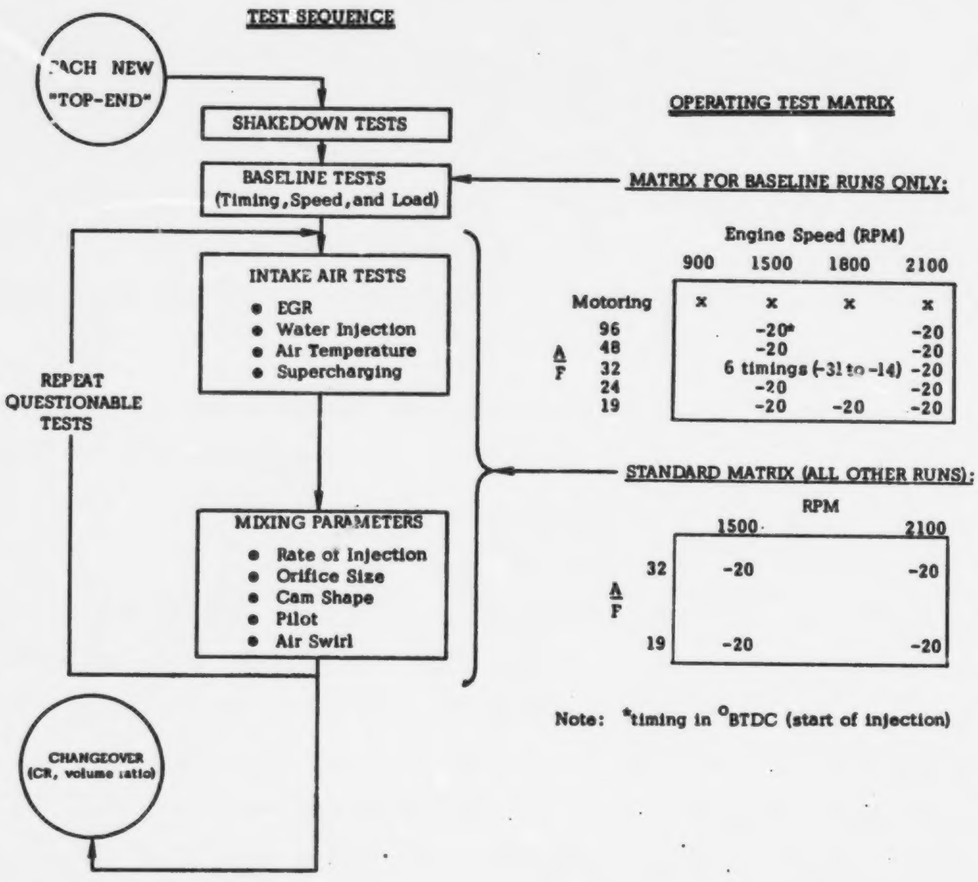
TEST SEQUENCE
EACH NEW "TOP-END"
SHAKEDOWN TESTS
BASELINE TESTS (Timing, Speed, and Load)
INTAKE AIR TESTS
• EGR
• Water Injection
• Air Temperature
• Supercharging
REPEAT QUESTIONABLE TESTS
MIXING PARAMETERS
• Rate of Injection
• Orifice Size
• Cam Shape
• Pilot
• Air Swirl
CHANGEOVER (CR, volume ratio)
OPERATING TEST MATRIX
MATRIX FOR BASELINE RUNS ONLY:
Engine Speed (RPM)
900
1500
1800
2100
Motoring
x
x
x
x
A/F
96
-20*
-20
48
-20
-20
32
6 timings (-31 to -14)
-20
24
-20
-20
19
-20
-20
-20
STANDARD MATRIX (ALL OTHER RUNS):
RPM
1500
2100
A/F
32
-20
-20
19
-20
-20

Note: *timing in °BTDC (start of injection)

The timing variations were over a range wide enough to uncover the characteristic nonlinearities in the NO vs. timing curve. Air/fuel ratio was selected over BMEP or IMEP as the "load" variable because the latter are inherently dependent variables.

In order to compare data from separate studies it was necessary to convert reported data into common units. For example, EGR percentage was converted to initial oxygen mole fraction by means of the expression:

$$X_{O_2} = .21 \left| 1 - \phi \left[CR^{-1} + EGR\,(1 - CR^{-1}) \right] \right| .$$

Swirl units were quite divergent and were handled by assigning data as low, medium or high swirl. Nitric oxide conversion formula were often necessary:

$$\text{lb } NO_x/1000 \text{ lbf} = (A/F)\,(M_{NO_2}/\overline{M})\,(\text{ppmNO}/10^6)$$

$$\text{lb } NO_x/1000 \text{ lbf} = (\text{g}NO_x/\text{BHP-hr})/(.454 \text{ BSFC})$$

$$\text{lb } NO_x/1000 \text{ lbf} = (\text{g}NO_x/\text{hr})/(.454 \text{ lbf/hr})$$

Reduced data for the effects of swirl, air density, air temperature, water injection, EGR, and timing are presented in Figures D-1 through D-6.

When A/F = 19 could not be reached because of excessive smoke or exhaust temperature (particularly during turbocharging), the minimum A/F was run instead. Additional baseline runs were repeated after about every 10 runs in order to check the validity of the baseline data (i.e., to detect any unplanned deviations or systematic drift).

Variables were changed one at a time in order to clarify the NO and smoke behavior. Runs with two effects which compensate or amplify one another would be appropriate for a low-emissions development program, but not for this study of mechanisms. In each case, extreme levels of the variables (for example, 30% EGR; a range of X5 in swirl, etc.) were selected in order to bring to the surface whatever NO and smoke changes were occurring.

The current data reduction procedure derives the following three key measurements:

(i) NO_x: Expressed in lb NO_2/1000 lb fuel, which is derived from the measured NO (ppm), the measured air/fuel ratio, known molecular weights, the C/H ratio of the fuel, and a correction for the dry measurement. No correction for humidity is applied because measured humidity variations in the compressed air are only about ± 5 grains H_2O/lb air, which corresponds to 1% correction to NO_x [Krause et al.(1973)]. Uncertainty of the NDIR measurement is ± 2%.

Values of gm NO_2/BHP-hr were obtained directly from the BSFC (lb fuel/BHP-hr) and the emission value (lb NO_2/1000 lb fuel) by applying a conversion factor of grams to pounds.

(ii) Soot: Expressed in percent opacity, as measured by a PHS meter with a shielded 3" stack, with estimated accuracy ± .2% opacity. Although Bosch units are also found in the literature and in fact are being recorded in the present program, the percent opacity manifests less scatter at low soot levels and correlates against mass concentration (mg/m^3) with less uncertainty than the Bosch unit.

(iii) ISFC: Expressed in lb/IHP-hr and derived from measured BMEP, fuel flow rate, engine speed, and FMEP which is known at each engine speed based on motoring data.

Table B-5

TEST MATRIX

TOP END → PARAMETER ↓	DI Standard	Direct Injection CR = 17/1	Direct Injection CR = 14/1	PC Standard	Prechamber CR = 17/1 $V/V_{tot} = 25\%$	Prechamber CR = 19/1 $V/V_{tot} = 15\%$	Prechamber CR = 17/1 $V/V_{tot} = 35\%$	Prechamber CR = 19/1 $V/V_{tot} = 25\%$	M.A.N.	Lanova
Baseline:		Original 27-point matrix	Revised 20-point matrix		20-point matrix	20-point matrix	20-point matrix	20-point matrix	20-point matrix	20-point matrix
Speed (RPM)		900 to 2100	900 to 2100		900 to 2100	900 to 2100	900 to 2100	900 to 2100	900 to 2100	900 to 2100
Load (A/F)		19 to 96	19 to 96		19 to 96	19 to 96	19 to 96	19 to 96	19 to 96	19 to 96
Timing (°BTDC)		-31 to -14	-31 to -14		-12 to +3	-12 to +3	-12 to +3	-12 to +3	-31 to -14	-31 to -14
Air Swirl (paddle RPM)	850	350, 1600	350, 1600	0						
Air Boost ("Hg abs)	30	50	50	30	50		50			
Air Temp (°F)	100	200		100	200					
Water Injection (W/F)	0	.5, 1.0, 1.5		0	.5, 1.0, 1.5					
EGR (%)	0	10, 20, 30	10, 20, 30	0	10, 20, 30		10, 20, 30			
No. x Fuel Orifice dia. (10^{-3} in)	6x10	8x10, 6x12, 4x14	8x10, 4x14	1 x 27	1x30, 1x34		1x30			
Fuel Orifice Area ($10^{-4} in^2$)	6	9, 12(6x12, 6x14)		6						
Fuel Rate Shape	⊓	⊿ ◺	⊿	⊓	⊿ ◺	⊿ ◺				
Fuel Pilot Injection	⊓		△⊓	⊓						
Fuel Temperature (°F)	100	200		100						
Number of Variations		17	10		12	2	5	0	0	0
Number of Variation Runs		80	36		48	8	20	0	0	0
Number of Baseline Runs		27	20		20	20	20	20	20	20
Number of baseline check runs		9	3		5	2	2	0	0	0
Number of runs repeated		8	4		5	3	3	0	0	0
Total Runs		124	63		78	33	45	20	20	20

APPENDIX C

COMPLETE DATA FROM SINGLE CYLINDER EMISSION TESTS

The following tables are a complete listing of single-cylinder data gathered for eight combustion chambers as noted in column 2 (e.g. DI-14 indicates direct injection, compression ratio = 14). The remaining table headings are given below to assist in using the listing.

VR	Volume ratio	dimensionless
PLACE	Data sheet and line number	dimensionless
PHI	Equivalence ratio	dimensionless
RPM	Engine speed	min^{-1}
TIM	Start of injection	deg. crank angle
SWIRL	Swirl level	1=low, 2=med, 3=high
PA	Air intake pressure	inches Hg
TA	Air intake temperature	$^{\circ}F$
H_2O	Water/fuel ratio	dimensionless
PCT EGR	Exhaust gas recirculation	as % of intake
ORIF DIA	Fuel orifice diameter	inches
FUEL RATE	Mean rate of injection	$mm^3/^{\circ}CA$
PILOT INJ	Pilot injection	40.10 indicates 10% at 40°CA BTDC
CONE ANGLE	Angle subtended by opposing fuel jets	deg.

AUTH	EN	VR CR	PLACE	PHI	RPM	TIM	SWIRL	PA	TA	H O 2	PCT EGR	ORFC DIA.	FUEL RATE	PILOT INJ	CONE ANGLE	PPM NOX	OPAC (SOOT)	BMEP	LB NOX/ 1K LB FUEL	OPACITY	ISFC	GNOX/BHP HR (MULTI)
RPW	DI	14	105- 6	.76	1500	-20	2	30	100	0.00	0	.010	7.0	0.00	160	1060	20.0	105.5	31.95	20.0	.370	6.58
RPW	DI	14	109- 9	.76	1500	-20	3	30	100	0.00	0	.010	7.0	0.00	160	1220	17.0	102.3	36.77	17.0	.368	7.57
RPW	DI	14	109-14	.76	1500	-20	1	30	100	0.00	0	.010	7.0	0.00	160	470	17.0	107.6	14.16	17.0	.346	2.72
RPW	DI	14	110- 4	.76	1500	-20	2	30	100	0.00	0	.014	6.9	0.00	160	1160	25.0	108.7	34.96	25.0	.363	7.03
RPW	DI	14	113- 6	.76	1500	-20	2	30	100	0.00	0	.010	5.1	0.00	160	1120	20.0	94.9	33.75	20.0	.365	7.00
RPW	DI	14	111- 3	.76	1500	-20	2	30	100	0.00	0	.010	6.5	0.00	160	1100	21.0	106.6	33.15	21.0	.367	6.76
RPW	DI	14	112- 5	.76	1500	-20	2	30	100	0.00	0	.010	7.0	40.10	160	1520	25.0	102.3	45.81	25.0	.374	9.60
RPW	DI	14	105- 3	.76	1800	-20	2	30	100	0.00	0	.010	6.2	0.00	160	1090	21.0	99.2	30.14	21.0	.363	6.37
RPW	DI	14	104-13	.76	2100	-20	2	30	100	0.00	0	.010	5.4	0.00	160	840	21.0	79.1	25.32	21.0	.378	6.09
RPW	DI	14	109- 8	.76	2100	-20	3	30	100	0.00	0	.010	5.4	0.00	160	980	30.0	78.1	29.54	30.0	.376	7.08
RPW	DI	14	109-13	.76	2100	-20	1	30	100	0.00	0	.010	5.4	0.00	160	540	18.0	86.5	16.27	18.0	.355	3.59
RPW	DI	14	110- 2	.76	2100	-20	2	30	100	0.00	0	.014	5.2	0.00	160	850	18.0	86.5	25.62	18.0	.357	5.68
RPW	DI	14	111- 4	.76	2100	-20	2	30	100	0.00	0	.010	5.2	0.00	160	1180	15.0	85.5	35.56	15.0	.362	8.02
RPW	DI	14	112- 3	.76	2100	-20	2	30	100	0.00	0	.010	5.4	40.10	160	1180	24.0	83.3	35.56	24.0	.367	8.18
RPW	DI	14	105- 7	.60	1500	-20	2	30	100	0.00	0	.010	7.0	0.00	160	1020	9.0	85.5	38.83	9.0	.346	7.80
RPW	DI	14	108- 4	.60	1500	-20	2	30	100	0.00	0	.010	7.0	0.00	160	900	10.0	81.2	34.26	10.0	.345	6.94
RPW	DI	14	108-13	.60	1500	-20	2	50	100	0.00	0	.010	7.0	0.00	160	1480	8.0	166.7	56.34	8.0	.338	9.88
RPW	DI	14	108- 5	.60	1500	-20	2	30	100	0.00	30	.010	7.0	0.00	160	220	37.0	74.9	8.38	37.0	.367	1.84
RPW	DI	14	108- 6	.60	1500	-20	2	30	100	0.00	20	.010	7.0	0.00	160	430	24.0	78.1	16.37	24.0	.355	3.44
RPW	DI	14	108- 7	.60	1500	-20	2	30	100	0.00	10	.010	7.0	0.00	160	890	15.0	80.2	33.88	15.0	.348	6.93
RPW	DI	14	104-14	.60	2100	-20	2	30	100	0.00	0	.010	5.4	0.00	160	800	13.0	68.6	30.46	13.0	.336	6.80
RPW	DI	14	106-11	.60	2100	-20	2	30	100	0.00	0	.010	5.4	0.00	160	740	15.0	66.5	28.17	15.0	.339	6.40
RPW	DI	14	109- 4	.60	2100	-20	2	50	100	0.00	0	.010	5.4	0.00	160	1110	10.0	130.8	42.26	10.0	.363	8.65
RPW	DI	14	106-14	.60	2100	-20	2	30	100	0.00	10	.010	5.4	0.00	160	610	18.0	64.4	23.22	18.0	.348	5.46
RPW	DI	14	106-13	.60	2100	-20	2	30	100	0.00	20	.010	5.4	0.00	160	390	29.0	62.2	14.85	29.0	.355	3.61
RPW	DI	14	106-12	.60	2100	-20	2	30	100	0.00	30	.010	5.4	0.00	160	260	35.0	61.2	9.90	35.0	.359	2.45
RPW	DI	14	108- 8	.45	1500	-20	2	30	100	0.00	0	.010	7.0	0.00	160	900	4.0	61.2	45.68	4.0	.315	9.04
RPW	DI	14	105- 8	.45	1500	-20	2	30	100	0.00	0	.010	7.0	0.00	160	940	6.5	64.4	47.71	6.5	.316	9.36
RPW	DI	14	106- 7	.45	1500	-31	2	30	100	0.00	0	.010	7.0	0.00	160	2210	5.0	63.3	112.18	5.0	.320	22.37
RPW	DI	14	106- 6	.45	1500	-27	2	30	100	0.00	0	.010	7.0	0.00	160	1460	5.5	65.4	74.11	5.5	.315	14.43
RPW	DI	14	106- 5	.45	1500	-23	2	30	100	0.00	0	.010	7.0	0.00	160	1060	7.0	65.4	53.80	7.0	.315	10.48
RPW	DI	14	106- 3	.45	1500	-17	2	30	100	0.00	0	.010	7.0	0.00	160	730	8.0	65.4	37.05	8.0	.318	7.27
RPW	DI	14	106- 4	.45	1500	-14	2	30	100	0.00	0	.010	7.0	0.00	160	640	8.0	63.3	32.49	8.0	.325	6.58
RPW	DI	14	109-10	.45	1500	-20	3	30	100	0.00	0	.010	7.0	0.00	160	1860	3.5	66.5	94.41	3.5	.298	17.29
RPW	DI	14	109-15	.45	1500	-20	1	30	100	0.00	0	.010	7.0	0.00	160	450	5.0	70.7	22.84	5.0	.300	4.16
RPW	DI	14	108-14	.45	1500	-20	2	50	100	0.00	0	.010	7.0	0.00	160	1350	4.0	127.7	68.52	4.0	.314	11.60
RPW	DI	14	108- 9	.45	1500	-20	2	30	100	0.00	30	.010	7.0	0.00	160	290	15.0	60.1	14.72	15.0	.319	2.96
RPW	DI	14	108-10	.45	1500	-20	2	30	100	0.00	20	.010	7.0	0.00	160	520	9.0	60.1	26.39	9.0	.320	5.34
RPW	DI	14	108-11	.45	1500	-20	2	30	100	0.00	10	.010	7.0	0.00	160	890	6.0	60.1	45.17	6.0	.317	9.05
RPW	DI	14	110- 5	.45	1500	-20	2	30	100	0.00	0	.014	6.9	0.00	160	880	9.0	64.4	44.67	9.0	.324	8.98
RPW	DI	14	111- 2	.45	1500	-20	2	30	100	0.00	0	.010	6.5	0.00	160	1440	4.0	68.6	73.09	4.0	.306	13.66
RPW	DI	14	113- 2	.45	1500	-20	2	30	100	0.00	0	.010	5.1	0.00	160	1120	7.5	63.3	56.85	7.5	.322	11.40
RPW	DI	14	112- 6	.45	1500	-20	2	30	100	0.00	0	.010	7.0	40.17	160	1370	8.0	66.5	69.54	8.0	.316	13.51
RPW	DI	14	104-15	.45	2100	-20	2	30	100	0.00	0	.010	5.4	0.00	160	800	6.0	50.6	40.61	6.0	.301	8.99
RPW	DI	14	106-15	.45	2100	-20	2	30	100	0.00	0	.010	5.4	0.00	160	810	6.0	49.6	41.11	6.0	.310	9.44
RPW	DI	14	109- 7	.45	2100	-20	3	30	100	0.00	0	.010	5.4	0.00	160	1500	5.0	50.6	76.14	5.0	.294	16.43
RPW	DI	14	109-12	.45	2100	-20	1	30	100	0.00	0	.010	5.4	0.00	160	420	5.0	52.7	21.32	5.0	.294	4.54
RPW	DI	14	108-16	.45	2100	-20	2	50	100	0.00	0	.010	5.4	0.00	160	1020	5.5	104.4	51.77	5.5	.322	9.87
RPW	DI	14	106-16	.45	2100	-20	2	30	100	0.00	30	.010	5.4	0.00	160	260	10.0	48.5	13.20	10.0	.303	2.99

AUTH	EN CR VR	PLACE	PHI	RPM	TIM	SWIRL	PA	TA	H_2O	PCT EGR	ORFC DIA	FUEL RATE	PILOT INJ	CONE ANGLE	PPM NOX	OPAC (SOOT)	BMEP	LB NOX/ 1K LB FUEL	OPACITY	ISFC	GNOX/BHP HR (MULTI)
RPW	DI-14	107- 3	.45	2100	-20	2	30	100	0.00	20	.010	5.4	0.00	160	430	7.0	47.5	21.83	7.0	.309	5.07
RPW	DI-14	108- 3	.45	2100	-20	2	30	100	0.00	10	.010	5.4	0.00	160	790	5.0	48.5	40.10	5.0	.303	9.07
RPW	DI-14	110- 3	.45	2100	-20	2	30	100	0.00	0	.014	5.2	0.00	160	680	8.0	51.7	34.52	8.0	.306	7.69
RPW	DI-14	113- 8	.45	2100	-20	2	30	100	0.00	0	.010	3.8	0.00	160	1180	6.0	52.7	59.89	6.0	.306	13.27
RPW	DI-14	111- 5	.45	2100	-20	2	30	100	0.00	0	.010	5.2	0.00	160	1190	8.0	50.6	60.40	8.0	.301	13.33
RPW	DI-14	112- 4	.45	2100	-20	2	30	100	0.00	0	.010	5.4	40.17	160	1180	7.5	50.6	59.89	7.5	.303	13.35
RPW	DI-14	106- 8	.30	1500	-20	2	30	100	0.00	0	.010	7.0	0.00	160	400	5.0	39.0	30.46	5.0	.290	6.40
RPW	DI-14	104-16	.30	2100	-20	2	30	100	0.00	0	.010	5.4	0.00	160	750	4.0	27.4	57.10	4.0	.280	15.28
RPW	DI-14	106- 9	.15	1500	-20	2	30	100	0.00	0	.010	7.0	0.00	160	360	4.5	-7.4	54.82	4.5	.495	-43.44
RPW	DI-14	105- 1	.15	2100	-20	2	30	100	0.00	0	.010	5.4	0.00	160	180	4.0	-3.2	27.41	4.0	.246	-82.50

AUTH	EN CP VR	PLACE	PHI	RPM	TIM	SWIRL	PA	TA	H_2O	PCT EGR	ORFC DIA.	FUEL RATE	PILOT INJ	CONE ANGLE	PPM NOX	OPAC (SOOT)	BMEP	LB NOX/ 1K LB FUEL	OPACITY	ISFC	GNOX/BHP HR (MULTI)
RPW	DI-17	62-10	.76	1500	-20	2	30	100	0.00	0	.010	7.0	0.00	160	1950	12.0	104.4	58.77	12.0	.343	11.20
RPW	DI-17	73- 7	.76	1500	-20	2	30	100	0.00	0	.010	7.0	0.00	160	2130	11.0	102.3	64.19	11.0	.340	12.18
RPW	DI-17	50-15	.76	1500	-20	2	30	100	0.00	0	.010	7.0	0.00	160	1750	12.0	111.8	52.74	12.0	.335	9.70
RPW	DI-17	48-12	.76	1500	-20	1	30	100	0.00	0	.010	7.0	0.00	160	2090	7.0	106.6	62.99	7.0	.327	11.40
RPW	DI-17	73- 5	.76	1500	-20	3	30	100	0.00	0	.010	7.0	0.00	160	2300	8.0	106.6	69.32	8.0	.338	12.96
RPW	DI-17	48- 5	.76	1500	-20	3	30	100	0.00	0	.010	7.0	0.00	160	3380	1.5	105.5	101.87	1.5	.312	17.63
RPW	DI-17	50- 8	.76	1500	-20	2	30	201	0.00	0	.010	7.0	0.00	160	2320	11.0	91.8	69.92	11.0	.327	13.01
RPW	DI-17	63- 5	.76	1500	-20	2	30	100	0.00	0	.012	6.3	0.00	160	1250	21.0	103.4	37.67	21.0	.352	7.37
RPW	DI-17	62-14	.76	1500	-20	2	30	100	0.00	0	.014	6.9	0.00	160	1370	25.0	100.2	41.29	25.0	.349	8.06
RPW	DI-17	64- 8	.76	1500	-20	2	30	100	0.00	0	.014	7.5	0.00	160	1480	41.0	102.3	44.60	41.0	.358	8.89
RPW	DI-17	64- 1	.76	1500	-20	2	30	100	0.00	0	.010	6.5	0.00	160	1390	20.0	107.6	41.89	20.0	.347	8.03
RPW	DI-17	71- 7	.76	1500	-20	2	30	100	0.00	0	.010	6.1	0.00	160	1430	21.0	103.4	43.10	21.0	.349	8.37
RPW	DI-17	71-13	.76	1500	-20	2	30	100	0.00	0	.010	5.1	0.00	160	1200	28.0	98.1	36.17	28.0	.363	7.38
RPW	DI-17	46-16	.76	1800	-20	2	30	100	0.00	0	.010	6.2	0.00	160	1750	9.0	97.1	52.74	9.0	.324	9.89
RPW	DI-17	47-12	.76	2100	-20	2	30	100	0.00	0	.010	5.4	0.00	160	1630	10.0	88.6	49.12	10.0	.327	9.76
RPW	DI-17	48- 7	.76	2100	-20	3	30	100	0.00	0	.010	5.4	0.00	160	2630	6.0	89.7	79.26	6.0	.311	14.96
RPW	DI-17	48-14	.76	2100	-20	1	30	100	0.00	0	.010	5.4	0.00	160	1810	5.5	80.2	54.55	5.5	.315	10.71
RPW	DI-17	50-12	.76	2100	-20	2	30	206	0.00	0	.010	5.4	0.00	160	1910	11.0	77.0	57.56	11.0	.325	11.77
RPW	DI-17	62-16	.76	2100	-20	2	30	100	0.00	0	.014	5.2	0.00	160	860	28.0	79.1	25.92	28.0	.348	5.65
RPW	DI-17	64-10	.76	2100	-20	2	30	100	0.00	0	.014	6.0	0.00	160	1340	31.0	83.3	40.39	31.0	.348	8.69
RPW	DI-17	63- 6	.76	2100	-20	2	30	100	0.00	0	.012	4.9	0.00	160	1140	22.0	84.4	34.36	22.0	.345	7.30
RPW	DI-17	64- 2	.76	2100	-20	2	30	100	0.00	0	.010	5.2	0.00	160	1110	22.0	85.5	33.45	22.0	.342	7.03
RPW	DI-17	71- 8	.76	2100	-20	2	30	100	0.00	0	.010	4.8	0.00	160	1400	15.0	81.2	42.19	15.0	.359	9.40
RPW	DI-17	71-14	.76	2100	-20	2	30	100	0.00	0	.010	3.8	0.00	160	1110	25.0	79.1	33.45	25.0	.365	7.64
RPW	DI-17	68- 2	.60	1500	-20	2	30	100	0.00	0	.010	7.0	0.00	160	1990	12.0	84.4	75.76	12.0	.307	13.47
RPW	DI-17	46- 8	.60	1500	-20	2	30	100	0.00	0	.010	7.0	0.00	160	2110	7.0	91.8	80.33	7.0	.312	14.26
RPW	DI-17	72-14	.60	1500	-20	2	30	100	0.00	0	.010	7.0	0.00	160	2050	10.5	87.6	78.04	10.5	.315	14.11
RPW	DI-17	67- 3	.60	1500	-20	2	50	100	0.00	0	.010	7.0	0.00	160	2220	11.0	168.8	84.51	11.0	.322	14.09
RPW	DI-17	66- 5	.63	1500	-20	2	60	100	0.00	0	.010	7.0	0.00	160	2030	7.5	177.2	74.06	7.5	.407	15.52
RPW	DI-17	67-13	.60	1500	-20	2	30	100	0.00	10	.010	7.0	0.00	160	1870	13.0	84.4	71.19	13.0	.307	12.66
RPW	DI-17	68- 3	.60	1500	-20	2	30	100	0.00	10	.010	7.0	0.00	160	1900	13.0	84.4	72.33	13.0	.307	12.86
RPW	DI-17	67-12	.60	1500	-20	2	30	100	0.00	20	.010	7.0	0.00	160	760	23.0	81.2	28.93	23.0	.316	5.33
RPW	DI-17	67-11	.60	1500	-20	2	30	100	0.00	30	.010	7.0	0.00	160	370	36.0	80.2	14.09	36.0	.319	2.63
RPW	DI-17	69- 8	.60	2100	-20	2	30	100	0.00	0	.010	5.4	0.00	160	1670	9.0	71.7	63.57	9.0	.306	12.48
RPW	DI-17	47-11	.60	2100	-20	2	30	100	0.00	0	.010	5.4	0.00	160	1710	4.0	69.6	65.10	4.0	.302	12.71
RPW	DI-17	67- 5	.60	2100	-20	2	50	100	0.00	0	.010	5.4	0.00	160	1620	8.5	146.6	61.67	8.5	.328	11.10
RPW	DI-17	66- 3	.63	2100	-20	2	60	100	0.00	0	.010	5.4	0.00	160	1470	7.0	177.2	53.63	7.0	.357	10.19
RPW	DI-17	41-11	.63	2100	-25	2	30	100	0.00	0	.010	5.4	0.00	160	2500	2.9	71.0	91.21	2.9	.397	23.29
RPW	DI-17	41-12	.63	2100	-25	2	30	100	.50	0	.010	5.4	0.00	160	1280	2.8	74.0	46.70	2.8	.393	11.68
RPW	DI-17	41-13	.63	2100	-25	2	30	100	1.00	0	.010	5.4	0.00	160	900	3.5	74.0	32.83	3.5	.393	8.21
RPW	DI-17	41-14	.63	2100	-25	2	30	100	1.50	0	.010	5.4	0.00	160	670	3.0	72.0	24.44	3.0	.398	6.24
RPW	DI-17	69-11	.60	2100	-20	2	30	100	0.00	10	.010	5.4	0.00	160	1460	11.0	71.7	55.58	11.0	.306	10.91
RPW	DI-17	69-10	.60	2100	-20	2	30	100	0.00	20	.010	5.4	0.00	160	790	21.0	69.6	30.07	21.0	.312	6.07
RPW	DI-17	69- 9	.60	2100	-20	2	30	100	0.00	30	.010	5.4	0.00	160	400	40.0	67.5	15.23	40.0	.318	3.16
RPW	DI-17	72-15	.45	1200	-20	2	30	100	0.00	0	.010	7.8	0.00	160	1610	7.0	64.4	81.72	7.0	.299	14.51
RPW	DI-17	47- 1	.45	1500	-20	2	30	100	0.00	0	.010	7.0	0.00	160	1710	1.0	63.3	86.80	1.0	.291	15.62
RPW	DI-17	72-13	.45	1500	-20	2	30	100	0.00	0	.010	7.0	0.00	160	1910	7.5	64.4	96.95	7.5	.297	17.69
RPW	DI-17	73- 1	.45	1500	-20	2	30	100	0.00	0	.010	7.0	0.00	160	1690	7.0	62.2	85.78	7.0	.301	15.99
RPW	DI-17	68- 5	.45	1500	-20	2	30	100	0.00	0	.010	7.0	0.00	160	1750	8.0	65.4	88.83	8.0	.292	15.89

```
    EN  VR  PLACE          RPM     SWIRL          H O  PCT ORFC FUEL PILOT CONE PPM  OPAC   BMEP    LB NOX/ OPACITY       GNOX/AHP HR
AUTH  CR            PHI         TIM        PA  TA   2  EGR DIA. RATE  INJ ANGLE NOX (SOOT)        1K LB FUEL          ISFC   (MULTI)
---- -- --  -- -- --- ---- --- --- --- --- ---- --- ---- ---- ----- ---- ---- ---- -----   ------- ------ ---- --------
RPW DI-17   65-15 .45 1500 -20   2  30 100 0.00  0  .010  7.0  0.00  160 1870  6.0  65.5    94.92    6.0  .292  16.89
RPW DI-17   65- 7 .45 1500 -20   2  30 100 0.00  0  .010  7.0  0.00  160 1800  5.5  65.4    91.37    5.5  .293  16.42
RPW DI-17   50-13 .45 1500 -20   2  30 100 0.00  0  .010  7.0  0.00  160 1670  3.7  65.4    84.77    3.7  .288  14.94
RPW DI-17   50-14 .45 1500 -14   2  30 100 0.00  0  .010  7.0  0.00  160 1150  5.9  65.4    58.37    5.9  .289  10.34
RPW DI-17   62- 9 .45 1500 -31   2  30 100 0.00  0  .010  7.0  0.00  160 2520  3.0  43.3   127.91    3.0  .376  33.00
RPW DI-17   62- 8 .45 1500 -28   2  30 100 0.00  0  .010  7.0  0.00  160 2470  3.0  49.6   125.37    3.0  .344  28.42
RPW DI-17   73- 8 .45 1500 -25   2  30 100 0.00  0  .010  7.0  0.00  160 3750  4.0  63.3   190.34    4.0  .299  35.10
RPW DI-17   48-11 .45 1500 -14   1  30 100 0.00  0  .010  7.0  0.00  160 1405  1.0  63.3    71.32    1.0  .282  12.41
RPW DI-17   48- 3 .45 1500 -20   3  30 100 0.00  0  .010  7.0  0.00  160 2540  1.2  63.3   128.93    1.2  .285  22.65
RPW DI-17   66- 8 .45 1500 -20   3  30 100 0.00  0  .010  7.0  0.00  160 3080  2.5  65.4   156.34    2.5  .291  27.82
RPW DI-17   48- 4 .45 1500 -14   3  30 100 0.00  0  .010  7.0  0.00  160 1710  1.0  63.3    86.80    1.0  .278  14.90
RPW DI-17   48-10 .45 1500 -20   1  30 100 0.00  0  .010  7.0  0.00  160 1830   .9  63.3    92.89     .9  .281  16.09
RPW DI-17   67- 4 .45 1500 -20   2  50 100 0.00  0  .010  7.0  0.00  160 1910  9.0 137.1    96.95    9.0  .295  15.22
RPW DI-17   49- 4 .45 1500 -20   2  60 100 0.00  0  .010  7.0  0.00  160 1910  3.0 176.2    96.95    3.0  .294  14.66
RPW DI-17   65- 9 .45 1500 -20   2  60 100 0.00  0  .010  7.0  0.00  160 1990  6.0 154.0   101.01    6.0  .312  16.51
RPW DI-17   49- 5 .45 1500 -14   2  60 100 0.00  0  .010  7.0  0.00  160 1350  3.0 173.0    68.52    3.0  .295  10.43
RPW DI-17   50- 7 .45 1500 -14   2  30 200 0.00  0  .010  7.0  0.00  160 1460  7.0  59.1    74.11    7.0  .291  13.56
RPW DI-17   50- 6 .45 1500 -20   2  30 202 0.00  0  .010  7.0  0.00  160 2060  6.0  58.0   104.56    6.0  .295  19.46
RPW DI-17   68- 8 .45 1500 -20   2  30 100 0.00 10  .010  7.0  0.00  160 1650  9.0  63.3    83.75    9.0  .299  15.45
RPW DI-17   68- 7 .45 1500 -20   2  30 100 0.00 20  .010  7.0  0.00  160  950 16.0  63.3    48.22   16.0  .297   8.85
RPW DI-17   68- 6 .45 1500 -20   2  30 100 0.00 30  .010  7.0  0.00  160  580 20.0  64.4    29.44   20.0  .295   5.35
RPW DI-17   54- 8 .45 1500 -20   2  30 100 0.00  0  .008  5.6  0.00  120 2010  1.0  66.5   102.02    1.0  .289  18.02
RPW DI-17   54- 9 .45 1500 -14   2  30 100 0.00  0  .008  5.6  0.00  120 1420  1.2  67.5    72.08    1.2  .286  12.55
RPW DI-17   52-13 .45 1500 -20   2  30 100 0.00  0  .012  6.3  0.00  160 1270  4.0  63.3    64.46    4.0  .287  11.43
RPW DI-17   52-14 .45 1500 -14   2  30 100 0.00  0  .012  6.3  0.00  160  825  7.0  63.3    41.88    7.0  .291   7.50
RPW DI-17   63-11 .45 1500 -28   2  30 100 0.00  0  .012  6.3  0.00  160 2320  3.0  62.2   117.76    3.0  .299  21.84
RPW DI-17   63-12 .45 1500 -31   2  30 100 0.00  0  .012  6.3  0.00  160 2720  2.5  60.1   138.06    2.5  .306  26.45
RPW DI-17   62-13 .45 1500 -20   2  30 100 0.00  0  .014  6.9  0.00  160  950 13.0  60.1    48.22   13.0  .305   9.19
RPW DI-17   63- 1 .45 1500 -28   2  30 100 0.00  0  .014  6.9  0.00  160 1710  8.0  59.1    86.80    8.0  .310  16.90
RPW DI-17   63- 2 .45 1500 -31   2  30 100 0.00  0  .014  6.9  0.00  160 2130  7.0  53.8   108.12    7.0  .333  23.19
RPW DI-17   51- 4 .45 1500 -20   2  30 100 0.00  0  .014  6.9  0.00  160 1020 11.0  63.3    51.77   11.0  .297   9.50
RPW DI-17   64- 5 .45 1500 -20   2  30 100 0.00  0  .014  7.5  0.00  160  990 17.0  62.2    50.25   17.0  .301   9.37
RPW DI-17   64- 6 .45 1500 -28   2  30 100 0.00  0  .014  7.5  0.00  160 1950  7.0  61.2    98.98    7.0  .306  18.84
RPW DI-17   64- 7 .45 1500 -31   2  30 100 0.00  0  .014  7.5  0.00  160 2390  6.5  58.0   121.31    6.5  .318  24.38
RPW DI-17   58- 1 .45 1500 -20   2  30 100 0.00  0  .010  5.1  0.00  160 1180 11.0  63.3    59.89   11.0  .300  11.10
RPW DI-17   71- 6 .45 1500 -20   2  30 100 0.00  0  .010  6.1  0.00  160 1250  9.0  61.2    63.45    9.0  .304  12.02
RPW DI-17   63-16 .45 1500 -31   2  30 100 0.00  0  .010  6.5  0.00  160 2950  2.0  63.3   149.74    2.0  .306  28.32
RPW DI-17   63-15 .45 1500 -28   2  30 100 0.00  0  .010  6.5  0.00  160 2470  2.5  66.5   125.37    2.5  .296  22.65
RPW DI-17   53-11 .45 1500 -20   2  30 100 0.00  0  .010  6.5  0.00  160 1905  2.0  63.3    96.69    2.0  .287  17.15
RPW DI-17   53-12 .45 1500 -14   2  30 100 0.00  0  .010  6.5  0.00  160 1340  3.5  63.3    68.02    3.5  .282  11.84
RPW DI-17   72-16 .45 1800 -20   2  30 100 0.00  0  .010  6.2  0.00  160 1830  5.5  59.1    92.89    5.5  .298  18.11
RPW DI-17   73- 3 .45 1800 -20   3  30 100 0.00  0  .010  6.2  0.00  160 2170  4.5  60.1   110.15    4.5  .293  21.00
RPW DI-17   47- 7 .45 2100 -20   2  30 100 0.00  0  .010  5.4  0.00  160 1670  1.0  48.5    84.77    1.0  .282  17.32
RPW DI-17   69- 6 .45 2100 -20   2  30 100 0.00  0  .010  5.4  0.00  160 1690  6.5  52.7    85.78    6.5  .283  17.13
RPW DI-17   68-11 .45 2100 -20   2  30 100 0.00  0  .010  5.4  0.00  160 1655  5.5  52.7    84.01    5.5  .283  16.78
RPW DI-17   51- 1 .45 2100 -20   2  30 100 0.00  0  .010  5.4  0.00  160 1460  3.0  52.7    74.11    3.0  .285  14.90
RPW DI-17   47- 9 .45 2100 -17   2  30 100 0.00  0  .010  5.4  0.00  160 1340  1.7  48.5    68.02    1.7  .283  13.95
RPW DI-17   47-10 .45 2100 -14   2  30 100 0.00  0  .010  5.4  0.00  160  970  2.0  48.5    49.24    2.0  .281  10.01
RPW DI-17   47- 8 .45 2100 -25   2  30 100 0.00  0  .010  5.4  0.00  160 2300   .5  46.4   116.74     .5  .286  24.57
RPW DI-17   41- 6 .40 2100 -25   2  30 100 0.00  0  .010  5.4  0.00  160 2050  1.0  40.1   117.06    1.0  .288  26.18
```

```
     EN  VR  PLACE        RPM    SWIRL         H O  PCT ORFC FUEL PILOT CONE PPM  OPAC  BMEP   LB NOX/ OPACITY      GNOX/BHP HR
AUTH  CR          PHI         TIM        PA  TA   2  EGR DIA. RATE  INJ ANGLE NOX (SOOT)       1K LB FUEL          ISFC  (MULTI)
---- -- --  -- -- --- ---- --- --- --- --- ---- --- ---- ---- --.-- ---- ---- ---- -----   ------- ------ ---- --------
RPW DI-17   48- 3 .45 2100 -20   1  30 100 0.00  0  .010  5.4  0.00  160 1710  2.1  48.5    86.80    2.1  .278  17.49
RPW DI-17   48- 6 .45 2100 -20   3  30 100 0.00  0  .010  5.4  0.00  160 2390   .6  48.5   121.31     .6  .273  24.02
RPW DI-17   66- 9 .45 2100 -20   3  30 100 0.00  0  .010  5.4  0.00  160 2860  2.2  48.5   145.17    2.2  .285  29.97
RPW DI-17   67- 6 .45 2100 -20   2  50 100 0.00  0  .010  5.4  0.00  160 1460  7.0 108.7    74.11    7.0  .310  13.36
RPW DI-17   65-11 .45 2100 -20   2  60 100 0.00  0  .010  5.4  0.00  160 1450  7.0 129.8    73.60    7.0  .322  13.30
RPW DI-17   49- 8 .45 2100 -20   2  60 100 0.00  0  .010  5.4  0.00  160 1630  3.0 139.3    82.74    3.0  .305  13.96
RPW DI-17   50-11 .45 2100 -20   2  30 205 0.00  0  .010  5.4  0.00  160 1930  2.2  45.4    97.96    2.2  .280  20.39
RPW DI-17   41- 7 .40 2100 -25   2  30 100  .50  0  .010  5.4  0.00  160 1520  1.2  40.1    86.80    1.2  .287  19.31
RPW DI-17   41- 8 .40 2100 -25   2  30 100 1.00  0  .010  5.4  0.00  160  750  1.7  40.1    42.83    1.7  .288   9.58
RPW DI-17   41- 9 .40 2100 -25   2  30 100 1.50  0  .010  5.4  0.00  160  590  1.7  40.1    33.69    1.7  .290   7.58
RPW DI-17   69- 5 .45 2100 -20   2  30 100 0.00 10  .010  5.4  0.00  160 1560  7.0  52.7    79.18    7.0  .283  15.82
RPW DI-17   69- 4 .45 2100 -20   2  30 100 0.00 20  .010  5.4  0.00  160 1020 15.0  52.7    51.77   15.0  .283  10.34
RPW DI-17   69- 3 .45 2100 -20   2  30 100 0.00 30  .010  5.4  0.00  160  660 15.0  51.7    33.50   15.0  .287   6.82
RPW DI-17   68-10 .45 2100 -20   2  30 100 0.00 30  .010  5.4  0.00  160  700 13.0  51.7    35.53   13.0  .287   7.23
RPW DI-17   54-11 .45 2100 -20   2  30 100 0.00  0  .008  4.2  0.00  120 1650  1.5  52.7    83.75    1.5  .282  16.62
RPW DI-17   53- 3 .45 2100 -20   2  30 100 0.00  0  .012  4.9  0.00  160  980  5.0  47.5    49.74    5.0  .285  10.35
RPW DI-17   62-15 .45 2100 -20   2  30 100 0.00  0  .014  5.2  0.00  160  760 11.0  46.4    38.58   11.0  .299   8.50
RPW DI-17   64- 9 .45 2100 -20   2  30 100 0.00  0  .014  6.0  0.00  160  860 13.0  48.5    43.65   13.0  .296   9.35
RPW DI-17   58- 5 .45 2100 -20   2  30 100 0.00  0  .010  3.8  0.00  160  980  7.0  49.6    49.74    7.0  .292  10.45
RPW DI-17   71- 9 .45 2100 -20   2  30 100 0.00  0  .010  4.8  0.00  160 1340  5.0  48.5    68.02    5.0  .299  14.76
RPW DI-17   54- 1 .45 2100 -20   2  30 100 0.00  0  .010  5.2  0.00  160 1520  3.0  50.6    77.15    3.0  .280  15.41

RPW DI-17   45- 8 .30 1500 -20   2  30 100 0.00  0  .010  7.0  0.00  160 1340  3.0  36.9   102.02    3.0  .281  20.67
RPW DI-17   65-14 .30 1500 -20   2  60 100 0.00  0  .010  7.0  0.00  160 1600  4.0 107.6   121.82    4.0  .298  20.08
RPW DI-17   40-12 .32 1500 -25   2  30 100 0.00  0  .010  7.0  0.00  160 1510  1.2  40.1   107.78    1.2  .295  22.34
RPW DI-17   40-13 .32 1500 -25   2  30 100  .50  0  .010  7.0  0.00  160 1510  1.0  40.1   107.78    1.0  .294  22.25
RPW DI-17   40-14 .32 1500 -25   2  30 100 1.00  0  .010  7.0  0.00  160 1040  1.2  40.1    74.23    1.2  .294  15.33
RPW DI-17   40-15 .32 1500 -25   2  30 100 1.50  0  .010  7.0  0.00  160  660  1.2  40.1    47.11    1.2  .295   9.76
RPW DI-17   41- 1 .31 1500 -15   2  30 100 0.00  0  .010  7.0  0.00  160  940  2.4  40.1    68.59    2.4  .283  13.66
RPW DI-17   41- 2 .31 1500 -15   2  30 100  .50  0  .010  7.0  0.00  160  600  2.6  40.1    43.78    2.6  .286   8.81
RPW DI-17   41- 3 .31 1500 -15   2  30 100 1.00  0  .010  7.0  0.00  160  460  2.6  40.1    33.56    2.6  .287   6.78
RPW DI-17   41- 4 .31 1500 -15   2  30 100 1.50  0  .010  7.0  0.00  160  320  2.5  40.1    23.35    2.5  .286   4.70
RPW DI-17   47- 6 .30 2100 -20   2  30 100 0.00  0  .010  5.4  0.00  160  830   .6  24.3    63.19     .6  .262  15.81
RPW DI-17   65-13 .30 2100 -20   2  60 100 0.00  0  .010  5.4  0.00  160 1270  3.5  83.3    96.69    3.5  .307  18.30

RPW DI-17   47- 5 .15 2100 -20   2  30 100 0.00  0  .010  5.4  0.00  160  200   .4 -10.5    30.46     .4  .259 -15.16
---- -- --  -- -- --- ---- --- --- --- --- ---- --- ---- ---- --.-- ---- ---- ---- -----   ------- ------ ---- --------
```

AUTH	EN CR VR	PLACE	PHI	RPM	TIM	SWIRL	PA	TA	H_2O	PCT EGR	ORFC DIA.	FUEL RATE	PILOT INJ	CONE ANGLE	PPM NOX	OPAC (SOOT)	BMEP	LB NOX/ 1K LB FUEL	OPACITY	ISFC	GNOX/BHP HR (MULTI)
RPW	PC1725	78-16	.76	15	-6	"	20	1 0	0.0	0	0. 0	7.0	0.00	12	420	12.0	90.7	12.66	12.0	.376	2.70
RPW	PC1725	80-12	.76	1500	-6	0	50	100	0.00	0	0.000	7.0	0.00	12	360	30.0	145.6	10.85	30.0	.445	2.54
RPW	PC1725	80- 4	.76	1500	-6	0	30	206	0.00	0	0.000	7.0	0.00	12	450	16.0	74.9	13.56	16.0	.386	3.09
RPW	PC1725	81-13	.76	1500	-6	0	30	100	.50	0	0.000	7.0	0.00	12	270	13.0	93.9	8.14	13.0	.366	1.68
RPW	PC1725	81-12	.76	1500	-6	0	30	100	1.00	0	0.000	7.n	0.00	12	230	3.0	90.7	6.93	3.0	.376	1.48
RPW	PC1725	81-14	.76	1500	-6	0	30	100	1.50	0	0.000	7.0	0.00	12	200	4.0	87.6	6.03	4.0	.386	1.33
RPW	PC1725	89-11	.76	1500	-6	0	30	100	0.00	0	0.000	7.0	0.00	8	350	34.0	79.1	10.55	34.0	.422	2.59
RPW	PC1725	90- 2	.76	1500	-6	0	30	100	0.00	0	0.000	7.0	0.00	30	390	30.0	77.0	11.75	30.0	.426	2.94
RPW	PC1725	78-13	.76	1800	-6	0	30	100	0.00	0	0.000	6.0	0.00	12	320	21.0	72.8	9.64	21.0	.408	2.43
RPW	PC1725	78- 6	.76	2100	-6	0	30	100	0.00	0	0.000	5.0	0.00	12	400	9.0	66.5	12.06	9.0	.393	3.08
RPW	PC1725	80- 6	.76	2100	-6	0	30	208	0.00	0	0.000	5.0	0.00	12	380	16.0	53.8	11.45	16.0	.424	3.35
RPW	PC1725	81- 8	.76	2100	-6	0	30	100	.50	0	0.000	5.0	0.00	12	270	2.0	70.7	8.14	2.0	.378	1.97
RPW	PC1725	81-10	.76	2100	-6	0	30	100	1.50	0	0.000	5.0	0.00	12	150	1.0	63.3	4.52	1.0	.405	1.21
RPW	PC1725	81- 9	.76	2100	-6	0	30	100	1.00	0	0.000	5.0	0.00	12	190	1.0	67.5	5.73	1.0	.389	1.44
RPW	PC1725	89- 9	.76	2100	-6	0	30	100	0.00	0	0.000	6.0	0.00	8	380	30.0	63.3	11.45	30.0	.418	3.16
RPW	PC1725	89-15	.76	2100	-6	0	30	100	0.00	0	0.000	5.0	0.00	30	490	14.0	65.4	14.77	14.0	.412	3.97
RPW	PC1725	84- 4	.60	1500	-6	0	30	100	0.00	0	0.000	7.0	0.00	12	470	4.5	77.0	17.89	4.5	.340	3.57
RPW	PC1725	79- 1	.60	1500	-6	0	30	100	0.00	0	0.000	7.0	0.00	12	460	4.5	77.0	17.51	4.5	.340	3.50
RPW	PC1725	84- 3	.60	1500	-6	0	30	100	0.00	10	0.000	7.0	0.00	12	430	5.0	78.1	16.37	5.0	.337	3.23
RPW	PC1725	84- 2	.60	1500	-6	0	30	100	0.00	20	0.000	7.0	0.00	12	290	5.5	77.0	11.04	5.5	.340	2.20
RPW	PC1725	84- 1	.60	1500	-6	0	30	100	0.00	30	0.000	7.0	0.00	12	130	14.0	66.5	4.95	14.0	.376	1.12
RPW	PC1725	78- 7	.60	2100	-6	0	30	100	0.00	0	0.000	5.0	0.00	12	450	2.5	58.0	17.13	2.5	.347	4.01
RPW	PC1725	83-12	.60	2100	-6	0	30	100	0.00	0	0.000	5.0	0.00	12	480	3.0	58.0	18.27	3.0	.347	4.28
RPW	PC1725	80- 9	.65	2100	-6	0	50	100	0.00	0	0.000	5.0	0.00	12	460	9.0	116.0	16.05	9.0	.410	3.76
RPW	PC1725	83-11	.60	2100	-6	0	30	100	0.00	10	0.000	5.0	0.00	12	450	3.0	59.1	17.13	3.0	.343	3.95
RPW	PC1725	83-10	.60	2100	-6	0	30	100	0.00	20	0.000	5.0	0.00	12	270	8.0	57.0	10.28	8.0	.351	2.45
RPW	PC1725	83- 9	.60	2100	-6	0	30	100	0.00	30	0.000	5.0	0.00	12	180	9.0	53.8	6.85	9.0	.363	1.72
RPW	PC1725	89- 4	.45	1200	-6	0	30	100	0.00	0	0.000	8.0	0.00	12	510	1.5	59.1	25.89	1.5	.320	4.93
RPW	PC1725	83-16	.45	1500	-6	0	30	100	0.00	0	0.000	7.0	0.00	12	520	1.5	57.0	26.39	1.5	.311	5.15
RPW	PC1725	79- 2	.45	1500	-6	0	30	100	0.00	0	0.000	7.n	0.00	12	520	2.0	60.1	26.39	2.0	.302	4.94
RPW	PC1725	79- 3	.45	1500	-9	0	30	100	0.00	0	0.000	7.0	0.00	12	670	2.5	58.0	34.01	2.5	.308	6.54
RPW	PC1725	79- 4	.45	1500	-12	0	30	100	0.00	0	0.000	7.n	0.00	12	820	3.0	55.9	41.62	3.0	.314	8.25
RPW	PC1725	79- 5	.45	1500	-3	0	30	100	0.00	0	0.000	7.0	0.00	12	480	2.0	55.9	24.36	2.0	.318	4.88
RPW	PC1725	79- 6	.45	1500	-0	0	30	100	0.00	0	0.000	7.0	0.00	12	550	1.5	54.9	27.92	1.5	.322	5.70
RPW	PC1725	80-11	.45	1500	-6	0	50	100	0.00	0	0.000	7.0	0.00	12	450	4.0	111.8	22.84	4.0	.340	4.26
RPW	PC1725	80- 3	.45	1500	-6	0	30	204	0.00	0	0.000	7.0	0.00	12	520	2.5	46.4	26.39	2.5	.316	5.52
RPW	PC1725	81-15	.45	1500	-6	0	30	100	.50	0	0.000	7.0	0.00	12	400	.5	55.9	20.30	.5	.314	4.02
RPW	PC1725	81-16	.45	1500	-6	0	30	100	1.00	0	0.000	7.n	0.00	12	250	.5	55.9	12.69	.5	.315	2.52
RPW	PC1725	82- 1	.45	1500	-6	0	30	100	1.50	0	0.000	7.0	0.00	12	170	0.0	54.9	8.63	0.0	.319	1.74
RPW	PC1725	83-15	.45	1500	-6	0	30	100	0.00	10	0.000	7.0	0.00	12	520	1.5	57.0	26.39	1.5	.311	5.16
RPW	PC1725	83-14	.45	1500	-6	0	30	100	0.00	20	0.000	7.0	0.00	12	280	2.0	57.0	14.21	2.0	.310	2.76
RPW	PC1725	83-13	.45	1500	-6	0	30	100	0.00	30	0.000	7.0	0.00	12	150	3.0	55.9	7.61	3.0	.313	1.50
RPW	PC1725	89-10	.45	1500	-6	0	30	100	0.00	0	0.000	7.n	0.00	8	540	3.0	57.0	27.41	3.0	.319	5.48
RPW	PC1725	89-16	.45	1500	-6	0	30	100	0.00	0	0.000	7.0	0.00	30	550	3.0	58.0	27.92	3.0	.317	5.52
RPW	PC1725	89- 3	.45	1800	-6	0	30	100	0.00	0	0.000	6.0	0.00	12	460	1.5	48.5	23.35	1.5	.321	5.16
RPW	PC1725	78- 8	.45	2100	-6	0	30	100	0.00	0	0.000	5.0	0.00	12	590	1.5	42.2	29.95	1.5	.301	6.72
RPW	PC1725	83- 8	.45	2100	-6	0	30	100	0.00	0	0.000	5.0	0.00	12	680	2.0	42.2	34.52	2.0	.301	7.74
RPW	PC1725	80- 8	.45	2100	-6	0	50	100	0.00	0	0.000	5.0	0.00	12	610	3.0	88.6	30.96	3.0	.341	6.39
RPW	PC1725	80- 5	.45	2100	-6	0	30	204	0.00	0	0.000	5.0	0.00	12	640	2.5	33.8	32.49	2.5	.295	7.72

AUTH	EN VR CR	PLACE	PHI	RPM	TIM	SWIRL	PA	TA	H_2O	PCT EGR	ORFC DIA.	FUEL RATE	PILOT INJ	CONE ANGLE	PPM NOX	OPAC (SOOT)	BMEP	LB NOX/ 1K LB FUEL	OPACITY	ISFC	GNOX/BHP HR (MULTI)
RPW	PC1725	81- 5	.45	2100	-6	0	30	100	.50	0	0.000	5.0	0.00	12	390	0.0	42.2	19.80	0.0	.301	4.44
RPW	PC1725	81- 6	.45	2100	-6	0	30	100	1.00	0	0.000	5.0	0.00	12	180	0.0	41.1	9.14	0.0	.305	2.09
RPW	PC1725	81- 7	.45	2100	-6	0	30	100	1.50	0	0.000	5.0	0.00	12	130	0.0	38.0	6.60	0.0	.317	1.62
RPW	PC1725	83- 7	.45	2100	-6	0	30	100	0.00	10	0.000	5.0	0.00	12	610	2.0	42.2	30.96	2.0	.301	6.95
RPW	PC1725	83- 6	.45	2100	-6	0	30	100	0.00	20	0.000	5.0	0.00	12	360	2.0	42.2	18.27	2.0	.299	4.08
RPW	PC1725	83- 5	.45	2100	-6	0	30	100	0.00	30	0.000	5.0	0.00	12	280	2.0	41.1	14.21	2.0	.304	3.25
RPW	PC1725	89- 8	.45	2100	-6	0	30	100	0.00	0	0.000	6.0	0.00	8	670	1.5	42.2	34.01	1.5	.309	7.82
RPW	PC1725	89-14	.45	2100	-6	0	30	100	0.00	0	0.000	5.0	0.00	30	550	1.5	41.1	27.92	1.5	.324	6.80
RPW	PC1725	79- 8	.30	1500	-6	0	30	100	0.00	0	0.000	7.0	0.00	12	530	1.5	31.6	40.35	1.5	.286	8.55
RPW	PC1725	78- 9	.30	2100	-6	0	30	100	0.00	0	0.000	5.0	0.00	12	460	1.5	19.0	35.02	1.5	.282	9.89
RPW	PC1725	79- 9	.15	1500	-6	0	30	100	0.00	0	0.000	7.0	0.00	12	120	2.5	0.0	18.27	2.5	1.314	46.74
RPW	PC1725	78-10	.15	2100	-6	0	30	100	0.00	0	0.000	5.0	0.00	12	100	3.0	-14.8	15.23	3.0	.308	-7.23

AUTH	EN VR CR	PLACE	PHI	RPM	TIM	SWIRL	PA	TA	H_2O	PCT EGR	ORFC DIA	FUEL RATE	PILOT INJ	CONE ANGLE	PPM NOX	OPAC (SOOT)	BMEP	LB NOX/ 1K LB FUEL	OPACITY	ISFC	GNOX/BHP HR (MULTI)
RPW	PC1735	95- 9	.76	1500	-6	0	30	100	0.00	0	0.000	7.0	0.00	12	460	13.0	93.9	13.86	13.0	.385	3.01
RPW	PC1735	97-15	.76	1500	-6	0	50	100	0.00	0	0.000	7.0	0.00	12	630	-0.0	168.8	18.99	-0.0	.405	3.98
RPW	PC1735	98- 4	.75	1500	-6	0	30	100	0.00	0	0.000	7.0	0.00	8	550	18.2	90.7	16.58	18.2	.383	3.60
RPW	PC1735	95- 7	.76	1800	-6	0	30	100	0.00	0	0.000	6.0	0.00	12	540	6.0	84.4	16.27	6.0	.382	3.71
RPW	PC1735	94- 4	.76	2100	-6	0	30	100	0.00	0	0.000	5.0	0.00	12	630	3.0	74.9	18.99	3.0	.368	4.40
RPW	PC1735	98- 5	.76	2100	-6	0	30	100	0.00	0	0.000	6.0	0.00	8	670	7.6	73.8	20.19	7.6	.373	4.77
RPW	PC1735	95-10	.60	1500	-6	0	30	100	0.00	0	0.000	7.0	0.00	12	550	1.0	82.3	20.94	1.0	.337	4.08
RPW	PC1735	94- 5	.60	2100	-6	0	30	100	0.00	0	0.000	5.0	0.00	12	730	2.5	61.2	27.79	2.5	.336	6.21
RPW	PC1735	96- 3	.45	1200	-6	0	30	100	0.00	0	0.000	8.0	0.00	12	670	.5	64.4	34.01	.5	.299	5.95
RPW	PC1735	95-11	.45	1500	-6	0	30	100	0.00	0	0.000	7.0	0.00	12	730	1.0	59.1	37.05	1.0	.315	7.25
RPW	PC1735	97-10	.45	1500	-6	0	30	100	0.00	0	0.000	7.0	0.00	12	720	1.8	60.1	36.55	1.8	.312	7.05
RPW	PC1735	97-16	.45	1500	-6	0	50	100	0.00	0	0.090	7.0	0.00	12	490	-0.0	116.0	24.87	-0.0	.328	4.44
RPW	PC1735	97- 9	.45	1500	-6	0	30	100	0.00	10	0.000	7.0	0.00	12	900	1.8	61.2	45.68	1.8	.413	11.65
RPW	PC1735	97- 8	.45	1500	-6	0	30	100	0.00	20	0.000	7.0	0.00	12	390	3.4	60.1	19.80	3.4	.311	3.81
RPW	PC1735	97- 7	.45	1500	-6	0	30	100	0.00	30	0.000	7.0	0.00	12	180	3.4	60.1	9.14	3.4	.313	1.77
RPW	PC1735	95-13	.45	1500	0	0	30	100	0.00	0	0.000	7.0	0.00	12	750	0.0	58.0	38.07	0.0	.317	7.53
RPW	PC1735	95-16	.45	1500	-12	0	30	100	0.00	0	0.000	7.0	0.00	12	1180	8.0	58.0	59.89	8.0	.318	11.90
RPW	PC1735	95-15	.45	1500	-9	0	30	100	0.00	0	0.000	7.0	0.00	12	780	2.5	60.1	39.59	2.5	.311	7.62
RPW	PC1735	95-12	.45	1500	-3	0	30	100	0.00	0	0.000	7.0	0.00	12	640	0.0	59.1	32.49	0.0	.315	6.35
HPW	PC1735	95-14	.45	1500	3	0	30	100	0.00	0	0.000	7.0	0.00	12	790	0.0	55.9	40.10	0.0	.326	8.23
RPW	PC1735	98- 3	.45	1500	-6	0	30	100	0.00	0	0.000	7.0	0.00	8	870	2.5	57.0	44.16	2.5	.317	8.78
RPW	PC1735	95- 8	.45	1800	-6	0	30	100	0.00	0	0.000	6.0	0.00	12	870	2.0	50.6	44.16	2.0	.315	9.47
RPW	PC1735	94- 6	.45	2100	-6	0	30	100	0.00	0	0.000	5.0	0.00	12	870	8.0	39.0	44.16	8.0	.329	11.13
RPW	PC1735	97- 6	.45	2100	-6	0	30	100	0.00	0	0.000	5.0	0.00	12	900	11.5	40.1	45.68	11.5	.317	10.98
RPW	PC1735	97-14	.45	2100	-6	0	50	100	0.00	0	0.000	5.0	0.00	12	960	-0.0	84.4	48.73	-0.0	.343	10.24
RPW	PC1735	97- 5	.45	2100	-6	0	30	100	0.00	10	0.000	5.0	0.00	12	870	12.5	39.0	44.16	12.5	.321	10.85
HPW	PC1735	97- 4	.45	2100	-6	0	30	100	0.00	20	0.000	5.0	0.00	12	460	13.7	40.1	23.35	13.7	.317	5.61
RPW	PC1735	97- 3	.45	2100	-6	0	30	100	0.00	30	0.000	5.0	0.00	12	230	18.2	40.1	11.67	18.2	.317	2.81
RPW	PC1735	98- 6	.45	2100	-6	0	30	100	0.00	0	0.000	6.0	0.00	8	730	17.5	33.8	37.05	17.5	.340	10.14
RPW	PC1735	96- 1	.30	1500	-6	0	30	100	0.00	0	0.000	7.0	0.00	12	690	1.0	31.6	52.53	1.0	.302	11.75
RPW	PC1735	94- 7	.30	2100	-6	0	30	100	0.00	0	0.000	5.0	0.00	12	380	9.0	12.7	28.93	9.0	.483	16.41
RPW	PC1735	96- 2	.15	1500	-6	0	30	100	0.00	0	0.000	7.0	0.00	12	150	3.0	.0	22.84	3.0	.460	20.46
RPW	PC1735	94- 8	.15	2100	-6	0	30	100	0.00	0	0.000	5.0	0.00	12	180	5.0	-13.7	27.41	5.0	.313	-16.16

AUTH	EN CR	VR PLACE	PHI	RPM	TIM	SWIRL	PA	TA	H2O	PCT EGR	ORFC DIA.	FUEL RATE	PILOT INJ	CONE ANGLE	PPM NOX	OPAC (SOOT)	BMEP	LB NOX/ 1K LB FUEL	OPACITY	ISFC	GNOX/BHP HR (MULTI)
RPW	M.A.N.	91-10	.76	1500	-21	0	30	100	0.00	0	0.000	*.0	0.00	0	1610	5.6	113.0	48.52	5.6	.328	8.80
RPW	M.A.N.	91- 8	.76	1850	-24	0	30	100	0.00	0	0.000	*.0	0.00	0	1300	6.2	106.8	39.18	6.2	.335	7.54
RPW	M.A.N.	91- 3	.76	2100	-21	0	30	100	0.00	0	0.000	*.0	0.00	0	1330	4.5	100.1	40.08	4.5	.340	8.18
RPW	M.A.N.	91-11	.60	1500	-21	0	30	100	0.00	0	0.000	*.0	0.00	0	1270	2.3	92.1	48.35	2.3	.310	8.60
RPW	M.A.N.	91- 4	.60	2100	-21	0	30	100	0.00	0	0.000	*.0	0.00	0	1280	2.1	85.7	48.73	2.1	.316	9.61
RPW	M.A.N.	92- 2	.45	1500	-21	0	30	100	0.00	0	0.000	*.0	0.00	0	940	1.2	67.1	47.71	1.2	.310	9.16
RPW	M.A.N.	91-12	.45	1500	-21	0	30	100	0.00	0	0.000	*.0	0.00	0	1080	1.2	68.9	54.82	1.2	.297	10.03
RPW	M.A.N.	91-14	.45	1500	-27	0	30	100	0.00	0	0.000	*.0	0.00	0	1750	3.6	68.9	88.83	3.6	.297	16.26
RPW	M.A.N.	91-13	.45	1500	-24	0	30	100	0.00	0	0.000	*.0	0.00	0	1500	2.0	68.9	76.14	2.0	.296	13.86
RPW	M.A.N.	92- 4	.45	1500	-18	0	30	100	0.00	0	0.000	*.0	0.00	0	730	1.6	65.3	37.05	1.6	.309	7.16
RPW	M.A.N.	92- 5	.45	1500	-15	0	30	100	0.00	0	0.000	*.0	0.00	0	560	1.6	64.2	28.42	1.6	.314	5.61
RPW	M.A.N.	91- 9	.45	1850	-21	0	30	100	0.00	0	0.000	*.0	0.00	0	1100	1.4	65.5	55.83	1.4	.293	10.62
RPW	M.A.N.	91- 5	.45	2100	-21	0	30	100	0.00	0	0.000	*.0	0.00	0	850	1.4	61.4	43.14	1.4	.304	9.07
RPW	M.A.N.	92- 6	.30	1500	-21	0	30	100	0.00	0	0.000	*.0	0.00	0	390	1.4	34.6	29.69	1.4	.316	7.28
RPW	M.A.N.	91- 6	.30	2100	-21	0	30	100	0.00	0	0.000	*.0	0.00	0	400	.9	33.5	30.46	.9	.292	7.89
RPW	M.A.N.	92- 7	.15	1500	-21	0	30	100	0.00	0	0.000	*.0	0.00	0	50	.8	-10.3	7.61	.8	1.149	-5.49
RPW	M.A.N.	91- 7	.15	2100	-21	0	30	100	0.00	0	0.000	*.0	0.00	0	90	.9	-6.4	13.70	.9	2.482	-61.60

AUTH	EN CR	VR PLACE	PHI	RPM	TIM	SWIRL	PA	TA	H2O	PCT EGR	ORFC DIA.	FUEL RATE	PILOT INJ	CONE ANGLE	PPM NOX	OPAC (SOOT)	BMEP	LB NOX/ 1K LB FUEL	OPACITY	ISFC	GNOX/BHP HR (MULTI)
RPW	LANOVA	115-14	.76	15	-20	[illegible]	30	1 0	0.0	0	0. 0	*.0	0.00	0	1350	10.0	92.7	40.69	10.0	.356	8.31
RPW	LANOVA	115-12	.76	1850	-20	0	30	100	0.00	0	0.000	*.0	0.00	0	1100	10.0	95.9	33.15	10.0	.353	6.87
RPW	LANOVA	115- 2	.76	2200	-20	0	30	100	0.00	0	0.000	*.0	0.00	0	910	7.2	93.8	27.43	7.2	.443	7.47
RPW	LANOVA	115-15	.60	1500	-20	0	30	100	0.00	0	0.000	*.0	0.00	0	1370	2.0	72.5	52.15	2.0	.347	11.01
RPW	LANOVA	115- 7	.60	2200	-20	0	30	100	0.00	0	0.000	*.0	0.00	0	870	3.8	70.4	33.12	3.8	.328	7.28
RPW	LANOVA	115-16	.45	1500	-20	0	30	100	0.00	0	0.000	*.0	0.00	0	1020	1.6	49.6	51.77	1.6	.351	12.34
RPW	LANOVA	116- 1	.45	1500	-23	0	30	100	0.00	0	0.000	*.0	0.00	0	1210	2.0	48.5	61.42	2.0	.358	15.03
RPW	LANOVA	116- 2	.45	1500	-26	0	30	100	0.00	0	0.000	*.0	0.00	0	1140	6.9	45.8	57.86	6.9	.371	14.98
RPW	LANOVA	116- 3	.45	1500	-17	0	30	100	0.00	0	0.000	*.0	0.00	0	850	1.6	50.1	43.14	1.6	.349	10.17
RPW	LANOVA	116- 4	.45	1500	-14	0	30	100	0.00	0	0.000	*.0	0.00	0	580	2.6	51.2	29.44	2.6	.345	6.83
RPW	LANOVA	115-13	.45	1850	-20	0	30	100	0.00	0	0.000	*.0	0.00	0	920	2.0	50.1	46.70	2.0	.334	11.06
RPW	LANOVA	115- 8	.45	2200	-20	0	30	100	0.00	0	0.000	*.0	0.00	0	700	3.2	49.6	35.53	3.2	.319	8.60
RPW	LANOVA	116- 5	.30	1500	-20	0	30	100	0.00	0	0.000	*.0	0.00	0	545	1.4	24.5	41.49	1.4	.365	13.78
RPW	LANOVA	115- 9	.30	2200	-20	0	30	100	0.00	0	0.000	*.0	0.00	0	305	1.6	22.4	23.22	1.6	.314	8.26

APPENDIX D

COMPILATION OF PUBLISHED DIESEL EMISSIONS DATA

Eighteen publications reporting tests of 51 engines have been compiled in order to determine what emissions behavior is representative of a wide class of engines--both trends (say, in NO vs. EGR), and variations from those trends for specific engines. In this way our single-cylinder test data could be placed in context. Only operational changes were tested for 37 of the 51 engines. Abbreviated information about the 14 more extensively tested engines (compression ratio, displacement, etc.) is listed in Table D-1, along with an indication of which of the parameters were varied.

Table D-1

PUBLISHED EMISSIONS DATA

First Author(year)	Engine#	Type	Comp. Ratio	N_{cyl}	V_{cyl}	Load	Speed	Timing	T_a	EGR	H_2O	P_a	Swirl	d_f	Rate
Pischinger (72)	3	DI	----	6	120	50-55 A/F	----	14	----	0-40	----	----	Low	----	(fumig)
"	4	DI	16.2	1	83	*	18-26	29-9	----	----	----	1-2	High	----	----
Parker (72)	5	DI	----	6	67	*	*	----	----	0-20	----	----	Med	----	----
Bascom (71)	7	DI	----	----	----	16-100 A/F	----	18-4	----	0-20	----	----	Med-Hi	----	(fumig)
Shahed (73)	8	DI	12.3	1	130	40-140 BMEP	15-21	20-28	100-300	0-33	----	----	----	----	----
Hames (71)	9	DI	----	6	"7IN"	20-200 BHP	12-21	10-16	----	----	----	----	----	5.5-6.5	5.7-8.3
Marshall (71)	10	DI	----	6	112	19-100 A/F	12-22	30-22	50-265	0-15	0-1.5	(TC)	----	(no effect)	----
Khan-C151 (71)	12	DI	16	1	62	.24-.84 ϕ	----	30-+5	----	----	----	----	----	10-13	----
Abthoff (69)	17	DI	20	1	33	25-90 A/F	15-30	----	----	----	----	.83-1.04	----	----	----
"	21	MAN	17	4	73	17-70 A/F	10-26	41-18	70-170	0-60	0-0.9	----	----	----	----
Walder (73)	27	DI	----	6	143	----	----	----	----	0-10	0-1.0	----	High	----	----
Khan-C142 (71)	29	DI	16	----	63	30-75 A/F	11-27	35-0	----	----	----	----	Lo-Hi	----	varied
Landen (63)	32	PC	17.5	1	----	----	12-24	25-0	90-250	----	----	1-3	----	----	2.4-4.8
McConnell (63)	34	DI	----	----	----	.3-.8 ϕ	8-20	15-+8	----	0-20	----	(TC)	----	----	----
Bosecker (71)	47	PC	----	----	----	0-300 BHP	9-22	----	----	----	0-3.0	(TC)	----	----	----
	48	PC	----	----	----	23-38 A/F	16-22	----	80-240	0-25	----	(TC)	----	----	----
Valdmanis (70)	51	DI	----	----	----	----	----	----	----	----	0-0.4	----	----	----	----
UNITS		----	----	----	in^3	as shown	100 RPM	°CA BTDC	°F	%	per fuel	atm	----	.001"	$mm^3/°CA$

*13-mode

```
                                                       H O  PCT ORFC FUEL PILOT CONE PPM  OPAC   AMEP   LB NOX/  OPACITY         GNOX/HHP HR
     EN  VR   PLACE        RPM      SWIRL               2   EGR DIA. RATE  INJ ANGLE NOX (SOOT)         1K LB FUEL         ISFC   (MULTI)
AUTH  CR              PHI       TIM      PA  TA
---- -- --    -- -- --- ---- --- --- --- --- ---- --- ---- ---- --.-- ---- ---- ---- -----  -------  ------  ----  --------
RPW PC1925    98-10 .76 1500  -6   0  30 100 0.00  0 0.000 7.0  0.00   12  300 31.9  87.6    9.04    31.9  .406    2.10
RPW PC1925    98- 9 .76 1800  -6   0  30 100 0.00  0 0.000 6.0  0.00   12  280 27.7  71.7    8.44    27.7  .423    2.21
RPW PC1925    99-14 .76 2100  -6   0  30 100 0.00  0 0.000 5.0  0.00   12  290 16.0  61.2    8.74    16.0  .423    2.46

RPW PC1925    99- 4 .60 1500  -6   0  30 100 0.00  0 0.000 7.0  0.00   12  380 11.0  77.0   14.47    11.0  .350    2.97
RPW PC1925    99-16 .60 2100  -6   0  30 100 0.00  0 0.000 5.0  0.00   12  320  9.6  52.7   12.18     9.6  .364    3.08

RPW PC1925    99- 5 .45 1500  -6   0  30 100 0.00  0 0.000 7.0  0.00   12  340  4.0  55.9   17.26     4.0  .326    3.54
RPW PC1925   101- 7 .45 1500  -6   0  30 100 0.00  0 0.000 7.0  0.00   12  320  6.0  52.7   16.24     6.0  .317    3.29
RPW PC1925   101-10 .45 1500  -6   0  30 100 0.00 10 0.000 7.0  0.00   12  330  6.0  52.7   16.75     6.0  .318    3.40
RPW PC1925   101- 9 .45 1500  -6   0  30 100 0.00 20 0.000 7.0  0.00   12  180  6.0  52.7    9.14     8.0  .318    1.86
RPW PC1925   101- 8 .45 1500  -6   0  30 100 0.00 30 0.000 7.0  0.00   12  120 13.0  51.7    6.09    13.0  .330    1.29
RPW PC1925    99- 7 .45 1500 -12   0  30 100 0.00  0 0.000 7.0  0.00   12  720 10.0  59.1   36.55    10.0  .313    7.11
RPW PC1925    99- 6 .45 1500  -9   0  30 100 0.00  0 0.000 7.0  0.00   12  480  5.0  60.1   24.36     5.0  .311    4.69
RPW PC1925    99- 8 .45 1500  -3   0  30 100 0.00  0 0.000 7.0  0.00   12  290  4.0  54.9   14.72     4.0  .330    3.07
RPW PC1925    99-10 .45 1500   0   0  30 100 0.00  0 0.000 7.0  0.00   12  450  2.0  57.0   22.84     2.0  .323    4.63
RPW PC1925    99-11 .45 1500   3   0  30 100 0.00  0 0.000 7.0  0.00   12  510  1.5  52.7   25.89     1.5  .340    5.62
RPW PC1925   100- 1 .45 2100  -6   0  30 100 0.00  0 0.000 5.0  0.00   12  370  2.2  43.3   18.78     2.2  .303    4.20
RPW PC1925   101- 6 .45 2100  -6   0  30 100 0.00  0 0.000 5.0  0.00   12  370  4.0  43.3   18.78     4.0  .291    4.05
RPW PC1925   101- 5 .45 2100  -6   0  30 100 0.00 10 0.000 5.0  0.00   12  360  4.0  43.3   18.27     4.0  .300    4.05
RPW PC1925   101- 4 .45 2100  -6   0  30 100 0.00 20 0.000 5.0  0.00   12  230  4.5  41.1   11.67     4.5  .324    2.84
RPW PC1925   101- 3 .45 2100  -6   0  30 100 0.00 30 0.000 5.0  0.00   12  170  6.5  41.1    8.63     6.5  .306    1.99

RPW PC1925    99-12 .30 1500  -6   0  30 100 0.00  0 0.000 7.0  0.00   12  430  1.5  33.8   32.74     1.5  .282    6.70
RPW PC1925   100- 2 .30 2100  -6   0  30 100 0.00  0 0.000 5.0  0.00   12  430  1.8  22.2   32.74     1.8  .265    8.19

RPW PC1925    99-13 .15 1500  -6   0  30 100 0.00  0 0.000 7.0  0.00   12  150  3.5   0.0   22.84     3.5  .819   36.45
RPW PC1925   100- 3 .15 2100  -6   0  30 100 0.00  0 0.000 5.0  0.00   12  100  3.0  -7.4   15.23     3.0  .248  479.26
---- -- --    -- -- --- ---- --- --- --- --- ---- --- ---- ---- --.-- ---- ---- ---- -----  -------  ------  ----  --------


                                                       H O  PCT ORFC FUEL PILOT CONE PPM  OPAC   AMEP   LB NOX/  OPACITY         GNOX/BHP HR
     EN  VR   PLACE        RPM      SWIRL               2   EGR DIA. RATE  INJ ANGLE NOX (SOOT)         1K LB FUEL         ISFC   (MULTI)
AUTH  CR              PHI       TIM      PA  TA
---- -- --    -- -- --- ---- --- --- --- --- ---- --- ---- ---- --.-- ---- ---- ---- -----  -------  ------  ----  --------
RPW PC1915    88- 4 .76 15    -6   0  30 1 0 0.0   0 0.  0 7.0  0.00   12  250 46.0  69.6    7.53    46.0  .473    2.13
RPW PC1915    88-15 .76 1800  -6   0  30 100 0.00  0 0.000 6.0  0.00   12  250 34.0  60.1    7.53    34.0  .485    2.37
RPW PC1915    86-14 .76 2100  -6   0  30 100 0.00  0 0.000 5.0  0.00   12  240 30.0  47.5    7.23    30.0  .479    2.49

RPW PC1915    88-13 .60 1500  -6   0  30 100 0.00  0 0.000 7.0  0.00   12  240 44.0  59.1    9.14    44.0  .419    2.38
RPW PC1915    86-15 .60 2100  -6   0  30 100 0.00  0 0.000 5.0  0.00   12  230 30.0  42.2    8.76    30.0  .423    2.76

RPW PC1915    88- 7 .45 1500  -6   0  30 100 0.00  0 0.000 7.0  0.00   12  230 24.0  47.5   11.67    24.0  .357    2.74
RPW PC1915    88- 9 .45 1500 -12   0  30 100 0.00  0 0.000 7.0  0.00   12  400 28.0  49.6   20.30    28.0  .346    4.56
RPW PC1915    88- 8 .45 1500  -9   0  30 100 0.00  0 0.000 7.0  0.00   12  320 20.0  50.6   16.24    20.0  .343    3.60
RPW PC1915    88-10 .45 1500  -3   0  30 100 0.00  0 0.000 7.0  0.00   12  210 20.0  45.4   10.66    20.0  .370    2.63
RPW PC1915    88-11 .45 1500   0   0  30 100 0.00  0 0.000 7.0  0.00   12  250  9.0  42.2   12.69     9.0  .382    3.29
RPW PC1915    88-12 .45 1500   3   0  30 100 0.00  0 0.000 7.0  0.00   12  290  2.0  36.9   14.72     2.0  .409    4.25
RPW PC1915    86-16 .45 2100  -6   0  30 100 0.00  0 0.000 5.0  0.00   12  250 12.0  31.6   12.69    12.0  .348    3.64

RPW PC1915    88- 6 .30 1500  -6   0  30 100 0.00  0 0.000 7.0  0.00   12  330  2.0  32.7   25.13     2.0  .290    5.34
RPW PC1915    87- 1 .30 2100  -6   0  30 100 0.00  0 0.000 5.0  0.00   12  250  2.5  17.9   19.03     2.5  .287    5.60

RPW PC1915    88- 5 .15 1500  -6   0  30 100 0.00  0 0.000 7.0  0.00   12  170  2.0   1.1   25.89     2.0  .277   12. 5
RPW PC1915    87- 2 .15 2100  -6   0  30 100 0.00  0 0.000 5.0  0.00   12  120  1.0 -10.5   18.27     1.0  .246  -19.34
---- -- --    -- -- --- ---- --- --- --- --- ---- --- ---- ---- --.-- ---- ---- ---- -----  -------  ------  ----  --------
```

Symbol	Author	Engine Code (Table D-1)	ϕ	Timing (^{O}BTDC)
○	Bascom	7	.70	12
●	Bascom	7	.70	16
+	Bascom	7	.70	24
□	Kahn	29	.30	20
■	Kahn	29	.45	20
◇	Kahn	29	.62	20

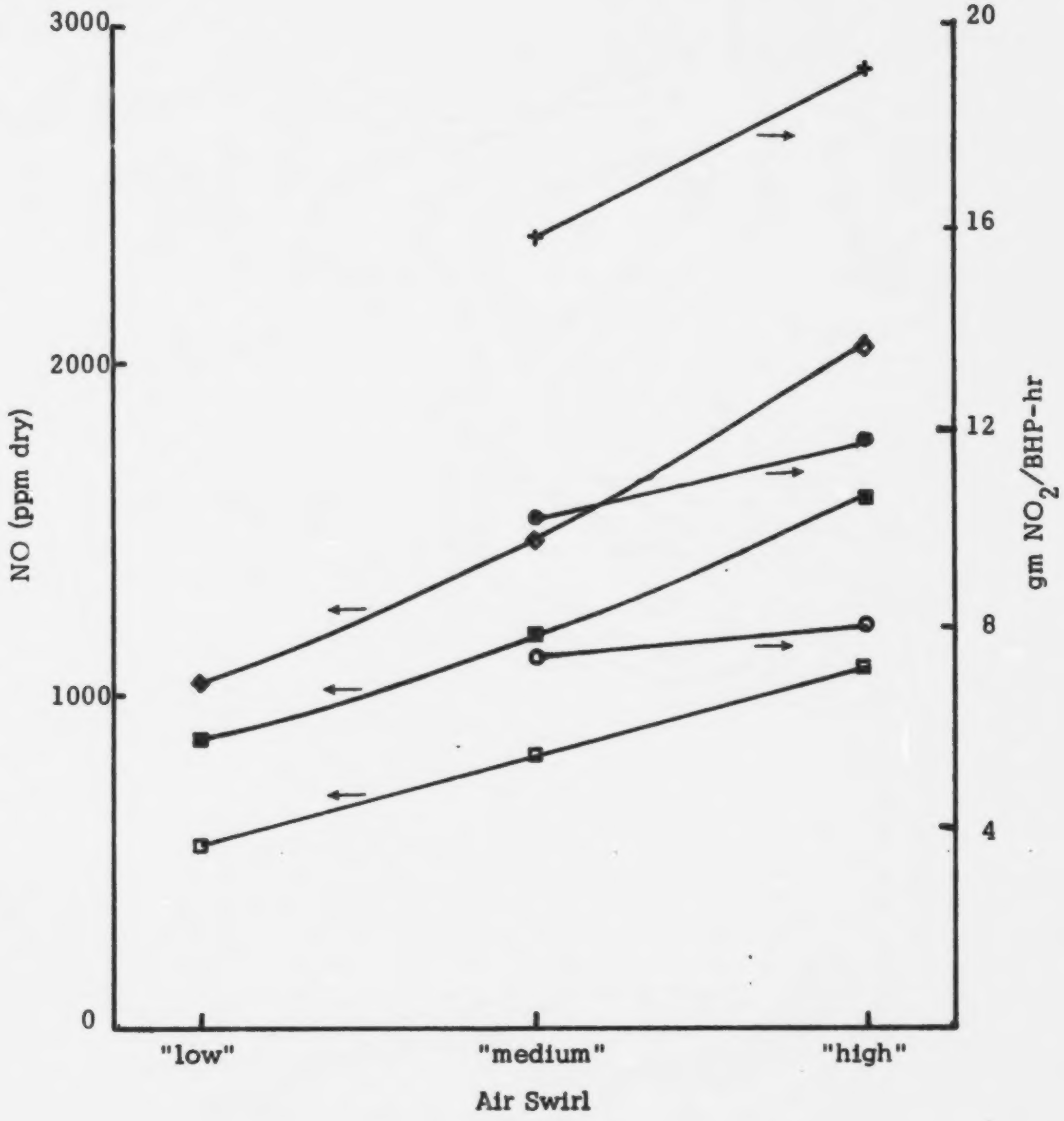

Figure D-1
EFFECT OF AIR SWIRL
(Previous Studies)

Figure D-2

EFFECT OF AIR DENSITY
(Previous Studies)

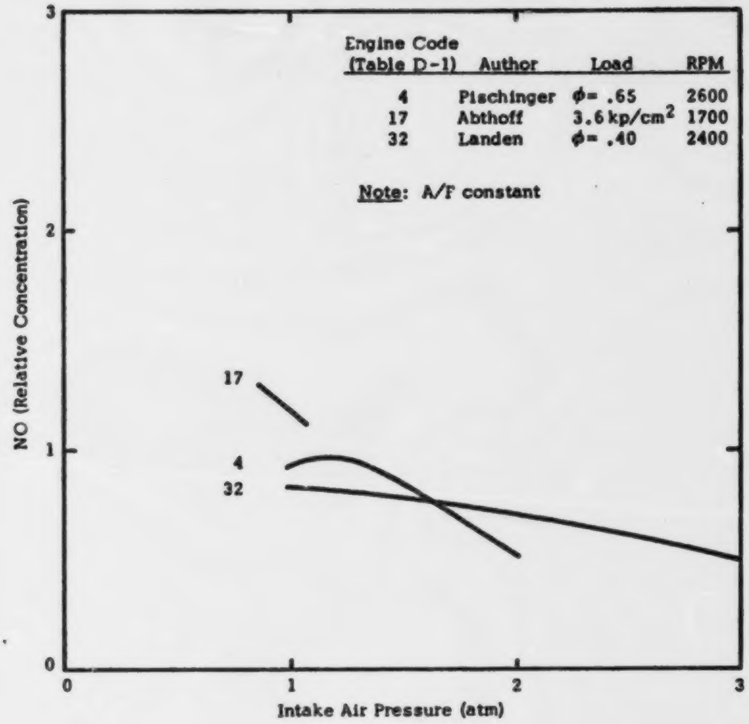

Figure D-3

EFFECT OF AIR TEMPERATURE
(Previous Studies)

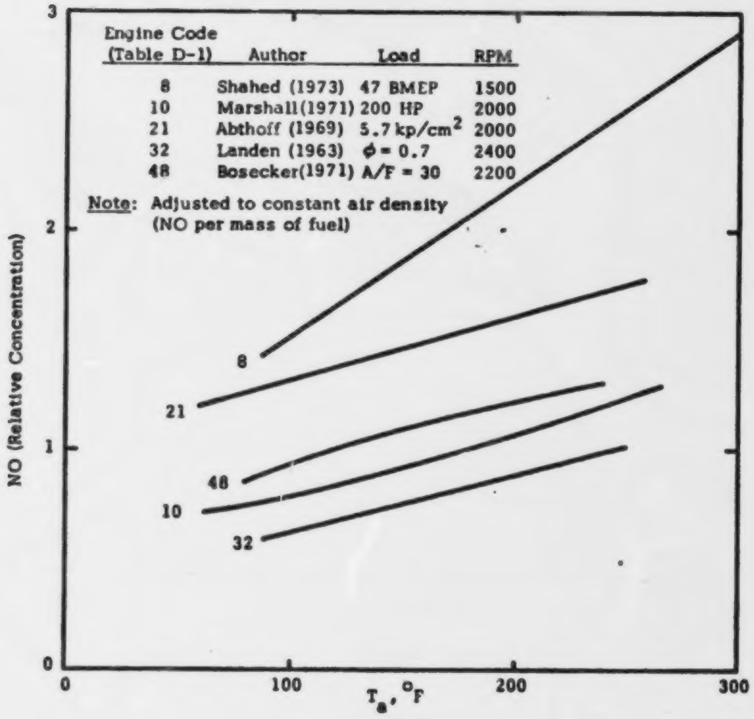

Figure D-4

EFFECT OF WATER INJECTION
(Previous Studies)

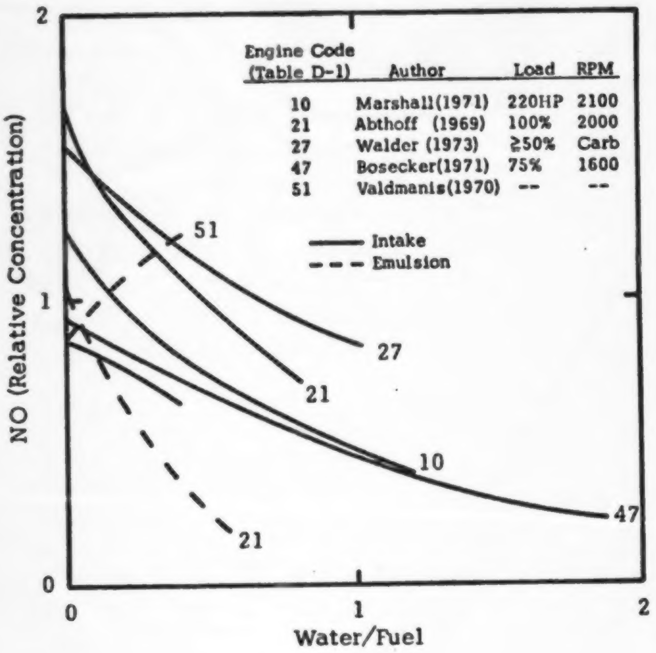

Figure D-5

EFFECT OF EGR
(Previous Studies)

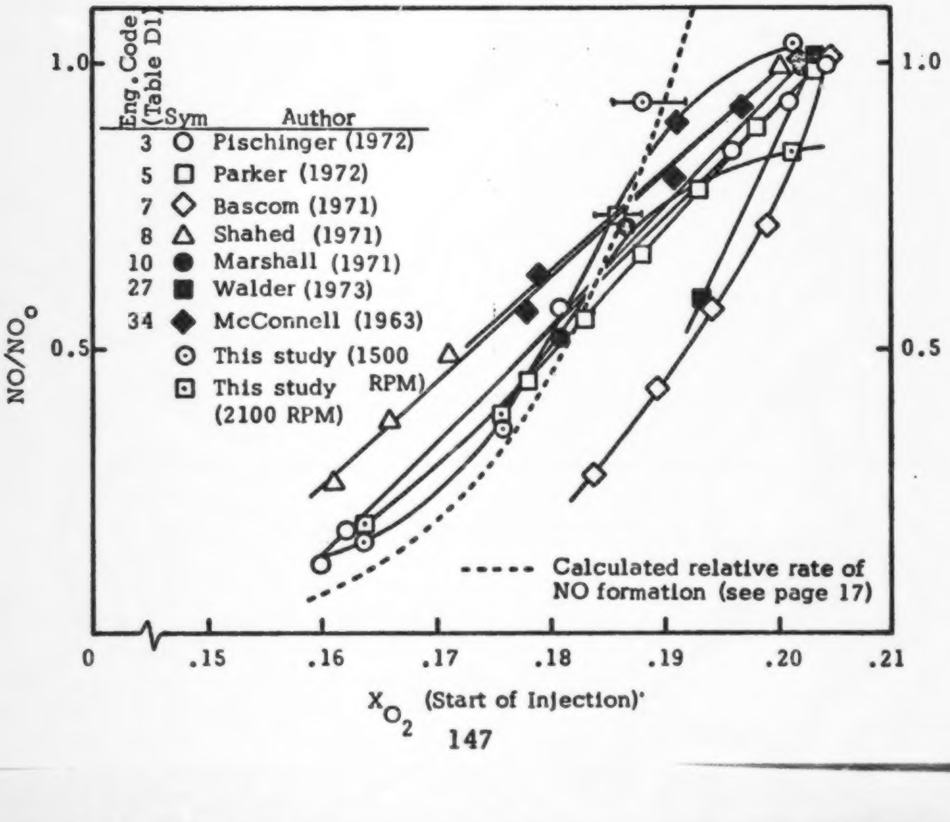

Figure D-6
EFFECT OF TIMING
(Previous Studies - DI Engines)

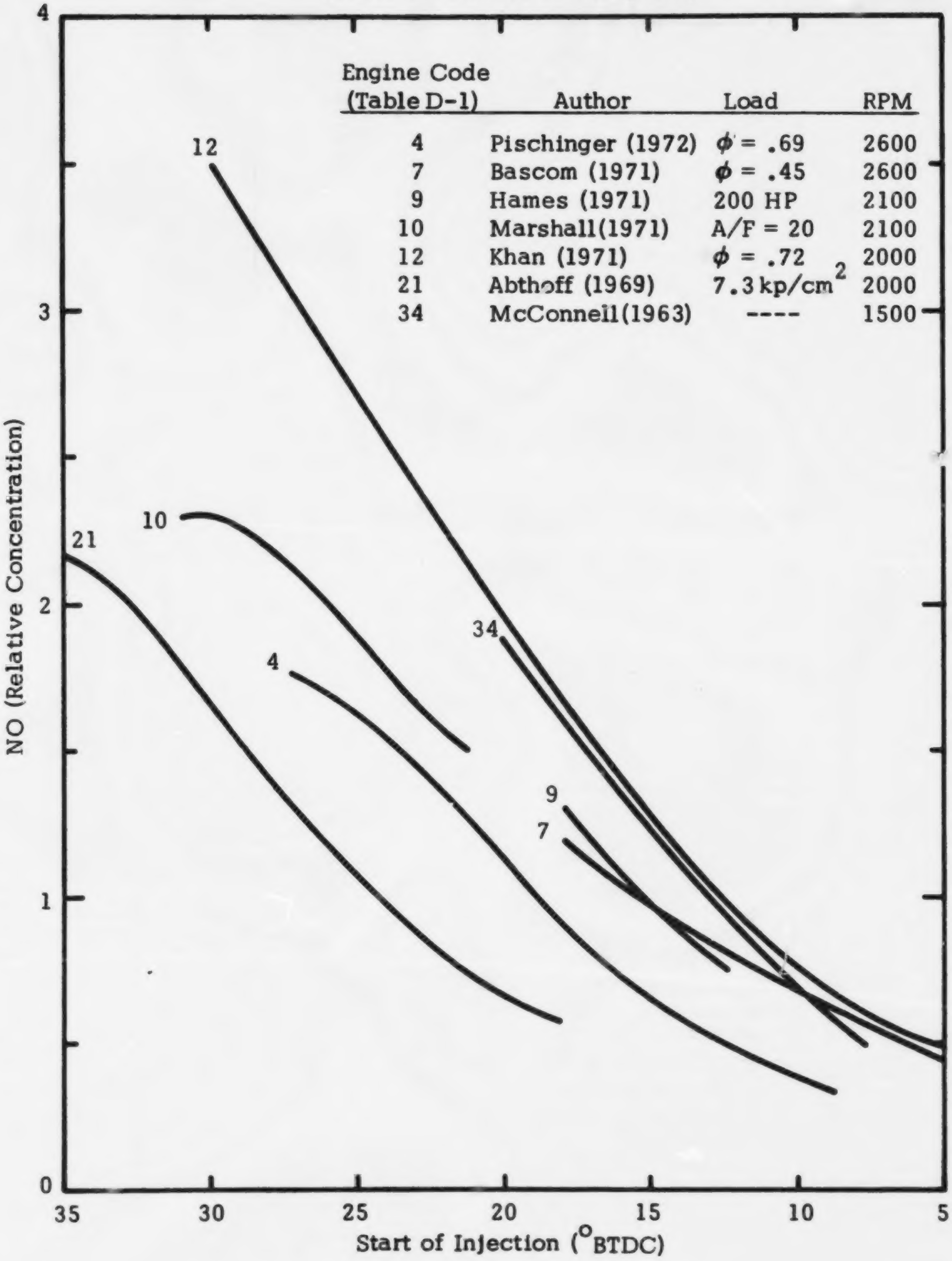

Engine Code (Table D-1)	Author	Load	RPM
4	Pischinger (1972)	$\phi = .69$	2600
7	Bascom (1971)	$\phi = .45$	2600
9	Hames (1971)	200 HP	2100
10	Marshall (1971)	A/F = 20	2100
12	Khan (1971)	$\phi = .72$	2000
21	Abthoff (1969)	$7.3\ kp/cm^2$	2000
34	McConnell (1963)	----	1500

APPENDIX E

EQUILIBRIUM ANALYSIS OF DIFFUSION FLAME STRUCTURE

An equilibrium diffusion flame model was developed in which it is assumed that all of the reactions are in equilibrium with the exception of the NO_x-formation reactions. This assumption may be justifiable since it is the nature of a diffusion flame that the reaction rates are fast compared to the transport rates (the reactions relax faster than the diffusion field can change). Moreover, and perhaps more importantly, there is some experimental evidence which supports this notion*.

Governing Equations

The equations governing the equilibrium diffusion are considerably simpler than those for finite-rate kinetics and are amenable to closed form solution or solution in terms of known tabulated functions for many geometrical configurations. The equations are most conveniently solved when expressed in terms of the enthalpy and the element mass fractions, defined as follows:

$$\tilde{Y}_j = \Sigma \mu_{ij} \frac{M_j}{M_i} Y_i$$

If it is assumed that (1) all diffusion pairs have equal diffusion coefficients and obey Fick's Law, (2) unit Lewis number, and (3) spherical symmetry, then the governing equations take the form

$$\rho \frac{\partial \tilde{Y}_j}{\partial t} = \nabla \cdot (\rho D \nabla \tilde{Y}_j)$$

$$\rho \frac{\partial h}{\partial t} = \nabla \cdot (\rho D \nabla h) \quad ,$$

---

*A. D. Tuteja and H. K. Newhall, "Nitric Oxide Formation in Laminar Diffusion Flames," Emission from Continuous Combustors (1972).

where $\mathcal{D}$ is the total derivative including convective transport.

These equations are readily solved for many cases. For droplet combustion (assuming quasi-steady conditions and ρD = constant), we have the boundary conditions

$$\frac{d}{d\eta}\begin{pmatrix}\tilde{Y}_j\\ h\end{pmatrix} - P\acute{e}\begin{pmatrix}\tilde{Y}_j - \tilde{Y}_{j-}\\ h - h_-\end{pmatrix} = 0 \text{ at } \eta = 1 \quad ,$$

where $\tilde{Y}_{j-}$ and h_- are the element mass fractions and enthalpy of the injected fuel. The solutions take the form

$$\tilde{Y}_j = \tilde{Y}_{j-} + (\tilde{Y}_{j_\infty} - \tilde{Y}_{j-})\ e^{-P\acute{e}/\eta}$$

$$h = h_- + (h_\infty - h_-)\ e^{-P\acute{e}/\eta} \quad ,$$

where $\eta = r/r_w$ and Pé is the usual ratio of convective to diffusive transport.

Once the element mass fractions $\tilde{Y}_j$ and enthalpy and h have been solved as a function of radius, the actual species distribution can be found from an equilibrium analysis. Equilibrium composition through the diffusion flame is accomplished with the aid of the NASA One-Dimensional Equilibrium (ODE) Program. The specified input for this program is the molecular structure (obtained from the element mass fractions) plus two thermodynamic state variables (here taken as enthalpy and pressure).

Sample Calculations

Sample calculations shown in Figure E1 are for methane gas injected into ambient air at 300°K. The Péclét number was taken as Pé = .51. The Burke-Schumann (flame sheet) model calculations were also obtained from the ODE Program by suppressing all species not present in the global reaction, viz.,

$$CH_4 + 2O_2 \longrightarrow CO_2 + 2H_2O \quad .$$

Figure E1

EQUILIBRIUM DIFFUSION FLAME-SPECIES MOLE FRACTIONS

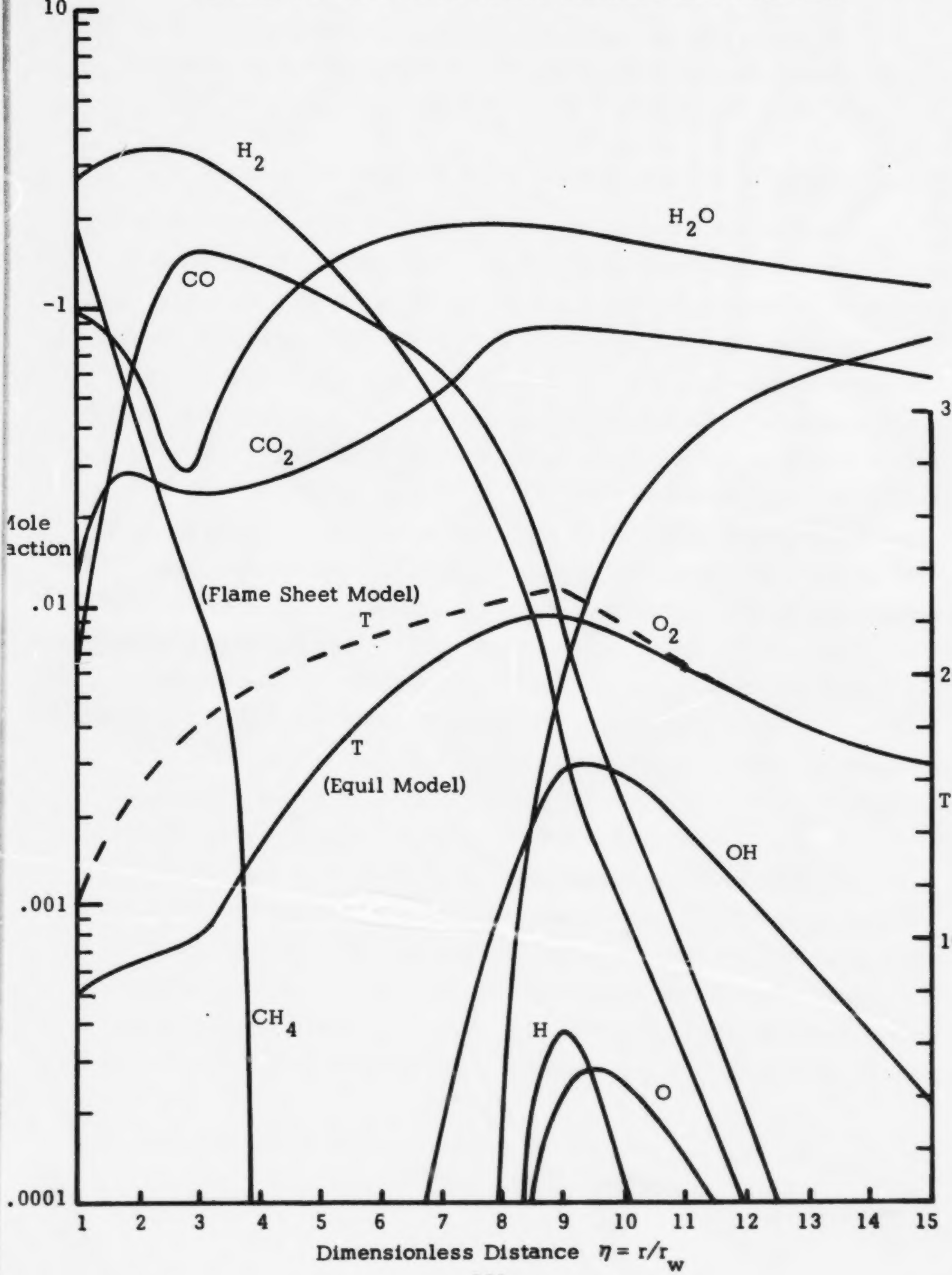

For the equilibrium calculations the spacial variation enters as a parameter only. Thus the computation must be performed at many locations through the flame zone to determine the profiles.

Notes Toward a Flame-Structure Model with Finite-Rate Chemistry

It may be necessary to go beyond the equilibrium chemistry approach of the previous section and consider finite rate reactions. If this becomes necessary, an asymptotic approach can be taken as follows. We neglect the bulk convection and nonsteady effects and consider only the balance between the molecular-diffusion transport term and the chemical source term. This assumption is justified because the governing equations simplify when attention is focused on the flame zone. (See Table E1 which suggests how the asymptotic theory would be developed). In general, the general conservation equations consist of the following four terms: (1) the unsteady term arising due to temporal changes in the field, (2) a convective term representing the transport of heat or mass to a point in the fluid by the mean fluid motion, (3) a diffusion term representing the transport of heat or mass due to gradients in the flow, and finally (4) a chemical reaction term representing the creation or destruction of species and heat by chemical kinetics. Of these four terms, only the last two are of significance if one confines attention to the flame zone itself. It can be rigorously demonstrated that in diffusion flames with large Damköhler numbers*, the flame zone is sufficiently thin that the flame responds in a quasi-steady manner to temporal changes and that convective transport is much less effective than diffusive transport. Thus the local diffusion flame problem can be treated as if it consists of a balance between the diffusion term and the chemical reaction term. Moreover, and perhaps more importantly, is the fact that this flame balance is independent of the geometric configuration. That is to say, it is a universal approximation and will apply equally to burning droplets, sprays, jets, or gaseous counter-flow. Furthermore, the model will be basically iterative because the chemical production in a given subzone will sensitively depend on the flow of species into it from other regions.

---

*The Damköhler number is the ratio of the characteristic mixing time to a characteristic chemical reaction time.

Table E1

Physical Motivation for Asymptotic Expansions

Flame Viewed from a Distance
(Outer Region)

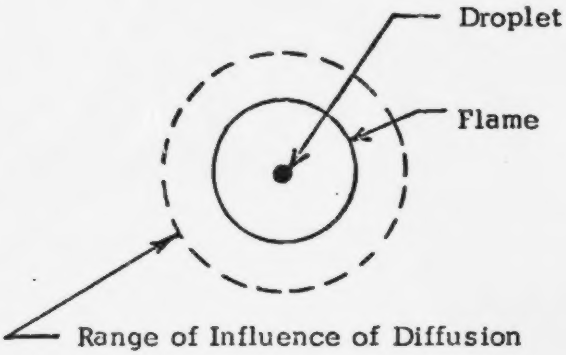

1. In the zones on either side of the flame one or other of the reactants is absent. Hence there is no reaction, and we have an unsteady-diffusion balance.
2. The flame zone appears to be a surface where the reactants disappear. We cannot satisfy all the boundary conditions, and must match with an inner solution.

Flame Viewed Close-up
(Inner Region)

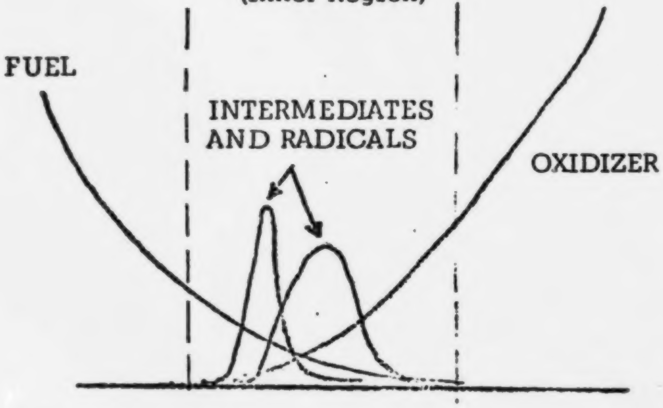

1. The region of interest is sufficiently small that relaxation is rapid, thus the flame zone is quasi-steady and we have a diffusion-reaction balance.
2. The droplet and the range of influence seem far away. We cannot satisfy boundary conditions so we must "match" with the outer solution.

As suggested earlier, the diffusion flame is amenable to a universal treatment. It is intended for our model to satisfy the following criteria, which are put forward both as a goal and as a guide as to what to include in the model:

(1) The model should predict temperature and reactant concentration profiles through the flame zone.

(2) It should predict the O-atom distribution and determine for once and for all if this is in equilibrium.

(3) It should include dissociation for this lowers the temperature and thus affects NO_x production rates.

(4) It should include sufficiently complex C-H-O kinetics to accurately predict the reaction intermediates of interest.

APPENDIX F

UNSTEADY DIFFUSION AS A FACTOR IN DROPLET COMBUSTION

Background

Some recent evidence, both experimental and theoretical, has suggested the possibility that droplets deviate from the classical quasi-steady behavior during combustion. The classical theories assume that the time for the diffusion field to establish itself is small compared to the droplet lifetime, so that at any instant of time the diffusion field corresponds to the steady-state associated with the instantaneous droplet size*. Strictly speaking, the relaxation time for diffusion only vanishes in the limit of zero gas density. Kirkaldy (1958) has pointed out the inherent unsteadiness of spherically symmetric diffusion problems (owing to the finite rate of diffusion). Nevertheless, the quasi-steady theories persist, probably because of the excellent predictions of burning rate (notably the so-called "d^2-law"). More recently, however, investigators have looked not just at overall burning rate but at flame radius, and observations seem to indicate that under some conditions burning occurs in a compound-unsteady fashion (flame and drop radii changing independently). Such observations of unsteadiness have been made by Nuruzzaman and Beér (1971) and Krier and Wronkiewicz (1972), although experimental resolution was not precise enough to rule out alternative explanations for unsteadiness such as droplet heat-up or natural convection. Theoretical studies of droplet combustion such as the exact numerical solutions of Kotake and Okayaki (1969) and the approximate solutions of Chervinsky (1969) have treated the unsteadiness due to droplet heat-up and diffusion. It is interesting to note that the d^2-law would be expected theoretically to hold true even under unsteady conditions, thus

---

*There are other relaxation times of importance in droplet combustion. These include the delay to spontaneous ignition, chemical relaxation time, and liquid-phase heat-up time. In the classical theories, as in the present case, these are assumed to be small compared to both the droplet lifetime and the diffusion relaxation time.

d^2-law measurements should not be taken as evidence for the quasi-steady theory.

The purpose of the present study is to determine the conditions under which the quasi-steady assumption breaks down and how unsteady diffusion affects flame temperature and NO_x formation. Thus we seek to develop a theory for unsteady droplet evaporation and combustion. The present effort will focus attention on the temporal variations of the flame position and temperature by adopting the flame sheet approximation. Thus the present study assumes that finite rate kinetic effects are confined to the immediate flame zone and do not affect the fuel and oxidizer mantles to any appreciable degree. A more realistic analysis of the structure of the flame zone itself is treated in Appendix E.

Governing Equations and Boundary Conditions

The present treatment will be limited to spherically symmetric evaporating or burning droplets in a constant pressure environment. It is further assumed that the diffusion velocity is given by Fick's law, Lewis number is unity, and that we can define a mean specific heat and a mean molecular weight for the mixture. The chemical rate processes are taken to be restricted to an interfacial flame surface and thus no rate terms appear in the field equations. Also, following Williams' (1965) Schvab-Zeldovich formulation, body forces, Soret and Dufour effects, and radiation are neglected.

In addition, liquid-phase heat conduction is neglected. While the influence of this phenomenon on droplet burning is not clear at the present time its inclusion is beyond the scope of the present effort*. In the present analysis the droplet has a constant and uniform internal temperature. Physically this means that all of the heat supplied from the gas-phase is used to evaporate additional fuel to sustain the combustion. Under these conditions we have the following set of equations:

---

*Those who are interested in pursuing the problem may examine the numerical solutions of Wise and Ablow (1957) or the analytical solution of Waldman (1971), both of which are based on a surface regression rate corresponding to the d^2-law and constant surface temperature. The analytical solutions of Waldman were recently extended by Sonalkar (1972) to include arbitrary surface temperature histories.

Continuity:

$$\frac{\partial \bar{\rho}}{\partial \tau} + \frac{1}{\eta^2} \frac{\partial}{\partial \eta} (\eta^2 \bar{\rho} \bar{v}) = 0 \tag{1}$$

Transport:

$$\bar{\rho} \frac{\partial S}{\partial \tau} + \bar{\rho} \bar{v} \frac{\partial S}{\partial \eta} = \frac{1}{\eta^2} \frac{\partial}{\partial \eta} \left(\eta^2 \frac{\partial S}{\partial \eta}\right) , \tag{2}$$

subject to the boundary condition at the droplet surface:

$$\frac{\partial S}{\partial \eta} + \bar{\rho} \bar{v} (S - S_-) = 0 \text{ at } \eta = \eta_s(t) \quad . \tag{3}$$

The initial conditions and boundary conditions at infinity are given by

$$S\,(r > r_s, 0) \;=\; S\,(\infty, t) \;=\; S_\infty \tag{4}$$

Let us define S. Since attention will be restricted here to the case of infinite Damkohler number, i.e., a flame sheet, it is appropriate to introduce a general Schvab-Zeldovich variable S which represents linear combination of the non-dimensionalized temperature and species variables:

$$S = \bar{T} + \bar{Y}_i$$

$$S = \bar{Y}_i - \bar{Y}_j \quad .$$

These variables then satisfy homogeneous equations. In the simple case of pure evaporation the quantity S may represent the mass fraction or temperature itself, of course. $\bar{T}$ and $\bar{Y}_i$ represent dimensionless temperature and reduced mass fraction, following Waldman (1968):

$$\bar{T} = C_p T/Q$$

$$\bar{Y}_i = Y_i/\alpha_i \quad \text{where } \alpha_i = \frac{|\nu_i'' - \nu_i'|\hat{M}_i}{\hat{M}} \quad . \tag{5}$$

In expression (3), $S_- = \overline{Y}_{i-} - \overline{T}_-$, where

$$\bar{T}_- = \frac{L}{Q} - \frac{C_{p_\ell}}{C_p} T_s \; .$$

The other nondimensionalized variables are as follows:

$$\begin{aligned} \eta &= r/r_r \\ \bar{\rho} &= \rho/\rho_\infty \\ \bar{v} &= \rho_\infty r_r v/\rho D \\ \tau &= \rho D t/\rho_\infty r_r^2 \end{aligned} \qquad (6)$$

where r_r is an (as yet unspecified) reference radial position. It is also assumed from here on that the product ρD is constant.

Analysis by Matched Asymptotic Expansions

By uncoupling the droplet regression rate from the gaseous diffusion rate, quasi-steady theories may fail to adequately account for certain unsteady effects, notably the relative motion of the flame and the droplet surface. We suggest here that the unsteady effects are likely to be important far from the droplet, and that the quasi-steady theories confine their attention to the droplet vicinity, and thus may fail to "see" these effects. Thus it is suggested that the droplet be viewed from afar as well as close up, and so analysis by matched asymptotic expansions seems apropos. The physical motivation for asymptotic expansions is demonstrated in Table F1.

Having proposed this notion, it is incumbent upon us to select an expansion parameter which will distinguish the two regions. The above notion suggests that the droplet radius is small compared to the diffusion field of interest. We can define the characteristic diffusion radius, r_r from diffusion theory, $r_r \approx \sqrt{D_\infty t_b}$, where t_b is the characteristic time of the problem (here taken as the burning time). The characteristic burning time can be obtained from the d^2-law (i.e., $r_s^2 = r_{so}^2 - \beta t$) by setting $r_s = 0$. It then follows that

$$\frac{r_{so}}{r_r} = \sqrt{\frac{\beta}{D_\infty}} \quad .$$

Table F1

Physical Motivation for Asymptotic Expansions

Droplet Viewed from a Distance (Outer Region)	Droplet Viewed from Close-up (Inner Region)
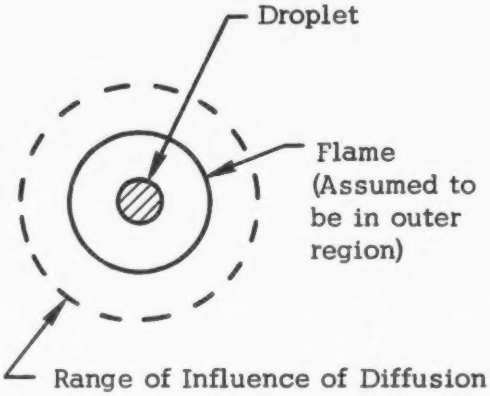 Droplet Flame (Assumed to be in outer region) Range of Influence of Diffusion	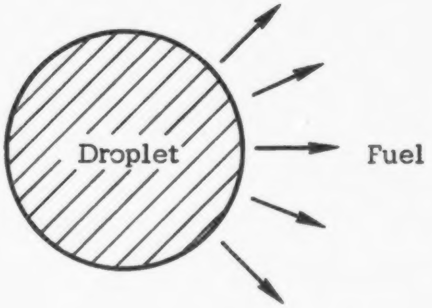
1. The droplet appears to be a point source of mass and sink for heat. We cannot satisfy the boundary conditions at the surface, so we must "match" with the inner solution.	1. On the scale of the droplet, the influence of the diffusion (and perhaps of the flame) is not felt because it acts on a larger scale. We cannot satisfy the boundary conditions at infinity so we must "match" with the outer solution.
2. Convective effects are negligible; this leads to an unsteady-diffusion balance.	2. Relaxation is rapid, the system is quasi-steady; this leads to a convection-diffusion balance.

Typical values for the evaporation constant and the diffusion coefficient ($\beta \approx 10^{-3}$ cm^2/sec, $D_\infty \approx 10^{-1}$ cm^2/sec) suggest taking the expansion parameter

$$\delta = \sqrt{\frac{\beta}{D_\infty}} \quad .$$

With δ so defined, the surface boundary conditions are to be applied at $\eta = \delta\zeta(t)$ [where $\zeta(t) = r_s(t)/r_{so}$]. In the limit $\delta \to 0$, the boundary conditions cannot be applied because the droplet literally vanishes. Recourse must be made to matched asymptotic expansions in order to observe the details of the inner region.

The analysis proceeds formally as follows: The lowest order solution must be dominated by the outer region, for which we postulate $y = \eta - \delta\zeta$ and for which we postulate the velocity to be small ($\bar{v}_{outer} = v = O(\delta)$), so that the primary outer region balance is between unsteadiness and diffusion. The first-order outer equations lead to the trivial solutions

$$\tilde{S}_o = S_\infty, \ \tilde{\rho}_o = 1, \ \tilde{v}_o = 0 \quad . \qquad (7)$$

We now turn our attention to the inner region where the following expansion scheme is postulated.

Inner Region: 1st Order

$$\begin{aligned} z &= \eta/\delta \\ S_{inner} &= \hat{S} = \hat{S}_o + O(\delta) \\ \bar{\rho}_{inner} &= \hat{\rho} = \hat{\rho}_o + O(\delta) \\ \bar{v}_{inner} &= \hat{v} = \delta^{-1}\,\hat{v}_{-1} + O(1) \end{aligned}$$

The inner region equations are determined by substituting the above in Eqs. (1)-(3) and taking the limit $\delta \to 0$, from which we obtain the inner region solutions:

$$z^2 \hat{\rho}_o \hat{v}_{-1} = C(t) = Pé\ \zeta(t)$$

and

$$\hat{S}_o = S_- + (S_s - S_-)e^{Pé}\ e^{-Pé\zeta/z}$$

where

$$Pé = \frac{(\rho v r^2)_s}{(\rho D r)_s}$$

is the Péclét number (ratio of convection to diffusion at the droplet surface and is determined by matching with the outer solution. The boundary condition for z → ∞ is obtained later by matching with the outer solution.

Notice that the lowest order inner solutions are independent of time, thus showing that on a scale of the droplet radius the quasi-steady approximation is valid. Note, however, that in eliminating the time derivative we cannot apply an arbitrary initial condition. In other words, we cannot account for the ignition phenomenon; this is consistent with the flame sheet approximation. Physically, the quasi-steadiness of the inner region means that the zone of interest is sufficiently small that timewise disturbances relax quite rapidly. This result agrees with the conclusion previously reached by Williams (1960) that unsteady effects have only higher order effects on the burning rate.

Following the formalism suggested by Van Dyke (1964) for matching and generation of the next order outer functions, we express the 1-term inner solution in outer variables, expand for small δ, and truncate terms of order greater than δ, to obtain the following 2-term outer expansion:

$$\hat{S} = S_- + (S_s - S_-)e^{Pé} - \delta\,\frac{(S_s - S_-)\,e^{Pé}\,Pé\,\zeta}{y} \tag{8}$$

$$\hat{v} = \delta\,\frac{Pé\,\zeta}{\hat{\rho}_o\, y^2}\ .$$

Matching the lowest order term of Eq. (8) with Eq. (7) gives

$$\mathrm{P\acute{e}} = \ln \left[\frac{S_\infty - S_-}{S_s - S_-} \right] = \ln (1 + B)$$

$$\text{or} \quad \dot{m} = 4\pi \rho D r_s \ln (1 + B)$$

which is the familiar result associated with the quasi-steady theories. Notice that the above expansion (Eq. (8)) also shows that the inner region induces additional perturbations in the outer region, and these will be unsteady as we shall see below. Formally, Eq. (8) suggests the following expansion in the outer region:

$$\left.\begin{aligned} \tilde{S} &= S_\infty + \delta \tilde{S}_1 + O(\delta^2) \\ \tilde{\rho} &= \bar{\rho}_\infty + \delta \tilde{\rho}_1 + O(\delta^2) \\ \tilde{v} &= \qquad \delta \tilde{v}_1 + O(\delta^2) \end{aligned}\right\}$$

The outer equations then take the form

$$\frac{\partial \tilde{\rho}_1}{\partial \tau} + \frac{1}{y^2} \frac{\partial}{\partial y} (y^2 \tilde{v}_1) = 0 \tag{9}$$

$$\frac{\partial \tilde{S}_1}{\partial \tau} = \frac{1}{y^2} \frac{\partial}{\partial y} \left(y^2 \frac{\partial \tilde{S}_1}{\partial y}\right) . \tag{10}$$

subject to $\tilde{S}_1(\infty, \tau) = \tilde{S}_1(y, o) = 0$. Fortunately, Eq. (10) is uncoupled from Eq. (9) and can be solved analytically. The solution is given by

$$\tilde{S}_1 = - \frac{f(o)}{y} \operatorname{erfc} \frac{y}{2\sqrt{\tau}} - \int_0^\tau \frac{df}{d\tau}(\tau') \frac{1}{y} \operatorname{erfc} \frac{y}{2\sqrt{\tau - \tau'}} \, d\tau' \tag{11}$$

where

$$f(\tau) = \lim_{y \to 0} y^2 \frac{\partial \tilde{S}_1}{\partial y}$$

and is to be determined from the matching as follows:

We expressed the 2-term outer solution in inner variables, expanded for small δ and truncated terms of order greater than δ to obtain the 2-term outer solution expressed in outer variables:

$$\tilde{S} = S_\infty - \frac{\delta f(\tau)}{y} \quad .$$

Matching with Eq. (8) gives

$$f(\tau) = (S_s - S_-)\, e^{Pe'}\, Pe'\zeta \tag{12}$$

Returning now to the velocity equation (9) the solution can be expressed as

$$\tilde{v}_1 = \frac{1}{y^2} \int_y^\infty y^2 \frac{\partial \tilde{\rho}_1}{\partial \tau}\, dy \quad .$$

Since $\tilde{\rho}_1$ can be determined from Eqs. (11) and (12) the quadrature can be completed. It is not in the present interest to do this, however, as we will not be seeking higher order inner perturbations. It is clear that such perturbations do exist and will be of increasing importance as ϵ becomes larger (e.g., for more rapidly burning droplets).

In order to examine the temporal history of the flame radius and flame temperature, it is necessary to construct the composite solution. This is so because the flame does not necessarily reside in either the inner or outer regions during its entire lifetime, though it may in some cases. Again following Van Dyke (1964) we can construct an additive composite solution. Thus, from Eqs. (7), (10), and (11) we obtain

$$\begin{aligned} S_c = S_\infty + (S_s - S_-) \Big\{ & e^{Pe'} e^{-Pe'\zeta/z} - \left(e^{Pe'} - \delta e^{Pe'} \frac{Pe'\zeta}{y}\right) \\ & - \delta e^{Pe'} \frac{Pe'\zeta(0)}{y} \operatorname{erfc} \frac{y}{2\sqrt{\tau}} - \frac{\delta e^{Pe'} Pe'}{y} \int_0^\tau \frac{d\zeta}{d\tau}(\tau - \tau') \operatorname{erfc} \frac{y}{2\sqrt{\tau'}}\, d\tau' \Big\} \quad . \end{aligned} \tag{13}$$

Equation (13) is readily expressed in terms of the original variables and the mass burning rate. Noting that

$$Pe'\zeta(t) = \frac{\dot{m}}{4\pi\rho D r_{so}} \quad ,$$

we obtain

$$S = S_\infty - \frac{(S_\infty - S_-)}{4\pi\rho D[r - r_s(t)]}\Big\{\dot{m}(t) - \dot{m}(o)\,\mathrm{erfc}\,\frac{r - r_s(t)}{2\sqrt{Dt}}$$

$$- \int_0^t \frac{d\dot{m}}{dt}(t-t')\,\mathrm{erfc}\,\frac{r - r_s(t')}{2\sqrt{Dt'}}\,dt' - 4\pi\rho D[r - r_s(t)]\Big[\exp\Big(\frac{-\dot{m}(t)}{4\pi\rho Dr}\Big) - 1\Big]\Big\} \;. \qquad (14)$$

It is worthwhile to note that this result is independent of the reference radius r_r. This is consistent with the notion that diffusion in an infinite domain is characterized by an infinite relaxation time. Notice also that Eq. (14) applies both to actual droplets (evaporating and burning) and to porous spheres. For porous spheres $\dot{m}(t)$ and $r_s(t)$ are constants and the equation simplifies somewhat.

Results and Discussion

Equation (14) can be used to determine the flame radius and flame temperature. To determine the former, choose $S = \bar{Y}_F - \bar{Y}_{ox}$ and set $S = 0$. (This assures that the reactants meet and react in stoichiometric proportions.) Thus, the flame radius is given implicitly by the equation

$$\bar{Y}_{ox_\infty} = \frac{(\bar{Y}_{ox}^\infty + \bar{Y}_{F-})}{4\pi\rho D[r_f(t) - r_s(t)]}\Big\{\dot{m}(t) - \dot{m}(o)\,\mathrm{erfc}\,\frac{r_f(t) - r_s(t)}{2\sqrt{Dt}}$$

$$- \int_0^t \frac{d\dot{m}}{dt}(t'-t)\,\mathrm{erfc}\,\frac{r_f(t') - r_s(t')}{2\sqrt{Dt'}}\,dt' - 4\pi\rho D[r_f(t) - r_s(t)]\Big[\exp\Big(\frac{-\dot{m}(t)}{4\pi\rho D r_f(t)}\Big) - 1\Big]\Big\} \qquad (15)$$

where $r_s(t)$ and $\dot{m}(t)$ are given by the quasi-steady solution in the inner region and hence are known.

Likewise, the flame temperature is determined by letting $S = (\bar{T} + \bar{Y}_{ox})$ or $(\bar{T} + \bar{Y}_F)$ and evaluating Eq. (21) at $r = r_f(t)$.

$$\bar{T}_f = \frac{\bar{T}_\infty \bar{Y}_{F-} + \bar{Y}^\infty_{ox} \bar{Y}_{F-} + \bar{T}_- \bar{Y}^\infty_{ox}}{\bar{Y}^\infty_{ox} + \bar{Y}_{F-}} \quad . \tag{16}$$

Equation (16) shows that flame temperature is constant in spite of the motion of the flame. This result is surprising in the light of the exact numerical solutions of Kotake and Okayaki (1969) which exhibit temporally varying flame temperature. We do not presently understand this discrepancy, perhaps it is attributable to the neglect of liquid-phase heat conduction in the present case.

As pointed out previously, Eq. (14) is the principle result of this analysis, being the first-order asymptotic solution to the unsteady droplet combustion problem. Equation (15), which gives an implicit solution for the flame radius, was programmed for solution on a computer. Figure F1 shows some typical results of the computation. It is seen that for the assumed initial conditions $[T(r > r_s) = T_\infty, Y(r > r_s) = Y_\infty]^*$ the flame radius is always increasing relative to the droplet radius (by contrast with the quasi-steady theory which predicts r_f/r_s = constant). It is also seen that the flame radius itself first increases then decreases in the latter stages of combustion.

Figure F2 confines attention to the flame-to-droplet radius over the envelope of validity. The theory is not valid at very early stages of the burning because it ignores the ignition process. Moreover, in the very last stages of the burning most of the mass is already consumed and the exact flame behavior is inconsequential. Thus, Figure F2 shows that over this envelope of validity the flame-to-droplet radius increases from 3 to 6. For comparison, the given conditions for quasi-steady theory predicts a flame-to-droplet radius

---

*Admittedly not a realistic simulation of the ignition or post-ignition conditions.

Figure F1.

TYPICAL RESULTS FROM THE UNSTEADY DIFFUSION THEORY

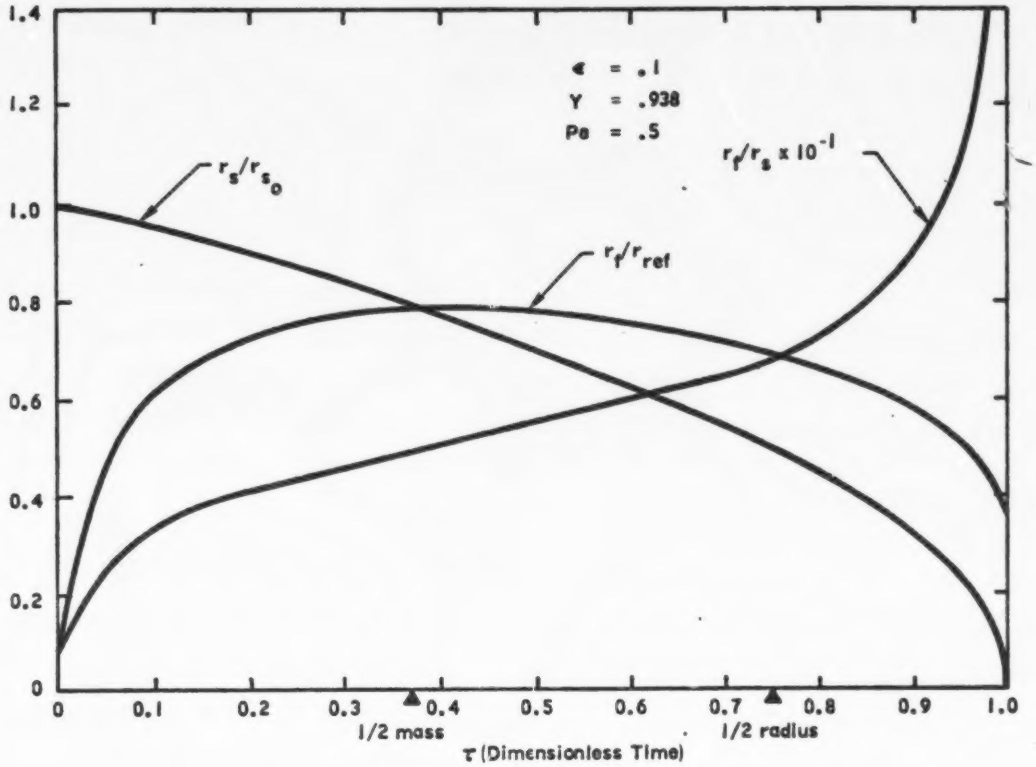

Figure F2.

FLAME ENVELOPE EXPANDS RELATIVE TO DROPLET SURFACE
(BOTH DECREASE DURING BURNING)

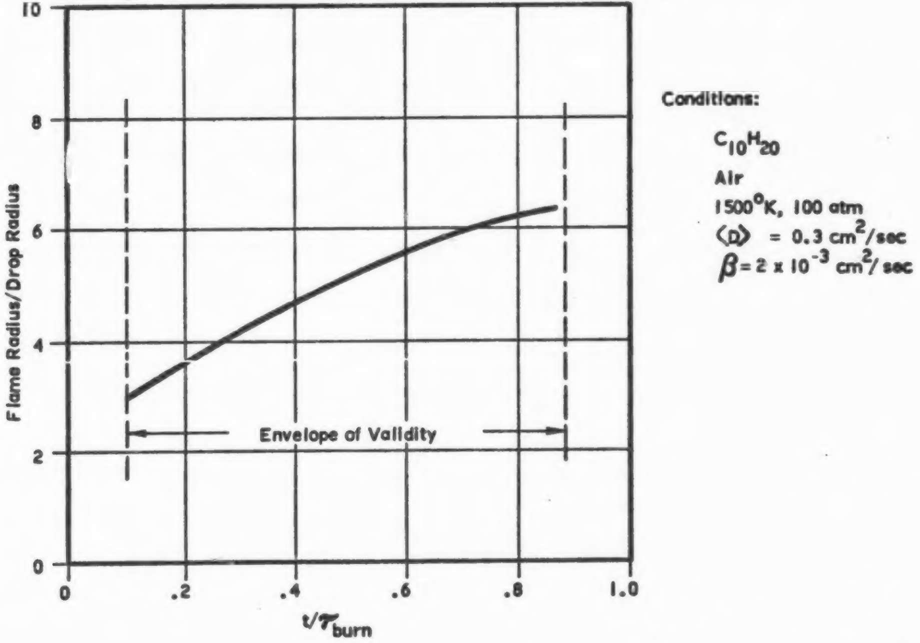

$$\frac{r_f}{r_s} = \frac{\text{Pé}}{\ln(1 + Y_{ox}^{\infty}/i)} \cong 7.8 \quad ,$$

somewhat in excess of the mean value obtained by the unsteady theory. Thus, the unsteady theory seems to be more appropriate than the quasi-steady theory.

It is also interesting to note that the parameter δ, which may be rewritten as

$$\delta = \sqrt{2\text{Pé}\,\frac{\rho_{\infty}}{\rho_{\ell}}} = \sqrt{\frac{2\text{Pé}}{RT}\,\frac{P_{\infty}}{\rho_{\ell}}}$$

is seen to be proportional to the gas-to-liquid-phase density ratio. Owing to the high pressure environment found in diesel combustion chambers it may yet turn out that unsteady effects are minimized in diesel engines. This point requires further examination before any definite conclusions can be reached.

SUPPLEMENTARY REFERENCES FOR APPENDIX F

(See also main list, p.107)

Chervinsky, A., "Transient Burning of Spherical Symmetric Fuel Droplets," Israel Journal of Technology 7, 35 (1969).

Kirkaldy, J. S., "The Time Dependent Diffusion Theory for Condensation on Spherical and Plane Surfaces," Canadian Journal of Physics 36, 446 (1958).

Krier, H. and Wronkiewicz, J. A., "Combustion of Single Drops of Fuel," Combustion and Flame 18, 159 (1972).

Nuruzzaman, A.S.M. and Beér, J. M., "On the Non-Steady State Nature of Droplet Combustion," Combustion Science and Technology 3, 17 (1971).

Sonalkar, R., "Examination of the Fuel Droplet Combustion Problem with Variable Surface Temperature," M.S. Thesis, Rensselaer Polytechnic Institute, Troy, New York (1972).

Tuteja, A. D. and H. K. Newhall, "Nitric Oxide Formation in Laminar Diffusion Flames," Emission from Continuous Combustors (1972).

Van Dyke, M., Perturbation Methods in Fluid Mechanics, Academic Press, New York (1964).

Waldman, C. H., "Theoretical Studies of Diffusion Flame Structures," Ph.D. Thesis, Princeton University (1968).

Waldman, C. H., "Heat Conduction Within a Burning Droplet," unpublished notes (1971).

Williams, F. A., "On the Assumptions Underlying Droplet Vaporization and Combustion Theories," J. Chemical Physics 33, 133 (1960).

Wise, H. and Ablow, C. M., "Burning of a Liquid Droplet. III. Conductive Heat Transfer within the Condensed Phase during Combustion," J. Chemical Physics 27, 389 (1957).

APPENDIX G

EXPERIENCE WITH WINDOWS FOR DIESEL COMBUSTION CHAMBERS

Optical access to a fired diesel combustion chamber was needed for high speed photography and spectroscopic species measurements. Windows were developed and used with combustion chambers of both the direct-injection and prechamber type. Before outlining the experience of window development, it will be useful to recall the design objectives or potential problem areas:

1. Optical Access: A line-of-sight configuration (two opposing windows) for the prechamber, and a single window directly above the piston for the direct-injected head. Windows must pass all light of $\lambda >$ 2100 Å. Also, for photography, windows of about 1 to 2" diameter (as large as feasible) to maximize the field of view.
2. Mechanical Properties: Sufficient tensile strength to withstand up to 100 atm peak chamber pressure.
3. Provision to prevent rapid soot accumulation.
4. Window installation must be free of leakage yet allow windows to be readily replaced.
5. Sufficient cooling must be considered.

Design objectives 1 and 2 were met by selecting fused quartz windows, a pair of 1.5" diameter x 3/8" thick for the prechamber and a single window 2.0" diameter x 1/2" thick for the direct-injection head.

The transmittance and relevant physical properties of type 125 quartz are given below in Figure G-1 and Table G-1, respectively.

Figure G-1

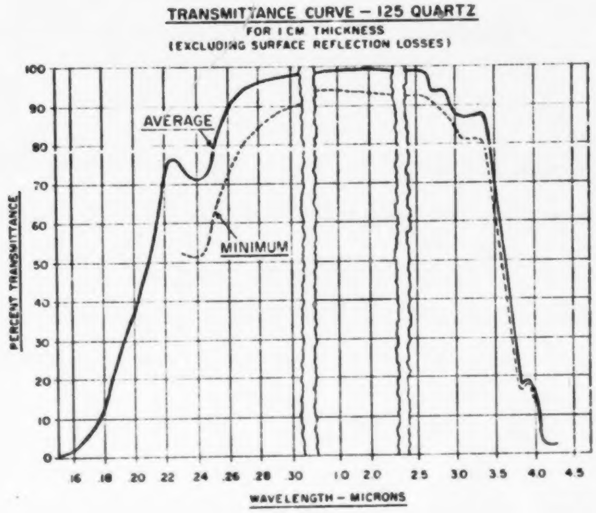

Table G-1

Physical Properties of Type 125 Quartz

Property	English and Metric System Value
Density	2.2 gm/cm^3
Hardness	4.9 Mohs' Scale
Tensile Strength	7,000 psi
Compressive Strength	$>$ 160,000 psi
Bulk Modulus	5.3 x 10^6 psi
Rigidity Modulus	4.5 x 10^6 psi
Young's Modulus	10.4 x 10^6 psi
Poisson's Ratio	.16
Coefficient of Thermal Expansion	5.5 x 10^{-7} cm/cm-°C (20°C-320°C)
Thermal Conductivity	3.3x10^{-3} gm cal-cm/cm^2-sec-°C
Specific Heat	.18 gm cal/gm
Fusion Temperature	1800°C
Softening Point	1670°C
Index of Refraction	1.4585

The following calculations support the notion that the windows would not break under combustion pressures.

For a disk of radius r(in) and tensile strength S(psi), the thickness t(in) to withstand pressure P(psi) is given by the expression

$$t = \sqrt{\frac{1.1\,P}{S}}\ r$$

For $S = 7000$ psi and $P = 1500$ psi, we derive $r/t \approx 2.2$. With a 40% safety factor (i.e. assume peak pressure 2100 psi), the required diameter-to-thickness ratio is

$$\boxed{d/t \equiv 4}$$

Window designs to allow spectroscopy without smoke observation were evaluated following very helpful communication from Bill Brown of Caterpillar and Dr. P. Flynn of Cummins. Options considered include:

1. Conventional window reportedly usable for only five to ten power strokes. Either inject fuel intermittently or remove and clean windows intermittently.

2. Continuously flushed window of reduced size (1/4" to 1/2"); six to twelve small jets provided to flush across the window surface. Based on a review of the flow rates and back pressures used by previous investigators, flushing appears feasible provided the back pressure exceeds twice the peak cylinder pressure. This technique has been used successfully by Ebersole et al. [SAE Paper 701C (1963)], on a smaller window by Dr. Flynn in prechamber engines, and by Dr. Landen who used a 1/8" diameter passage, 1/2" long. Preliminary calculations show that four holes of 300μ diameter can be continuously purged at sonic flow without adding more than 10% to the cylinder contents. Mr. Brown suggests that this approach only works when the unmixed potential core of the jet completely covers the window. This requires a continuous wall jet completely around the circumference of the window with a height of .08" for the 1/4" window. The momentum of the jet must be large compared to the momentum of the eddies in the cylinder.

3. Burn off smoke as it accumulates by heating the window, focused radiation, or other means. At Caterpillar, a plate with a temperature gradient was inserted in the gas stream from a combustor. The hot end of the plate did not collect soot, but the cold end did. The boundary of the soot was at a temperature of 700 to 800°F. This data fits Mr. Brown's experience on diesel piston crowns. To burn off smoke, there is some experience indicating 1000 to 3000 watt/in^2 is necessary.

4. Massive blast of air at BDC on the intake stroke; only the smoke accumulated in one cycle need be removed. Although smoke buildup would occur eventually, it may be considerably postponed in this manner.

Two configurations were selected based on a naturally heated window and a window with continuous flushing. Preliminary calculations given below show that the center of a 2" x 1/2" thick window will rather quickly reach a steady state temperature which is too hot for soot accumulation ($T > 1000^\circ K$).

To simplify the analysis, we assume that a steady heat flux of 13 watt/cm^2 [taken from Le Feuvre et al. (1969)]* is applied to the surface of a semi-infinite quartz body. The temperature gradient within the glass will be on the order of:

$$\frac{\Delta T}{\Delta Z} \approx \frac{\dot{q}}{k} .$$

Substituting $\dot{q} = 13$ watt/cm^2 and $k = 3.3 \times 10^{-3}$ cal/cm-sec°K we obtain $\Delta T/\Delta Z \approx 1000^\circ K/cm$. The actual temperature profiles are non-linear; thus the temperature drop across a 1/2" window would be more than 1000°K. It can be concluded that the exposed surface of the window will exceed the soot burn-up temperature. The heat loss in the radial direction to the cylinder head does not alter this conclusion as long as the window diameter-to-thickness ratio is large ($d/t = 4$ in this case).

---

*Le Feuvre, T., Myers, P. S. and Uyehara, O. A., "Experimental Instantaneous Heat Fluxes in a Diesel Engine and Their Correlation," SAE Paper No. 701C, SAE Trans. 78, 1969.

3. Burn off smoke as it accumulates by heating the window, focused radiation, or other means. At Caterpillar, a plate with a temperature gradient was inserted in the gas stream from a combustor. The hot end of the plate did not collect soot, but the cold end did. The boundary of the soot was at a temperature of 700 to 800°F. This data fits Mr. Brown's experience on diesel piston crowns. To burn off smoke, there is some experience indicating 1000 to 3000 watt/in^2 is necessary.

4. Massive blast of air at BDC on the intake stroke; only the smoke accumulated in one cycle need be removed. Although smoke buildup would occur eventually, it may be considerably postponed in this manner.

Two configurations were selected based on a naturally heated window and a window with continuous flushing. Preliminary calculations given below show that the center of a 2" x 1/2" thick window will rather quickly reach a steady state temperature which is too hot for soot accumulation ($T > 1000^\circ K$).

To simplify the analysis, we assume that a steady heat flux of 13 watt/cm^2 [taken from Le Feuvre et al. (1969)]* is applied to the surface of a semi-infinite quartz body. The temperature gradient within the glass will be on the order of:

$$\frac{\Delta T}{\Delta Z} \approx \frac{\dot{q}}{k} \quad .$$

Substituting $\dot{q} = 13$ watt/cm^2 and $k = 3.3 \times 10^{-3}$ cal/cm-sec°K we obtain $\Delta T/\Delta Z \approx 1000^\circ K/cm$. The actual temperature profiles are non-linear; thus the temperature drop across a 1/2" window would be more than 1000°K. It can be concluded that the exposed surface of the window will exceed the soot burn-up temperature. The heat loss in the radial direction to the cylinder head does not alter this conclusion as long as the window diameter-to-thickness ratio is large ($d/t = 4$ in this case).

---

*Le Feuvre, T., Myers, P. S. and Uyehara, O. A., "Experimental Instantaneous Heat Fluxes in a Diesel Engine and Their Correlation," SAE Paper No. 701C, SAE Trans. 78, 1969.

Although a flushed-window (slotted gasket) was also built, the uncooled windows worked well enough to obviate the need for the more complex flushed system. The precup windows become prohibitively opaque after about 20 to 30 seconds of running at full load and 1500 rpm. However, the windows clean up to an adequate transparency (approximately 70%) after 20 to 30 seconds of motoring. Apparently this is due to oxidation of the freshly deposited soot by hot compressed air. The larger the precup volume, the cleaner the windows can be maintained.

After the soot problem was solved, the spectroscopic measurements were delayed by two window problems: cracking and poor sealing. Quartz window cracking had occurred because of precup deformation when hold-down bolts were tightened; an extra .010" clearance solved the problem. Sealing was accomplished when a trial-and-error series of tests led to the use of a soft brass and asbestos sandwich-gasket.

The final configurations are shown below in Figure G-2.

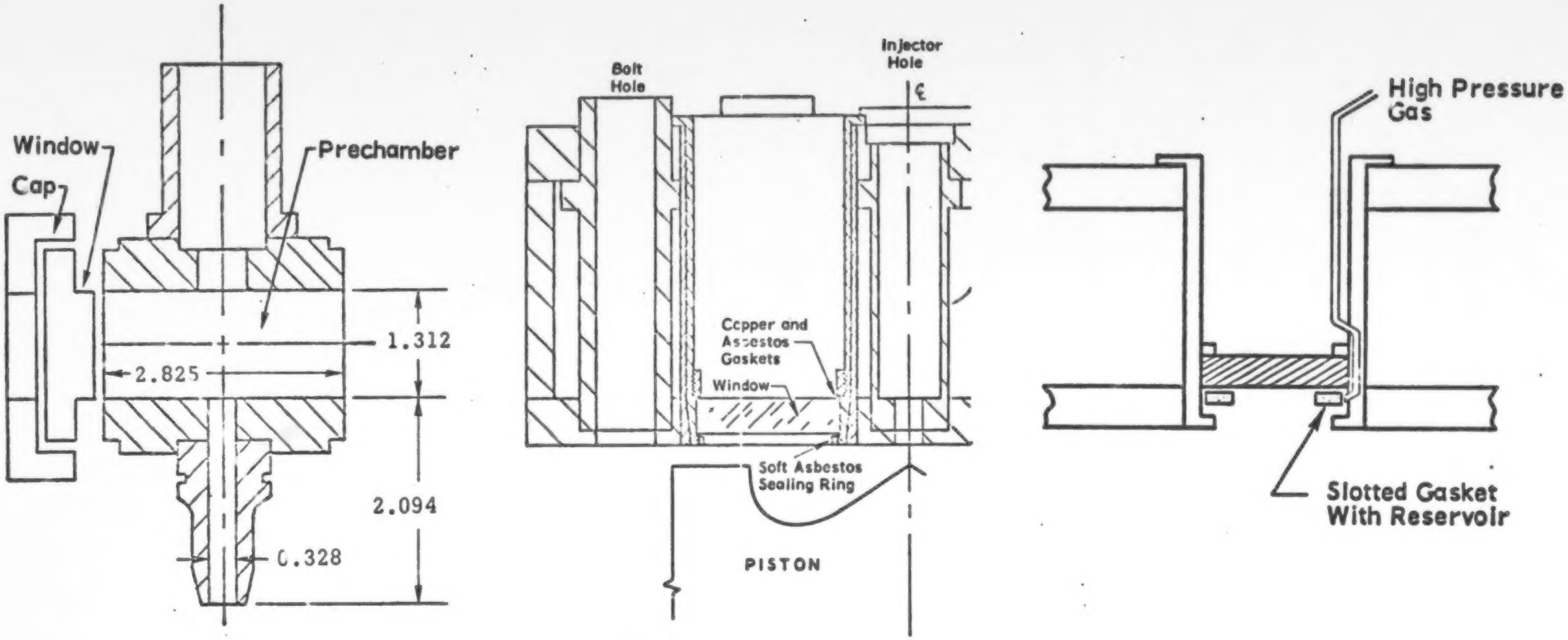
Window
Cap
Prechamber
1.312
2.825
2.094
0.328
Bolt Hole
Injector Hole
℄
Copper and Asbestos Gaskets
Window
Soft Asbestos Sealing Ring
PISTON
High Pressure Gas
Slotted Gasket With Reservoir

(a) Window for Prechamber Engine

(b) Window for Direct Injection Engine

(c) Schematic for Optional Flushed Window

Figure G-2